

Modelling of Long and Short Term Blood Pressure Control Systems

Violeta McLoone

A Thesis submitted in partial fulfillment for the degree of

Doctor of Philosophy



NUI MAYNOOTH

Ollscoil na hÉireann Má Nuad

Faculty of Science and Engineering
Department of Electronic Engineering

Supervisor: Prof. John V. Ringwood
Head of Department: Dr. Ronan Farrell

June 2014

Declaration Of Authorship

I, Violeta McLoone, declare that the thesis, entitled ‘Modelling of Long and Short Term Blood Pressure Control Systems’, and the work presented in the thesis are both my own, and have been generated by me as the result of my own original research. I confirm that:

- This work was done wholly or mainly while in candidature for a research degree at this University.
- Where any part of this thesis has previously been submitted for a degree or any other qualification at this University or any other institution, this has been clearly stated.
- Where I have consulted the published work of others, this is always clearly attributed.
- Where I have quoted from the work of others, the source is always given. With the exception of such quotations, this thesis is entirely my own work.
- I have acknowledged all main sources of help.
- Where the thesis is based on work done by myself jointly with others, I have made clear exactly what was done by others and what I have contributed myself.

Signed:

Date

Abstract

Blood pressure levels are tightly controlled in the body by a variety of interconnected mechanisms at the short-, medium- and long-term scale. In pathophysiological conditions, blood pressure may be chronically elevated above normal levels, which can lead to the development of cardiovascular disease and increased mortality. Building a complete picture of the mechanisms involved in blood pressure control is vital for the development of a better understanding of the processes that may lead to hypertension.

Mathematical models of physiological systems can greatly aid in our understanding of the systems under study, and can also be used in teaching and research tools. This thesis develops a range of mathematical models of various blood pressure control systems and present a diverse set of generic modelling tools, which can be applied to other aspects of human physiology also.

A set of nonlinear grey-box models of varying complexities are developed in this thesis to model the process of salt-induced hypertension in Dahl rats. The models successfully replicate the multiphasal response of blood pressure to high salt intake and provide information on the magnitudes and time scales of the various response components.

The renal vasculature response to sympathetic nerve activity is also modelled by a nonlinear grey-box model. The model represents the renal blood flow response to electrical renal nerve stimulation, under the condition of renal denervation, which can aid in the development of an overall model of the neural control of blood pressure.

In contrast, a linear black-box modelling approach is taken in this thesis to represent the arterial baroreflex, since baroreflex impairment has been associated with a number of conditions such as hypertension, myocardial infarction and heart failure. A measure of the gain of the baroreflex, the baroreflex sensitivity index, can be a useful diagnostic and prognostic tool in cardiology. This thesis develops a rigorous system identification approach to baroreflex sensitivity estimation, based on a linear black-box model of the baroreflex.

Finally, this thesis presents a novel visual, hierarchical, implementation of Arthur Guyton's famous integrative physiology model (Guyton et al., 1972b), in a modelling and simulation environment, which could potentially facilitate its use and further development.

Acknowledgements

First and foremost, I would like to thank my supervisor Prof. John Ringwood, without whom this thesis wouldn't exist. John has provided me with abundant help, endless support for (too) many years of working together, and he has given me a great deal of encouragement, especially when life got in the way of my studies.

I would also like to thank our collaborators Prof. Simon Malpas, Dr. Sarah-Jane Guild and Prof. Bruce Van Vliet for all the help, experimental data, lessons in physiology, and fun times! It was a pleasure working with you.

My sincerest gratitude goes to the staff and my fellow postgrads in the Department of Electronic Engineering. Special thanks go to Joanne and Ann for all the great moral support and advice, to John M. and Denis for the technical support, to Claire for being a great friend (and who understands me so well), and to all the lads - Shane L., Kev, Giorgio, Shane B., Lorcan, Damian, Niall and Francesco for the countless laughs, discussions and help along the way.

This thesis would not have been possible without the support of my amazing family. A huge thank you is owed to my wonderful parents and great role models, for all the help and support throughout the years, and especially during write-up time. I certainly couldn't have done it without you! A big thank you to my sister for the moral support and for being my best friend! I love you and miss you! To my grandmother and Jeni, who looked after my babies (big and small!) and helped me settle into motherhood while attempting to finish my studies - a huge thank you. To my two beautiful, smart and amazing girls, Maya and Anthea - you make it all worthwhile!

I would also like to thank my extended family and friends, especially Stanis, Stoyan and Vania, for being there for me when I needed them.

And finally, the biggest thank you goes to my amazing husband *Séamus*, for truly being my better other half. You possess all the wonderful qualities that I do not and we make a great team. Without you, this thesis would never have materialised.

This work was undertaken with the financial support of the Irish Research Council for Science Engineering and Technology (IRCSET), the John and Pat Hume scholarship and the Ireland Newfoundland Partnership Education and Research Scholarship Scheme.

Contents

Declaration Of Authorship	i
Abstract	ii
Acknowledgements	iii
List of Figures	ix
List of Tables	xiii
List of Abbreviations	xvii
1 Introduction	1
1.1 Motivation	2
1.2 Objectives	4
1.3 Contributions of this thesis	5
1.4 List of publications	6
1.4.1 Journal publications	6
1.4.2 Full-length peer-reviewed conference papers	7
1.5 Thesis outline	7
2 Background	9
2.1 Blood pressure control mechanisms in the body	10
2.1.1 Short-term blood pressure control	10
2.1.2 Medium-term blood pressure control	11
2.1.3 Long-term blood pressure control	12
2.2 The neural baroreflex	14
2.2.1 Baroreflex sensitivity	15

2.2.2	Purpose of the baroreflex sensitivity index	16
2.2.3	Hypertension and the baroreflex	17
2.2.4	Current methods for baroreflex sensitivity estimation	18
2.3	Blood flow regulation	28
2.3.1	Sympathetic nerve activity	29
2.3.2	Hormones	29
2.3.3	Myogenic responses	30
2.3.4	Tissue metabolites	30
2.3.5	Paracrine factors	31
2.3.6	Interactions between effectors	33
2.3.7	Models of RBF response to SNA stimulation	34
2.4	Hypertension	35
2.4.1	Salt-sensitivity and salt-induced hypertension	37
2.4.2	Dahl salt-sensitive and salt-resistant rats	42
2.4.3	Renal function curves	44
2.5	Summary	45
3	Implementation of Guyton’s integrative physiology model in Simulink	47
3.1	Introduction	47
3.2	Model Development and Simulation	49
3.3	Modelling	50
3.4	Simulation	52
3.5	Modelling and simulation environments	53
3.5.1	Diagrams and equations	54
3.5.2	Markup languages	54
3.5.3	Graphical modelling and simulation environments	56
3.5.4	High-level languages	59
3.6	Existing large-scale physiology models	59
3.7	Guyton’s model implementation	63
3.8	Discussion	69
3.9	Conclusions	70
4	A model for salt-induced hypertension in Dahl rats	73
4.1	Introduction	73

4.2	Experimental Protocols	74
4.2.1	Protocol 1: Time evolution of salt-induced changes of blood pressure in Dahl-S rats	74
4.2.2	Protocol 2: Reversibility of salt-induced changes in blood pressure in Dahl-S rats	75
4.2.3	Protocol 3: Response of blood pressure in Dahl-S and Dahl-R rats to a pseudo random binary sequence (PRBS) salt input . . .	76
4.2.4	Protocol 4: Time evolution of salt-induced blood pressure changes in Hybrid rats	77
4.3	Model structure development	78
4.3.1	3-component model	79
4.3.2	4-component model	80
4.3.3	5-component model	82
4.4	Model parameter determination	82
4.5	Results	85
4.5.1	3-component model	86
4.5.2	4-component model	89
4.5.3	5-component model	93
4.5.4	F-test	97
4.5.5	Renal function curves	99
4.6	Discussion	101
4.7	Conclusion	103
5	Baroreflex sensitivity estimation	105
5.1	Experimental protocol	105
5.2	System characteristics and implications	106
5.3	Outline of the SID framework for BRS estimation	107
5.3.1	Families of model structures	107
5.3.2	Persistence of excitation	108
5.3.3	Identification in closed-loop	109
5.3.4	Model parameter determination	111
5.4	Results of the system identification approach to BRS estimation	113
5.4.1	Data preprocessing	113
5.4.2	Persistence of excitation	116

5.4.3	Model order and parameter determination	116
5.4.4	BRS calculation	122
5.5	Discussion	124
5.5.1	Comparison with other methods	126
5.5.2	Results comparison with other methods	128
5.6	Conclusions	131
6	Nonlinear model of renal vasoaction	133
6.1	Introduction	133
6.2	Experimental protocol	135
6.3	Model structure development	137
6.3.1	Model A	137
6.3.2	Model B	139
6.3.3	Stimulation/recovery models	140
6.4	Model optimisation	140
6.4.1	Manual parametrisation	142
6.4.2	Genetic algorithms	142
6.4.3	Gradient techniques	143
6.4.4	Combination of GAs and gradient techniques	144
6.5	Results	145
6.5.1	Model A vs Model B	145
6.5.2	Stimulation/recovery models	147
6.6	Discussion	151
6.7	Conclusions	154
7	Conclusions and future work	156
7.1	Summary and conclusions	156
7.2	Future work	160
	Appendices	163
A	Salt-induced hypertension model results	164
A.1	3-component model results	164
A.2	4-component model results	168
A.3	5-component model results	171

B Baroreflex sensitivity estimation results	177
B.1 Persistence of excitation figures	178
B.2 ARMAX model parameters - standing position	186
B.3 ARMAX Model parameters - supine position	191
References	197

List of Figures

2.1	The baroreflex	15
2.2	The baroreflex loop with two external noise sources n_r and n_s	16
2.3	Steady-state renal function curves, representing: line a - a normotensive salt-resistant individual, line b - a normotensive salt-sensitive individual, line c - a hypertensive salt-resistant individual and line d - a hypertensive salt-sensitive individual. The figure is a modified version of Figure 4 in Van Vliet et al. (2006)	45
3.1	Stages of the modelling process	49
3.2	Multiscale modelling hierarchy (Hunter and Nielsen, 2005).	51
3.3	Spatial (top) and temporal (bottom) scales encompassed by the Human Physiome Project along with corresponding markup language (based on Hunter et al. (2002)).	55
3.4	Existing integrative physiology models	61
3.5	Novel Simulink implementation of the 1992 version of Guyton’s model	64
3.6	First order system with steady-state gain k_{ss} and a time constant τ	65
3.7	First order system step response with steady-state gain $k_{ss} > 1$ and time constant τ	66
3.8	Comparison between the MODSIM and the Simulink implementations of the 1992 version of Guyton’s model for an experiment with reduced kidney mass and increased salt intake	68
4.1	SIH Protocol 1, individual and ‘mean animal’ responses for the Dahl-S and control Dahl-R animals	75
4.2	SIH Protocol 2, individual and ‘mean animal’ responses	76

4.3	SIH Protocol 3, individual and ‘mean animal’ responses for the Dahl-S and control Dahl-R animals	77
4.4	SIH Protocol 4, individual and ‘mean animal’ responses for the hybrid animals	78
4.5	SIH 3-component model structure	79
4.6	SIH 4-component model structure	81
4.7	SIH 5-component model structure	83
4.8	Simplex method operations	84
4.9	‘Mean animal’ model response for the 3-component model structure . .	87
4.10	Model component contribution for the 3-component ‘mean animal’ model	89
4.11	‘Mean animal’ model response for the 4-component model structure . .	90
4.12	Model component contribution for the 4-component ‘mean animal’ model	91
4.13	‘Mean animal’ model response for the 5-component model structure . .	94
4.14	Model component contribution for the 5-component ‘mean animal’ model	95
4.15	Steady-state pressure-natriuresis relationships for the ‘mean’ salt-sensitive and salt-resistant animals of Protocol 1	99
4.16	Steady-state pressure-natriuresis relationships for four hybrid rats . . .	100
5.1	A closed-loop system	109
5.2	Irregularly sampled EuroBaVar beat-to-beat data compared to the interpolated regularly sampled data (Subject 5, supine position)	114
5.3	Butterworth bandpass filter response	115
5.4	Filtered SAP and RR interval data compared with the original unfiltered data for Subject 5 in the supine position	115
5.5	Persistence of excitation in <i>SAP</i> for Subject 5 in the supine position . .	116
5.6	Plot of actual and modelled data for Subject 5 in the supine position . .	121
5.7	Baroreflex gain for Subject 5 in the supine position	122
5.8	BRS estimates for all EuroBaVar subjects in the standing position . . .	124
5.9	BRS estimates for all EuroBaVar subjects in the supine position	125
5.10	Correlation of our LF and HF BRS estimates in the standing position with results from methods reported in Laude et al. (2004)	130
5.11	Correlation of our LF and HF BRS estimates in the supine position with results from methods reported in Laude et al. (2004)	131

6.1	Summary of vasoactive mechanisms, adapted from Richardson et al. (1998)	134
6.2	Experimental data for Rabbit 1 during electrical nerve stimulation and recovery (includes data for all 7 frequencies of stimulation)	136
6.3	Scaled data for Rabbit 1 during electrical nerve stimulation and recovery (includes data for all 7 frequencies of stimulation)	136
6.4	Feedforward/feedback vasoaction model configuration	137
6.5	Block diagram of vasoaction Model A	138
6.6	Typical large-signal response to SNA activation	139
6.7	Block diagram of vasoaction Model B	140
6.8	Block diagram of Model B, during stimulation	141
6.9	Block diagram of Model B, during recovery	141
6.10	‘Frequency’ transform function for the manually optimised Model A (Manual) and the computer optimised Model A and Model B	146
6.11	Local vasodilator ‘Activation level’ for the manually optimised Model A (Manual) and the computer optimised Model A and Model B	146
6.12	Model B (stimulation/recovery) ‘Frequency transform’ function for three animals	149
6.13	Local factors ‘Activation level’ function for the stimulation model of three animals (Model B)	150
6.14	Local factors ‘activation level’ function for the recovery model of three animals (Model B)	150
6.15	Hysteresis effect diagram	151
6.16	Comparison of model output and experimental results for Rabbit 1 (Model B: stimulation and recovery plotted together)	152
6.17	Comparison of model output and experimental results for Rabbit 2 (Model B: stimulation and recovery plotted together)	152
6.18	Comparison of model output and experimental results for Rabbit 3 (Model B: stimulation and recovery plotted together)	153
B.1	Persistence of excitation in <i>SAP</i> for EuroBaVar Subjects 1-6 in the standing position	178
B.2	Persistence of excitation in <i>SAP</i> for EuroBaVar Subjects 7-12 in the standing position	179

B.3 Persistence of excitation in <i>SAP</i> for EuroBaVar Subjects 13-18 in the standing position	180
B.4 Persistence of excitation in <i>SAP</i> for EuroBaVar Subjects 19-21 in the standing position	181
B.5 Persistence of excitation in <i>SAP</i> for EuroBaVar Subjects 1-6 in the supine position	182
B.6 Persistence of excitation in <i>SAP</i> for EuroBaVar Subjects 7-12 in the supine position	183
B.7 Persistence of excitation in <i>SAP</i> for EuroBaVar Subjects 13-18 in the supine position	184
B.8 Persistence of excitation in <i>SAP</i> for EuroBaVar Subjects 19-21 in the supine position	185

List of Tables

4.1	‘Mean animal’ model MAEs and parameters for the 3-component SIH model	88
4.2	Average individual animal MAEs and parameters for the 3-component SIH model	88
4.3	Average MAEs and parameters for the control Dahl-R rats for the 3-component SIH model	88
4.4	‘Mean animal’ model MAEs and parameters for the 4-component SIH model	92
4.5	Average individual animal MAEs and parameters for the 4-component SIH model	92
4.6	Average MAEs and parameters for the control Dahl-R rats for the 4-component SIH model	93
4.7	‘Mean animal’ model MAEs and parameters for the 5-component SIH model	93
4.8	Average individual animal MAEs and parameters for the 5-component SIH model	96
4.9	Average MAEs and parameters for the control Dahl-R rats for the 5-component SIH model	96
4.10	Mean F-test values for the Dahl-S rats of Protocols 1, 2 and 3 and the hybrid rats of Protocol 4	98
4.11	Mean F-test values for the control Dahl-R rats of Protocols 1 and 3	99

5.1	ARMAX model structures and corresponding MAEs for each EuroBaVar subject in the standing and supine positions; n_a , n_b , n_c are the orders of the A , B and C polynomials, respectively, and n_d is the number of step delays in Equation (5.1); MAE is the mean absolute error	120
5.2	ARMAX model parameters for Subject 5 in the supine position, with model structure [6 4 1 2]; a_i , b_i and c_i are the parameters of the A , B and C polynomials, respectively.	121
6.1	Dynamic parameters for the manually optimised vasoaction Model A and the computer optimised vasoaction Model A and Model B	145
6.2	Dynamic blocks parameters for the stimulation vasoaction models (Model B) for 3 animals	148
6.3	Dynamic blocks parameters for the recovery vasoaction models (Model B), for 3 animals	148
A.1	SIH modelling results for individual salt-sensitive animals of Protocol 1, 3-component model	164
A.2	SIH modelling results for individual salt-sensitive animals of Protocol 2, 3-component model	165
A.3	SIH modelling results for individual salt-sensitive animals of Protocol 3, 3-component model	165
A.4	SIH modelling results for individual hybrid animals of Protocol 4, 3-component model	166
A.5	SIH modelling results for individual salt-resistant animals of Protocol 1, 3-component model	166
A.6	SIH modelling results for individual salt-resistant animals of Protocol 3, 3-component model	167
A.7	SIH modelling results for individual salt-sensitive animals of Protocol 1, 4-component model	168
A.8	SIH modelling results for individual salt-sensitive animals of Protocol 2, 4-component model	168
A.9	SIH modelling results for individual salt-sensitive animals of Protocol 3, 4-component model	169

A.10 SIH modelling results for individual hybrid animals of Protocol 4, 4- component model	169
A.11 SIH modelling results for individual salt-resistant animals of Protocol 1, 4-component model	170
A.12 SIH modelling results for individual salt-resistant animals of Protocol 3, 4-component model	170
A.13 SIH modelling results for individual salt-sensitive animals of Protocol 1, 5-component model	171
A.14 SIH modelling results for individual salt-sensitive animals of Protocol 2, 5-component model	172
A.15 SIH modelling results for individual salt-sensitive animals of Protocol 3, 5-component model	173
A.16 SIH modelling results for individual hybrid animals of Protocol 4, 5- component model	174
A.17 SIH modelling results for individual salt-resistant animals of Protocol 1, 5-component model	175
A.18 SIH modelling results for individual salt-resistant animals of Protocol 3, 5-component model	176
B.1 ARMAX model parameters, Subject 1, standing position, $n_d=1$	186
B.2 ARMAX model parameters, Subject 2, standing position, $n_d=1$	186
B.3 ARMAX model parameters, Subject 3, standing position, $n_d=3$	186
B.4 ARMAX model parameters, Subject 4, standing position, $n_d=2$	187
B.5 ARMAX model parameters, Subject 5, standing position, $n_d=0$	187
B.6 ARMAX model parameters, Subject 6, standing position, $n_d=0$	187
B.7 ARMAX model parameters, Subject 7, standing position, $n_d=0$	187
B.8 ARMAX model parameters, Subject 8, standing position, $n_d=0$	187
B.9 ARMAX model parameters, Subject 9, standing position, $n_d=0$	188
B.10 ARMAX model parameters, Subject 10, standing position, $n_d=1$	188
B.11 ARMAX model parameters, Subject 11, standing position, $n_d=1$	188
B.12 ARMAX model parameters, Subject 12, standing position, $n_d=0$	189
B.13 ARMAX model parameters, Subject 13, standing position, $n_d=2$	189
B.14 ARMAX model parameters, Subject 14, standing position, $n_d=4$	189
B.15 ARMAX model parameters, Subject 15, standing position, $n_d=0$	189

B.16 ARMAX model parameters, Subject 16, standing position, $n_d=1$	189
B.17 ARMAX model parameters, Subject 17, standing position, $n_d=1$	190
B.18 ARMAX model parameters, Subject 18, standing position, $n_d=4$	190
B.19 ARMAX model parameters, Subject 19, standing position, $n_d=4$	190
B.20 ARMAX model parameters, Subject 20, standing position, $n_d=3$	190
B.21 ARMAX model parameters, Subject 21, standing position, $n_d=0$	190
B.22 ARMAX model parameters, Subject 1, supine position, $n_d=1$	191
B.23 ARMAX model parameters, Subject 2, supine position, $n_d=2$	191
B.24 ARMAX model parameters, Subject 3, supine position, $n_d=1$	191
B.25 ARMAX model parameters, Subject 4, supine position, $n_d=1$	192
B.26 ARMAX model parameters, Subject 5, supine position, $n_d=2$	192
B.27 ARMAX model parameters, Subject 6, supine position, $n_d=2$	192
B.28 ARMAX model parameters, Subject 7, supine position, $n_d=1$	192
B.29 ARMAX model parameters, Subject 8, supine position, $n_d=1$	192
B.30 ARMAX model parameters, Subject 9, supine position, $n_d=2$	193
B.31 ARMAX model parameters, Subject 10, supine position, $n_d=1$	193
B.32 ARMAX model parameters, Subject 11, supine position, $n_d=0$	193
B.33 ARMAX model parameters, Subject 12, supine position, $n_d=1$	194
B.34 ARMAX model parameters, Subject 13, supine position, $n_d=0$	194
B.35 ARMAX model parameters, Subject 14, supine position, $n_d=0$	194
B.36 ARMAX model parameters, Subject 15, supine position, $n_d=4$	194
B.37 ARMAX model parameters, Subject 16, supine position, $n_d=0$	194
B.38 ARMAX model parameters, Subject 17, supine position, $n_d=0$	195
B.39 ARMAX model parameters, Subject 18, supine position, $n_d=2$	195
B.40 ARMAX model parameters, Subject 19, supine position, $n_d=1$	195
B.41 ARMAX model parameters, Subject 20, supine position, $n_d=4$	196
B.42 ARMAX model parameters, Subject 21, supine position, $n_d=1$	196

List of Abbreviations

AA	Arachidonic acid
ANF	Atrial natriuretic factor
ANG I	Angiotensin I
ANG II	Angiotensin II
ANS	Autonomic nervous system
AR	Auto-Regressive
ARMA	Autoregressive moving average model
ARMAX	Auto-regressive moving average model with exogenous input
ARX	Auto-regressive model with exogenous input
ATP	Adenosine triphosphate
BJ	Box-Jenkins (model)
BP	Blood pressure
BRS	Baroreflex sensitivity
CNS	Central nervous system
CO	Cardiac output
DAE	Differential algebraic equations
DFT	Discrete Fourier transform
ECG	Electrocardiography
GA	Genetic algorithm

HF	High-frequency
HR	Heart rate
IUPS	International Union of Physiological Sciences
LF	Low-frequency
MAP	Mean arterial pressure
MI	Myocardial infarction
MAE	Mean absolute error
ML	Markup language
MSE	Mean squared error
NO	Nitric oxide
ODE	Ordinary differential equation
PEM	Prediction error method
PRBS	Pseudo-random binary sequence
RAAS	Renin-angiotensin-aldosterone system
RBF	Renal blood flow
RR	R-R interval
SAP	Systolic arterial pressure
SIH	Salt-induced hypertension
SNA	Sympathetic nerve activity
TF	Transfer function
TPR	Total peripheral resistance
TRS	Trigonometric regressive (approach)
VLF	Very low-frequency
XML	Extensible markup language

To Maya and Anthea

Chapter 1

Introduction

The state of homeostasis is the maintenance of a relatively constant internal bodily environment, despite external changes (Guyton and Hall, 2006). All systems in the body function to achieve desirable conditions, but the circulatory system's role to maintain nutrient and oxygen supply to satisfy all tissues' needs, is of utmost importance. The regulation of blood pressure at stable and healthy levels, in order to ensure effective blood flow supply, is thus central to achieving homeostasis.

Blood pressure can be determined according to the simplified relationship (Guyton and Hall, 2006):

$$BP = CO \cdot TPR \tag{1.1}$$

where

- BP is blood pressure, measured in mmHg, and refers to the mean arterial pressure (MAP),
- CO is cardiac output, evaluated as the product of heart rate and stroke volume (in l/s), and
- TPR is the total peripheral resistance, as seen by the heart (in mmHg s/l).

Blood pressure is controlled by numerous mechanisms in the body, on a variety of time scales, in order to sustain sufficient blood flow and perfusion pressure to satisfy the metabolic requirements of various tissues and organs.

In the short term, the autonomic nervous system (ANS) can adjust CO and TPR in seconds while, in the longer term, hormones and the renal-body fluid system become more prevalent. Provided that arterial pressure is maintained at optimum levels, individual organs and tissues can also regulate their local blood flows to meet their individual needs. In pathophysiological conditions, blood pressure may be chronically elevated above normal levels (hypertension), giving rise to the hypertrophy or remodelling of affected organs, such as the heart, the brain and the kidneys, and ultimately leading to increased morbidity and mortality (Guyton and Hall, 2006).

The mechanisms that control blood pressure are only a few of countless control systems in the body, with some acting at cell level, others at a tissue or organ level, and others still operating at an overall-body level to regulate the relationships between organs. Most control systems in the body work in closed loop and more specifically, in a negative feedback control loop (Guyton and Hall, 2006). Negative feedback control loops operate in a manner to decrease the ‘error’ between a system output and a desired output or setpoint. An example of a negative feedback control loop, which will be examined in further detail in this thesis, is the arterial baroreflex. Positive feedback systems (such as the process of blood coagulation) and adaptive control systems (e.g. control of muscle contractions) are also present in the body and have important roles within it (Guyton and Hall, 2006).

The study of control systems is a well developed discipline within the engineering field and many principles developed to study control systems are highly valuable in the examination of biological and physiological systems. There is much to be gained from developing models of such physiological systems based on collected experimental data, in order to improve the understanding of their operation.

1.1 Motivation

In the second half of the last century, mathematical modelling of biological and physiological systems experienced a rise in popularity, and modelling and simulation of physiological systems is now a common feature of biomedical research (Gavaghan et al., 2006).

The development of mathematical models based on experimental data has multiple

benefits, as the models can:

- Help to improve the understanding of the system under study, by identifying the time scales and magnitudes of various interconnected mechanisms and their responses (Guyton et al., 1972b),
- Be used in clinical settings - mathematical models can be used in applications to enhance decision-making, diagnosis or predict survival outcomes (Weiss et al., 1978; Pedersen et al., 1996; Lewenstein, 2005; La Rovere et al., 2008),
- Be used as part of software-based teaching and assessment (Coleman and Randall, 1983; Kofranek et al., 2005), or in human body and pharmacological simulators (Ottesen et al., 2004), and
- Enhance experiment design - model development and experiment design can work in an iterative fashion to improve data collection and analysis (Guild et al., 2001).

Mathematical models have been a useful research tool for the last 60 years, but with the advances in computational capability, model development and simulation is now easier than ever, allowing ever increasing complexities of physiological systems to be modelled. In addition to the advent of cheap and powerful computing, another form of technology has also expanded immensely. The development of various modern implantable sensors (Tabrizchi and Pugsley, 2000; Bolger and Lowry, 2005; Tan et al., 2008), as well as the arrival of the telemetry technology (Budgett et al., 2007; Russell et al., 2012), have allowed the collection of high quality data in vivo, which can now be collected, recorded and logged with the least possible disturbance to the subjects and for much longer time scales than ever before (Van Vliet and Montani, 2008). With minimal technological restrictions, both on the computational implementation and experimental side, integrative physiological models can now be further enhanced to encompass very short and very long time scales.

1.2 Objectives

Since mathematical modelling can make a very beneficial contribution to the study of physiological systems, the main objective of this thesis is to develop a variety of models, of different types and complexities, to represent the operation of various blood pressure control systems and to derive useful indices from the model characteristics.

Mathematical models can be categorised in many different ways; for instance, they can be linear or nonlinear, static or dynamic, continuous- or discrete-time, they can be empirical (derived from experimental data) or physical (where the equations are based on a knowledge of the exact system characteristics), deterministic or stochastic (Ljung, 1999). The type of model chosen to represent a particular system will depend on the type of system under study, whether the inner workings of the system are known or unknown, and also what the purpose of the model is.

A variety of the aforementioned diverse model types are employed in this thesis, to demonstrate the application-based selection of the modelling techniques. The modelling and simulation routines developed and used in this thesis are relatively uncomplicated from an engineering perspective, but can be a tremendous addition, not only to the study of the systems considered here, but also to the wider category of physiological systems. The relative simplicity of the modelling concepts will hopefully be of benefit to researchers of non-mathematical backgrounds, thus making the subsequent use and further development of the models more feasible.

Developing a diverse range of models and applications is both a strength and a weakness of the thesis. There can be a perceived lack of focus on a specific application area; however, the wide range of modelling techniques, applied across a variety of systems of various time scales, provide a comprehensive ‘toolbox’ for modelling and simulation studies of physiological systems in general. A particular strength of the thesis is its investigation of both linear and non-linear systems. Mathematical modelling of linear systems is simpler due to the availability of a general theory of linear systems, and an assortment of tools for linear system modelling and analysis is available. Nonlinear system models, on the other hand, need to be customised to the particular application. Establishing whether there is a need to use a nonlinear model is an important step in the modelling exercise. Exploring systems within a regulatory loop, and where only

spontaneous signals without external excitation into the system are considered, would likely lead to a linear model, since there are only minor deviations from equilibrium, and the tendency of the regulatory loop is to bring the system back to equilibrium (e.g. analysis of spontaneous baroreflex data). In contrast, if an open-loop system is considered, where significant external excitation is applied, a nonlinear model would likely be necessary, as shown in Chapter 6, where a model for renal vasoaction is developed.

In summary, a number of mathematical models for blood pressure control systems are developed in this thesis with the purpose of:

- Extending our understanding of how systems work and at what time scales,
- Developing rigorous approaches to physiological estimation methods,
- Deriving indices of clinical importance, and
- Assigning physiological meaning to model responses and structure.

The specific topics addressed, where it was felt that a positive and constructive contribution could be made, are modelling of salt-induced hypertension, baroreflex sensitivity estimation and modelling of local vasoaction.

The final objective of this thesis was the implementation of the inspiring integrative model of the circulatory system, developed by Dr. Arthur Guyton (Guyton et al., 1972b), in a visual environment, in a hierarchical manner, with systems and subsystems represented at different resolution scales. A new visualisation approach is taken, with the aim of facilitating the use and further study of the model in a more user friendly manner. User-selected ‘concealing’ of some of the model complexity from the user would facilitate work on specific subsystems in the model without the need to consider the maximum detail in all other subsystems.

1.3 Contributions of this thesis

This thesis presents the development, implementation, simulation and use of a number of mathematical models, and claims the following key novel contributions:

- The development of three mathematical models, of varying complexity, that represent the relationship between high salt intake and the development of hypertension

in Dahl rats; The merits of increasing model complexity versus improvements in the model fit are evaluated and discussed,

- The design of a set of non-linear models of local vasoaction, under the conditions of renal denervation and artificial sympathetic nerve activity stimulation, is executed, and
- The development of a rigorous method for baroreflex sensitivity estimation, through the use of a black-box model of the baroreflex is carried out. The baroreflex sensitivity gain is estimated, based on the frequency response of the obtained model of the baroreflex.

The thesis also provides a review of existing baroreflex sensitivity estimation techniques, including time and frequency domain methods, methods that use external stimulation of the system, along with those that work on subjects at rest.

In addition, the thesis provides a detailed overview of integrative physiology modelling, including:

- The steps of model development and simulation,
- The available modelling and simulation environments, and
- Published integrative physiology models

A significant accomplishment of this work is also the implementation of the latest version of Guyton's integrative physiology model (Guyton et al., 1972b) in MATLAB's Simulink (The Mathworks Inc.) modelling and simulation environment. Even though the model itself is not novel, its implementation in a hierarchical form with system and subsystems at different resolution scales is considered beneficial for future use.

1.4 List of publications

1.4.1 Journal publications

- Mangourova, V., Ringwood, J., Guild, S.-J. and Malpas, S. Nonlinear modelling of renal vasoaction, *Biomedical Signal Processing and Control*, Vol.2, No.3, pp 258-266, July 2007

- McLoone, V., Ringwood, J. and Van Vliet, B. A multi-component model of the dynamics of salt-induced hypertension in Dahl-S rats, *BMC-Physiology*, Vol.9, No.20, Oct. 2009
- McLoone, V., Ringwood, J. and Van Vliet, B. A 5-component mathematical model for salt-induced hypertension in Dahl-S and Dahl-R rats, *Computer Methods and Programs in Biomedicine*, Vol.101, No.2, pp 220-229, Feb 2011
- McLoone, V., Ringwood, J. and Van Vliet, B. Graphical simulation environments for modelling and simulation of integrative physiology, *Computer Methods and Programs in Biomedicine*, Vol.102, No.3, pp 295-304, June 2011

1.4.2 Full-length peer-reviewed conference papers

- Mangourova, V. and Ringwood, J. Gray box modeling of arterial vasoaction, in *Proceedings of the Irish Signals and Systems Conference (ISSC)*, Dublin, June 2006, pp 315-320
- McLoone, V., Ringwood, J. and VanVliet, B. A 5-component model for salt-induced hypertension, in *Proceedings of the IFAC Symposium on Modelling and Control in Biomedical Systems (MCBMS09)*, Aalborg, August 2009, pp 175-180
- McLoone, V. and Ringwood, J. A system identification approach to baroreflex sensitivity estimation, in *Proceedings of the Irish Signals and Systems Conference (ISSC)*, NUI Maynooth, June 2012

1.5 Thesis outline

This thesis describes the development, optimisation, implementation and use of several diverse mathematical models of various blood pressure control systems.

In order to set the scene for the thesis, Chapter 2 begins by providing a general outline of blood pressure control at the short, medium and long term, including the local and systemic mechanisms for blood pressure regulation. Since the following chapters develop mathematical models of a number of specific blood pressure control systems, Chapter 2 also includes detailed overviews of the physiological phenomena pertaining to salt-related hypertension, local vasoaction and baroreflex sensitivity estimation.

Mathematical models of specific systems in the body can aid in the development of a deeper understanding of the systems under study; however, models can also be incorporated into large integrative models, which can be used as valuable teaching and research tools. Chapter 3 examines the history and current ‘state of the art’ in integrative physiology modelling and simulation. The steps and considerations involved in the process of developing an integrative model are first described. Subsequently, the simulation of an integrative model is considered and a comprehensive review of existing modelling and simulation environments and their advantages and drawbacks, in terms of integrative physiological modelling, is provided. A review of the published integrative physiology models is also included. Chapter 3 culminates with the implementation of the latest available version of Guyton’s integrative physiology model (Guyton et al., 1972b) in a hierarchical structure, within MATLAB’s Simulink modelling and simulation environment (The Mathworks Inc, Natick, MA, USA), which will potentially aid its visualisation and hopefully further its development and update.

Chapters 4, 5 and 6 then follow with the development, implementation and simulation of a number of novel mathematical models of specific long and short term blood pressure control systems. Chapter 4 considers the long term regulation of blood pressure and presents three models, of varying complexity, relating high salt intake to the development of hypertension in Dahl rats. Salt-induced hypertension data from four very different experimental protocols is employed for model development, training and validation, thus promoting a model structure that performs well under a wide variety of conditions.

Chapters 5 and 6 are devoted to the modelling of two short-term blood pressure control systems. Chapter 5 describes a novel, rigorous, model-based approach for baroreflex sensitivity estimation and clearly articulates the assumptions, constraints and advantages of the method, whilst comparing it to existing techniques.

Chapter 6, on the other hand, specifically addresses the peripheral arc of short-term blood pressure control, and presents a set of novel non-linear mathematical models for renal arterial vasoaction developed using artificial sympathetic nerve stimulation.

Finally, Chapter 7 provides the concluding remarks of this thesis and discusses future research opportunities.

Chapter 2

Background

The partial failure of one or more blood pressure control mechanisms, leading to poor regulation of blood pressure, possibly plays a major role in the development of hypertension; thus, a better understanding of the processes involved in blood pressure control is essential for the prediction and prevention of serious cardiovascular conditions. Since a number of interconnecting mechanisms, on a variety of time scales, are involved in blood pressure regulation, a real difficulty exists in developing a true understanding of the individual subsystems and the system as a whole. Mathematical modelling and simulation of the various processes involved can bring us a step closer to building a better understanding of the overall blood pressure control system.

Section 2.1 in this chapter provides a succinct overview of the various blood pressure control mechanisms, acting at the short (secs), medium (minutes to hours) and long (hours to days) term. In addition, this chapter also provides some background information needed for the development of a number of mathematical models, presented in the following chapters. Section 2.2 describes the arterial baroreflex in detail and provides a review of the existing baroreflex sensitivity estimation techniques, while Section 2.3 provides an overview of the vasoactive mechanisms, and especially those active in the renal vasculature. Section 2.4 gives a general overview of hypertension and, in particular, examines salt-induced hypertension in detail.

2.1 Blood pressure control mechanisms in the body

When blood pressure needs to be adjusted, as noted in Equation (1.1), cardiac output and/or peripheral resistance needs to be varied. Cardiac output can be modified by varying heart rate or stroke volume, while a change in resistance to blood flow can be achieved by varying blood vessel diameter. Overall, blood pressure control is achieved through a mixture of interrelated regulatory systems, including neural, hormonal and local mechanisms, on a variety of time scales. Briefly, in the seconds after an acute blood pressure change, the central nervous system control mechanisms are most effective. In the minutes to hours after a BP change hormonal mechanisms, stress-relaxation and capillary fluid shift mechanisms become more prominent, while hours to days later, the renal-body fluid mechanism is the primary blood pressure control system. A succinct overview of the main well known blood pressure control systems is presented next.

2.1.1 Short-term blood pressure control

The autonomic nervous system (ANS) plays a major role in short term blood pressure control. The sympathetic and parasympathetic branches of the ANS act in concert to regulate blood pressure levels, by modifying heart function and the vasculature, and are controlled by the vasomotor center in the brain. Sympathetic and parasympathetic innervation of the heart can effectively modify heart rate and cardiac output in the following manner:

- Stimulation of the sympathetic nerves increases heart rate and heart contractility, thus increasing cardiac output and blood pressure, while
- Parasympathetic (vagal) nerves can decrease heart rate and, to a much smaller extent, heart contractility, thus decreasing cardiac output and blood pressure.

Sympathetic innervation of the peripheral circulation, on the other hand, can vary peripheral resistance, and thus blood pressure, as follows:

- Sympathetic nerve activity (SNA) in small arteries and arterioles causes vasoconstriction and increased resistance to blood flow, therefore increasing blood pressure, while
- SNA-mediated constriction of some larger arteries, and especially of the veins,

which act like reservoirs, increases venous return to increase cardiac output.

There are numerous mechanisms for blood pressure regulation, mediated by the autonomic nervous system, including the central nervous system's ischemic response (Guyton, 1948), the Bainbridge reflex (Jones, 1962), chemoreceptor reflexes (De Burgh Daly and Scott, 1958), and the baroreflex (Cowley Jr. et al., 1973). The most important feature of the nervous system control of blood pressure is the speed of response, where significant changes in blood pressure levels can be achieved within seconds.

The baroreceptor reflex, or the baroreflex, is one of the most important short-term blood pressure control mechanisms, since it ensures minimum variability of blood pressure during normal daily life (Guyton and Hall, 2006). The baroreflex modifies heart rate and peripheral resistance when blood pressure deviates from normal levels. The health of the baroreflex can be assessed via the baroreflex gain, or sensitivity, which can be measured as the change in heart period induced by a change in systolic blood pressure (ms/mmHg), with higher baroreflex sensitivity (BRS) values being more desirable. BRS is used in clinical settings as a measure of health and disease and can be invaluable as a prognostic factor in patients with cardiovascular disease (La Rovere et al., 1988). Low values of baroreflex sensitivity are generally associated with poor prognosis and can be a predictor of mortality in heart failure and post-myocardial infarction patients (Frenneaux, 2004). Since one of the main objectives of this work is the development of a new approach to baroreflex estimation, Section 2.2 will provide a more detailed account of the physiology of the baroreflex and will also review existing methods for BRS estimation.

2.1.2 Medium-term blood pressure control

A number of blood pressure control mechanisms are activated on a medium-term time scale, such as minutes to hours, after a change from normal pressure levels (Guyton and Hall, 2006). These, mainly hormonal, mechanisms provide blood pressure regulation at times when the nervous system mechanisms become less effective but longer-term control systems have not yet been activated.

The renin-angiotensin system is an important hormonal contributor to blood pressure regulation, especially in the case of hypotension, or low blood pressure. When arterial pressure falls, the enzyme renin is secreted in the kidneys and stimulates the production

of angiotensin I (ANG I), whose main role is to form Angiotensin II (ANG II) with the aid of the angiotensin converting enzyme. ANG II is a powerful vasoconstrictor of the arterioles and thus elevates blood pressure by increasing peripheral resistance. The peak renin-angiotensin vasoconstrictor response is attained approximately twenty minutes after an acute blood pressure fall, since Angiotensin II production and activation is a multi-step process, including the secretion of renin, ANG I formation, conversion to Angiotensin II and receptor binding (Guyton and Hall, 2006).

In the case of hypotension, sympathetic activation of the adrenal gland causes the release of epinephrine and norepinephrine by the adrenal medulla. The release of these two hormones raises blood pressure by increasing heart rate and heart muscle contractility, while also mediating arterial and venous vasoconstriction.

A rise in blood pressure above normal levels, on the other hand, activates the stress-relaxation mechanism of the vasculature, which involves the gradual stretching of a vessel due to rising pressure, in order to reduce peripheral resistance. The stress-relaxation response can remain active from a few minutes to a number of hours, until a longer-term mechanism takes over.

The capillary fluid shift mechanism is another blood pressure control mechanism and works by adjusting the blood volume available in the vasculature. At low-blood pressure levels at the capillaries, extra fluid can be shifted into the circulatory system from surrounding tissues while, if blood pressure rises above normal, the fluid can be absorbed back into the tissue, thus reducing blood volume and pressure.

2.1.3 Long-term blood pressure control

Apart from its medium-term blood pressure effect, the renin-angiotensin system also contributes to long-term BP regulation, over a period of hours or days. ANG II decreases salt and water excretion by the kidneys, thus increasing blood volume and blood pressure over hours or days. In effect, the renin-angiotensin system is an important modulator of the most powerful blood pressure control mechanism in the human body, the renal-body fluid system, and the numerous paths by which ANG II affects it will be described in subsequent paragraphs.

The exact balance of fluid intake and excretion is paramount for homeostasis and main-

tenance of an appropriate BP level. The renal-body fluid system is the long-term control mechanism for fluid balance regulation, thereby also maintaining normal BP over days, months, or years. The mechanism, described initially by Guyton et al. (1972a), is a feedback loop, which detects changes in BP and modifies excretion of salt and water accordingly, thus altering extracellular fluid volume and bringing BP back to normal levels. As BP rises, the kidneys excrete higher amounts of urine, a process known as pressure diuresis, in order to reduce extracellular fluid volume and BP. Sodium excretion also increases concurrently, referred to as pressure natriuresis. Conversely, in the hypotensive case, renal tubular reabsorption of salt and water increases in order to raise extracellular fluid volume and increase BP.

The renin-angiotensin system is the main mediator of the renal-body fluid system. As described in Section 2.1.2, when BP falls, renin is released, instigating the formation of ANG I and then ANG II. ANG II causes the kidneys to retain salt and water in a number of ways:

- It causes selective vasoconstriction in the renal arterioles, thus diminishing blood flow through the kidneys and allowing less fluid to be filtered,
- ANG II-mediated vasoconstriction, leading to low blood flow levels through the peritubular capillaries, increases sodium and water reabsorption by the renal tubules, and
- ANG II has a direct effect on the tubular cells to increase salt and water reabsorption.

In addition to the direct effects of ANG II in increasing fluid retention under low pressure conditions, angiotensin II also triggers the release of aldosterone from the adrenal glands, with aldosterone causing further salt and water retention (Reinhardt et al., 1996).

Other substances with a role in BP control such as vasopressin, atrial natriuretic factor and endothelin have also been identified, with Cowley Jr. (1992) providing a detailed review of most known factors.

2.2 The neural baroreflex

The arterial baroreflex is the most important short-term blood pressure control mechanism. The baroreflex is a negative feedback control system which detects changes in blood pressure and, through adjusting heart rate and peripheral resistance, attempts to minimise blood pressure fluctuations. The arterial baroreceptors are mechanical stretch receptors, located in a number of sites, most abundantly in the aortic arch and the carotid sinuses, and are central to the baroreflex. When the blood vessels stretch due to pressure, the baroreceptors are depolarised, resulting in action potentials being sent towards the central nervous system through afferent nerves. At higher blood pressure levels, the stretch applied on blood vessels is also higher, leading to higher firing frequencies of the baroreceptors. The autonomic nervous system, then, through efferent nerves, varies cardiac output and vascular resistance, thus controlling blood pressure. A diagram of the baroreflex loop is shown in Figure 2.1.

As shown in Figure 2.1, the baroreceptors located in the aortic arch relate information via the vagus nerves about the blood pressure being supplied to the systemic circulation, while the carotid sinus baroreceptors send information via the glossopharyngeal nerves about blood pressure supplied to the brain. Both sets of afferent nerves release neurotransmitters in the solitary tract nucleus in the brainstem.

An increase in blood pressure, resulting in higher than normal baroreceptor firing rates, causes an inhibition of the sympathetic branch of the autonomic nervous system and activation of the parasympathetic limb through efferent (vagal) nerves. The resulting effects are a decrease in heart rate and heart contractility, vasodilation of the peripheral veins and arterioles and decreased venous return, all contributing to a lower cardiac output and peripheral resistance. Conversely, low blood pressure leads to the stimulation of the sympathetic nervous system and downregulation of the parasympathetic branch, causing vasoconstriction in the peripheral circulation, and increases in heart rate, cardiac contractility and venous return.

According to various studies, there is a delay of between 200 and 600ms between the baroreceptor signalling and the resulting effect on the sinus node in the heart, mediated by the parasympathetic nerves, while the effect on the peripheral vasculature due to sympathetic vasomotor activity, can take much longer (up to 2-3s.) (Eckberg and

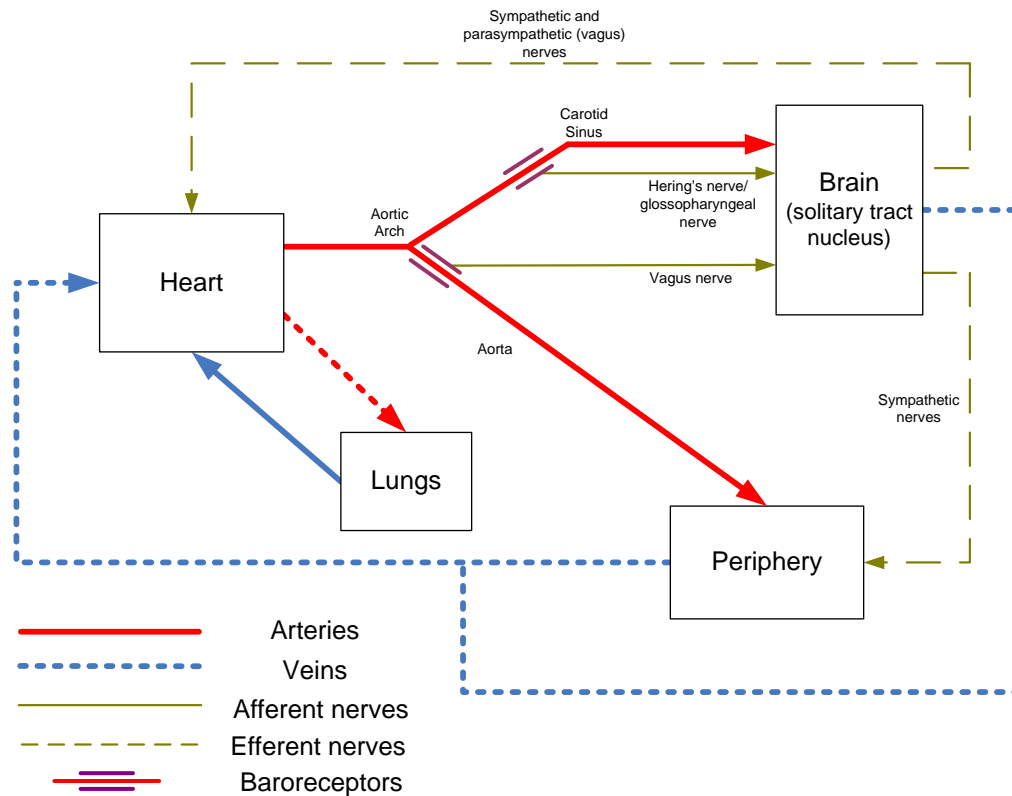


Figure 2.1: The baroreflex

Sleight, 1992; Pagani et al., 1988).

Low-pressure receptors found in the pulmonary circulation, as well as chemoreceptors found at sites similar to the baroreceptors, act in conjunction with arterial baroreceptors to counteract changes in blood pressure.

2.2.1 Baroreflex sensitivity

Baroreflex sensitivity is, in effect, a frequency-dependent dynamic gain, and measures how much the RR interval (the interval between one R wave and the next on a cardiogram, also the inverse of the heart rate) changes due to variations in blood pressure, and is measured in ms/mmHg (Eckberg and Sleight, 1992; Westerhof et al., 2004; Tiinanen et al., 2008). Most research groups use systolic arterial pressure (SAP) and RR interval for BRS estimation; however, some groups have employed other measures, such as mean arterial pressure and heart rate. A single standard method for BRS estimation does not exist. There is a large variety of BRS estimation techniques, including both

time and frequency domain methods, leading to very differing estimates of BRS. The unavailability of a single BRS ‘gold-standard’ estimation technique causes difficulty in defining what gain values can be considered normal. If BRS is to be used in clinical settings as a determinant of health and disease, it is vital that an exact definition is agreed upon and that ranges for normal, reduced and failed baroreflex are defined.

Figure 2.2 shows a diagram representing the baroreflex as a feedback control loop. On the top side of the loop the RR interval is regulated via the central nervous system, while on the bottom side of the loop SAP is determined through the influence of the peripheral vasculature and the heart. There are two external noise sources, affecting SAP and RR interval, and those include influences such as respiration, central modulation of the sinus node or vasomotor activity (Baselli et al., 1988). The gain of the central nervous system (CNS) block represents the baroreflex sensitivity.

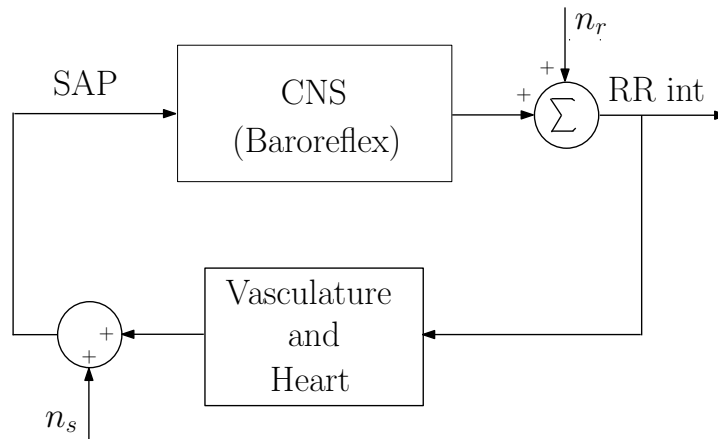


Figure 2.2: The baroreflex loop with two external noise sources n_r and n_s

2.2.2 Purpose of the baroreflex sensitivity index

Baroreflex impairment has been associated with a number of conditions such as hypertension, myocardial infarction (MI) and heart failure. A measure of the baroreflex gain provides information on the neural regulation and autonomic control of the cardiovascular system.

In some cases of cardiovascular disease, a reduction in responsiveness of the sinus node to vagal neural modulation can be observed, in addition to an increase of sympathetic

cardiac and peripheral stimulation. This effect is particularly common in heart failure patients (Osterziel et al., 1995). Impaired baroreflex may contribute to end organ damage also (Lanfranchi and Somers, 2002), through sustained high levels of sympathetic activity, while diminished gain has also been related to higher mortality in heart failure patients (La Rovere et al., 2008; Osterziel et al., 1995).

The most important use of BRS in a clinical setting, however, is its use as a prognostic factor in cardiology, especially as a predictor of cardiac mortality in patients following MI. A number of studies address the issue of BRS as a determinant of future adverse outcome in patients following MI (Laude et al., 2004; La Rovere et al., 1988; Van de Vooren et al., 2007; La Rovere et al., 2008).

In addition, the relationship between baroreflex sensitivity and hypertension has come under investigation (Parmer et al., 1992; Thrasher, 2005) and is gaining importance, and BRS has been found to be useful as an overall prognosis risk marker in hypertensive patients (Ormezzano et al., 2008). The possibility of lowering the long-term blood pressure of chronic hypertensive patients through electric stimulation of the carotid sinus is also under investigation (Heusser et al., 2010).

2.2.3 Hypertension and the baroreflex

During prolonged blood pressure increases, the baroreceptors reset to new pressure levels, in order to continue to reduce blood pressure variability (Eckberg and Sleight, 1992; Guyton and Hall, 2006). In hypertensive subjects, where the baroreceptors are centered around the new, increased, baseline pressure, reductions in pressure down to normotensive levels actually provokes a baroreflex response to increase BP. Because of the resetting of the baroreceptors, the baroreflex has been considered mainly as a short-term blood pressure control system, and its role in the development of hypertension has not been confirmed. Subjects with hypertension, however, have been shown to have an impaired baroreflex (Parmer et al., 1992) and the reduction in baroreflex gain has been found to be proportional to the degree of blood pressure increase (Eckberg and Sleight, 1992). Parmer et al. (1992) have also shown that normotensive subjects with a family history of hypertension have lower BRS values compared to their normotensive counterparts without a family history of diagnosed hypertension. Since an impaired baroreflex can precede the development of hypertension, it is impossible to disregard the

possibility that the baroreflex may be involved with the pathogenesis of hypertension. BRS has also been found to decrease with increasing age, especially for males over 60 years (Monahan et al., 2001; Kardos et al., 2001), possibly due to stiffness of the arteries in the baroreceptor locations, which can lead to reduced baroreceptor firing rates and thus reduced inhibition of the sympathetic nervous system. In addition, increased levels of both renal and muscle SNA have been found in hypertensive subjects, both young and old, but it has not been established whether this is due to the baroreflex (Grassi et al., 1998; Thrasher, 2005).

2.2.4 Current methods for baroreflex sensitivity estimation

There are a variety of mathematical methods used for baroreflex sensitivity estimation, including both time domain and frequency domain techniques. Some methods employ external excitation (injections of vasoactive drugs, the Valsalva manoeuvre, etc. (Eckberg and Sleight, 1992)) in their experimental protocols, while others use recordings of spontaneous BP and RR interval (Robbe et al., 1987; Pinna et al., 1996). A form of data pre-processing or selection (such as sequence selection) is also performed as part of some estimation techniques (Davies et al., 1999; Gouveia et al., 2005; Choi et al., 2006). In a number of cases, thresholds, such as the minimum variation in BP and RR interval, and the minimum correlation (time domain) or coherence (frequency domain) between the BP and RR signals, are also sometimes employed (Davies et al., 1999; Laude et al., 2004; Choi et al., 2006).()

Time domain methods

A variety of time domain BRS estimation methods have been developed, where some form of regression model is usually fit to the RR-SAP data (in rare cases HR and MAP are used instead of RR and SAP respectively), and include methods with or without external excitation in the experimental protocols.

Sequence methods are techniques for baroreflex sensitivity estimation, where a pre-processing step is applied to the beat-to-beat data before fitting a regression line between the RR and SAP signals. The preprocessing step includes the selection of sequences of concurrently increasing or decreasing contiguous SAP and RR interval values.

In general, for each selected sequence, the slope of the regression line is calculated and the baroreflex gain estimate is obtained by averaging the slopes for all sequences. The sequence methods are very popular due to their simplicity and have been applied in a large number of studies (Choi et al., 2006; Davies et al., 1999; Kardos et al., 2001; Gouveia et al., 2005).

Minimum thresholds are usually applied to the pre-processing data selection process to ensure that sequences are not just random occurrences but are, in fact, the baroreflex in action. Each sequence is usually required to contain a minimum of three or four data points. Sometimes, a requirement is imposed that a SAP value changes by a minimum of up to 1mmHg, compared to the previous beat, in order to be included in a sequence (Davies et al., 1999; Kardos et al., 2001). A change of up to 5ms in the RR interval between two beats can also be required (Davies et al., 1999). Once the slope of the regression line for a particular sequence has been calculated, a minimum coefficient of correlation between SAP and RR from 0.7 up to 0.85 can also be imposed (Choi et al., 2006; Davies et al., 1999), in order to consider the slope of that sequence for BRS calculation. Some research groups also require a minimum of between 2 and 5 valid sequences for each subject in order to obtain a BRS estimate for that subject (Laude et al., 2004). The issue of delay or ‘lag’ between a change in SAP and the associated change in RR interval also needs to be considered, and different lag values have been employed previously (Choi et al., 2006).

Low correlation, too few points in a sequence, or an insufficient number of sequences can all be a major problem associated with the traditional sequence techniques for BRS estimation, especially in patients with cardiac disease or autonomic dysfunction (Oka et al., 2003).

Gouveia et al. (2005) have suggested a variation to the traditional sequence methods described above where, instead of averaging the slopes obtained from individual sequences, the baroreflex gain is calculated by fitting a regression line through all RR interval and SAP pairs, from all sets of baroreflex sequences. The work was further developed by Gouveia et al. (2006) by altering the data pre-processing step and instead of selecting sequences of concurrently increasing SAP-RR values, segments of data were selected based on ‘SAP ramps’ only. A signal segment was selected based on the SAP value changing by a minimum of 1mmHg from one beat to the next (a ‘SAP ramp’),

without a necessary change in the RR interval. The ‘SAP ramp’ approach to selecting sequences allows the inclusion of a larger number of beats in the overall regression line calculation, as there is no requirement for a concurrent change in RR interval.

Gouveia et al. (2009) have also introduced an ‘events-based’ sequence method where instead of identifying sequences of concurrently increasing or decreasing SAP and RR interval values, segments of data were selected on the basis of high correlation (0.8) between SAP and RR interval. The minimum segment length of each event was 3 beats, while the maximum achievable length for each individual segment was determined on the basis of correlation between SAP and RR interval only. In effect, the difference between the traditional sequence methods and the events-based technique is the omission of the minimum thresholds for change in SAP and RR interval from one beat to the next. The benefits of the events-based method is the inclusion of a larger number of beats in the overall regression line calculation (approximately 50% of all beats are included in events), compared to the traditional sequence method (where only about 25% of all beats are included in sequences). Estimates by the events-based and traditional sequence methods are highly correlated but the events-based technique has a higher success rate in estimating BRS values in subjects with a diminished baroreflex response.

An alternative means of obtaining a larger number and/or longer sequences, as well as a higher correlation value, especially in cases of patients with autonomic dysfunction, is to use some excitation during the experiment, such as deep respiration (Oka et al., 2003). The effect of deep respiration is to induce changes in venous return and increase BP variability; however, other unknown mechanisms, apart from the baroreflex, could possibly be activated as well. An experiment with controlled breathing, where subjects are required to breathe at a set frequency (Davies et al., 1999), which provides an alternative method of putting excitation into the system, produces a similar result as deep respiration and also leads to a higher likelihood of obtaining a BRS estimate, compared to standard sequence methods.

Other BRS estimation techniques use an external excitation to perturb the baroreflex loop and then fit a linear regression line to the whole SAP and RR interval data, rather than using sequences or events. The excitation can be invasive, as in the Oxford method (Palmero et al., 1981; Parmer et al., 1992), or non-invasive as with the Valsalva

manoeuvre (Palmero et al., 1981; Oka et al., 2003) and the neck chamber (Ludbrook et al., 1977) techniques, described below:

- The Oxford method for BRS estimation is an invasive technique, comprising a bolus injection of a vasoactive drug, which causes either an increase or decrease of blood pressure. Successive RR intervals are plotted against the corresponding SAP values with a lag, or delay, of one beat. The slope of the regression line is considered as an index of baroreflex sensitivity (Eckberg and Sleight, 1992). A correlation coefficient for the data is also calculated to determine the certainty of the BRS estimate. The most common vasoactive drugs used with the Oxford method are phenylephrine, adrenaline, angiotensin II, methoxamine or noradrenaline. Some issues associated with the Oxford method need to be noted (Eckberg and Sleight, 1992):
 - Angiotensin II can cause a large variety of additional effects to rising BP, especially tachycardia instead of bradycardia, i.e. when BP increases, instead of seeing an associated lengthening of the RR interval, an increase in heart rate and a shortening of the RR interval is found.
 - Phenylephrine, on the other hand, can cause a reduction instead of an increase in carotid sinus diameter at times when BP is rising. Since baroreceptors work by detecting a larger stretch of the blood vessel when blood pressure increases, a diameter decrease would cause the baroreceptors to send messages of decreasing pressure instead.
 - Cardiopulmonary afferent activity may be altered by vasoactive drugs, due to the activation of low-pressure receptors, which can send either conflicting messages to the brain, or can enforce the baroreflex, thus leading to an overestimation of the baroreflex gain.
 - Sinus node function may also be affected by vasoactive drugs, thus RR interval may change independently of the baroreflex.
 - Hysteresis of the baroreceptor curve can be noticed, i.e., when depressor drugs are used to lower blood pressure, the BRS estimates are lower than those when pressure is on the rise due to vasoconstrictory drugs, and
 - Patients who already have cardiovascular disease may not be suited to further

drug infusion, thus making the technique unusable in certain clinical settings.

Despite some of its shortfalls, the Oxford method is still the main method against which results from other BRS estimation techniques are usually compared (Parmer et al., 1992; Davies et al., 1999; Pagani et al., 1988; Maestri et al., 1998).

- The neck chamber excitation for BRS estimation involves application of suction or pressure (i.e. negative or positive pressure changes) to the carotid artery via a neck chamber. The applied pressure provides a reduction or increase of carotid artery diameter, thus activating the carotid baroreceptors (Eckberg and Sleight, 1992). Different pressures are applied and the resulting RR intervals are recorded. Similar to the sequence and Oxford methods, a regression line is computed for the SAP-RR interval changes and the resulting slope is taken as the BRS estimate. An advantage over the Oxford method is the non-pharmacological nature of the technique, as additional blood pressure control mechanisms are not activated. A major pitfall, however, is the differential stimulation of the carotid and aortic baroreceptors, where baroreceptors at the two locations can receive opposing information on pressure changes.
- The Valsalva manoeuvre comprises the exhaling of air against a closed glottis, which has an effect to alter intrathoracic pressure. Subjects initially rest in the supine position for 10 minutes. They are then required to blow into a mouth-piece at 40mmHg for 15s, in the sitting position. The SAP and RR intervals are recorded and the slope of the linear regression between the two is estimated at a particular point in the experiment (Oka et al., 2003). Baroreflex gain estimates obtained using this method correlate well with the Oxford technique. Similar to the neck suction method, the Valsalva manoeuvre has the advantage that it does not incorporate drug infusions; however, the manoeuvre may be difficult to perform on some patients.

Another BRS estimation method, which uses a linear regression model, but also uses spontaneous SAP and RR interval data, is a statistical Z-coefficient method for BRS estimation, proposed by Ducher et al. (1995), where a coefficient of statistical dependence between two events is calculated. The two probabilistic events used for BRS estimation are the SAP and RR interval values. Pairs of SAP and RR interval values with high Z-coefficient are selected, as a pre-processing step. The linear regression for those values

is calculated and the slope is considered to be the BRS estimate (Cerutti et al., 1999). The method needs long recording periods to reliably estimate the required probability functions. An additional requirement for high correlation between RR interval and SAP can also be imposed (Laude et al., 2004).

Apart from a simple linear regression gain, a number of more complex time series models for BRS estimation have also been described in the literature. Porta et al. (2000) have developed three models of different complexity, with the simplest of their models shown in Equation (2.1):

$$RR_i = \sum_{k=0}^Q b_{1k} \cdot SAP_{i-k} + u_i \quad (2.1)$$

where RR interval is a function of SAP only and u_i is an external uncorrelated disturbance.

The second model developed by Porta et al. (2000), shown in Equation (2.2), incorporates a coloured noise disturbance w_i , defined in Equation (2.3).

$$RR_i = \sum_{k=0}^Q b_{1k} \cdot SAP_{i-k} + w_i \quad (2.2)$$

$$w_i = \sum_{k=0}^Q h_k \cdot w_{i-k} + u_i \quad (2.3)$$

In the most complex of the models by Porta et al. (2000), Equation (2.2) is modified by introducing respiration (*RESP*) as an additional measured disturbance.

$$RR_i = \sum_{k=0}^Q b_{1k} \cdot SAP_{i-k} + \sum_{k=0}^P b_{2k} \cdot RESP_{i-k} + w_i \quad (2.4)$$

Faes et al. (1999) and Nollo et al. (2001) (Equation (2.5)) include an autoregressive term on the *RR* measurement to estimate BRS in patients following MI.

$$RR_i = \sum_{k=1}^R a_k \cdot RR_{i-k} + \sum_{k=0}^Q b_{1k} \cdot SAP_{i-k} + w_i \quad (2.5)$$

A similar model is used by De Cecco and Angrilli (1998), while Patton et al. (1996) combine the models in Equation (2.4) and (2.5) by incorporating SAP, RR interval and

respiration dynamics. The model by Patton et al. (1996) is defined in Equation (2.6) as follows:

$$RR_i = \sum_{k=1}^R a_k \cdot RR_{i-k} + \sum_{k=n_{ds}}^Q b_{1k} \cdot SAP_{i-k} + \sum_{k=n_{dr}}^P b_{2k} \cdot RESP_{i-k} + w_i \quad (2.6)$$

and a specific breathing protocol is used to stimulate *RESP* and, consequently, *RR*. In the model in Equation (2.6), n_{dr} and n_{ds} are the delays associated with respiration and systolic arterial pressure respectively.

In general, the modelling problem is to determine the dimension P , Q and R of the regressors a_k , b_{1k} and b_{2k} and then to determine the parameter values for $a_1 \dots a_P$, $b_{10} \dots b_{1Q}$ and $b_{20} \dots b_{2R}$. Note that, while a consistent notation has been adopted here to associate an input variable to a model with a parameter set (e.g. *RESP* is associated with the parameter set b_{2k}), the values determined for the orders P , Q and R , and the parameter sets a_k , b_{1k} and b_{2k} , will not necessarily be the same across different models.

A nonlinear model, based on a Volterra-Wiener framework, was proposed by Wu et al. (2008), who applied it to spontaneous SAP-RR data from normotensive and hypertensive subjects. It is, however, questionable whether the added complexity of a non-linearity is justifiable in cases where the subjects are at rest (Patton et al., 1996). Under such conditions, small signal variation requirements for local linearisation are usually met.

Baselli et al. (1988, 1994) have proposed a *closed-loop* model to represent the relationship between *RR*, *SAP* and *RESP*. The model is identified using a closed-loop approach, based on the joint input-output approach (see Section 5.3.3); however, they use ‘per-beat’ data, making spectral estimates unreliable (Ljung, 1999).

In another approach, which respects the closed-loop nature of the baroreflex, bivariate autoregressive modelling has been employed to calculate the transfer functions between the signals on the feedforward and feedback side of the loop simultaneously (Hytti et al., 2006). Nollo et al. (2001), Faes et al. (1999) and Pitzalis et al. (1998) take this approach to evaluate model components in the time domain and subsequently calculate the frequency response of these components.

Frequency domain methods

Frequency domain or spectral methods for BRS estimation rely on an assumed linear relationship between SAP and RR interval, i.e. only the frequency components found in the input are propagated to the output, albeit with different amplitude and/or phase. In general, two main frequency bands are considered for baroreflex operation (Pagani et al., 1986; Davies et al., 1999; Glos et al., 2007):

- A low-frequency (LF) band of 0.04-0.15Hz, associated with both sympathetic and parasympathetic activity, and
- A high-frequency (HF) band of 0.15-0.4Hz due to mostly vagal parasympathetic modulation, related to respiration (Malliani et al., 1994)

Robbe et al. (1987) defines a further very low frequency (VLF) band, between 0.02Hz and 0.06Hz, associated with vasomotor activities, due to temperature and task adaptation.

A transfer function method was first proposed by Robbe et al. (1987) and comprises the calculation of the gain or modulus of the transfer function between SAP and RR interval in the VLF, LF and HF bands, using spectral techniques. The Fourier transfer function $H_{RS}(f)$ is defined as:

$$H_{RS}(f) = \frac{G_{RS}(f)}{G_S(f)} \quad (2.7)$$

where $G_{RS}(f)$ is the cross-spectral density function between SAP and RR and $G_S(f)$ is the spectral density of SAP.

A coherence function in the frequency domain represents the amount of linear coupling between two signals and is often calculated in conjunction with the modulus of the transfer function. The coherence, $C_{RS}(f)$ is defined as follows:

$$C_{RS}(f) = \frac{|G_{RS}(f)|^2}{G_R(f)G_S(f)} \quad (2.8)$$

where $|G_{RS}(f)|$ is the magnitude of $G_{RS}(f)$ and $G_R(f)$ and $G_S(f)$ are the spectral densities of RR and SAP respectively.

The coherence function $C_{RS}(f)$ can be used as a measure of the significance of the coupling between *SAP* and *RR* at a frequency f . Only the Fourier transfer function (gain) points with corresponding ‘high’ coherence values (arbitrarily defined as $C_{RS}(f) > 0.5$ by Robbe et al. (1987)), are considered for the final BRS estimate. The coherence values were found to be very low in the VLF band, and highest in the LF band.

The frequency-dependent gain quantity, $\alpha(f)$, defined in Equation (2.9), has also been used as an estimate of BRS (Pagani et al., 1988).

$$\alpha(f) = \sqrt{\frac{G_R(f)}{G_S(f)}} \quad (2.9)$$

The α -index is also evaluated over the LF and HF bands and, similarly to the Fourier transfer function method, a high level of coherence is also required.

In general, spectral densities are calculated using the discrete Fourier transform (DFT). Finding the frequency response of an autoregressive or input/output time domain model has also been used as a base for the determination of spectral densities (Task Force of the European Society of Cardiology and the North American Society of Pacing and Electrophysiology, 1996); however, such a calculation route strictly places associated BRS methods within the time domain class of BRS estimation techniques.

A large number of research groups employ spectral methods for BRS estimation. Choi et al. (2006) used both the transfer function method and the α -index for BRS estimation, to study the effect of posture in the EuroBaVar data set. The DFT was employed for spectral estimation, and a minimum coherence threshold of 0.5 was required. Both the transfer function and α -index methods performed well in distinguishing the standing from the supine position.

Davies et al. (1999) employed an α -index method, using AR modelling for spectral estimation, in a study to determine the reproducibility of BRS estimates in control subjects and in patients with chronic heart failure. A coherence threshold of 0.5 was used and controlled breathing was also employed to increase BP variability in chronic heart failure patients. The α -index was poorly reproducible in the HF band for all subjects, while the LF results were reproducible for the controls, but not for the patients. In a study by Glos et al. (2007), the α -index is used to examine the effects of positive pressure ventilation on BRS. The coherence threshold in this study was 0.56 and the

DFT method was used for spectral estimation. Apart from calculating the α -index using the standard procedure, they also consider the phase shift between SAP and RR interval. Maestri et al. (1998) performed a study to compare different methods for estimating BRS, including the transfer function method in Robbe et al. (1987) and the α -index method in Pagani et al. (1988).

Pitzalis et al. (1998) estimated BRS in a method similar to that in Pagani et al. (1988), while controlling breathing at 6, 10 or 16 breaths per minute. The phase lag between RR and SAP was estimated to vary between 0.25s and 1.2s, with higher respiration rates leading to lower delays. This result is similar to Eckberg's conduction time of the baroreceptor-cardiac reflex arc (Eckberg and Sleight, 1992) and is a bit lower than the estimation in Pagani et al. (1988).

Rüdiger et al. (1999) propose an alternative approach to the autoregressive and DFT methods for spectra estimation. The trigonometric regressive (TRS) approach provides estimates of the power spectra and the usual transfer function estimates are calculated. Their results are well correlated with other spectral techniques.

Using the coherence function to ensure reliability of the spectral methods for BRS estimation has come under some criticism. As in the sequences technique, in pathological subjects' low coherence is unavoidable, since baroreflex is impaired or SAP variability is low (Pinna and Maestri, 2002); therefore, subjects who may need the measurement the most cannot be assessed using these spectral methods. Pinna and Maestri (2002), hence, suggest that, in clinical settings, it is best to impose no thresholds but to simply use the average gain over the whole frequency band as the BRS measurement. This leads to a bias in the BRS estimate but the results are considered adequate enough for use in clinical settings.

Finally, a novel, systematic and rigorous system-identification approach to BRS estimation will be presented in Chapter 5 of this thesis. The new approach falls into the time domain method category, since a time-series model of the $SAP \rightarrow RR$ is identified; however, the BRS estimate is calculated over both the LF and HF bands from the model spectral response.

2.3 Blood flow regulation

Following on from Sections 2.1 and 2.2, where the chief short-, medium- and long-term blood pressure control mechanisms were briefly discussed, and the baroreflex was considered in more detail, this section provides a short overview of the control of blood flow at local level. Short- and medium-term blood pressure control, as described in Section 2.1, is closely related to the regulation and distribution of blood flow to various organs and tissues in the body to satisfy their local metabolic needs. Important metabolic needs include oxygen and nutrient delivery, carbon dioxide removal and the transport of hormones. The levels of blood flow through the small arteries and arterioles is regulated via varying peripheral resistance by numerous vasoactive mechanisms, causing vasodilation and vasoconstriction in the smooth muscle surrounding the blood vessels. In order to maintain a normal workload on the heart, the minimum necessary blood flow is delivered to each site in order to balance out each tissue's perfusion and metabolism (Guyton and Hall, 2006); therefore, a combination of vasoactive factors maintain local blood flow within narrow limits.

This section outlines the main blood flow effectors, with the purpose of providing a background for the development of a mathematical model for the renal blood flow (RBF) response to SNA in the renal vasculature.

According to the site of action, the various blood flow effectors can be classified into central and local. Central effectors act on a systemic level to ensure that different parts of the body obtain the necessary amount of cardiac output, whereas local effectors are activated in specific tissues to serve their own metabolic needs (Richardson et al., 1998). Local blood flow regulators can counteract the effects of central factors to achieve a balance that satisfies local needs.

Neurohumoural blood flow effectors, which include the sympathetic and parasympathetic nervous system and circulating hormones, can be considered of central origin and are described first, followed by local blood flow effectors, including metabolic activity, myogenic responses and paracrine factors.

2.3.1 Sympathetic nerve activity

The autonomic nervous system, and in specific sympathetic nerve activity, is the principal central blood flow effector, especially on a short-term basis. SNA causes the release of the neurotransmitter norepinephrine (or noradrenaline) from nerve endings, causing the vascular smooth muscle surrounding small arteries and arterioles to constrict (DiBona and Kopp, 1997). The vasoconstrictive action of norepinephrine is mediated by binding to α -adrenergic receptors on the vascular smooth muscle walls. Sympathetic innervation is well distributed throughout the vasculature, allowing rapid control of peripheral resistance with a time delay between stimulation and response of around 0.6s in the renal vasculature in rabbits (Guild et al., 2001).

2.3.2 Hormones

Various hormones are released into the circulatory system and display vasoactive properties when bound to specific receptors, giving them the ability to cause vasoconstriction or vasodilation. Effects of the same hormone on different vascular beds can vary, depending on the type and concentration of receptors present in the area.

As previously noted, angiotensin plays a major role in blood pressure and blood flow control with ANG II being the most potent vasoconstrictive hormone (Guyton and Hall, 2006), though it can take up to several minutes to become fully active, since it needs to circulate in the blood stream (Guyton, 1987). Sigmon and Beierwaltes (1993) have demonstrated the vasoconstrictor characteristics of ANG II in the kidney, intestine and lungs. The vasoactive properties of ANG II have been shown to be caused by binding to AT_1 receptors, as vasoconstriction can be reversed with AT_1 receptor blockers, such as losartan (Sigmon and Beierwaltes, 1993) and valsartan (Madrid et al., 1997).

Epinephrine is released by the adrenal medulla in the kidney during SNA stimulation, stress, or in other physiological conditions when blood pressure needs to be increased. In general, epinephrine has been shown to be a potent vasoconstrictor by binding to α -adrenergic receptors (Muravchick and Bergofsky, 1976). Epinephrine can, however, elicit skeletal vasodilation (Diana et al., 1990), which was found to be due to the action of β_2 -adrenergic receptors. This differential action of epinephrine in different organs may be explained by the necessity to reduce blood flow to one organ in order to increase

it in another, e.g. during ‘fight-or-flight’ skeletal muscles have higher oxygen demand than the skin, therefore more blood would be supplied to the former.

Vasopressin (or antidiuretic hormone) is a vasoconstrictive substance, acting on V_1 receptors to increase peripheral resistance. The normal concentration levels of vasopressin in the vasculature are usually below active levels to achieve constriction; however, its concentration increases during conditions such as hemorrhage (Cowley Jr. et al., 1980) or dehydration (Aisenbrey et al., 1981), when blood flow to the periphery may need to be restricted to increase blood pressure.

Atrial natriuretic factor (ANF), on the other hand, is a vasodilatory hormone, secreted mainly in the heart, but plays a major role in reducing renal vasoconstriction and in the inhibition of renin secretion (Maack, 1996).

2.3.3 Myogenic responses

The myogenic response of small blood vessels represents a property of the smooth muscle to constrict, thus reducing blood flow, as the result of a sudden increase in pressure. Conversely, a loss of pressure would cause the vascular smooth muscle to relax and dilate in order to increase blood flow through the vessel (Guyton and Hall, 2006). The myogenic response, found to be activated by wall tension, is most powerful in medium sized blood vessels (small arteries and arterioles), it varies in strength from one vascular bed to another (Schubert and Mulvany, 1999), and has been found to be active in the renal vasculature among others (Guyton and Hall, 2006).

2.3.4 Tissue metabolites

Tissue metabolites are small molecules of substances that can have vasoactive properties under certain physiological conditions. An increase in nutrient or oxygen demands by a tissue, for example, leads to a marked arterial vasodilation. Some common tissue metabolites are adenosine, carbon dioxide (CO_2), potassium and hydrogen ions and a more detailed account of their function follows.

- Adenosine is a substance with a differential vasoaction. A bolus administration of adenosine has been shown to cause vasoconstriction in the renal vasculature (Marraccini et al., 1996; Hansen and Schnermann, 2003) by activating A_1 adenosine

receptors. A vasodilatory effect, however, has been reported after a continuous infusion of adenosine and resulting from the activation of A₂ adenosine receptors in the kidney (Hansen and Schnermann, 2003) and in skeletal muscle (Guyton and Hall, 2006).

- CO₂ levels increase during high oxidative metabolism, for instance, during exercise in the skeletal muscle circulation, and CO₂ has been found to cause arterial vasodilation. The vasodilatory action of CO₂ has also been found in other vascular beds, such as in the coronary arteries, the brain and the intestine, with the exception of pulmonary circulation where CO₂ has been found to cause vasoconstriction (Piuze, 1960).
- Carbon monoxide has been found to cause vasodilation in numerous vascular beds, due to hypoxia, shear stress and stretch, as well as in pathophysiological conditions, such as septicemia (Thorup et al., 1999). O'Donaghay and Walker (2000) have demonstrated that carbon monoxide causes dose dependant vasodilation in the renal vasculature, while Naik and Walker (2001) and Naik et al. (2002) have demonstrated that carbon monoxide production results in mesenteric artery vasodilation.
- Both hydrogen and potassium ions have been found to have vasoactive properties (Guyton and Hall, 2006). Low concentrations of hydrogen ion cause arterial vasoconstriction, while high concentration result in vasodilation (Haddy and Scott, 1968). Potassium ions cause vasodilation in the coronary, skeletal and renal vasculature, as well as the intestine and stomach (Haddy and Scott, 1968).

2.3.5 Paracrine factors

Paracrine effectors on blood flow relate to the release of locally acting substances such as nitric oxide (NO), endothelin-1 and arachidonic acid. A short overview of some of these mechanisms of local blood flow regulation is included here.

- NO is a potent vasodilator and is an endothelium derived relaxing factor. NO achieves vasodilation within seconds (Wunsch et al., 2000), similar to sympathetic stimulation, so *it can be regarded as an important substance opposing SNA-stimulated vasoconstriction* in peripheral arterioles (Reid and Rand, 1992). One

of the main triggers of NO release is the shear stress exerted on the arterial walls by blood flow (Boulanger and Vanhoutte, 1998). Neurohumoral and paracrine substances affect endothelial cell receptors to stimulate NO synthase also, by increasing intracellular calcium levels (Rajagopalan and Harrison, 1996). Studies have shown that administration of NO synthesis blockers increase blood pressure and vascular resistance and cause a decrease in blood flow (Zatz and DeNucci, 1991; Madrid et al., 1997; Eppel et al., 2003).

- Endothelin-1 is a vasoactive substance released mainly by the endothelium cells, which line the entire circulatory system, but also by vascular and airway smooth muscle cells. According to Ergul (2002) and Hishikawa et al. (1995) the sensing mechanisms, which stimulate the release of endothelin-1, are low sheer stress, pulsatile stretch, and pressure. The receptors associated with endothelin-1 are ET_A , found in vascular smooth muscle cells and mediating vasoconstriction, and ET_B situated in endothelial cells and causing vasodilation (Ergul, 2002; Boulanger and Vanhoutte, 1998). The overall effect of endothelin-1 in each vascular bed would depend on the relative density of each type of receptor.
- Prostaglandins are short-acting local vasoactive substances derived from fatty acids. Two of their important representatives, PGE_2 and PGI_2 , are synthesised in the kidney and have vasodilatory effects in the vasculature. Their receptors are EP and IP respectively. The response to PGE_2 is twice as strong as the one to PGI_2 but the production of PGI_2 by the vascular smooth muscle cells is much greater, therefore the IP receptor activation may be the primary antagonist of vasoconstriction (Imig, 2000).
- Two other tissue-derived vasoactive factors are histamine and bradykinin. Histamine is an arterial vasodilator but can have vasoconstrictive properties in the veins. It becomes activated in cases of allergic reactions and tissue injury and causes edema in the surrounding tissues (Guyton and Hall, 2006). Bradykinin has a similar action to histamine, causing edema in cases of tissue inflammation, as well as regulating blood flow to the skin, salivary and gastrointestinal glands (Guyton and Hall, 2006).

2.3.6 Interactions between effectors

Numerous blood flow effectors directly modify the vascular resistance in order to increase or decrease blood flow to a particular organ. However, some vasoactive factors can also indirectly influence blood flow control by stimulating the synthesis and release of other vasoactive substances, which can either counteract or emphasise the action of the original blood flow effector. A few examples follow.

SNA, for instance, causes the release of norepinephrine, which causes vasoconstriction, but SNA stimulation also has an effect on the endocrine glands in the vicinity of the kidney, causing the release of epinephrine and norepinephrine into the blood system as well. Sympathetic stimulation also stimulates the release of renin by the kidney, thus stimulating the production of ANG II (Guyton and Hall, 2006).

ANG II has been demonstrated to stimulate an increase in endothelin-1 production in renal endothelial cells (Ikeda et al., 1995), while Ma et al. (2001) have shown that intravenous administration of ANG II stimulates continuously discharging low amplitude renal SNA. ANG II also stimulates the release of vasopressin (Brooks et al., 1986), thus strengthening its vasoconstrictory effect. ANG II, however, can also stimulate the synthesis of NO in endothelial cells, when binding to AT₂ receptors, causing attenuated vasoconstrictive response or even vasodilation in some vascular beds (Pueyo et al., 1998; Sigmon and Beierwaltes, 1993; Patzak et al., 2001; Horiuchi et al., 1999).

Vasopressin has been shown to stimulate endothelin-1 production proportional to its concentration (Ikeda et al., 1995), while it also stimulates the synthesis of vasodilatory prostaglandins in a dose-dependant manner (Hassid and Williams, 1983).

NO is reported to inhibit the release of norepinephrine at the sympathetic neuroeffector junctions, directly opposing sympathetic nerve activity-mediated vasoconstriction (Schwarz et al., 1995; Egi et al., 1994), while ANF inhibits renin and aldosterone synthesis and antagonises the antinatriuretic effects of ANG II (Cogan, 1991).

Since there are numerous interactions between the various blood flow/pressure effectors, it is clear that a balance between them ensures that the perfusion pressure is maintained at the precise level to satisfy the metabolic needs of each organ or tissue.

2.3.7 Models of RBF response to SNA stimulation

Sympathetic nerve activity is a major blood flow effector in the renal vasculature. Characterising the relationship between SNA and blood flow is important since the kidneys receive a large proportion of the total cardiac output (approx. 20 - 25%). Numerous attempts have been made to model the blood flow response to SNA stimulation in previous studies, with most focusing on linear models, and often failing to capture some essential features of the response.

Leonard et al. (2000) have studied the RBF response to electrical nerve stimulation of various amplitudes and frequencies but the provided frequency responses, characterising the relationship, have not been parameterised. Steady-state blood flow was found to reduce with increasing voltage and/or frequency of stimulation, indicating an increase in vascular constriction; however, the actual blood flow response curves were not modelled. In a similar study, Eppel et al. (2003) examine the steady-state reduction in blood flow due to various frequencies of renal nerve stimulation, ranging from 0.5 to 8Hz, but does not consider the transient response.

Navakatikyan et al. (2000) developed a linear, first-order, pole-only, model to specify the relationship between SNA and RBF. They modelled the blood flow response to a range of frequencies of sympathetic nerve stimulation (0.5-3Hz); however, due to the low frequency nature of the stimulus, and the simplicity of the model, only certain features of the relationship were described, leaving an incomplete representation of the system. In a study by Guild et al. (2001), a linear 4th order model (4 poles, 2 zeros and a delay) was identified to represent the RBF response to a pseudo-random binary sequence (PRBS) of sympathetic stimulation. The renal nerves, however, were only stimulated at relatively low frequencies (up to 1Hz). Thus, the local blood flow effectors, typically likely to counteract SNA stimulation, may not have been sufficiently activated. As a result, even though the model yields good results for the experimental conditions reported in Guild et al. (2001), the linear model structure would fail to represent the blood flow response at higher frequencies of stimulation.

Berger and Malpas (1998) developed a black-box ARMAX model to represent the relationship between RBF, SNA and BP. They found that SNA in conscious animals had a much larger impact on RBF than previously reported and was a bigger determinant of RBF than blood pressure.

Despite the numerous studies investigating the relationship between SNA stimulation and RBF, none of the above models were based on the characteristics of the physiological system. Mathematical models can be useful in developing an understanding of the system under study, but in order to achieve structural information, models which exploit aspects of the physical system description, rather than a global black-box modelling approach, are more suitable. While the black-box approach can give a very good model fit for specific experimental data, it does little to reveal the generic structure of the real system.

2.4 Hypertension

This section presents a concise overview of hypertension in general, and salt-induced hypertension in particular, with the aim to lay the background for the development of a non-linear multi-component model of hypertension due to a high-salt diet in the Dahl salt-sensitive (Dahl-S) rat.

Hypertension, or high blood pressure, is a condition where blood pressure is chronically elevated above certain guidelines of ‘normal’ levels. Systolic blood pressure (SBP) of 140mmHg and above, combined with diastolic blood pressure (DBP) of over 90mmHg, giving a mean arterial pressure of over 110mmHg, are considered to be the lower boundary values of mild hypertension (Guyton and Hall, 2006; Carretero and Oparil, 2000).

Hypertension can be divided into two major categories: essential (or primary) and secondary hypertension. Essential hypertension accounts for about 90-95% of all high blood pressure cases, and by definition, its etiology is not exactly unknown (Carretero and Oparil, 2000; Guyton and Hall, 2006). It has been widely agreed that both hereditary and environmental factors play a part in the development of essential hypertension (Carretero and Oparil, 2000). A large number of genes, some of which have already been identified, can be involved in the development of essential hypertension, and usually a combination of mutations in a number of genes in an individual would lead to a sustained hypertension (Mullins et al., 2006). In addition, a variety of environmental and life-style factors, such as obesity, insulin resistance, stress, alcohol, sedentary life-style and high-salt intake in salt-sensitive individuals, have also been identified to contribute

to rising blood pressure (Carretero and Oparil, 2000; Guyton and Hall, 2006; Korner, 2007). Some of these factors have also been found to have a genetic determinant, thus a combination of genetic and environmental factors is possibly the cause of hypertension in most individuals.

Secondary hypertension occurs in about 5-10% of the population with high blood pressure and is caused by an identifiable, already existing, disorder or condition (Guyton and Hall, 2006). Common causes for secondary hypertension are renal disease and renal failure, as well as vascular disease, such as remodelling of blood vessels and aortic coarctation. In addition, a number of monogenic (or Mendelian) types of hypertension have been identified, which are caused by the mutation of a *single* gene and include, among others, Liddle's syndrome and glucocorticoid-remediable aldosteronism (Luft, 2003). Over-production of aldosterone (as in primary aldosteronism) or cortisol (Korner, 2007), over-activity of the renin-angiotensin system and renal artery stenosis (Guyton and Hall, 2006) are some of the common underlying mechanisms in secondary hypertension.

Untreated high blood pressure carries a major health risk for cardiovascular disease (Carretero and Oparil, 2000) and even mild hypertension is associated with shortened life expectancy (Guyton and Hall, 2006). High blood pressure, also associated with increased blood volume, places greater demands on the kidneys to process the extra fluids, and thus can result in renal disease and renal failure (Whelton et al., 1992). Hypertension has also been identified as one of the main risk factors for stroke (Sacco et al., 1997) and heart failure (Levy et al., 1996). In addition, hypertension leads to vascular remodelling or hypertrophy, which can be associated with increased peripheral resistance (Rizzoni et al., 1996), resulting in an increased work load for the heart.

Among other well known factors that contribute to hypertension, the effects of a high-salt diet have been widely studied in the past century, and high salt intake, possibly in combination with other factors, such as stress, has been recognised as a possible cause of essential hypertension in a large proportion of the population in the developed world. The following section provides an overview of salt-induced hypertension in animals and humans alike.

2.4.1 Salt-sensitivity and salt-induced hypertension

As already outlined in the previous section, hypertension presents a major health risk, and high intake of dietary salt, or sodium, has been shown to be one of the possible etiological factors for the development of hypertension (He and MacGregor, 2004; Meneton et al., 2005).

Sodium balance in the body is maintained through a number of mechanisms, including the renin-angiotensin-aldosterone system, atrial natriuretic factor and the sympathetic nervous system. Thus, under normal circumstances, even large changes in sodium intake would not result in a marked variation in BP (Guyton et al., 1980; Korner, 2007).

The question arises as to why it appears that, in populations with high salt intake, blood pressure levels tend to be higher than in those with lower levels of dietary sodium and why all individuals with high salt intake do not develop hypertension. The phenomenon of salt-sensitivity in a proportion of the population would explain selective blood pressure increases in some individuals and not others.

Salt-sensitivity definition

Salt-induced hypertension (SIH) is a process whereby a subject develops high BP due to a high salt intake. Salt-sensitivity has been defined arbitrarily, depending on the study, however a well accepted protocol for classifying individuals as salt-sensitive or salt-resistant has been used by Kawasaki et al. (1978) and Fujita et al. (1980). In both studies, individuals were given a low salt diet for several days, followed by a high-salt diet for a week. The difference between the BP levels on the last day of low-salt and the last day on high-salt diet was noted. Subjects with a BP increase of more than 10% from the initial value were considered salt-sensitive.

In some studies (e.g. Weinberger et al. (1986)), BP response to salt loading/depletion was studied on a short term scale (24 hours). The relationship between the blood pressure response to acute (24-h) salt loading/depletion and the effect of a week-long high/low-sodium diet was confirmed by Weinberger et al. (1993) and Sharma et al. (1994). In both studies a strong correlation was found between the two experimental protocols used to determine salt-sensitivity. In addition, Van Vliet et al. (2006) have shown a strong correlation between the BP response of Dahl-S rats to salt loading in

the short term (a few days to a week) and the subsequent development of hypertension due to high salt intake in the longer term (over a few months, which would equate to years in terms of the human species).

Finally, in addition to the effect on blood pressure, high salt intake has also been associated with increased cardiovascular morbidity and mortality, in a manner independent of hypertension (Meneton et al., 2005; O'Shaughnessy and Karet, 2006). Some of the serious effects of high dietary salt include an increase in left ventricular mass, stiffness and thickening of the arteries, platelet aggregability and susceptibility to stroke, as well as renal hypertrophy (Tobian and Hanlon, 1990; De Wardener and MacGregor, 2002). Additional possible effects of high salt intake, not related to the cardiovascular system, are bone density depletion, due to the relationship between calcium and sodium excretion, and cancer of the stomach (De Wardener and MacGregor, 2002).

Salt-induced hypertension prevalence in the population

Around 25 - 35% of normotensive individuals have been found to be salt-sensitive (Weinberger et al., 1986; Korner, 2007) and the degree of salt-sensitivity can be dependent on the subject's race and on the levels of potassium intake (Adrogué and Madias, 2007; Morris Jr et al., 1999), with low potassium intake exacerbating salt-sensitivity. In individuals with mild to moderate hypertension, the cases of salt-sensitivity are more numerous, with up to 50% of the those with high blood pressure affected (Weinberger et al., 1986).

A genetic component to salt-sensitivity has been identified and salt-sensitivity has been shown to be more common in the elderly, in Afro-Caribbeans and in those with Type II diabetes (Weinberger et al., 1987; Weinberger, 1996; Luft and Weinberger, 1997; O'Shaughnessy and Karet, 2006). Impaired regulation of renal sodium handling seems to present a common problem in the Mendelian types of hypertension and hypotension (O'Shaughnessy and Karet, 2006; Luft, 2001).

The negative effects of salt-sensitivity are particularly evident in a 30-year study of salt-sensitivity in normotensive and hypertensive individuals, where Weinberger et al. (2001) found that salt-sensitive subjects were more likely to develop hypertension with age than were salt-resistant individuals. In addition, salt-sensitive subjects who were initially normotensive, were found to have the same risk of cardiovascular mortality as

those who were hypertensive from the start, and a much higher risk compared to those who were salt-resistant.

Historically, and from an evolution viewpoint, human kidneys were designed to preserve salt and excrete potassium easily, since their largely vegetarian diet was low in salt and high in potassium, due to the location of most prehistoric human populations far from salt sources (Denton et al., 1995; Tobian, 1991; Adrogué and Madias, 2007; O'Shaughnessy and Karet, 2006).

In primitive tribes of modern times, which do not consume salt, blood pressure does not rise with age (Gonzalez-Albarra et al., 1998; O'Shaughnessy and Karet, 2006; Meneton et al., 2005), while a move to an urbanised society causes up to 30% of rural migrants to develop hypertension (Tobian, 1991), similarly to western populations. The Lou tribe in rural Kenya, for instance, have a diet low in sodium and high in potassium and do not manifest a rise in blood pressure with age. However, when Lou people migrate to Nairobi, with an associated increase in salt intake, their BP and weight rise, without an increase in calorie intake (Poulter et al., 1990). A similar effect has been noted in the Yi farmers in China, who have a primitive life-style and a low-salt, high potassium diet, with only rare cases of hypertension and cardiovascular disease (He et al., 1991a). When Yi farmers migrate to Xichang City, however, their salt intake rises, potassium intake decreases and blood pressure rises with age, similar to that of local Han people (He et al., 1991b).

The migration effect on blood pressure has been attributed to factors such as stress, alcohol consumption, smoking and weight gain, which would have been minimal in a peaceful rural environment. These factors may have some contribution to hypertension. It is worth noting, however, that in the case of the example of the Yi farmers, those who migrated and those who did not both smoked and both consumed similar amounts of alcohol, clearly indicating that salt intake was the key contributory factor to hypertension (He et al., 1991a). It is also true that stress may cause some rise in blood pressure but the Yanomamo Indians of the Venezuela-Brazil border live in an uncultured, highly stressful and violent society, without a rise in BP with age. Their lack of hypertension has been attributed to a low-salt diet of approximately 0.5 g/day of NaCl (Oliver et al., 1975). The nomadic Quash'Qai people of Iran, on the other hand, have a primitive life style, but consume large amounts of salt and demonstrate an associated increase in

BP with age, similar to that in the developed world (Page et al., 1981). One study of Italian nuns, who consume the same amount of salt as lay women from the surrounding geographic area, but are not exposed to normal everyday life, show that the nuns do not develop hypertension with age and have fewer cases of cardiovascular disease (Timio et al., 1997). Consequently, it is very likely that a combination of compounding factors contribute to salt-induced hypertension or the age-related increase of blood pressure in the developed world. Stress, high-fat diet and the lack of exercise might all play a role in the development of hypertension and cardiovascular disease, especially in the presence of a high-salt diet. Furthermore, Deter et al. (1997) have shown that during stress, blood pressure rises much more in salt-sensitive normotensive individuals than in their salt-resistant counterparts. Therefore, it is very likely that a genetic predisposition to salt-sensitivity would cause a rise in blood pressure under conditions of high-salt intake, combined with stress and an unhealthy life style.

The population of Northern Japan offers an example of possibly the highest salt intake in the World in the 1950s and 1960s, with some sub-populations consuming on average 27g/day and up to 61g/day (Sasaki, 1962) (the recommended salt intake is up to 6g/day), leading to wide-spread hypertension and vascular morbidity and mortality and the highest prevalence of cerebral hemorrhage in the World (Meneton et al., 2005). Up to 70% of the people there were found to be hypertensive at the age between 50 and 60 years (Meneton et al., 2005) and high blood pressure was found to be associated with low potassium intake (Sasaki, 1962).

In general, a linear relationship has been noted between the average salt intake within and across populations and their average levels of blood pressure, and a similar relationship exists between blood pressure levels and age (Stamler, 1997; Dahl, 2005).

Alteration in renal function, impairment of the renin-angiotensin-aldosterone system (RAAS), or genetics, can contribute to a faulty blood pressure response to salt (Weinberger et al., 1987), as well as possibly an overactive sympathetic nervous system (Johnson et al., 2002; Leenen et al., 2002), also contributing to salt-sensitivity. In any case, regardless of the causes of salt-induced hypertension, a reduction of the overall salt intake by a population with high dietary salt has been shown to have positive effects on blood pressure, in particular, and health outcomes in general (He and MacGregor, 2004; Meneton et al., 2005), especially for those with hypertension.

Salt-induced hypertension in animal studies

Animal experimental protocols have provided much insight into the issue of salt-induced hypertension. Animal studies are advantageous since they can be performed over longer periods than those on human subjects, especially compared to the life span of the subjects, and with more stringently defined protocols and interventions. The development of telemetry technology, in particular, has provided a great opportunity to continuously monitor physiological responses during lengthy experimental protocols without the need of frequent handling or interventions, such as sedation.

Animal studies on the effect of high dietary salt have shown a variety of blood pressure responses. A rise in blood pressure during the days following the onset of high salt intake, frequently used in humans to determine if an individual is salt-sensitive or salt-resistant (Fujita et al., 1980; Kawasaki et al., 1978), has been demonstrated in a number of animal species too. Mice (Leonard et al., 2006), Dahl-S (Van Vliet et al., 2006) and Sprague-Dawley (Osborn and Hornfeldt, 1998) rats, dogs (Manning et al., 1979) and monkeys (Srinivasan et al., 1980, 1984) all manifest a blood pressure increase within a few days to a week after the initiation of high salt intake. In addition, a distinct effect of high dietary salt, in raising blood pressure slowly and over a prolonged period of time, has been demonstrated in studies of chimpanzees (Denton et al., 1995; Elliott et al., 2007) and rats (Dahl, 1961; Van Vliet et al., 2006), and the blood pressure increase has been found to be proportional to the level of dietary salt (Meneely et al., 1953).

The different phases of salt-induced hypertension have distinct features (gain and time constant of response) and are probably due to different mechanisms. Van Vliet and Montani (2008) have provided a detailed overview of the phases and characteristics of salt-induced hypertension, encompassing a variety of animal species and humans.

The initial, ‘acute’ phase, evident within days to weeks of high salt intake, and corresponding to the re-establishment of sodium balance, has been shown to be reversible after removing the high-salt input (Srinivasan et al., 1980; Van Vliet et al., 2006). In salt-resistant individuals, sodium balance is normally established without a marked variation in blood pressure, due to the large number of subsystems in the body responsible for sodium excretion (RAAS, ANF, SNS). In salt-sensitive subjects, however, one or more of the regulatory systems responsible for sodium handling and blood pressure regulation, might be malfunctioning, and therefore a change in renal perfusion pressure

is required to maintain a balance between salt intake and excretion.

The longer-term effect of salt on blood pressure, which might occur over months, years or the time scale of a life-time, and resembling the increase in blood pressure with age in humans, has been shown to be partially irreversible in some cases (Van Vliet et al., 2006) and fully reversible in others (Denton et al., 1995), with the level of reversibility probably depending on the duration and level of salt exposure. It has been suggested that this slow and progressive increase in blood pressure with prolonged high-salt intake could be related to vascular remodelling, renal lesions or fibrosis (Van Vliet et al., 2006) and compromised glomerular filtration rate (Tobian, 1991), which have been shown to develop during salt-loaded hypertension.

2.4.2 Dahl salt-sensitive and salt-resistant rats

In the last century, animals, and in particular rodents, have been bred to create experimental models of various physiological and pathophysiological conditions, in an attempt to classify the genes involved, as well as to study the developmental stages of the conditions. Numerous animal models of hypertension have been developed with genetic, endocrine, mechanical or monogenic etiology, such as the spontaneously hypertensive rat (SHR), the Dahl salt-sensitive (Dahl-S) rat, the deoxycorticosterone acetate (DOCA)-salt rat, the two-kidney one-clip (2K1C) model, the transgenic TGR(mRen2)²⁷ rat and the Milan hypertensive rat. Each experimental model mimics a particular subtype of hypertension and they all lead to different outcomes in relation to actual levels of blood pressure, life expectancy and end organ damage (Pinto et al., 1998). Additionally, not all antihypertensive drugs are effective for the treatment of each of the models of hypertension, with some being solely efficient in reducing blood pressure and others also helping prevent end organ damage.

The Dahl-S rat has been specifically bred from Spraug-Dawley rats, for their genetic susceptibility to salt-induced hypertension (Dahl et al., 1968). The Dahl-S rat's blood pressure response to salt has been studied in detail and has been found to be a multi-component event, with both an acute and a slower, progressive form of hypertension (Van Vliet et al., 2006). The slow and progressive blood pressure increase due to high dietary salt is on an accelerated time scale compared to other species, since the rats were specifically bred to be highly salt-sensitive, and the resulting hypertension tends

to be self-sustaining after the removal of the high-salt input (Dahl and Schackow, 1964). On the other hand, most Dahl-S rats fed a high-salt diet (8% NaCl) for 2 weeks only, seem to return to normal pressures, while rats exposed to the high salt diet for 6 weeks are severely hypertensive even after many subsequent months on a normal diet (Dahl et al., 1968). Renal failure is common among Dahl-S rats on a high-salt diet, even in those whose blood pressure is not excessively high (Dahl et al., 1968)

The Dahl salt-resistant (Dahl-R) rats, in contrast, do not develop hypertension even at high levels of salt intake; however, a high-salt diet increases morbidity and mortality in salt-resistant rats, due to vascular injury.

F_2 hybrid rats, resulting from breeding the cross-bred progeny of Dahl-S and Dahl-R rats, provide an opportunity to study a range of blood pressure responses from complete salt-resistance to moderate or severe salt-induced hypertension (Van Vliet and Montani, 2008).

The exact means by which Dahl-S rats, and some of their hybrid off-spring, become hypertensive are not completely clear. Renal involvement has been confirmed, however, with transplant studies, in which salt-resistant recipients become hypertensive after receiving a kidney from a hypertensive salt-sensitive rat, and vice versa - the blood pressure of a hypertensive Dahl-S rat is reduced after receiving a kidney transplant from a salt-resistant donor (Dahl and Heine, 1975). A reduction in the kidney's capacity to excrete salt and water, resulting in an elevated cardiac output, has been identified as a possible cause of the salt-induced hypertension in Dahl-S rats, who have also been found to have fewer glomeruli, increased renal resistance and a lower glomerular filtration rate (GFR) (Simchon et al., 1989; Tobian, 1991) than Dahl-R rats under the same experimental conditions. Lower levels of prostaglandins E_2 have also been noted in the Dahl-S rat, leading to a higher level of sodium reabsorption. A decrease in other vasodilatory prostaglandins, accompanied by an increase in the vasoconstrictory prostaglandin thromboxane, is also believed to cause sodium retention (Tobian, 1991). Interestingly, in a study including F_2 hybrid rats, some of the hybrid animals exhibit an acute salt-sensitivity component only, while others develop a progressive form of SIH too, with others still being completely salt-resistant (Van Vliet et al., 2006). Such data can be very useful in describing the separate components of salt-induced hypertension, which may exist on their own or in combination with each other.

2.4.3 Renal function curves

The renal function curve, also referred to as the chronic pressure-diuresis/natriuresis relationship, defines the pressure level at which steady-state balance between sodium intake and excretion is achieved, after the regulatory mechanisms, contributing to renal function and blood pressure control, have been activated (Van Vliet and Montani, 2008). Under normal condition in non-salt-sensitive individuals, the renal function curve is very steep, nearly vertical, indicating that sodium balance is achieved without the need to change blood pressure levels much, as shown in Figure 2.3 (lines *a* and *c*).

Numerous regulatory systems are involved in establishing sodium balance, including the RAAS, SNA and ANF. Atrial natriuretic factor is released by the heart during blood pressure increases and stimulates sodium excretion by the kidneys, thus reducing pressure back to normal levels. Aldosterone, renal SNA and ANG II, on the other hand, increase salt and water reabsorption when blood pressure falls, and ANG II increases the secretion of antidiuretic hormone, which reinforces the fluid retention and activates thirst and the desire for salt (Guyton and Hall, 2006; DiBona, 1989). With a well functioning RAAS, even a 50-fold increase in salt intake may only cause a BP increase of 4-6mmHg (Guyton and Hall, 2006). Nevertheless, when one or more of the additional regulatory mechanisms malfunction, the renal-body fluid system may need to reset blood pressure to levels appropriate for maintaining salt balance, thus when salt intake increases, blood pressure rises accordingly to increase salt excretion (see Figure 2.3, lines *b* and *d*).

A schematic of the features of a renal function curve has been presented in Figure 2.3. Line *a* represents a normotensive, salt-resistant individual, with a very steep renal function curve. As the slope of the curve decreases, salt-sensitivity increases, leading to line *b*. A shift in the curve to higher blood pressure levels (to the right) is associated with chronic hypertension (line *c*) and again, if the curve has a decreased slope, salt-sensitivity is also present (line *d*). In Dahl-S rats fed a high salt diet for a short time (e.g. one week), the renal function curve is similar to line *b*, and in this thesis, it is referred to as ‘acute salt-sensitivity’, with the increase in blood pressure fully reversible when the salt intake is returned to normal levels. If the high salt intake is maintained over a prolonged period of time, however, the slope of the line decreases progressively (‘progressive acute salt-sensitivity’), a change which is also accompanied by a rightward

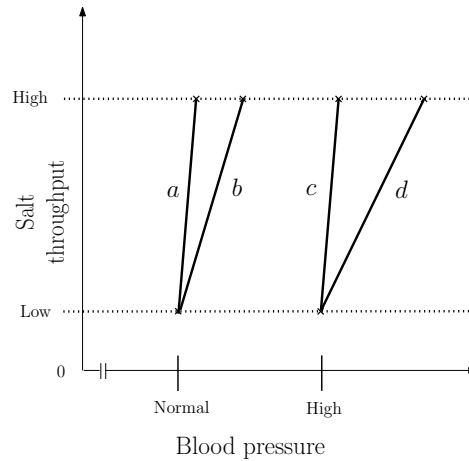


Figure 2.3: Steady-state renal function curves, representing: line *a* - a normotensive salt-resistant individual, line *b* - a normotensive salt-sensitive individual, line *c* - a hypertensive salt-resistant individual and line *d* - a hypertensive salt-sensitive individual. The figure is a modified version of Figure 4 in Van Vliet et al. (2006)

shift towards higher blood pressure levels (Van Vliet et al., 2006), which is referred to here as a self-sustained hypertension here (line *d*).

The mathematical models of the blood pressure response to high-salt intake, presented in Chapter 4, are developed in line with the mechanisms of SIH outlined here in Section 2.4, giving a ‘transparent’ structure, based on the underlying physiology, and also providing a capacity to generate the renal function curves shown in Figure 2.3.

2.5 Summary

This chapter has presented an overview of the main blood pressure control mechanisms at the short, medium and long terms. The overview lays a background for the development of a number of mathematical models related to blood pressure regulation.

Section 2.2 relates to the arterial baroreflex and provides a review of the existing baroreflex sensitivity estimation techniques, which lays the foundation for a novel system-identification approach to baroreflex sensitivity estimation, presented in Chapter 5.

Section 2.3 provides an overview of the vasoactive mechanisms, and especially those active in the renal vasculature, which provides the foundation of a mathematical model

for renal vasoaction, presented in Chapter 6.

Finally, Section 2.4 gives a general overview of hypertension and, in particular, examines salt-induced hypertension in detail, as a background to modelling of salt-induced hypertension in Dahl rats, as presented in Chapter 4.

Chapter 3

Implementation of Guyton's integrative physiology model in Simulink

In his 1972 “Circulation: Overall Regulation” paper (Guyton et al., 1972b) Arthur Guyton affirms his observation that systems analysis should be used to its full potential in order to study physiology from an analytical perspective. Mathematical models are a useful tool to develop a deeper understanding of a physiological system under study. In order to achieve structural information, the emphasis should be on models which employ the physical system description. Guyton's integrative physiology model, first published in 1972, is a remarkable example of such a model, which incorporates a large number of systems and was developed at a time when computational technology was not nearly as advanced as it is today.

3.1 Introduction

The extensive Guyton circulation model, developed in 1972 (Guyton et al., 1972b), is based on collective knowledge of physiology, and the model features and parameters originate from collected experimental data. The model simulates and predicts a large variety of both animal and human physiological conditions and circulatory stresses.

The model revolutionised the way physiology was studied, which was presented in a

number of ways:

1. The model assembled the available knowledge on the dynamics of the body's circulatory components and how they interacted with each other,
2. The model presented a diagrammatic form, which allowed the totality of the model to be viewed and interactions examined, and
3. The model was specified using the basic components of integrators, summers and (sometimes nonlinear) gains, the fundamental building blocks of analogue computers, facilitating computation.

The model comprises 354 mathematical blocks, where each block represents a particular physiological signal or function. Originally, the model was implemented in the Fortran programming language and was also published in a graphical format (Guyton et al., 1972b). The original model has been enhanced and extended over the years, and was translated in the C programming language in 1988, and an unpublished version of the model from 1992, accompanied by the MODSIM environment (Montani et al., 1989), has been made available.

The benefits of developing and utilising large physiological models for both teaching and research purposes, have withstood the test of time, with numerous research groups currently developing tools to enhance, store and make use of such models. A large number of modern modelling and simulation environments is now available; unfortunately, no common medium for development and sharing of integrative physiological models has been agreed. Ideally, a common platform should be used to model, simulate and store existing models and to allow updates in the knowledge and understanding of the underlying physiological systems to be added easily by the research community. Projects, such as the IUPS (International Union of Physiological Sciences) Physiome Project (Hunter et al., 2008), attempt to directly address this issue with mixed success, to date.

This chapter will examine the requirements of integrative physiology where modelling and simulation is concerned, and the currently available tools that can satisfy those requirements. A graphical modelling and simulation environment is proposed as an integrated solution and a validated Simulink version of Guyton's most recent (1992) model (Montani, 2008) is presented as an example of such a solution, together with a

discussion of outstanding issues which need to be resolved.

3.2 Model Development and Simulation

The development of mathematical models used for computation and simulation generally follow a similar pattern, as shown in Figure 3.1. Initially, the system is represented as a set of continuous- or discrete-time equations, derived either from first principles, or through a system identification process, where model parameters are optimised using measured experimental data. An appropriate mathematical representation is also selected (difference/differential equations, state-space, transfer function) at this time. For complex models, a hierarchical structure would allow users to conceal some of the detail, thus employing an approach of grouping parts of the model into systems and subsystems, which would improve the legibility of the model. A simulation environment, which satisfies the model representation requirements would then need to be selected, and a suitable interface with the end user, as well as the model developer, is also needed.

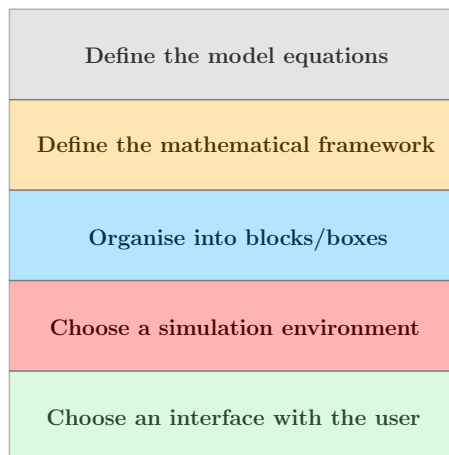


Figure 3.1: Stages of the modelling process

Guyton's original model followed a similar path of development, where the equations were based on physiological principles and experimental data, and were represented in a block diagram form with only a small set of simple mathematical operations (summers, integrators and gains, some of which are nonlinear), components typical of analog computer systems. For digital computer implementation, the model equations were discre-

tised and translated into C-like code and the model was simulated using the aforementioned MODSIM environment. Implementing a large model in a high level programming language, such as C or Fortran, has its limitations in both execution (sequential code) and readability and newer models and implementations, such as QHP (Quantitative Human Physiology) or HumMod (Hester et al., 2011), have similar drawbacks.

A more detailed discussion of the requirements and constraints in the process of modelling and simulation in the integrative physiology field follows.

3.3 Modelling

In order to take a structured approach to the discussion of modelling and simulation for integrative physiology, one must question the objective of the modelling and simulation exercises. In modelling, the following set of objectives are pertinent:

- Develop a set of continuous-time equations which represent the underlying physiological components (Garfinkel, 1983; Keener et al., 1998; Carson and Cobelli, 2000; Ottesen et al., 2004),
- Parameterise the equations using experimental data (Ljung, 1999), and
- Validate the model on previously unseen data (Cobelli et al., 1984)

In terms of defining a set of model equations, which represent the underlying physiological phenomena, a number of modelling approaches are available:

- White-box models, where each parameter represents a physical physiological quantity,
- Grey-box models (and the sub-classes of off-white, smoke-grey, steel-grey and slate-grey (Ljung, 2008)), where some links between the physiological structure and model parameters exists, and
- Black-box models, such as neural networks, where the model structure and parameters are not associated with particular physiological features and the model simply reproduces experimental data.

The type of model that should be developed is determined by the purpose of the model and the availability of system knowledge and experimental data. Even though all model

types can be valuable in the biomedical field, Guyton's model would fall in the grey-box model category, and this model type is perfectly suited for teaching and research purposes, where the link between model parameters and particular features in the underlying physiology are important. Grey-box models allow us to simulate various experiments and study their effects on the model parameters, and thus the physiology features these parameters represent.

It is also worth mentioning that when defining the model equations of large integrated models, such as Guyton's model, a variety of time scales can be incorporated. In addition, the model can be hierarchically built using progressively larger 'component' sizes, with a good example of such a hierarchy suggested by Hunter and Nielsen (2005) in Figure 3.2.

Organ systems (cardiovascular, respiratory, etc)
Organs
Tissues (Muscle, nerve, etc)
Cells
Organelles (Cell membranes, nucleus, etc)
Cell function (Membranes receptors, ion channels, etc)
Proteins, carbs. and lipids
Gene regulation, transcription, etc
Genes

Figure 3.2: Multiscale modelling hierarchy (Hunter and Nielsen, 2005).

An appropriate mathematical representation needs to be selected for any physiological model implementation. A set of possible representations are differential equations, state space models or transfer functions (TF), where the latter can be used for linear systems only. The model representation will, again, depend on the purpose of the model. It is beneficial to use representations that relate to physical or intuitive quantities, and

ones that help with the visualisation of important connections in the model. Using transfer functions, for example, allows us to easily note important features in the model components, such as time constants and gains; however, with a TF representation, initial conditions, which are vital for physiological systems, cannot be set.

A number of formalised modelling methods (Ljung and Glad, 1994), some of which have the ability to deal with non-homogeneous systems (i.e. systems with mixtures of mechanical, flow, electrical, etc. elements), such as bond graphs, are available. A variety of system identification routines (Ljung, 1999) can be used to estimate parameter values from experimental data, but care needs to be taken that the operating region, for which the model is valid, is well defined.

3.4 Simulation

Mathematical models of physiological systems are sets of equations that represent the system response and whose parameters may or may not have a direct relationship with specific physiological quantities, depending on the model type (white-, grey-, black-box). In order to use a mathematical model to simulate the physiological system response to a particular input or with respect to a set of initial conditions, a computer implementation of the model is vital.

One can document the steps required in simulating a system (physiological or otherwise) on a digital computer as:

1. Model equations are assembled - structure and form, including interconnections,
2. Model parameters are determined (white, various shades of grey, black),
3. Model equations are discretized, and
4. Equations are implemented in computer code

In the case of item 3 above, it is useful to observe that there is no 'perfect' form of discretization, which preserves all the properties of the original continuous-time system (e.g. time response, frequency response, etc.) with exact fidelity (Ascher and Petzold, 1998). The same model, simulated using different discretisation techniques, may produce significantly different responses, depending on the nature of the system. Certain nonlinear systems, stiff systems (systems containing both fast and slow dynamics) and

systems containing algebraic loops may all be sensitive to the simulation engine and/or discretization used.

Most discretisation methods are based on numerical integration techniques (e.g. Euler, Runge-Kutta, methods based on the Adams-Moulton and Adams-Bashford families, etc.) (Hairer et al., 1993; Hairer and Wanner, 1996; Molar and Van Loan, 2003), with some based on frequency response mapping (e.g. pole-zero mapping) (Hori et al., 1992). The 1992 Fortran implementation of Guyton's model (Montani, 2008), for example, uses a first order forward-difference discretization method.

In order to select a suitable discretisation technique, one must decide which particular features of the continuous-time response of the system are most important to preserve in the discrete-time approximation (Yates, 1978). Consequently, it is crucial that any models that are published, or made available to the wider community, also carry information on the discretisation method of choice and how to solve issues, such as algebraic loops, in order for results to be reproducible.

It is also important to note that, depending on the environment selected for model simulation, one may not need to discretise the continuous-time system 'by hand' before implementation. Advanced modelling and simulation environments, such as MATLAB's Simulink (The Mathworks Inc.), allow the user to implement the system using continuous-time blocks and then configure the simulation to use an 'integration method' from a set of routines built into the software.

3.5 Modelling and simulation environments

A wide variety of modelling and simulation environments, with different features and functionality, are available, and some are tailored to specific domains, while others are generic. This section provides a succinct overview of the main modelling and simulation environments in use and examines their suitability for integrative physiology modelling.

3.5.1 Diagrams and equations

The original (for example, see Grodins (1959)) environment for the communication of mathematical models is using block diagrams and differential or difference equations. Specification of sets of continuous-time equations (with associated block diagrams) is still prevalent in the published literature (Ringwood and Malpas, 2001; Karaaslan et al., 2005). This form, usually specified in continuous-time, utilises well-accepted standard mathematical and block-diagram notation, but is not directly computer readable and is purely for representation purposes, with no simulation potential or information.

3.5.2 Markup languages

Markup languages (ML) are used to process, define and present text in a way that it could be human- and machine- readable. A large number of markup languages have been developed for many types of applications, with the most well known being HTML, or HyperText Markup Language. HTML is used to define how text, images and multimedia are displayed in web browsers. XML, or eXtensible Markup Language, can be used to create new, application specific markup languages, for example MathML, which is used for defining mathematical expressions (Foster, 1999).

The main benefit of using markup languages to specify content is the simplicity and transportability of the definitions, which makes them machine independent and future proof. In terms of defining biomedical models using markup languages, there are numerous examples of such 'MLs':

- The set of markup languages associated with the IUPS Physiome project, which provides a framework for modelling the human body, incorporating biochemical, biophysical, and anatomical information on cells, tissues, and organs (see Fig.3.3, and also Khodade et al. (2007)), namely (Hunter et al., 2002):

ProteinML , which can describe pathway models,

CellML (Cuellar et al., 2003), which provides a representation of the mathematical relationships of biophysical models at the cell level, allows nesting of models,

TissueML , which describes models at the tissue level,

FieldML (Chang et al., 2007), describing spatially and temporally varying fields (such as electric fields) related to cell structure,

AnatML , which deals with physiology at the organ level, and

PhysioML (Ward et al., 2006), which addresses the organ system and organism level,

- CML (Chemical ML) (Murray-Rust and Rzepa, 2003), which provides a representation for managing molecular information, from macromolecular sequences to inorganic molecules and quantum chemistry,
- SBML (Systems Biology ML) (Hucka et al., 2003), which describes models of biochemical networks, such as signal transduction, metabolic pathways and gene regulation, and
- SysML (Systems ML) (Bock, 2006), which caters for 'systems' engineering, typically supporting block diagrams of interconnected systems.

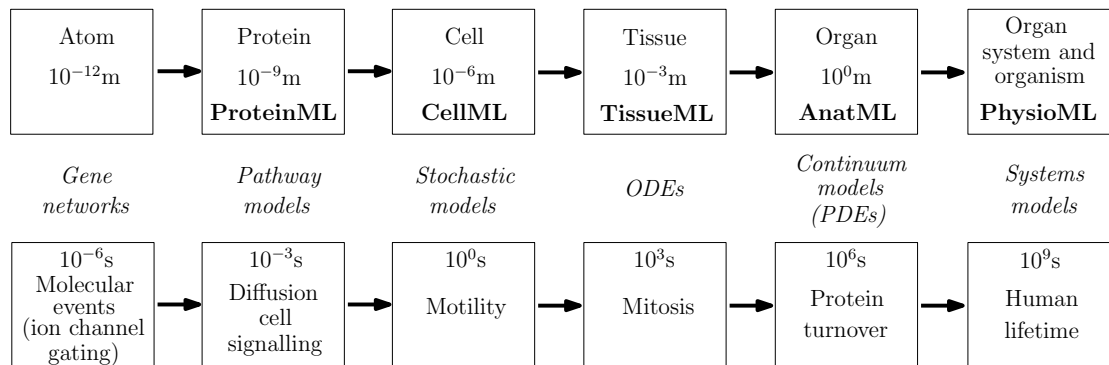


Figure 3.3: Spatial (top) and temporal (bottom) scales encompassed by the Human Physiome Project along with corresponding markup language (based on Hunter et al. (2002)).

CellML, promoted by the IUPS Physiome Project (Hunter et al., 2008), is a subset of Content MathML, which is the 'active' version of MathML (the other one is Presentation MathML). CellML has been suggested as a potential solution platform for cell function and to standardise the interface to other computer programs and probably represents the most developed of the IUPS Physiome 'MLs'. A CellML model contains both the essential model equations, written in ascii/markup, and associated 'metadata' which contains (Cuellar et al., 2003):

- The units in which the variables associated with the model component are measured,
- Author, literature reference, creation date, and
- Biological context.

An element of hierarchy is also provided for in CellML via the *encapsulation* and *containment* grouping relationships. Simulation tools are available for CellML models, via a CellML application programming interface (API) (Cuellar et al., 2003), and graphical tools for the development of CellML models are under development. CML and SBML appear to overlap in scope with some of the IUPS Physiome 'MLs', while PhysioML (Ward et al., 2006) is somewhat unique in its ability to control the interface display and can perform 'computational steering', which refers to the selection of particular variables which can be altered during computation. However, there is currently no means to incorporate model descriptions in PhysioML though there may be an option in the future to achieve this using MathML. SysML operates at a high (systems) level and it allows for the incorporation of 'systems-level' information, including hardware, software, information, processes, personnel, and facilities.

3.5.3 Graphical modelling and simulation environments

Graphical modelling and simulation tools are, generally, an excellent choice for presenting mathematical models as they facilitate the visual understanding of the interconnected systems under study, while also providing a simulation engine to run the model. There is a wide range of graphical modelling and simulation environments available, some of which are commercial proprietary products, while others are free and/or open source. In general, graphical simulation packages offer very fast development times for models, assisted by libraries of standard blocks and, in many cases (e.g. Simulink/MATLAB, Scicos/Scilab), an associated macro language parser which allows high-level calculations.

The range of graphical modelling/simulation environments includes the following (with many more available):

- MATLAB/Simulink - a commercial, easy to use, software, which allows fast block diagram graphical model development and provides a solver for ordinary differ-

ential equations (ODEs) and an iterative solution to algebraic equations.

- Scicos/Scilab (The Scilab Consortium) - a free software for numerical computation providing a powerful computing environment for engineering and scientific applications. It is similar to MATLAB/Simulink, and can be compatible with it too; however, the functionality is not quite as advanced.
- Dymola/Modelica (The Modelica Association) (Larsson, 2006) - the modelling environment Dymola, by Dynasim, is an object oriented tool for modelling and simulation of dynamic systems of various fields including, mechanical, thermal, control, pneumatic, hydraulic systems etc. Dymola is integrated with the Modelica modelling language, which supports the integration and reuse of code developed in different modelling and simulation environments.
- VisSim (Adept Scientific) - a visual tool for modeling and simulating nonlinear dynamic systems. A free VisSim viewer is available for sharing the model with others. Compatible blocks can be created in the C, Fortran or Pascal programming languages.
- 20-Sim (Controllab) - a modeling and simulation graphical tool with equations and blocks for electrical, mechanical, hydraulic systems etc. It allows subsystems creation and has a graphical environment with simulator, as well as visual representation of results through a plotting tool.
- SimApp - a dynamic simulation software for modeling systems in the time and frequency domains. It uses a block diagram method of building models and can help model full systems that cross various technical disciplines.
- Xcos - a block diagram environment, which enables the simulation of complex systems - discrete, continuous, defined by symbolic equations (Modelica) and Scicos.
- Easy-5 - a family of software tools used to model, simulate and analyze dynamic systems (multi-domain modeling and simulation of dynamic physical systems), graphical, schematic-based application, offering a comprehensive set of pre-packaged 'components'.
- Cytoscape - open source bioinformatics software platform for visualizing molecular interaction networks and biological pathways and integrating these networks with

annotations, gene expression profiles and other state data.

- SAAM II - modeling and simulation tool with a user-friendly interface based on compartmental models.
- SIMUL8 - allows the user to pick from a predefined set of simulation objects and statistical distributions to create a model; it also allows hierarchical modelling but the main focus is on discrete event simulation.
- MapleSim - a physical modeling and simulation commercial tool built on a foundation of symbolic computation technology; it can be used for the development of engineering models, including multi-domain systems, plant modeling, and control design.

A large number of other environments, such as MATRIXx, ExtendSim/Extend 6, Jsim, EcosimPro etc, are also available.

Of the listed packages, Simulink (Nuruzzaman, 2005) is probably the most popular, though it has become relatively expensive and there are some compatibility difficulties between the many releases. The Scilab/Scicos (Campbell et al., 2006) environment is unlikely to suffer the same fate, being an open-source platform, but does not yet offer the same level of functionality as MATLAB/Simulink. Modelica, which is promoted by the non-profit Modelica Association, has the advantage of being object oriented and can model complex heterogeneous systems. The most popular simulation engine for Modelica, Dymola is, however, a commercial product, though other (free) simulation engines, including OpenModelica and Modelicac are also available. In addition, a Modelica to XML translation is available (Pop and Fritzson, 2003), which would allow sharing of the model in a generic format.

In terms of capability, Simulink performs best with pure ordinary differential equations, with algebraic equations solved iteratively, which can require excessive computation (though insertion of small artificial delays can circumvent this). Modelica/Dymola provides a more natural way to simulate differential algebraic equations (DAEs) directly. In terms of model storage, Simulink uses a proprietary format, though translators (Dempsey, 2003; Hornych et al., 2002) are available to convert between representations, but these are unlikely to preserve the full detail of the original model description.

A particularly promising open-source offering under development is the ProMoT (Max

Planck Institute) (Process Modelling Tool) environment (Tränkle et al., 1999), which can build structured dynamic simulation models that are based on differential and algebraic equations. Developed originally for process engineering, it has been more recently applied to systems biology, with library modules available for application domains such as separation processes, membrane processes, fuel cells, metabolic cellular processes and signal transduction. Simulation is via the DIVA package, which uses some commercial libraries for numerical computation, but a further open-source simulation module (DIANA, Dynamic sImulation And Numerical Analysis tool) is currently under development. ProMoT uses symbolic reduction for efficient simulation, which deals effectively with algebraic loops. The scripting language, Python, is used as a command-line interface, and an interface is provided to MATLAB, with other interfaces possible using the SBML standard. Example applications which use ProMoT include those in Bettenbrock et al. (2006) and Waschler et al. (2006).

3.5.4 High-level languages

High-level languages such as Basic, Fortran, C, C++ and Java are a popular choice for the implementation of large, computationally intensive models (e.g. marine hydrodynamics applications (Clement, 1999)), due to the speed of simulation. The main issue with using high-level languages is the necessity to ‘manually’ discretise the equations of continuous time systems before implementing, as well as solving the problems arising from potential algebraic loops. Since there are many discretization techniques available, the same continuous time system may be implemented in very different manners in discrete time, thus leading to disparate results between different implementations. In addition, the code obtained after implementation, in general, runs in a sequential manner (with the exception of subroutines and loops), which would not represent well for e.g. a physiological system, where all parts of the body ‘run’ in parallel.

3.6 Existing large-scale physiology models

Since Guyton first published his original circulatory model in 1972 (Guyton et al., 1972b), it has served as an inspiration and basis for many other integrative physiology models, summarised in Figure 3.4.

A model of overall regulation of the bodily fluids was published in 1979 by Ikeda et al. (1979) and provides a more detailed representation of the renal system than Guyton's original model (Guyton et al., 1972b).

In 1983, a model called HUMAN (Coleman and Randall, 1983) was developed, which markedly extended Guyton's model and allowed the simulation of various pathologies and treatment options on a virtual patient. HUMAN was implemented in sequential Fortran code and suffered with similar drawbacks as Guyton's Fortran implementations. HUMAN was later developed further by Guyton's colleagues and is now available under the QCP (Quantative Circulatory Physiology) Windows software package (Abram et al., 2007). The QCP model consists of 4000 variables (compared to 150 in Guyton's original model from 1972) and hundreds of mathematical functions. QCP describes the cardiovascular, renal, neural, respiratory, endocrine and metabolic relationships in multiple organ systems in the human body. Having been written in the C programming language and being only available as a compiled program, QCP could not be altered in any way by its users, so further development by the wider community was impossible. In order to address this issue, QCP was translated into QHP (Hester et al., 2008) and then HumMod (Hester et al., 2010), which is a slightly extended version of the QCP model, but written in XML, so that it is human- and machine-readable. The code is compiled in C++ and is available for free download on <http://hummod.org/downloads>, but with the lack of a clear block diagram with the model structure, it is difficult to envisage future contribution to it from external sources.

Meanwhile, the MODSIM environment (Montani et al., 1989) was used to simulate a 1992 version of Guyton's model, while block diagrams, clearly describing the model structure and connections, are available for this version of the model, as well as the model equations in code (Montani, 2008).

In 1998 a Simulink model of the human circulatory system was published by Wabel and Leonhardt (1998). This model was based on an earlier model by Coleman (1979), since Wabel saw the need to present the model in a graphical block-diagram simulation environment for improved user friendliness as a teaching and research tool.

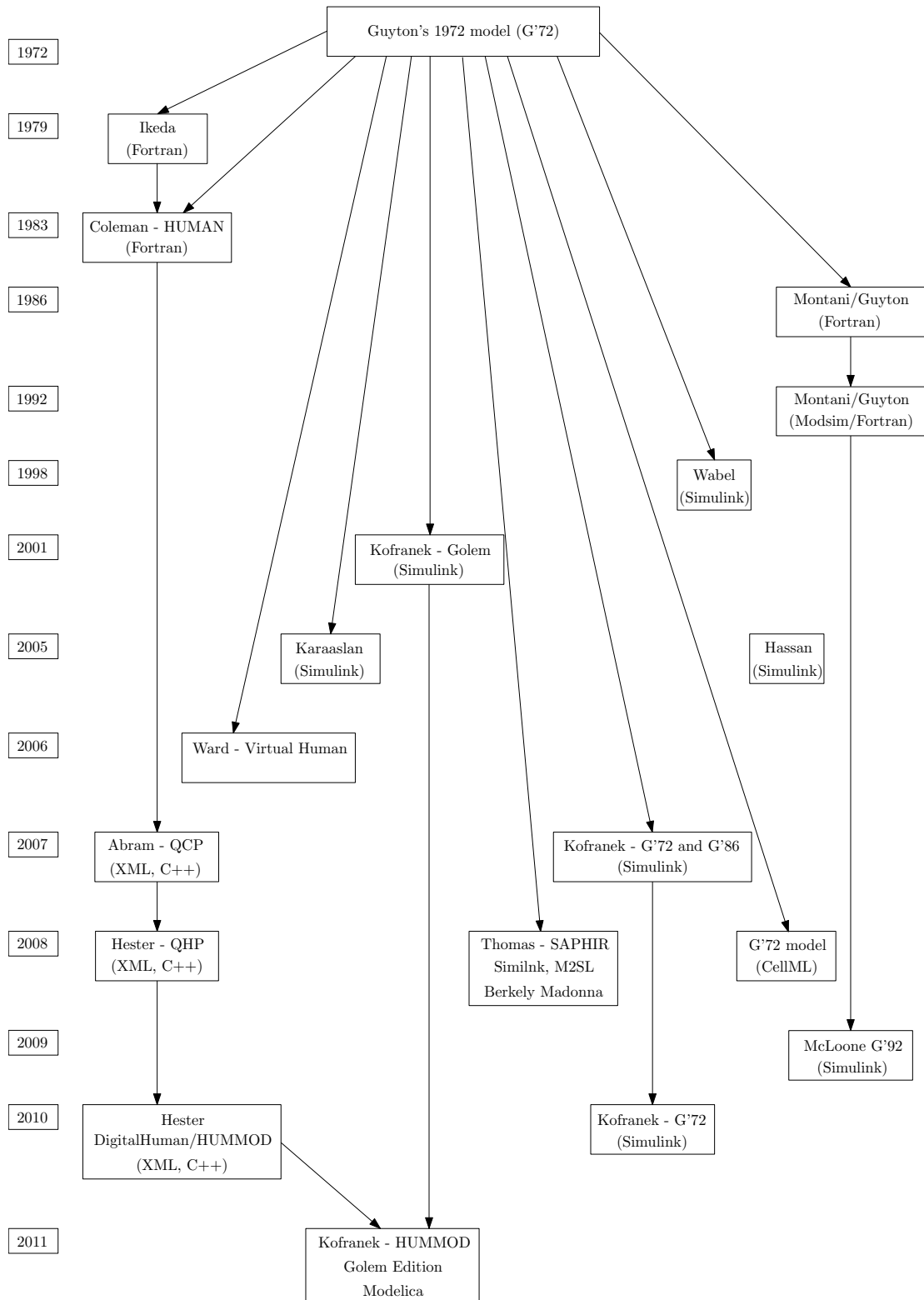


Figure 3.4: Existing integrative physiology models

In 2001 Kofranek et al. (2001) published the development of GOLEM, a multimedia medical training simulator for teaching purposes. The mathematical model behind the simulator was based on models by Guyton et al. (1972b), Cameron (1977), Ikeda et al. (1979) and Coleman and Randall (1983) and was designed for the teaching of acid/base and electrolyte equilibrium, respiration, circulation and the renal system, and it was implemented in the Simulink environment. In 2011, the the HumMod model (Hester et al., 2010) was also implemented in the Modelica environment and was later incorporated in the GOLEM simulator (Kofrnek et al., 2011).

In 2005 Karaaslan et al. (2005) also developed a mathematical model of the cardiovascular system in Simulink, which was based on models by Guyton et al. (1972b), Coleman and Hall (1992) and Uttamsingh et al. (1985). In the same year, Hassan et al. (2005) published a cardiovascular model with disorders also.

In 2006 the Virtual Human/Virtual Soldier project was developed to create complex mathematical models to represent individual soldiers and the models are implemented in PhysioML (Ward et al., 2006). The idea behind this project is to use the holographic medical representations to improve medical diagnosis on and off the battlefield.

In 2007 Kofranek et al. (2007) published a Simulink implementation of Guyton's original model from 1972, as well as an extended version of the model from 1986.

Also in 2007, the SAPHIR project (Thomas et al., 2008) was set up to implemented a collaborative open-source 'toolbox' or library of models and subsystem modules, so that researchers working on different platforms, different modelling and simulation environments, different organs/systems or timescales can share new developments (and implementations of older models, such as Guyton's model from 1972 (Guyton et al., 1972b) and Ikeda's model from 1979 (Ikeda et al., 1979)). The Simulink implementation of Guyton's model under the SAPHIR project, however, is in discrete-time and loses the natural relationship between the model diagrams and the computer implementation in continuous time, as well as creating some odd computational difficulties.

In 2008 Guyton's model (Guyton et al., 1972b) was implemented in the XML-based environment CellML (available at http://models.cellml.org/workspace/guyton_2008). Due to the differences between procedural code (in this case C-code) and declarative languages (CellML), some aspects of the original model were not able to be encapsulated by the CellML model (such as the damping of variables). This may effect the

transient behaviour of the model, however the steady-state behaviour would remain the same.

3.7 Guyton's model implementation

Where modelling of physiological systems is concerned, the question of what level to define the model at always arises. Models can be defined at a multitude of levels and, potentially, models at different spatial levels and different levels of timescale resolution can be integrated. The necessity of such integrated implementation needs to be assessed, taking into consideration the computational intensity, the purpose of the model, and the aptness of carrying a large complexity.

An example of model implementation at the 'macro' level (systems physiology, organ systems) has been shown by Cabrera et al. (1999), who look at the dynamics of lactate production during exercise. The model is in a block diagram form and at the 'Organ systems' (or inter-organ) level in Figure 3.2.

The 1992 version of Guyton's model (Montani, 2008), which is implemented here in the Simulink environment, is at the 'Organ systems' level also and an example of the systems and subsystem levels is shown in Figure 3.5. The top level is shown and two subsystem levels, including one at the lowest, first order, dynamic level.

The 1972 published version of Guyton's model has been implemented by a number of researchers (Kofranek et al., 2007; Thomas et al., 2008) in the Simulink format suggested in this study. A 1986 version of Guyton's model, which was not published, has also been implemented by Kofranek et al. (2007).

In this present study, the most current version of Guyton's model from 1992 was implemented in Simulink, using a set of model diagrams, similar to those published in 1972, and a Fortran code implementation of the model equations in discrete time (Montani, 2008). Our Simulink version of the model was implemented in continuous time, i.e. using continuous-time integrator blocks, while the discretization method for model simulation in Simulink can be chosen from a variety of solvers, with either a fixed- or variable-step size.

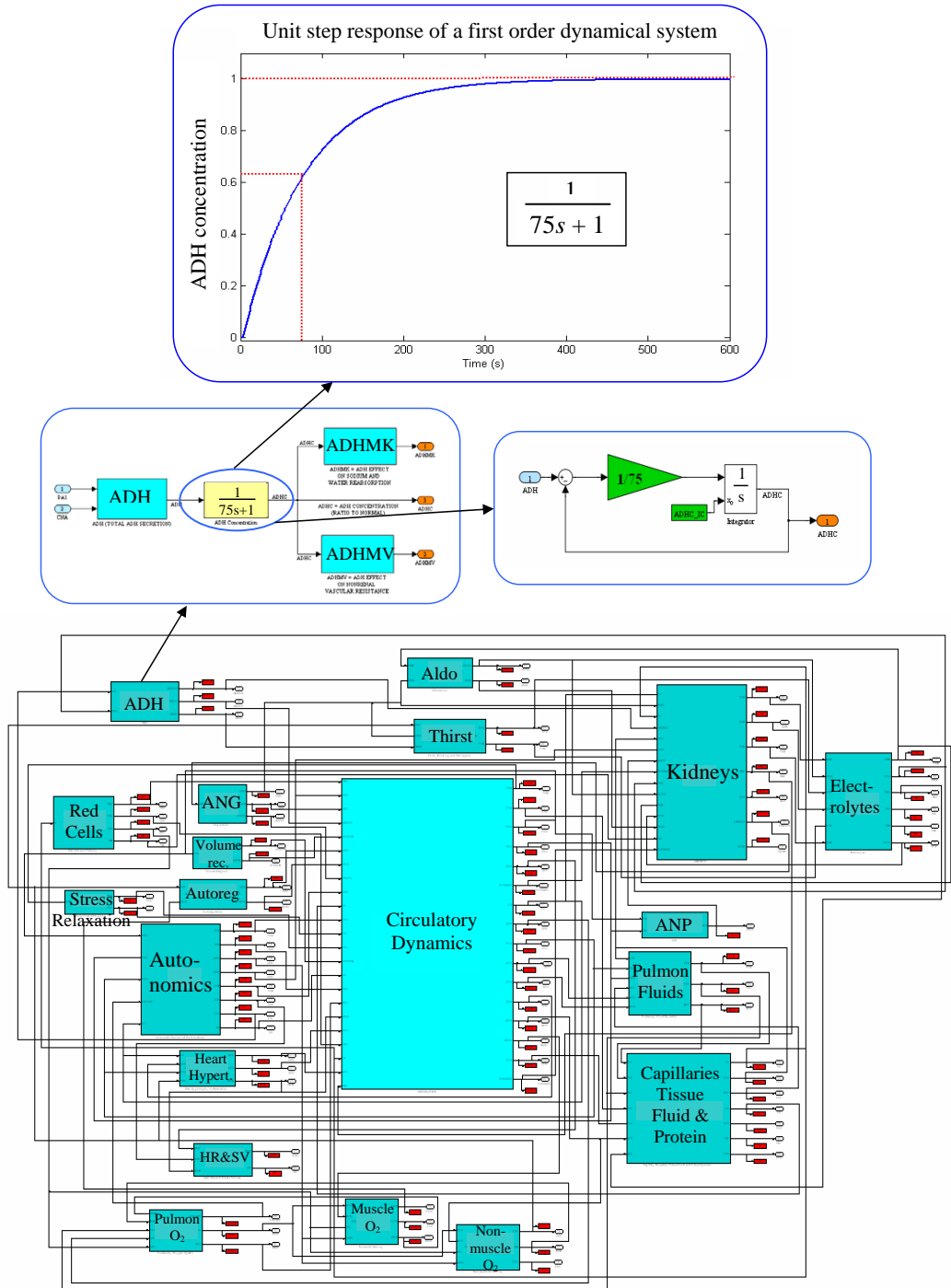


Figure 3.5: Novel Simulink implementation of the 1992 version of Guyton's model

Since the model size, and number of variables and parameters, has increased immensely since the first version of the model from 1972, a hierarchical structure with multiple layers of subsystems were used. At the lowest level, a first order dynamic system was implemented as in the original model diagram (Guyton et al., 1972b) with an integrator, a gain and a summer (the basic blocks of an analog computer), as shown in Figure 3.6, and this level was subsequently 'masked' as a transfer function in the s-domain of the form:

$$G(s) = \frac{Y(s)}{X(s)} = \frac{k_{ss}}{1 + s\tau}. \quad (3.1)$$

This transfer function representational form allows an easy deduction of the system's steady-state gain k_{ss} and time constant τ . Figure 3.7 shows a sample step response of such a first order system, where $k_{ss} > 1$.

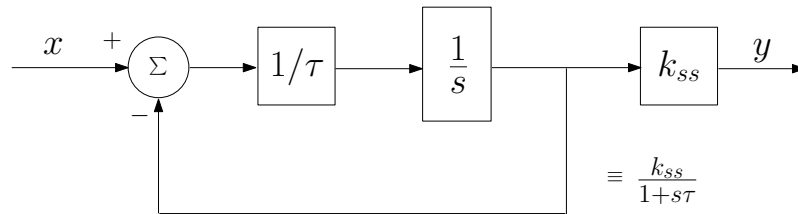


Figure 3.6: First order system with steady-state gain k_{ss} and a time constant τ

Some issues transpired during the model implementation and validation. In the Fortran implementation of the model (Montani, 2008), first order 'damping dynamics' were included. These seem to have been added to avoid numerical instability; however, it is not completely clear whether these dynamics have any physiological function or are simply a feature of the model computer implementation and due to, in particular, a possibly unsuitable discretization method. In addition, most of these discrete-time first order dynamic 'damping' equations included specific integration step sizes, as expected, while a few of the equations did not feature a particular step size. A discrete-time dynamic equation not a function of the integration step size has no continuous-time counterpart and cannot be implemented in our Simulink model without making unreasonable assumptions, such as that the step size is included in the gain parameter, which defines the time constant of the system.

An example of a first order damping equation from the model code used in the MODSIM implementation, the calculation of angiotensin secretion, where a step size is included,

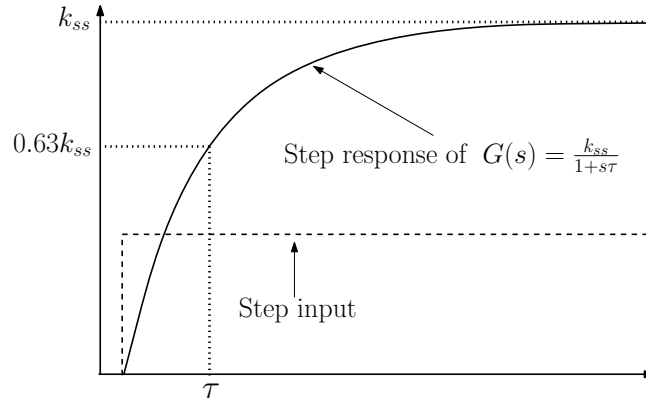


Figure 3.7: First order system step response with steady-state gain $k_{ss} > 1$ and time constant τ

is as follows:

$$ANX1 = ANX1 + (ANX - ANX1)/(ANV * I) \quad (3.2)$$

where:

ANX = angiotensin secretion,

ANX1 = actual ANX after damping,

ANV = time constant of angiotensin secretion, and

I = time incrementation step.

Alternatively, an example of a dynamic equation without the necessary step size is the damping of renal peritubular capillary reabsorption (RFAB1):

$$RFAB = RFAB + (RFAB1 - RFAB)/(RFABDP) \quad (3.3)$$

where:

RFAB = RFAB1 after damping,

RFAB1 = renal peritubular capillary reabsorption, and

RFABDP = RFAB damping factor.

We can only assume that the step size was incorporated into the RFABDP time constant parameter. This is an inadequate implementation solution, since the integration

step sizes seem to vary during model simulation, giving somewhat unpredictable results.

The Simulink model implementation presented here was validated against the 1992 version of Guyton's model, implemented in Fortran and simulated in the MODSIM environment (Montani, 2008). A sample 'reference' experiment, is included here and it is similar to those described in Guyton et al. (1972b) and Thomas et al. (2008). The experiment simulates a reduced kidney mass to 30% of normal and increased salt intake to 9 times normal at the start of the experiment. The responses of the MODSIM implementation and our Simulink version of the model are shown in Figure 3.8. It can be seen that the Simulink model output is comparable to the MODSIM simulation output, while the small difference in response could be due to a number of factors, namely the different discretization methods used and the issues with damping dynamics, as explained earlier. A variable step solver, based on numerical differentiation formulas, was used for the Simulink model, as the system is highly stiff, with time constants varying from a few seconds to over thirty days. It is possible to use a fixed step integration method; however, due to the stiffness of the system, simulation can take a very long time to complete, since the step size must be chosen according to the shortest time constant.

The Simulink models by Kofranek et al. (2007) and especially the 1986 version of Guyton's model (Kofranek et al., 2007), also produce similar results to ours. The model presented in this work, however, is more recent and also presents the first order dynamics in transfer function form, which is more intuitive and gives direct information on steady-state gain and time constant.

The Simulink implementation of Guyton's model under the SAPHIR project (Thomas et al., 2008) differs significantly from the model presented here. Thomas et al. (2008) specified the model in discrete-time, using discrete-time integration blocks and a forward Euler method. In addition, all subsystems were treated as 'atomic subunits'; thus, all computations within a subsystem were executed before moving to the next subsystem. Variable integration step sizes were also employed. All of these described features mimic closely the Fortran implementation of the model and thus do not provide the desirable properties of:

- Providing a generic representation of the underlying continuous-time physiology,

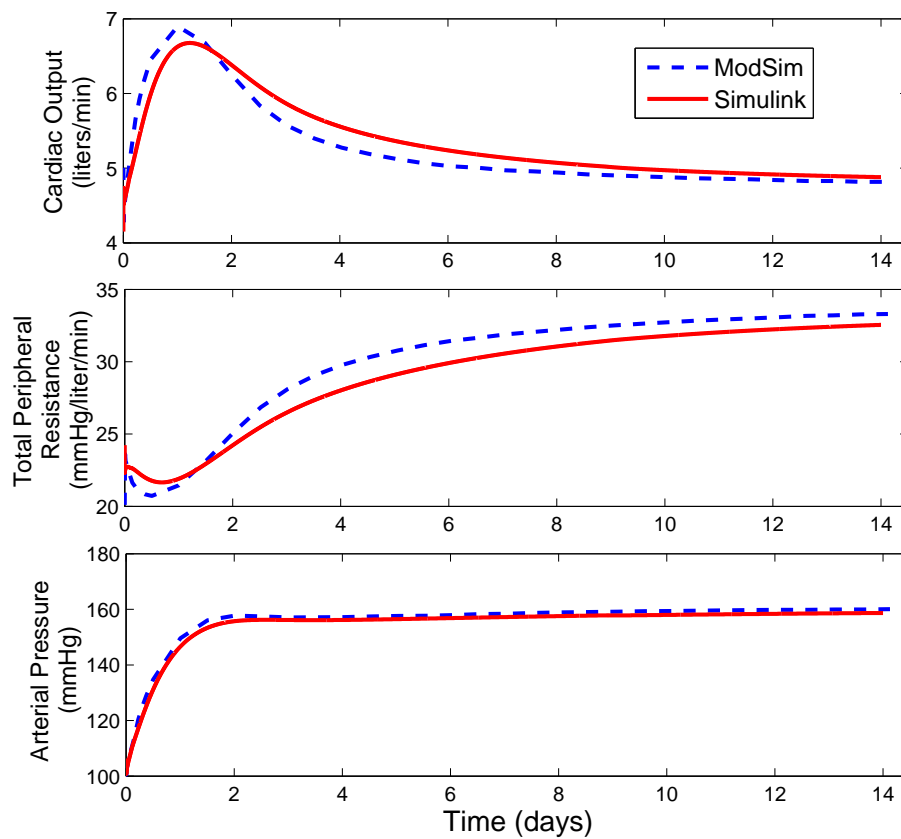


Figure 3.8: Comparison between the MODSIM and the Simulink implementations of the 1992 version of Guyton's model for an experiment with reduced kidney mass and increased salt intake

and

- Using a numerical integration technique, appropriate for the stiff system under consideration, which can be applied consistently across all model subsystems, without recourse to any custom discretization within the model.

Correctly addressing the above two issues is vital if a transportable, open-access model is to be developed. Nevertheless, the use of custom discretization can, in some cases, result in shorter simulation times, but also results in a model where the model and discretization are inextricably intertwined.

3.8 Discussion

Considering the numerous large scale physiological model implementations in the last 40 years, it becomes quite clear that such mathematical models should be managed in a 'community' way to embrace collaboration and advancement in the field and in the current modelling standards. The essential objective of any evolution of the modelling standard is to preserve the original inter-operability ethos, while taking advantage of technological developments and addressing perceived weakness in the 'standard' as experience with it builds. MATLAB's Simulink environment has proven quite popular for the development of large (and small) physiological models, however the commercial nature of the software is becoming problematic. Ironically, MATLAB and its Simulink toolbox were built on the original EISPACK (Smith et al., 1976) and LINPACK (Dongarra et al., 1979) open source libraries. EISPACK AND LINPACK, developed as Fortran libraries to implement eigensystem and linear algebra routines and originating from the Argonne National Laboratory, aimed to be portable, robust and reliable. The Numerical Algorithms Group (NAG) then provided these routines in a commercial package. Issues with MATLAB/Simulink, such as the incompatibility of new and older versions of the software, are becoming frustrating. Building libraries of physiological models is a long-term goal, and as such, it would be difficult to re-implement older models in the newer versions of MATLAB/Simulink at regular intervals, just to keep them compatible with newer developments. Open source standards generally preserve inter-version compatibility as a priority, since they aim to serve community, rather than commercial, needs, therefore a free and/or open-source modelling and simulation environment for community-wide model development would be a natural choice. The benefit of using a well developed commercial tool such as MATLAB's Simulink, however, lies in the fast and easy model development and validation.

Our Simulink model was developed in a single week, though requiring significantly more time to 'validate' it against the 1992 MODSIM Fortran implementation (mainly due to the custom implementation features in the Fortran code). This highlights two issues:

1. The model development time in Simulink can be extremely fast, once the underlying physiological structure is known, even when the model is complex, and

2. Discretization issues can be significant in getting agreement between different implementations of the same model.

Due to the large number of modelling/simulation environments, it may be difficult to impose a single standard on all researchers, who may have very different backgrounds. Simply using a common interface could be a practical solution to the problem (e.g. CellML or QHP); however metadata containing information about the numerical integration method needs to be included.

In summary, three main components are necessary for successful model development, implementation and improvement:

- A modelling tool - preferably graphical, which allows networks or interconnections of subsystems to be built up in a hierarchical manner,
- Simulation tools, with the ability to simulate ODEs, DAEs and partial differential equations and implement a variety of numerical integration methods, including the efficient solution of stiff systems, and
- A non-proprietary interface standard, probably XML-based, which allows models to be readable across a wide variety of platforms.

3.9 Conclusions

Over forty years ago, Dr. Arthur Guyton suggested that circulatory physiology was starting to change into, and use the techniques of, engineering science (Guyton et al., 1972b) and his model made large strides towards this change. Unfortunately, his famous circulatory physiology model has not developed significantly since 1992 in the practical form of a block diagram of systems and subsystems. A variety of simulation environments and existing large scale physiological model implementations have been examined here with a view to present options for future modelling and simulation developments; however not many environments allow the desired visual diagrammatic representation and speed of implementation.

Some computer implementations of the original 1972 Guyton model exist (Thomas et al., 2008; Kofranek et al., 2007), as well as an implementation of a 1986 version of the model (Kofranek et al., 2007); however the Simulink model presented here is the

first implementation of the most recent 1992 version of the model. If a core model is to be created and made available for extension/improvement, it should be the most up to date model recognised by the research and teaching community.

Guyton's model has been expanded previously under the QHP project, and with the QHP computer program now being open source, the community can, in theory, contribute to it. This new model, however, is implemented in an XML format and is difficult to read. In addition, appropriate structures have not been put in place to deal with model additions and a repository system for alternative model subsystems has not been created.

Technical implementation issues also make QHP unsuitable for development as a community project. Differential equations are implemented using one of three provided methods, where the model developer has to nominate a particular discretization method for each equation. The discretization methods include a first order (forward difference) Euler method and a stiff system discretization method, while the third method is undefined. The QHP model is defined in an XML format, while the model solver can be downloaded only in executable form from the QHP website, but details of its features are not available. QHP could be a good solution with further development. A graphical environment for faster development time would be very beneficial while better transparency and documentation in relation to the solver is required. Finally, a repository system, catering for community contributions to the model needs to be created, if it is truly to be treated as an open-source resource.

For the present, Simulink remains one of the few viable options for large scale model visualisation and implementation. Both development and validation are fast and easily executed with an intuitive graphical environment and results display. MATLAB also allows us to emulate the continuous-time nature of physiological systems by using continuous-time dynamic blocks and allows us to select an appropriate solver for the system. Nevertheless, compatibility issues impinge significantly on the utility of Simulink as a community platform on which an integrated physiology model can evolve.

Finally, if a common XML standard is to be agreed upon, as a model sharing interchange standard, three important features must be complied with:

- The model needs to be specified in continuous-time as a fundamental representation,

- Discretization information needs to be included as metadata, and
- Graphical editing tools, allowing block diagram representation with hierarchical visualisation capabilities must be available.

These features would ensure the successful reproduction and simulation of the model in any chosen environment, given suitable conversion tools, such as in Pop and Fritzsou (2003), Dempsey (2003) and Hornych et al. (2002).

Chapter 4

A model for salt-induced hypertension in Dahl rats

4.1 Introduction

As previously outlined in Section 2.4.1, a large proportion of the human population is salt-sensitive and salt-sensitive individuals are more likely to develop hypertension and cardiovascular disease (Weinberger et al., 2001). A common animal displaying salt-sensitivity is the Dahl-S rat, frequently used to study the interacting factors causing salt-induced hypertension (SIH) (Dahl and Schackow, 1964). The availability of new measurement and instrumentation technologies has allowed continuous long-term collection of blood pressure data, providing the opportunity to study the exact time course of the development of SIH (Van Vliet et al., 2006). This study examines the data from four different experimental protocols involving Dahl-S rats and a number of mathematical models are developed to describe the relationship between high salt intake and blood pressure.

4.2 Experimental Protocols

All experimental protocols, previously described in Van Vliet et al. (2006) and McLoone et al. (2009), include 3-month old male Dahl-S and Dahl-R rats from the Brookhaven strain, provided with food and water ad libitum, at an ambient temperature of 22°C, and a 12-h light/12-h dark cycle. Blood pressure was measured in the abdominal aorta and the measurements were transmitted using telemetry technology. A recovery period of at least 1 week, following surgery to implant the blood pressure measurement and telemetry device, was allowed before the experiments commenced. BP was recorded continuously for the duration of the protocols, and the daily mean BP levels were calculated as the average level of mean arterial pressure sampled once or twice each minute. The control, or regular salt, diet contained 0.7% NaCl, while the experimental, high-salt, diet contained 4% NaCl. Four distinct experimental protocols were used in this chapter. Protocols 1 and 3 comprise two data sets each, one for Dahl-S rats and one for Dahl-R rats, while protocol 2 contains one data set for Dahl-S rats and protocol 4 includes one data set for hybrid rats (progeny of Dahl-S and Dahl-R rats).

4.2.1 Protocol 1: Time evolution of salt-induced changes of blood pressure in Dahl-S rats

Experimental protocol 1, described in detail in Van Vliet et al. (2006), was conducted on nine Dahl-S rats. After a control week on a regular salt diet (0.7% NaCl), a step increase in dietary salt intake (4% NaCl) was applied for 6 weeks, followed by a 4-week recovery period with regular salt intake. A set of seven Dahl-R rats were used as control subjects and were fed the same diet as the Dahl-S rats. Figure 4.1 shows plots of the individual animals and the average responses for the Dahl-S and Dahl-R groups, as well as the associated salt intake levels. The average responses are referred to as the ‘mean animal’ in this thesis and represent the signal obtained by averaging all data recordings within a data set at each point in time. It is important to note that the ‘mean animal’ is an average response across all animals in the data set and no actual animal has such response, though some animals’ responses can be very similar to the mean response.

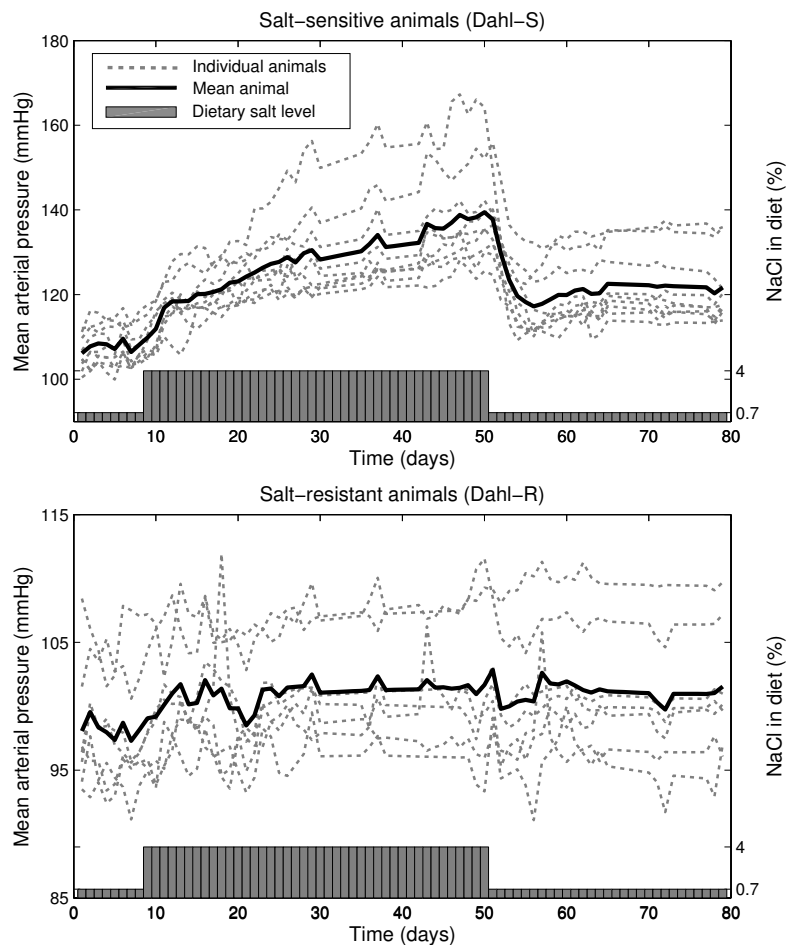


Figure 4.1: SIH Protocol 1, individual and ‘mean animal’ responses for the Dahl-S and control Dahl-R animals

4.2.2 Protocol 2: Reversibility of salt-induced changes in blood pressure in Dahl-S rats

Experimental protocol 2 investigated the reversibility of salt-induced hypertension and was originally reported in Van Vliet et al. (2006). The experiment was performed on five male Dahl-S rats. During weeks 1, 3, 7 and 11 of the experiment, the animals were given a normal salt diet of 0.7% NaCl, while during weeks 2, 4-6 and 8-10, dietary salt intake was increased to 4% NaCl. Figure 4.2 shows a plot of the mean arterial pressure response to salt intake for the individual rats and gives the average, or ‘mean animal’ response as well.

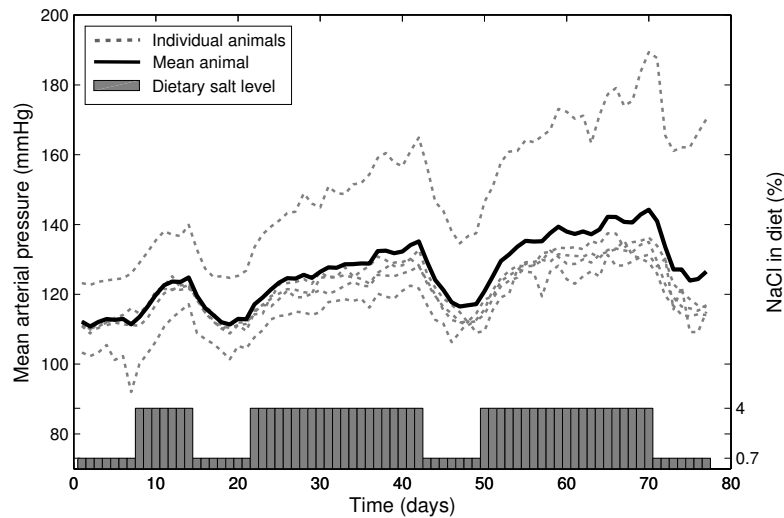


Figure 4.2: SIH Protocol 2, individual and ‘mean animal’ responses

4.2.3 Protocol 3: Response of blood pressure in Dahl-S and Dahl-R rats to a pseudo random binary sequence (PRBS) salt input

Protocol 3, described in McLoone et al. (2009), investigates the effect of short-term variations in salt intake on the daily MAP levels of eight Dahl-S rats and five control Dahl-R rats. The salt levels in the diet were varied between regular- and high-salt levels in a pseudo-random binary sequence manner where, at each day of the experiment, the level of salt was either changed (from high to regular or from regular to high) or it stayed the same. The protocol was 72 days long in total.

The dietary salt level was manipulated in the following manner, 000000000 1111110 1010110 0110111 0110100 1001110 0010111 1001010 0011000 0100000, with each ‘0’ representing a 24-hour exposure to a regular-salt diet (0.7% NaCl) and each ‘1’ representing a 24-hour exposure to high-salt diet (4% NaCl). Figure 4.3 shows plots of the MAP responses of individual animals, as well as the ‘mean animal’, for the salt-sensitive and salt-resistant rats, in addition to the salt intake levels.

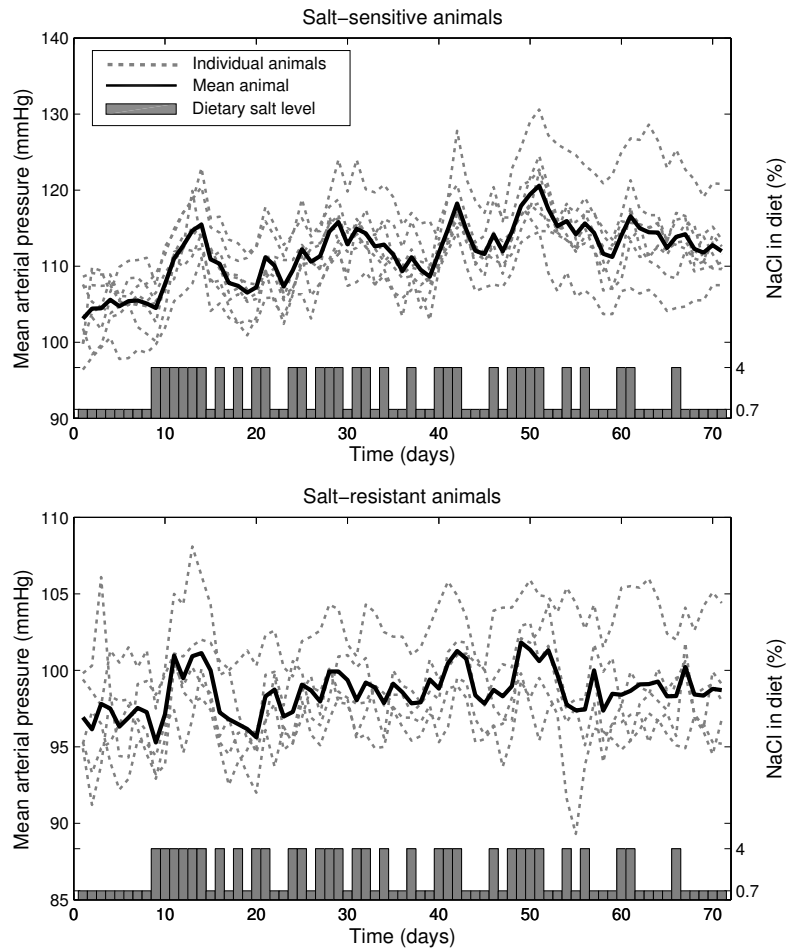


Figure 4.3: SIH Protocol 3, individual and ‘mean animal’ responses for the Dahl-S and control Dahl-R animals

4.2.4 Protocol 4: Time evolution of salt-induced blood pressure changes in Hybrid rats

Protocol 4, described in detail in Van Vliet et al. (2006) and similar to Protocol 1, was conducted to study the BP response to a step increase in salt level in the diet of rats. Thirteen male F_2 -hybrid rats, the progeny of a cross between Dahl-S and Dahl-R rats, were studied. Following a control week on a regular-salt diet containing 0.7% NaCl, a high salt diet of 4% NaCl was provided for 10 weeks and then returned to a regular-salt diet for 1 week. The 24-hour average MAP responses are presented in Figure 4.4 for individual animals and for the mean of the hybrid rat data set.

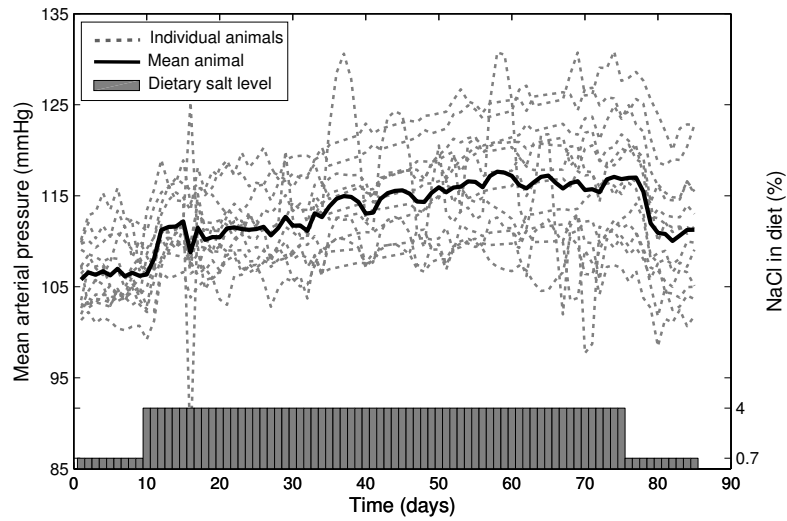


Figure 4.4: SIH Protocol 4, individual and ‘mean animal’ responses for the hybrid animals

4.3 Model structure development

Based on the literature motivation, presented in Section 2.4.1, for a multi-phasal response of blood pressure to a high-salt intake, a number of model structures, of varying complexity, are developed in this chapter. The model structures aim to represent the main features of the blood pressure response, without fitting noise or random variations, which are generally animal-specific and lead to overfitting. The ‘mean animals’ for each data set were used to determine the model structures, since the average of all data in a data set is relatively noise-free and emphasises the main characteristic features present in most of the animals within the data set. For each of the model structures, the model input was defined as the salt content of the animal’s diet (in %), while the model output was the MAP variation from baseline. The baseline pressure was taken as the mean blood pressure over the week before a high-salt diet was commenced. Three incremental model structures will be presented in the following sections, and an attempt will be made to provide a potential explanation for each component of each structure, in order to deliver a model with as much physiological fidelity as possible with respect to the available experimental data. The initial model contains 3 components, while additional elements are subsequently included, in 4- and 5-component models, in order to improve the model fit and to provide sufficient flexibility to capture more subtle, but important features in the MAP response.

4.3.1 3-component model

An initial three-component model, presented in Figure 4.5, was developed to capture the main blood pressure response features and incorporates the following basic elements:

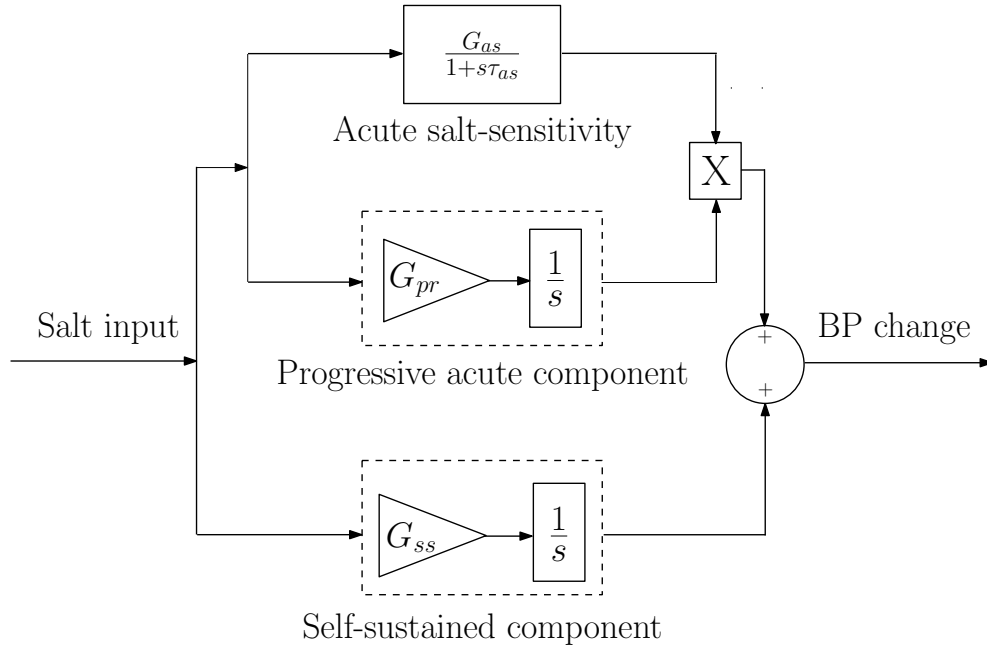


Figure 4.5: SIH 3-component model structure

- An ‘Acute salt-sensitivity’ component, comprising a first order transfer function with a steady state gain G_{as} (mmHg/%NaCl) and a time constant τ_{as} (days). The element of the blood pressure response resulting from this model component is an exponential, and is evident in the data from all four experimental protocols, shown in Figures 4.1 - 4.4. The ‘acute salt-sensitivity’ component represents the reversible rise in BP over the days to weeks, following a step increase in salt intake and shown in studies in salt-sensitive humans (Kawasaki et al., 1978), monkeys (Srinivasan et al., 1984), mice (Leonard et al., 2006), and rats (Osborn and Hornfeldt, 1998; Van Vliet et al., 2006). This component possibly denotes the re-establishment of sodium balance, as described in Section 2.4.1. The gain G_{as} determines the degree of acute salt-sensitivity and is inversely proportional to the slope of the chronic pressure natriuresis curve, shown in Figure 2.3.
- A ‘Progressive-acute’ component is included, consisting of an integrator term with gain G_{pr} , which creates a progressive and irreversible amplification of the gain G_{as}

of the ‘Acute salt-sensitivity’ component of the model, and is proportional to the length of high-salt diet exposure. In practice, G_{as} is amplified by a factor of ‘ $G_{pr} \cdot (\text{increase in dietary salt content above baseline level of } 0.7\% \text{ NaCl}) \cdot (\text{time spent above baseline salt level in days})$ ’. This effect is consistent with progressive worsening of the acute salt-sensitivity and has been demonstrated in chimpanzees (Denton et al., 1995), rats (Dahl et al., 1968) and humans (Weinberger and Fineberg, 1991). The ‘Progressive acute’ component represents the effect of high salt intake to increase acute salt-sensitivity and has an effect to progressively decrease the slope of the pressure-natriuresis curve. Again, physiological changes due to the prolonged exposure to high-salt diet and/or high blood pressure are possibly responsible for the increase in salt-sensitivity.

- A ‘self-sustained’ component consisting of a simple integrator with a gain G_{ss} , simulating a slow, progressive and irreversible BP increase in blood pressure while salt intake remains high and even after returning to baseline level of 0.7%NaCl. A self-sustaining hypertension due to exposure to a high-salt diet, which continues after the end of a high-salt intake period, is evident again in all four protocols, but is most obvious in the BP data of Protocol 1 (Figure 4.1), where the animals were allowed a number of weeks to recover from the high-salt diet, yet blood pressure remained well over the baseline up to the end of the experiment. As already outlined in Section 2.4.1, a possible cause for this element of the blood pressure response may be the presence of some renal injury or vascular remodelling and has been previously shown in outbred rats also (Dahl, 1961).

4.3.2 4-component model

Even though the three-component model includes elements to represent the general characteristics of the blood pressure response to a step increase in salt intake, some aspects of the response cannot be modelled. The tendency of blood pressure to undershoot when the high-salt input has been removed, and before it settles to its new steady state value, is evident in Protocols 1, 2 and 4, but most apparent in the data from Protocol 1 (Figure 4.1). It is impossible to achieve the undershooting response without including an additional component to the three-component model.

The four-component model, featuring a ‘compensatory’ element, and designed to help

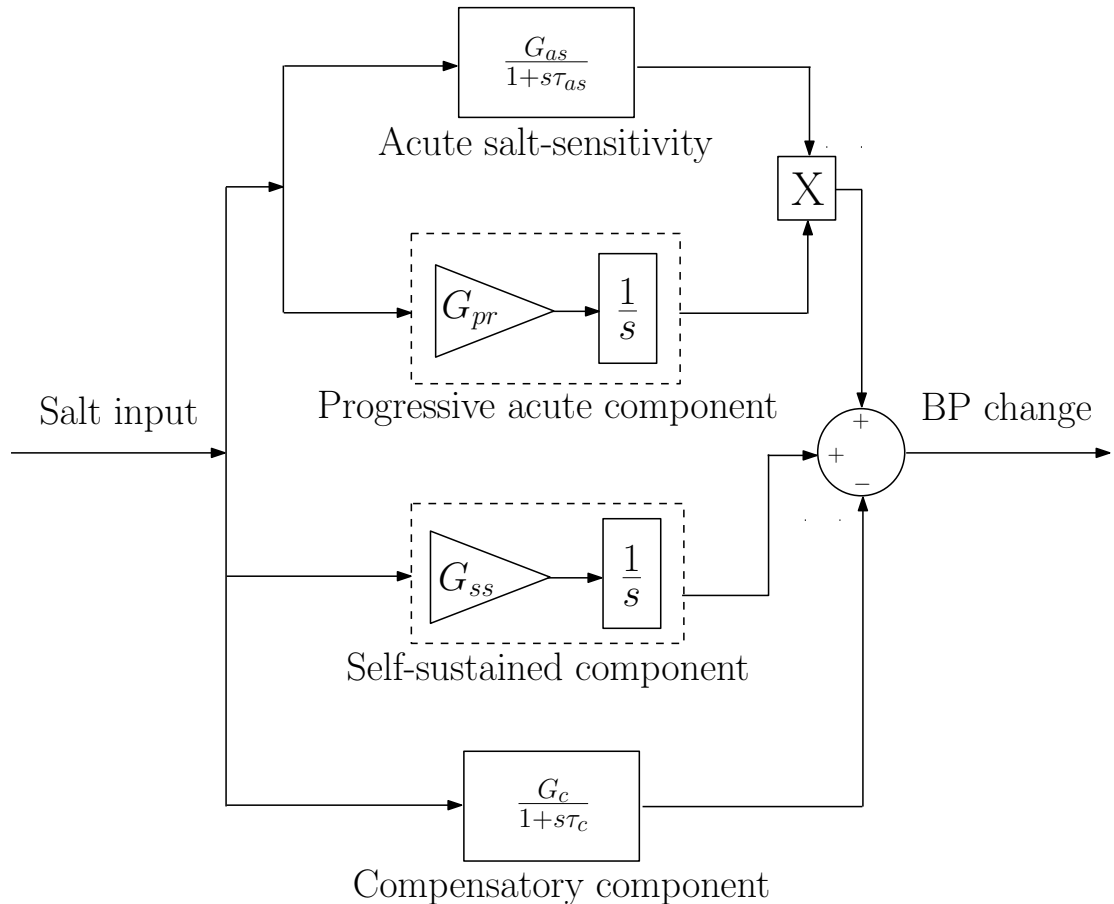


Figure 4.6: SIH 4-component model structure

model the overshoot in the data, is shown in Figure 4.6. The ‘Compensatory’ component consists of a first order transfer function, whose response opposes the increase in BP due to high salt intake (the output of the ‘Compensatory’ component is *subtracted* at the summation point of all BP responses shown in Figure 4.6). This compensatory effect is generally consistent with the physiology of the blood pressure control system, where numerous systems balance their effects to maintain the required blood pressure levels. Systems that, under normal circumstances, counteract the blood pressure increase due to high salt intake, include the renin-angiotensin-aldosterone system (Cholewa and Mattson, 2001; Denton et al., 1995) atrial natriuretic factor (Mullins et al., 2006) and nitric oxide release (Simchon et al., 1989), however some of these systems may be impaired in Dahl-S rats (Simchon et al., 1989).

4.3.3 5-component model

A close examination of the data in all four protocols confirmed that the transient BP response during a step increase in salt intake is actually different to the response during step decrease in salt intake. Consequently, a further set of dynamic components was added to the 4-component model to enhance the model response by accounting for different rates of BP increase and decrease during the stimulation and relaxation phases of the experiments (increase and decrease of salt contents in the diet). The resulting 5-component model comprises an additional switch, along with separate ‘stimulation’ and ‘relaxation’ dynamics of the ‘Acute salt-sensitivity’ component (Figure 4.7). Consequently, during high salt intake, the ‘Stimulation’ component of ‘Acute salt-sensitivity’ is activated, while when the high salt stimulus is removed, the ‘Recovery’ component takes over. This is reasonable, since substances involved in BP control may have different formation and dispersion mechanisms and rates, leading to different time constants.

4.4 Model parameter determination

The parameters of all model structures, proposed during the model development process, were initially determined by visual inspection to fit the ‘mean animal’ for each of the data sets. Subsequently, the parameters of each model structure was numerically optimised for the ‘mean animal’ of each data set, as well as for all individual animals from all available data sets.

The MatLab Simulink environment was used for model implementation, while the parameter optimisation was accomplished using a Nelder-Mead simplex algorithm (Nelder and Mead, 1965), implemented in the MATLAB Optimisation toolbox. The objective function to be minimised (J) was defined as the mean squared error (MSE) between model results and experimental data, defined in Equation (6.2). The MSE was used as a measure of model fit since it disregards whether the number is negative or positive and, thus, avoids the positives and negatives canceling each other out, but also the MSE penalises larger errors more heavily.

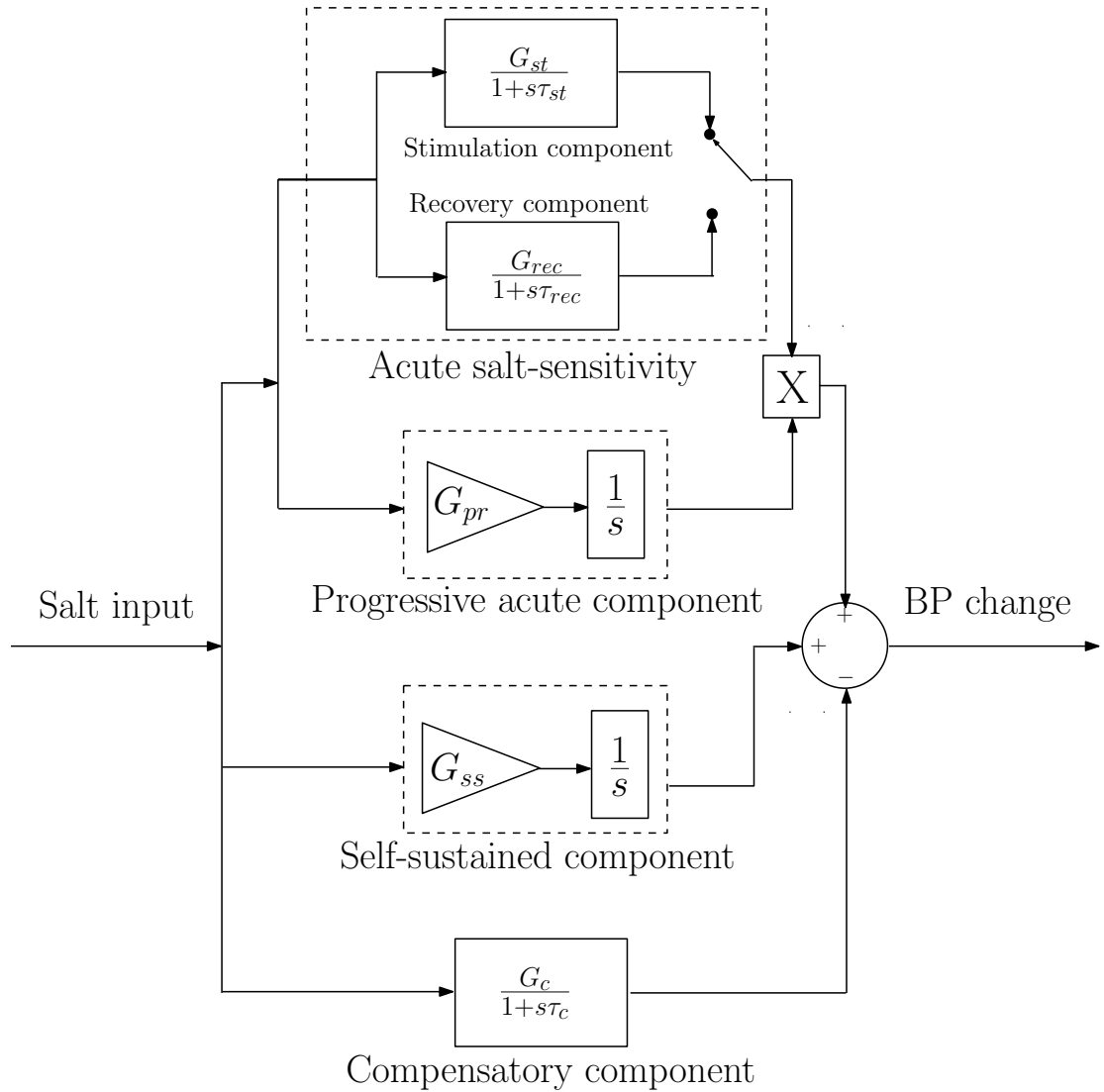


Figure 4.7: SIH 5-component model structure

$$J = \frac{1}{N} \sum_{i=1}^N (y_i - \hat{y}_i)^2 \quad (4.1)$$

where,

- N is the number of samples in the data,
- \hat{y}_i is the blood pressure data obtained from the model simulations, and
- y_i is the experimental blood pressure data.

The Nelder-Mead simplex optimisation algorithm was selected due to its suitability for multidimensional unconstrained problems. The simplex method is an iterative direct search technique, which employs $(n + 1)$ -point simplices in n -dimensional space (for

example for a 2-dimensional problem a simplex has the shape of a triangle). The value of the function to be minimised is obtained at each vertex of the simplex, and at each iteration, the simplex point with the highest function value is replaced with a new lower-value point. This movement of the simplex towards the function minimum is achieved using some basic operations:

- reflection and/or expansion,
- contraction, and
- reduction.

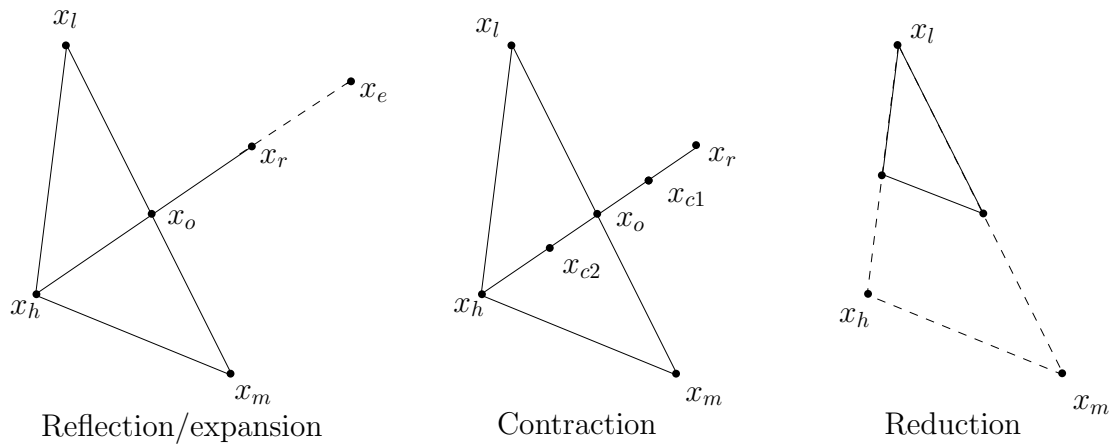


Figure 4.8: Simplex method operations

The simplex method operators are illustrated in Figure 4.8 (for a two-dimensional problem). Briefly, the reflection operation is used in the following manner: each simplex has three starting points, in the case of a two-dimensional problem. A new simplex point (x_r) is obtained by reflecting the point with the highest objective function value (x_h) through the centroid (x_o) of the two lower simplex points (x_l and x_m). If the new simplex point x_r is found to have the lowest objective function value of all simplex points (i.e. point x_r has the best data fit), the expansion operation can be applied, so that the vertex point x_r can be expanded along the same direction to search for the function minimum, and the point x_e is obtained.

If the initial reflection operation is not successful, i.e. a lower value than x_h is not achieved, the contraction operation can be applied, so that the new point is moved back in direction towards the original point (x_h) in search for an improvement in the

function value, obtaining either x_{c1} or x_{c2} , depending on the value of the function $f(x_r)$ relative to $f(x_h)$. At any stage, when the objective function is evaluated at a particular point, if a point better than x_h is found, x_h is replaced and the process starts again, with the reflection operation. If the basic operations of expansion and contraction fail to find a better point than x_h , the simplex appears to contain the minimum objective function point and therefore reduction of the simplex is applied around the best current point x_l . The simplex search can then begin from the start until a convergence criterion is met.

The simplex method is a fast and computationally efficient optimisation technique, which does not require knowledge of the gradient of the objective function. However the simplex method does not guarantee that a global minimum will be obtained and the final result is dependent on the starting point, therefore a variety of initial conditions should be tried.

4.5 Results

In this section, the results for each data set are presented for each of the three model structures. Each set of results will include parameter values and errors for the four different experimental protocols, which include 6 data sets in total:

- Protocol 1 comprises two data sets, one for nine Dahl-S rats and one for seven Dahl-R rats,
- Protocol 2 contains one data set for five Dahl-S rats,
- Protocol 3 includes two data sets, one for eight Dahl-S rats and one for five Dahl-R rats, and
- Protocol 4 has one data set for 13 hybrid rats.

Error results were obtained by comparing experimental data with the model response and are presented in the form of the mean absolute error (MAE), rather than the MSE form used for model optimisation. The MAE indicates the average difference between each point in the data and the corresponding point in the model response in mmHg, which is a more intuitive measure of model fit.

The results presented in this chapter include:

- the model parameters and errors obtained for the ‘mean animal’ of each data set, and
- the *average* parameter values and *average* errors for the *individual* animals across each data set, accompanied by the associated standard deviations.

A detailed account of the results for each individual animal can be found in Appendix A, while summary results are shown in the following section.

The results of an F-test, which assesses whether the increase in model complexity in the 4- and 5-component models, compared to the 3-component model, is justified, are presented in Section 4.5.4.

4.5.1 3-component model

This section presents error and parameter estimation results for the 3-component model structure, and includes plots with the model responses compared to the experimental data.

Figure 4.9, parts A, B and C, show a comparison of the model results with the experimental data for the ‘mean animal’ of each data set involving Dahl-S rats from protocols 1, 2 and 3, while plot D shows the ‘mean animal’ response for the hybrid rats in Protocol 4.

The 3-component model seems to capture well the main characteristics of the model response, shown in Figure 4.9, especially in the case where the high-salt intake is sustained over a number of days to weeks, as in Protocols 1 and 2. In the case of the PRBS-style stimulus in Protocol 3, the 3-component model seems to lack the complexity to respond to rapid changes in salt-intake. Another issue evident from the model responses is the inability to represent the undershooting blood pressure response when salt intake switches from high to low, most evident in the Protocol 1 results (Figure 4.9 A).

Table 4.1 presents the mean absolute errors and the model parameters resulting from the optimisation of the 3-component model to fit the ‘mean animals’ from the four experimental protocols, while Figure 4.10 shows the contribution of each of the elements in the 3-component model to the overall BP response.

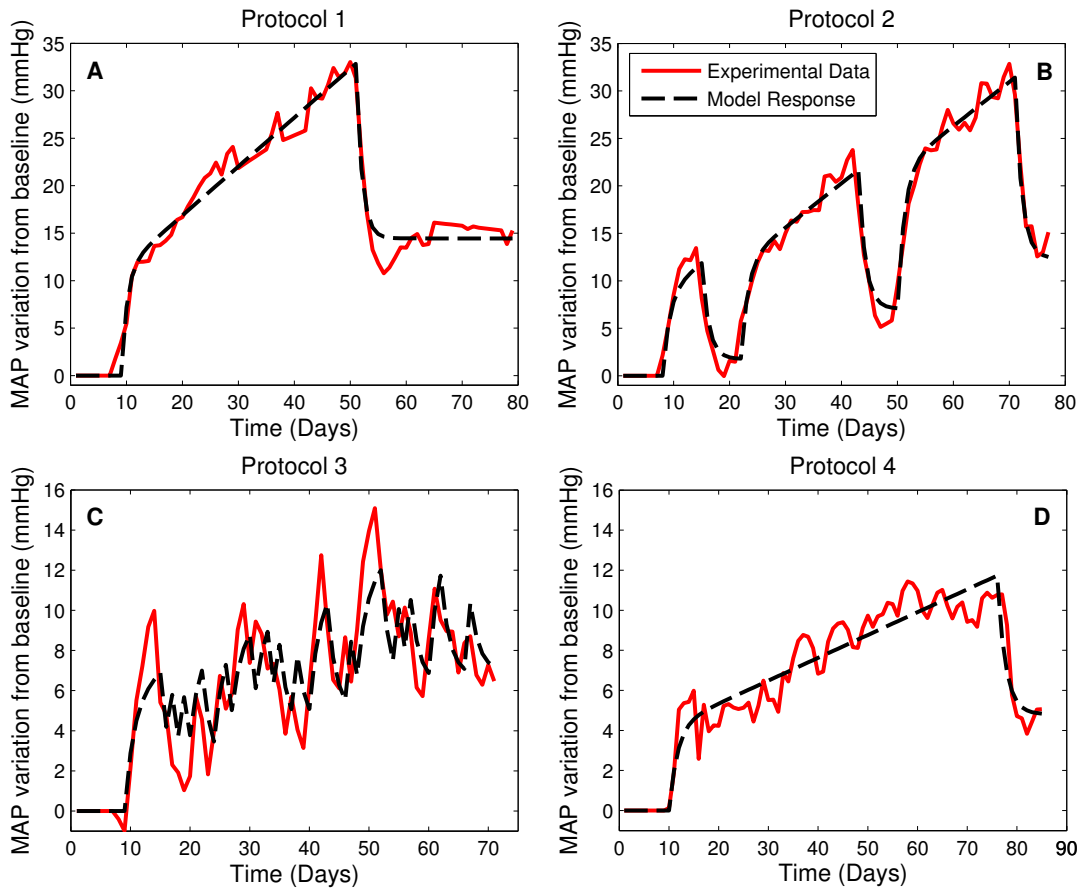


Figure 4.9: ‘Mean animal’ model response for the 3-component model structure

From both the parameter values and the plot of the various model component responses, it is evident that each of the model components plays an important role in the blood pressure response to high salt intake. The acute salt-sensitivity component, as expected, represents the blood pressure increase within a few days of the onset of high-salt intake. In addition, both irreversible model components, namely G_{ss} and G_{pr} seem to have a large effect on the BP levels, with a large self-sustained BP increase due to G_{ss} and a substantial increase in the acute salt-sensitivity response due to G_{pr} .

The promising results obtained for the ‘mean animals’ shown in Figure 4.9 led to the parameter optimisation of the 3-component model for each individual animal as well. Table 4.2 shows the average values of the model parameters and the associated standard deviations for the four experimental data sets comprising salt-sensitive and hybrid animals, and, for comparison, the results for the control salt-resistant animals from Protocols 1 and 3 are given in Table 4.3. There is a significant variation in the parameter values between control animals, reflected in the standard deviation values. This

Table 4.1: ‘Mean animal’ model MAEs and parameters for the 3-component SIH model

<i>Protocol</i>	<i>Protocol1</i>	<i>Protocol2</i>	<i>Protocol3</i>	<i>Protocol4</i>
<i>MAE</i>	1.192	1.257	1.727	0.872
G_{as}	3.3975	2.626	1.660	1.275
$\tau_{as}(\text{days})$	1.0698	1.283	1.548	1.701
G_{pr}	0.0046	0.007	0.002	0.003
G_{ss}	0.1043	0.077	0.066	0.022

Table 4.2: Average individual animal MAEs and parameters for the 3-component SIH model

<i>Protocol</i>	<i>Protocol1</i>	<i>Protocol2</i>	<i>Protocol3</i>	<i>Protocol4</i>
<i>MAE</i>	1.915 ± 0.644	2.213 ± 0.796	2.034 ± 0.335	1.112 ± 0.271
G_{as}	3.4680 ± 0.4264	2.617 ± 1.655	1.6593 ± 0.6819	1.268 ± 0.599
$\tau_{as}(\text{days})$	1.3035 ± 0.4649	1.470 ± 0.489	1.5784 ± 0.2884	1.852 ± 0.287
G_{pr}	0.0045 ± 0.0035	0.013 ± 0.008	0.0065 ± 0.0129	0.004 ± 0.003
G_{ss}	0.1035 ± 0.0284	0.073 ± 0.079	0.0647 ± 0.0463	0.025 ± 0.024

variation, however, is not surprising considering the diversity of BP responses to identical stimuli, shown in Figures 4.1–4.4, due to differences in the salt-sensitivity levels between animals.

Table 4.3: Average MAEs and parameters for the control Dahl-R rats for the 3-component SIH model

<i>Protocol</i>	<i>Protocol1</i>	<i>Protocol3</i>
<i>MAE</i>	0.842 ± 0.191	1.293 ± 0.081
G_{as}	1.041 ± 0.732	0.681 ± 0.426
$\tau_{as}(\text{days})$	2.101 ± 2.834	6.459 ± 10.723
G_{pr}	-0.004 ± 0.003	0.014 ± 0.013
G_{ss}	0.027 ± 0.010	-0.011 ± 0.043

A comparison between the results for the salt-sensitive (Table 4.2) and salt-resistant (Table 4.3) animals show that the acute salt-sensitivity component gain G_{as} is much lower for the salt-resistant animals, as expected, while the progressively increasing G_{pr} gain and the self-sustained component G_{ss} gain are either very small or even negative

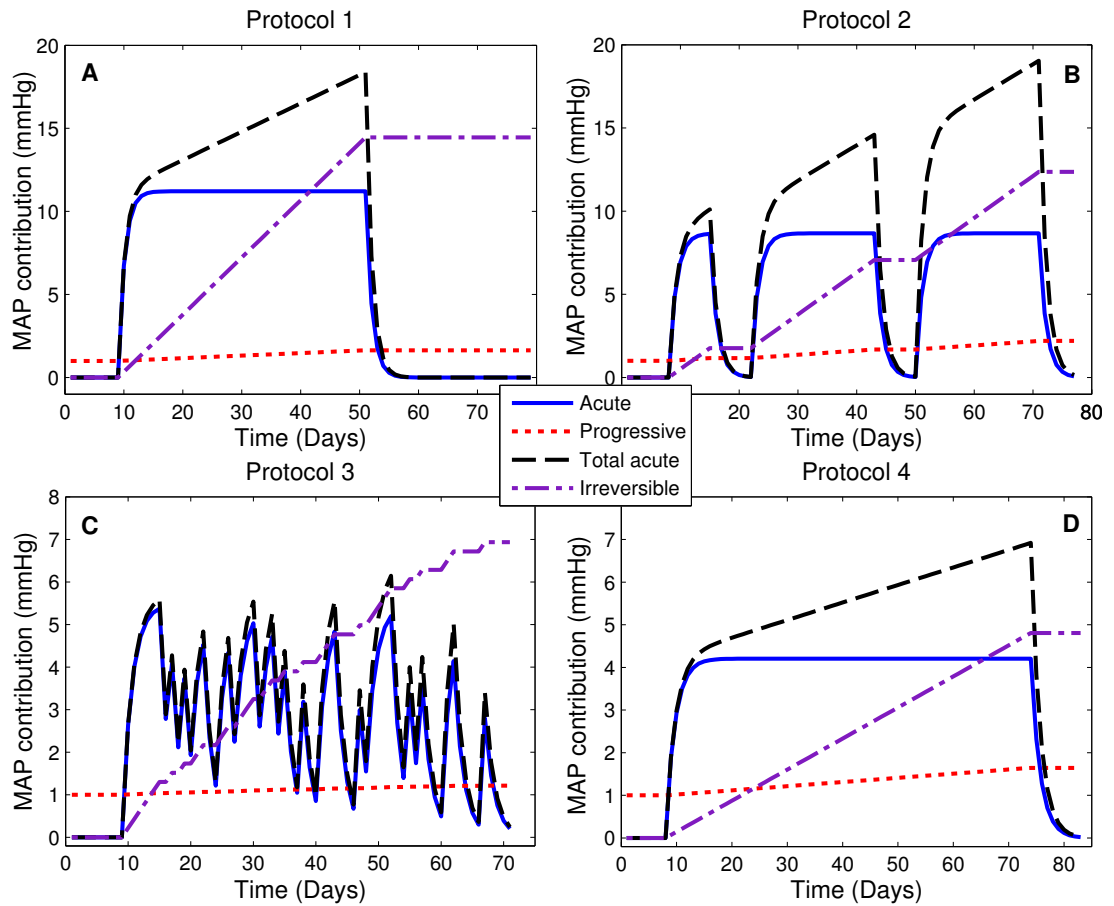


Figure 4.10: Model component contribution for the 3-component ‘mean animal’ model

for some individual salt-resistant animals. A negative value of the G_{pr} gain leads to a decrease in the total acute salt-sensitivity component, while a negative G_{ss} value results in a long-term blood pressure decrease, which appears to be irreversible for the duration of the experiments. The time constant of the acute salt-sensitivity component τ_{as} is longer for the Dahl-R animals, indicating that if they have any BP increase due to high-salt intake, it is much slower than in the Dahl-S case. The hybrid animals of Protocol 4 (Table 4.2) have average parameter values that fit between those of the Dahl-S and Dahl-R animals, as their genetic make-up varies between salt-sensitive and salt-resistant.

4.5.2 4-component model

Figure 4.11 presents the 4-component model response compared to the experimental data for the ‘mean animals’ for the salt-sensitive animals in Protocols 1, 2 and 3 (plots

A, B and C, respectively) and the hybrid animals of Protocol 4 (plot D). The additional compensatory component in the 4-component model (shown in Figure 4.6) provides for a better fit across all data sets. The improvement in model fit, however, is most noticeable in the case of Protocol 3, where the rapid blood pressure changes are followed much better by the model response, compared to the response of the 3-component model, shown in Figure 4.9 C.

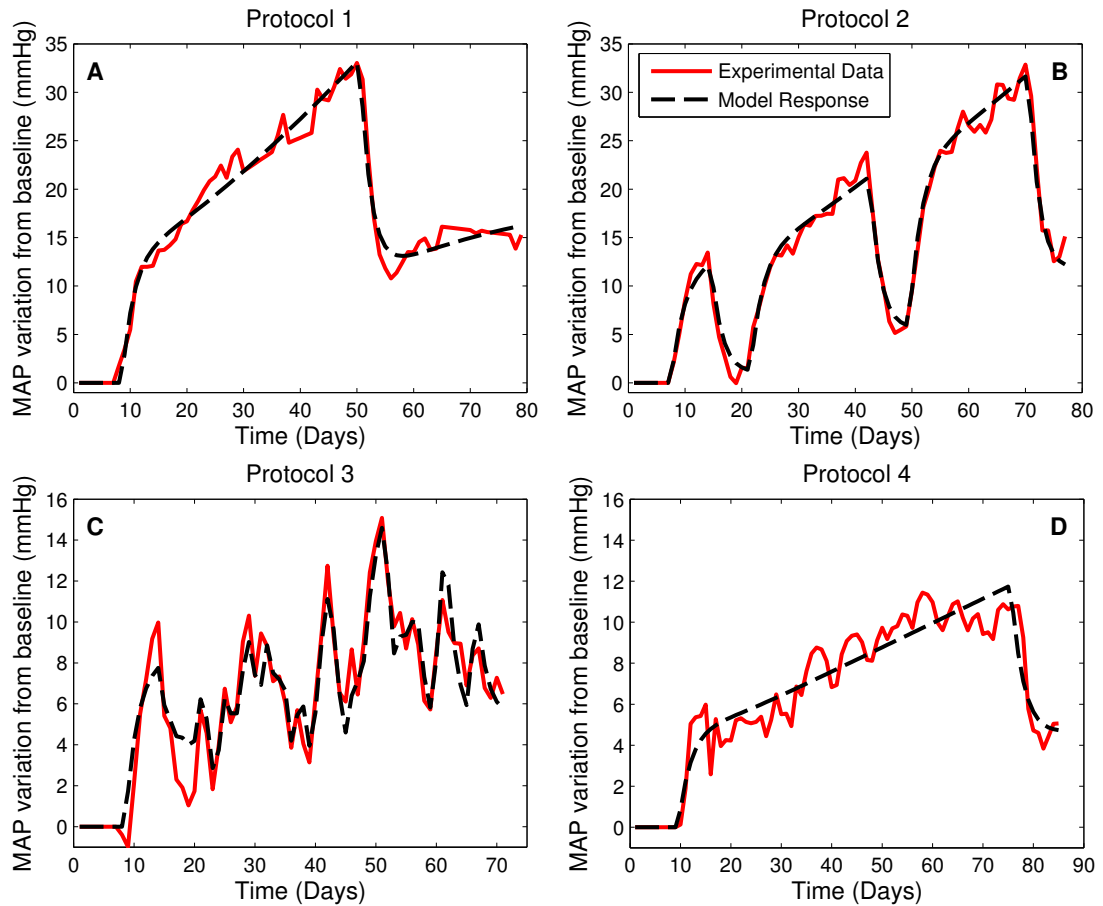


Figure 4.11: ‘Mean animal’ model response for the 4-component model structure

Figure 4.12 shows each of the model components’ response for the mean animals. It is evident that the compensatory component has a major contribution to the model response and allows for the BP undershoot, when high-salt intake is ceased, to be modelled. This has a direct effect to improve significantly the model response to the PRBS salt input signal (Figure 4.11 C) where multiple cessations of salt stimulation are present.

The improvement in the 4-component model response is also accompanied by a reduc-

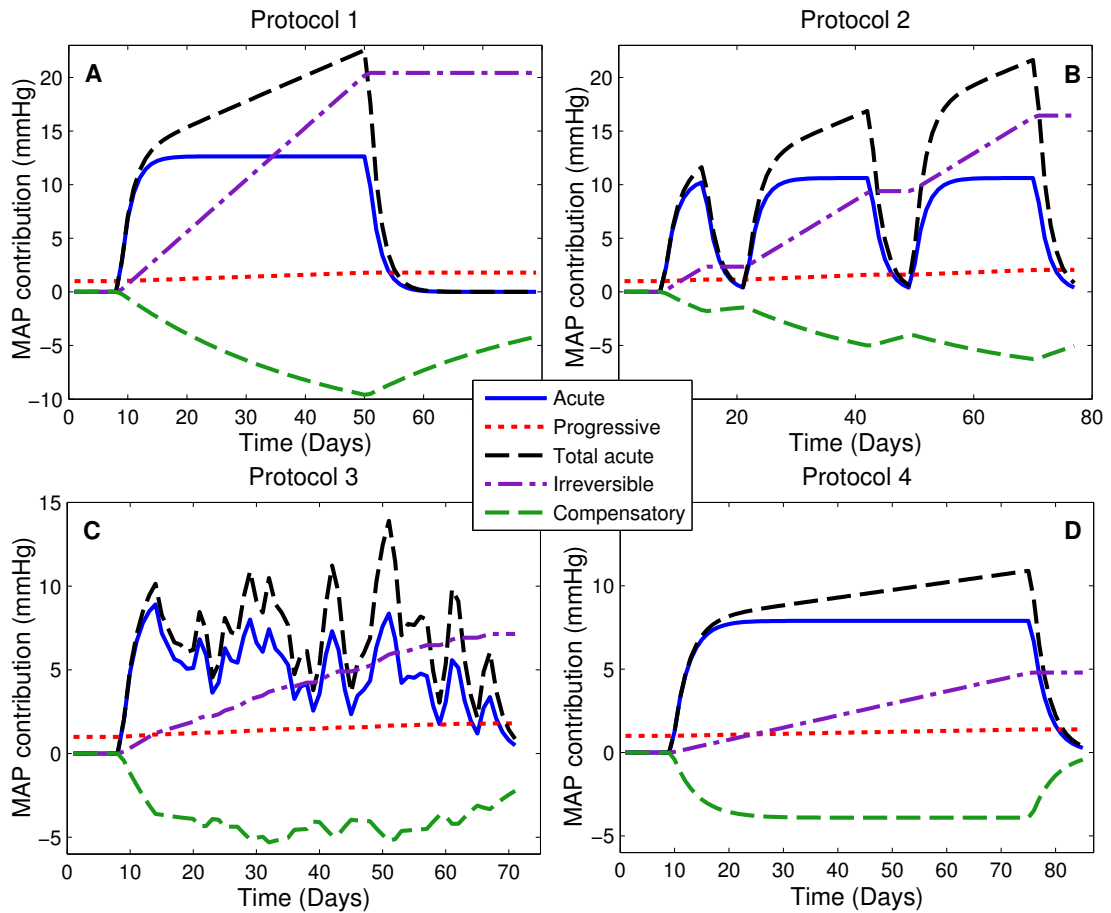


Figure 4.12: Model component contribution for the 4-component 'mean animal' model

tion in the MAE values across the 'mean animals' of the various data sets compared to the 3-component model. The MAE and parameter results for the 'mean animals' of the salt-sensitive and hybrid animals of Protocols 1, 2, 3 and 4 are detailed in Table 4.4.

The average individual animal MAEs and model parameters for the salt-sensitive and hybrid data sets are given in Table 4.5 and those for the individual control salt-resistant animals are shown in Table 4.6. As before, the average acute salt-sensitivity gain G_{as} is higher for the salt-sensitive rats compared to that of the hybrid and salt-resistant rats. Similarly, the longer term progressive salt-sensitivity (G_{pr}) and self-sustaining (G_{ss}) gains are highest for the salt-sensitive animals, while the gain values for the hybrid rats are similar to those of the salt-resistant rats, and are lower possibly due to the lower genetic predisposition to salt-sensitivity. In the case of the salt-sensitive animals, G_{ss} is lowest in the Dahl-S rats of Protocol 3, presumably due to the lack of a

Table 4.4: ‘Mean animal’ model MAEs and parameters for the 4-component SIH model

<i>Protocol</i>	<i>Protocol1</i>	<i>Protocol2</i>	<i>Protocol3</i>	<i>Protocol4</i>
<i>MAE</i>	1.084	0.999	0.972	0.892
G_{as}	3.829	3.216	2.906	2.391
$\tau_{as}(\text{days})$	1.893	1.981	2.066	2.819
G_{pr}	0.006	0.007	0.008	0.002
G_{ss}	0.147	0.102	0.068	0.022
G_c	4.135	2.581	2.583	1.187
$\tau_c(\text{days})$	34.1811	29.217	9.999	4.321

prolonged continuous exposure to a high-salt diet. The compensation gain G_c is lower for the hybrid and salt-resistant animals, since the increase in BP due to the remaining components is also low.

Table 4.5: Average individual animal MAEs and parameters for the 4-component SIH model

<i>Protocol</i>	<i>Protocol1</i>	<i>Protocol2</i>	<i>Protocol3</i>	<i>Protocol4</i>
<i>MAE</i>	1.728 ± 0.447	2.045 ± 0.899	1.479 ± 0.257	1.107 ± 0.279
G_{as}	5.792 ± 2.845	3.819 ± 2.164	3.076 ± 2.527	2.968 ± 1.549
$\tau_{as}(\text{days})$	2.645 ± 1.229	2.61 ± 1.038	2.7 ± 1.460	2.955 ± 0.853
G_{pr}	0.005 ± 0.005	0.009 ± 0.006	0.017 ± 0.017	0.0017 ± 0.0015
G_{ss}	0.129 ± 0.046	0.139 ± 0.153	0.074 ± 0.027	0.029 ± 0.025
G_c	4.584 ± 3.199	8.54 ± 10.684	4.732 ± 3.872	2.019 ± 1.608
$\tau_c(\text{days})$	18.609 ± 10.899	30.659 ± 24.978	19.324 ± 12.249	6.899 ± 3.738

Table 4.6: Average MAEs and parameters for the control Dahl-R rats for the 4-component SIH model

<i>Protocol</i>	<i>Protocol1</i>	<i>Protocol3</i>
<i>MAE</i>	0.799 ± 0.148	1.234 ± 0.148
G_{as}	2.034 ± 2.099	2.256 ± 0.482
$\tau_{as}(days)$	3.561 ± 5.229	2.194 ± 0.204
G_{pr}	-0.003 ± 0.004	0.003 ± 0.002
G_{ss}	0.029 ± 0.011	0.017 ± 0.019
G_c	1.155 ± 1.953	2.537 ± 0.549
$\tau_c(days)$	30.057 ± 37.333	5.558 ± 1.338

4.5.3 5-component model

The 5-component model response for the ‘mean animals’ of each of the experimental data sets is shown in Figure 4.13. The plots in Figure 4.13 demonstrate the ability of the model to mimic the BP response very closely and this is confirmed by a reduction in the mean absolute errors for the ‘mean animals’, as shown in Table 4.7. Virtually all the correlated components of the blood pressure response to high-salt intake have been captured by the 5-component model. Figure 4.14 demonstrates each of the model components’ contribution towards the final overall response.

Table 4.7: ‘Mean animal’ model MAEs and parameters for the 5-component SIH model

<i>Protocol</i>	<i>Protocol1</i>	<i>Protocol2</i>	<i>Protocol3</i>	<i>Protocol4</i>
<i>MAE</i>	0.942	0.9728	0.734	0.859
G_{st}	6.461	5.319	6.119	1.664
$\tau_{st}(days)$	5.656	3.032	2.547	1.384
G_{rec}	15.655	6.956	0.640	4.328
$\tau_{rec}(days)$	1.828	1.953	2.124	3.286
G_{pr}	0.0015	0.003	0.004	0.004
G_{ss}	0.118	0.094	0.068	0.017
G_c	3.003	2.936	3.940	0.457
$\tau_c(days)$	8.656	5.931	2.976	2.794

The average individual animal errors and parameters are given in Table 4.8 for the salt-

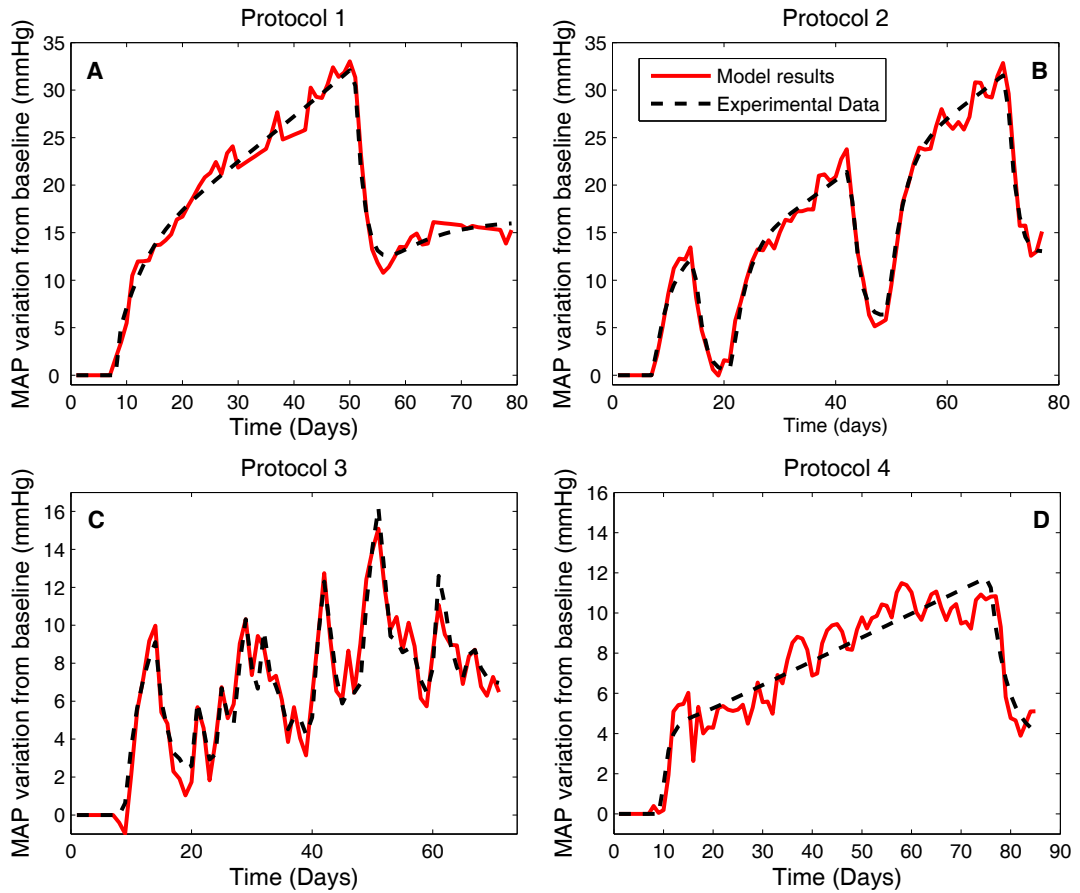


Figure 4.13: ‘Mean animal’ model response for the 5-component model structure

sensitive animals of Protocols 1,2 and 3 and the hybrid rats of protocol 4 and in Table 4.9 for the salt-resistant animals of Protocols 1 and 3. Again, as for the ‘mean animals’, there is a reduction in the average MAE, compared to the 4-component model, across all protocols involving salt-sensitive animals. However, in the case of the salt-sensitive animals from Protocol 3, the reduction is smaller than for Protocols 1 and 2. For the salt-resistant and hybrid animals the reduction in the average MAE compared to the 4-component model is also not very large.

The addition of separate stimulation and recovery components for the ‘Acute salt sensitivity’, with gains G_{st} and G_{rec} and time constants τ_{st} and τ_{rec} , has allowed us to provide a more complex shape of the short-term BP response. The flexibility of having different time constants during step increases and step decreases in salt intake is an important improvement since physiological responses often occur at different time scales during stimulation and recovery. The stimulation and recovery time constants have different values, with τ_{st} generally being larger than τ_{rec} , which demonstrates the

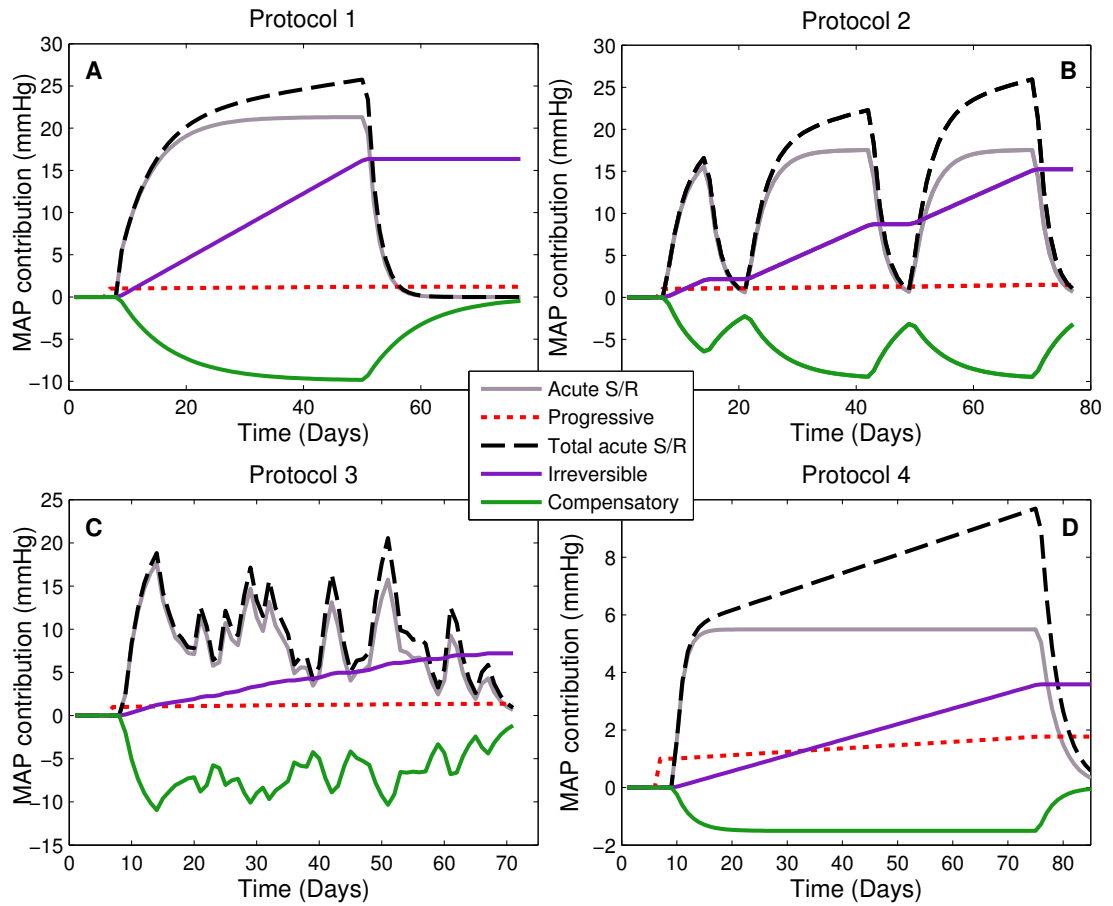


Figure 4.14: Model component contribution for the 5-component 'mean animal' model

necessity of including separate dynamics for increase and decrease in salt intake. One notable exception to this is the average recovery time constant τ_{rec} of the salt-sensitive animals in Protocol 2 being similar in size to the stimulation time constant τ_{st} . This is misleading, since the large average recovery value is due to one individual animal having a much larger τ_{rec} than the rest, but the model fit of that particular animal is also not very good, therefore the time constant can be taken as an outlier in the set of results.

In the cases where salt intake is not sustained and continuous, such as in Protocol 3, or where the animals are not salt-sensitive, the additional model components, compared to the 4-component model, could be redundant.

An F-test is applied to the individual animals results, and is described in the following section, to verify if the 5-component model provides enough improvement in results to justify the additional components.

Table 4.8: Average individual animal MAEs and parameters for the 5-component SIH model

<i>Protocol</i>	<i>Protocol1</i>	<i>Protocol2</i>	<i>Protocol3</i>	<i>Protocol4</i>
<i>MAE</i>	1.553 ± 0.259	1.584 ± 0.611	1.304 ± 0.226	1.065 ± 0.277
<i>G_{st}</i>	9.766 ± 4.909	9.550 ± 5.056	5.814 ± 2.281	2.856 ± 1.091
<i>τ_{st}(days)</i>	8.766 ± 10.005	3.239 ± 1.650	4.565 ± 4.574	3.416 ± 5.354
<i>G_{rec}</i>	17.628 ± 11.497	7.497 ± 5.548	1.359 ± 1.221	6.224 ± 3.101
<i>τ_{rec}(days)</i>	2.224 ± 1.041	3.781 ± 3.075	1.631 ± 1.018	3.552 ± 1.186
<i>G_{pr}</i>	0.001 ± 0.001	0.003 ± 0.003	0.006 ± 0.004	0.003 ± 0.003
<i>G_{ss}</i>	0.126 ± 0.030	0.086 ± 0.118	0.068 ± 0.048	0.021 ± 0.018
<i>G_c</i>	6.358 ± 4.608	7.249 ± 6.244	2.931 ± 3.043	1.655 ± 1.227
<i>τ_c(days)</i>	14.711 ± 20.753	4.067 ± 3.078	2.142 ± 2.497	3.479 ± 1.750

Table 4.9: Average MAEs and parameters for the control Dahl-R rats for the 5-component SIH model

<i>Protocol</i>	<i>Protocol1</i>	<i>Protocol3</i>
<i>MAE</i>	0.764 ± 0.16	1.1205 ± 0.066
<i>G_{st}</i>	2.111 ± 0.806	4.447 ± 0.946
<i>τ_{st}(days)</i>	2.699 ± 2.69	2.745 ± 2.491
<i>G_{rec}</i>	14.099 ± 18.263	1.388 ± 0.615
<i>τ_{rec}(days)</i>	55.148 ± 61.182	0.979 ± 0.462
<i>G_{pr}</i>	0.001 ± 0.001	0.001 ± 0.001
<i>G_{ss}</i>	0.032 ± 0.082	0.016 ± 0.019
<i>G_c</i>	22.571 ± 50.729	2.876 ± 1.002
<i>τ_c(days)</i>	104.5805 ± 222.35	1.590 ± 1.252

4.5.4 F-test

An F-test (Ludden et al., 1994) was performed to assess whether the increase in model complexity from 3 to 4 components and from 4 to 5 components is justified, especially for the salt-sensitive and hybrid animals. In general, an F – value, shown in Equation (4.2) can be calculated to compare the performances of two models, a simple and a more complex one, with respect to the number of model parameters.

$$F - value = \frac{(RSS1 - RSS2)/(DF1 - DF2)}{RSS2/DF2} \quad (4.2)$$

with

$$DF1 = n - p1 \quad DF2 = n - p2 \quad (4.3)$$

where

- $RSS1$ and $RSS2$ are the residual sum of squares or the square of the error between model response and experimental data for model 1 and model 2 respectively, where model 1 is the simpler of the two models,
- $DF1$ and $DF2$ are the degrees of freedom of model 1 and model 1 respectively,
- n is the number of points in the data set, and
- $p1$ is the number of parameters in model 1 and $p2$ is the number of parameters in model 2.

As the result of the F-test is, essentially, a ratio of performance versus complexity between the simpler and the more complex models, an F – value of 1 signifies that the two models perform equally well for their respective degree of complexity, while an F – value greater than 1 signifies some merit in the use of the more complex model. The degree to which the F – value exceeds 1 can also be used as a measure of confidence (P – value) on the F – value, taking into account the number of samples in the data set and the number of parameters used.

In this study, two sets of F – values were calculated for each data set, one comparing the 3- and 4-component models ($F_{3/4}$) and the other comparing the 4- and 5-component models ($F_{4/5}$). The average F – values with their associated confidence intervals are

presented in Table 4.10 for the salt-sensitive animals of all protocols and for the hybrid animals of Protocol 4. Table 4.11 gives the F-test results for the control salt-resistant animals of Protocols 1 and 3. An increase in model complexity from 4 to 5 components gives higher $F - values$ than an increase in complexity from 3 to 4 components for the salt-sensitive and hybrid animals, with the exception of the Dahl-S rats from Protocol 3, where there is a very large improvement in model fit in the 4-component model, compared to the 3 component model, while the improvement in the 5-component model fit in comparison to the 4-component model seems much more moderate. The hybrid animals of Protocol 4 have, on average, an $F - value < 1$ for a change from 3 to 4 components ($F_{4/5} = 0.8$), while the $F - value > 1$ for a change from 4 to 5 components ($F_{4/5} = 3.77$). This indicates that adding the compensatory component to the 3-component model structure on its own, without the addition of different stimulation and recovery dynamics, did not improve the hybrid animals model fit enough, compared to the increase in model complexity. The $F - value$ for a change from 3 components to 5 components for the hybrid animals is 2.35, however, which indicates a moderate improvement in the results. Increase in model complexity from 3 to 4 or from 4 to 5 components is possibly not well justifiable for the salt resistant or hybrid animals, even though the $F - values > 1$ in most cases. As a result of the lack of some of the response features in the Dahl-R and hybrid rats compared to the Dahl-S rats, it appears that not all model components are necessary to represent the responses of the former two. It is the intent, however, to have a general model, which can represent both salt-sensitive and salt-resistant animals, thus some model components may inadvertently appear redundant in the latter case but are essential in the former.

Table 4.10: Mean F-test values for the Dahl-S rats of Protocols 1, 2 and 3 and the hybrid rats of Protocol 4

<i>Protocol</i>	$F_{3/4}$	$P_{3/4}$	$F_{4/5}$	$P_{4/5}$
<i>Protocol1</i>	5.01	< 0.01	7.51	0.001
<i>Protocol2</i>	10.76	< 0.001	18.7	< 0.001
<i>Protocol3</i>	23.49	< 0.001	8.65	< 0.001
<i>Protocol4</i>	0.8	< 0.5	3.77	< 0.05

Table 4.11: Mean F-test values for the control Dahl-R rats of Protocols 1 and 3

<i>Protocol</i>	$F_{3/4}$	$P_{3/4}$	$F_{4/5}$	$P_{4/5}$
<i>Protocol1</i>	3.5	> 0.1	2.34	> 0.1
<i>Protocol3</i>	3.6	> 0.1	5.82	< 0.05

4.5.5 Renal function curves

In previous studies, the slope of the steady-state pressure-natriuresis relationship has been used to define the acute salt-sensitivity of BP (Guyton, 1980; Kimura and Brenner, 1997). The 5-component model (Figure 4.7) can be used to generate steady-state pressure-natriuresis relationship curves, which allow the visualisation of the progression of the development of SIH and worsening of the subjects' salt-sensitivity with prolonged high salt intake.

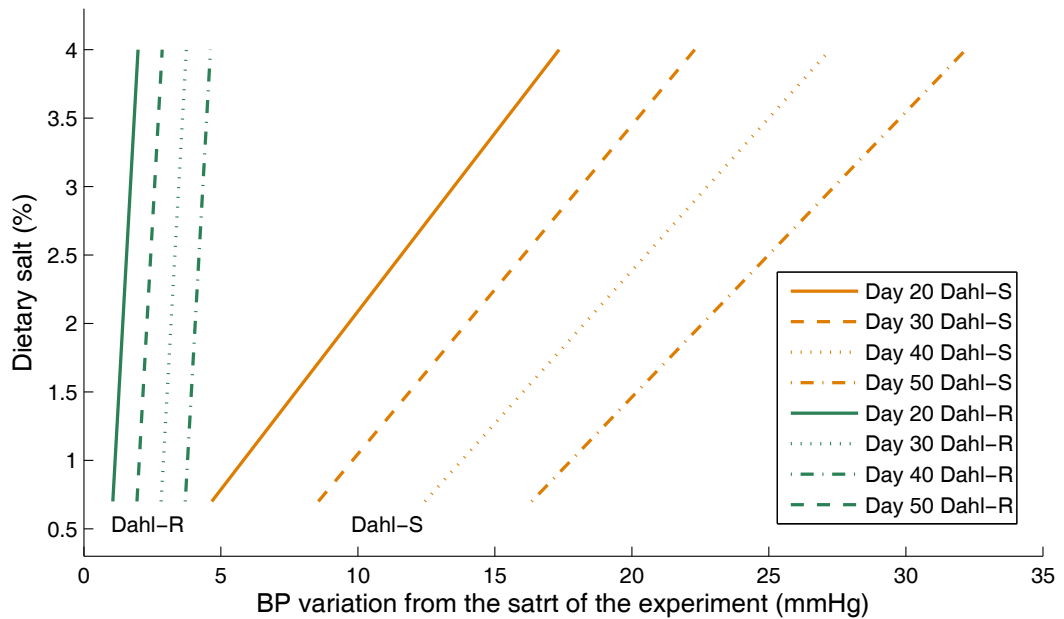


Figure 4.15: Steady-state pressure-natriuresis relationships for the ‘mean’ salt-sensitive and salt-resistant animals of Protocol 1

A combination of the ‘Acute salt-sensitivity’ and ‘Compensatory’ components impact on the initial slope of the chronic pressure-natriuresis relationship. The slope is determined by the magnitude of the animals response to high salt intake and is inversely proportional to the G_{st} gain, and directly proportional to the compensatory component gain G_c . Thus, for animals that are very salt-sensitive, the slope has a low value.

The ‘Progressive acute’ component in the model results in a further reduction of the slope value with continued exposure to high salt diet and this reduction is inversely proportional to the G_{pr} gain. This effect corresponds to an increase in acute salt-sensitivity with time. The ‘Self-sustained’ component in the model contributes to the pressure-natriuresis relationship by shifting the curve to the right, i.e. towards higher resting BP levels (Van Vliet et al., 2006; Van Vliet and Montani, 2008). Since this component of the BP response is self-sustained, even when salt intake reduces back to normal, the shift in the pressure-natriuresis curve is also permanent and the G_{ss} gain is proportional to the amount of rightward shift in the curve. All of the effects described here can be clearly seen in Figure 4.15 for the mean salt-sensitive animal of Protocol 1. In the same figure, the pressure-natriuresis curve progression is also shown for the mean salt-resistant animal from Protocol 1. The rightward shift in the Dahl-R rat curve is very small, compared to that of the salt-sensitive animal, and there is no overall reduction in the slope of the relationship. A further example of the different characteristic pressure–natriuresis relationships exhibited by four hybrid rats is shown in Figure 4.16.

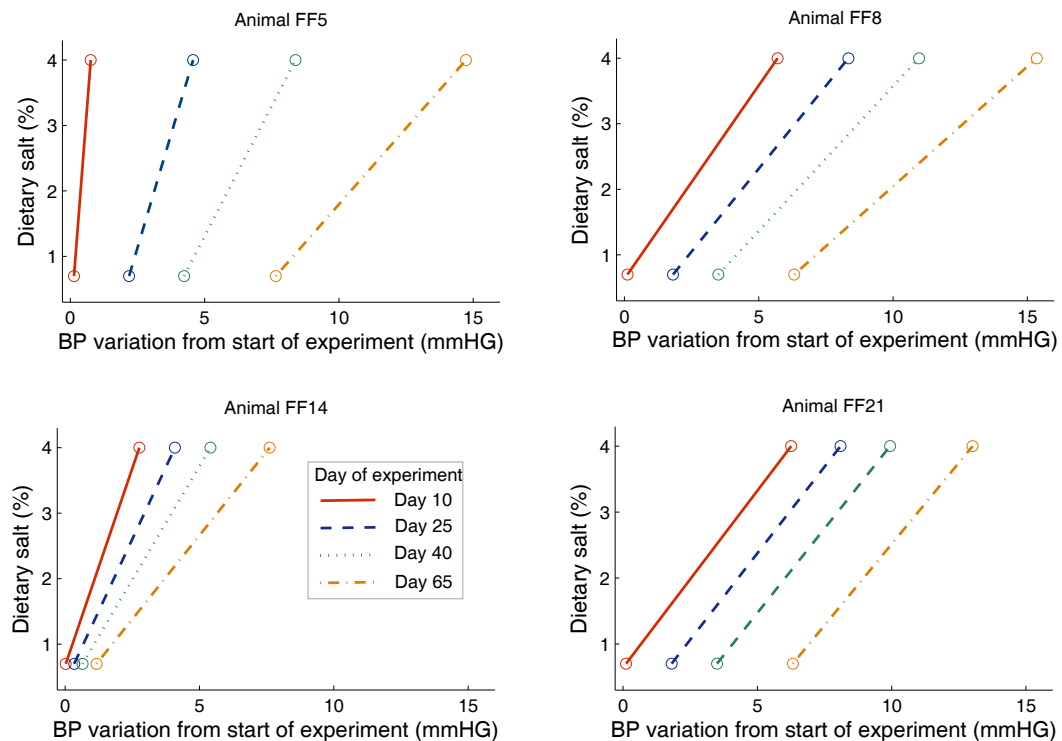


Figure 4.16: Steady-state pressure-natriuresis relationships for four hybrid rats

4.6 Discussion

Dahl-S rats have been specifically bred for their genetic predisposition to develop hypertension, due to a high-salt intake level, in an accelerated manner (within weeks of the initiation of salt-loading). The combination of genetic and environmental factors in the etiology of hypertension in the Dahl-S rat makes them valuable for investigation of the underlying mechanisms of the disease. The process of salt-induced hypertension has been studied in detail recently due to the availability of the telemetry technology, which allows continuous recording of long-term experimental data (Van Vliet et al., 2006; Van Vliet and Montani, 2008).

In this present study, the blood pressure response to a high-salt intake in the Dahl-S rat is represented as a multi-component process by a non-linear mathematical model. Three different model structures, of varying complexity, have been proposed to characterise the relationship between salt and blood pressure.

The simplest model, shown in Figure 4.5, consists of 3 elements representing distinct phases in the blood pressure response to salt intake. The ‘Acute salt-sensitivity’ component is a completely reversible first order exponential, whose time constant τ_{as} of 1-3 days resembles the effect of re-establishment of salt balance during salt-loading (Van Vliet et al., 2006; Osborn and Hornfeldt, 1998). The G_{as} gain of the acute salt-sensitivity component is proportional to the degree of salt-sensitivity in the subject.

The ‘Progressive acute’ model component was included to represent the progressive worsening of some subjects’ salt-sensitivity with continued high salt consumption. This component is an integrator, whose response, in practice, amplifies the gain of the ‘Acute salt-sensitivity’ component. The effect of progressive worsening of salt-sensitivity caused by an extended exposure to high dietary salt is particularly evident in the animals from Protocol 2, as shown in Figures 4.2 and 4.9 (B). Similar effects of reversible progressive increase in blood pressure, due to high salt intake, has been found in chimpanzees (Denton et al., 1995). In humans, progressive worsening of salt-sensitivity has often been contributed to the process of aging; however, the lifetime exposure to high dietary salt in the developed world could provide an alternative hypothesis (Weinberger and Fineberg, 1991).

The ‘Self-sustained’ model component consists of an integrator with a very low gain and represents a slow, irreversible increase in blood pressure due to high salt intake, which has been well described previously (Dahl, 1961; Van Vliet et al., 2006). The exact mechanisms underlying the effects of the ‘Progressive acute’ and the ‘Self-sustained’ components are not known; however, there are a number of possible explanations behind these features of the blood pressure response. Both the progressive worsening of salt-sensitivity and the irreversible hypertension due to prolonged salt exposure could be attributed to vascular remodelling and/or renal damage such as fibrosis and hypertrophy or lesions (Rapp and Dene, 1985; Jaffe et al., 1970; Chen et al., 1993). Changes in renal structure have been identified as a possible cause for the development of salt-sensitivity in rats (Johnson et al., 2002).

The 3-component model performed relatively well for most data sets used in this study, but not all features of the blood pressure response to salt were captured. A further ‘Compensatory’ element (Figure 4.6) was added to the model with the purpose of improving the data fit. The ‘Compensatory’ component is represented by a first order exponential, which counteracts the blood pressure increase due to salt. Considering that blood pressure control is achieved by balancing numerous physiological systems, it is reasonable to expect that a balance of model component responses would yield a better overall model fit. Physiological systems that could counteract the blood pressure increase due to high-salt intake are the renin-angiotensin-aldosterone system (Cholewa and Mattson, 2001; Denton et al., 1995) atrial natriuretic factor (Mullins et al., 2006) and nitric oxide release (Simchon et al., 1989) though it is impossible to assign an exact physiological significance to the ‘Compensatory’ model component without further experiments.

The 4-component model is a significant improvement over the 3-component model and the results shown in Figure 4.11 confirm this view. The addition of the compensatory component provides a most noticeable improvement in the data fit for Protocol 3, also reflected in the high associated F-value in Table 4.10. The compensatory component also aids in representing the blood pressure undershoot, clearly visible in Figure 4.11 (A); however, the BP data is still not entirely accurately represented. The addition of a fifth component, which allows for different rates of blood pressure response during salt-loading and depletion, achieves a much better result.

The separate ‘Stimulation’ and ‘Recovery’ dynamics in the ‘Acute salt-sensitivity’ component are first order exponentials with different characteristics during salt-loading and depletion. The response of the 5-component model captures very closely the characteristics of the experimental data for all protocols, and includes all major features of the BP response to high salt intake, especially for the salt-sensitive animals. The goodness-of-fit is also reflected in the improvement of the mean absolute errors compared to the 3- and 4-component models. The increase in complexity in the 5-component model may not be justifiable for the salt-resistant or hybrid animals, as reflected in the low F- and P-values in Tables 4.10 and 4.11. The Dahl-R and hybrid rats have an attenuated response to salt intake compared to their salt-sensitive counterparts, thus some of the model components may not be significantly activated. The model is primarily aimed at the Dahl-S rats, however, and it should be able to represent their BP response with a reasonable accuracy, even if some of the features are redundant for some of the hybrid and the salt-resistant animals. An example of the functionality of the 5-component model is its ability to generate the steady-state renal function curves at any point in time during the experiment as already outlined in Section 4.5.5.

Finally, the parameters of the 3 models presented in this work were optimised for the ‘mean animal’ of each data set and for each individual animal also.

An attempt was made to train each model using all but one animal within a data set, in order to predict the final animal’s response which is, in effect, making use of separate training and validation data. This, however, has the effect to average the model parameters across all animals, but one, and did not yield good results unless the ‘validation’ animals response was similar to that of the ‘mean animal’. The large inter-animal variability, thus, requires that models are trained separately for each animal. In order to obtain a truly generic model, additional variables would need to be recorded during the experiment and included in the SIH model.

4.7 Conclusion

This study highlights the multi-component nature of salt-induced hypertension in Dahl-S rats by describing five distinct model components, whose combined responses represent the time course of BP response to high salt intake. The 5-component model de-

veloped here is, so far, the most comprehensive model of the dynamics of salt-induced hypertension in Dahl-S rats and it helps gain an insight into the processes involved in blood pressure control. The model components are reasonably intuitive, though it is not possible, with the available experimental data, to assign exact physiological meaning to the various model elements. Nevertheless, it is believed that the 5-component model articulates clear and distinct characteristics, which may correspond with completely separate physiological phenomena.

Additional explanatory variables and protocols may also be studied in the future in order to provide the model with the ability to model inter-animal variation in blood pressure as, presently, the model is optimised to simulate the response of individual animals only. The measurement of additional variables could also aid in identifying, with more certainty, the underlying physiology behind each model component.

Chapter 5

Baroreflex sensitivity estimation

Many studies have been conducted to develop reliable techniques for baroreflex sensitivity (BRS) estimation over the years and a detailed overview is available in Section 2.2. Some protocols have provided external stimuli to the patients, while others studies been conducted in spontaneous conditions. This chapter develops a systematic approach to BRS estimation, which accounts for the closed loop nature of the system, and the EuroBaVar data set (Laude et al., 2004) has been employed to evaluate the quality of the approach. The following sections of this chapter will examine the experimental protocol and then will describe in detail the new BRS estimation technique developed in this work. Finally, a comparison between this new method and existing methods will be provided.

5.1 Experimental protocol

The EuroBaVar data set (Laude et al., 2004), used in this study, was provided by the European Society of Hypertension working group on baroreflex and cardiovascular variability. The data comprises non-invasive spontaneous blood pressure recordings for twenty one subjects, obtained using a Finapres 2300 device (Ohmeda, Helsingki, Finland). Concurrent electrocardiography (ECG) recordings were also made, using a Datex Cardiocap II device (Datex Engstrom, Helsinki, Finland). Data was collected

over 10-12 min in the supine position and 10-12 min in the standing position, for each subject. Systolic, mean and diastolic pressures, as well as RR interval, are provided on a per-beat basis. The collected raw data, including the ECG recording from which the RR interval signal was derived, is also available, sampled at 500Hz.

The twenty one subjects who participated in the study comprised four men and seventeen women. They ranged in age from 17 to 68 years. Two subjects were confirmed to have baroreflex failure; one was a recent heart transplant patient, while the other was a diabetic with cardiac autonomic neuropathy. Twelve subjects were normotensive outpatients; of the remaining subjects, one was an untreated hypertensive, two were treated hypertensives and four were healthy volunteers. One woman was pregnant in her first term. The records of two subjects were duplicated in order to test if the results were reproducible, therefore the total data set contains twenty three sets of data.

5.2 System characteristics and implications

Based on the experimental protocol, outlined in the previous section, some observations about the EuroBaVar data set are noteworthy. The characteristics of the system under study, as well as the method of data collection and recording, will determine the type of data preprocessing needed and the required system identification framework.

- In the EuroBaVar data set, the subjects are at rest in either the supine or standing positions, with no external excitation applied. The spontaneous nature of the data results in relatively small variations in SAP and RR around their equilibrium values; therefore, it is reasonable to assume that a linear model could be employed to represent the $SAP \rightarrow RR$ relationship.
- A further implication of the small variation in the spontaneous SAP and RR signals is the possible poor excitation of the baroreflex. Poor excitation of the system can affect the identifiability of the baroreflex across a range of frequencies.
- The EuroBaVar data is collected under closed-loop conditions, i.e. the baroreflex loop was intact. This consideration is vital when selecting a system identification routine, as the feedforward and feedback paths of a closed-loop system can only be separately identified within a limited set of conditions. It is also worth noting, when examining Figure 2.2, that no external inputs to the closed-loop system (n_s

or n_r) are available as measured signals and that there is also no measured *SAP* setpoint or desired reference value.

- The EuroBaVar data is available on a ‘per beat’ basis i.e. a measurement of *SAP* and *RR* is provided after each RR interval, so the data is irregularly sampled, i.e. it is on a non-uniform time base. This has important implications for any frequency domain calculations, or model generalisation.

5.3 Outline of the SID framework for BRS estimation

Ljung (1999) identifies a framework within which a system identification problem can be placed, from a mathematical perspective, given the conditions under which the data were recorded and the nature of the data itself. The framework encompasses both time- and frequency domain models, though the focus in this study will be on time domain models.

5.3.1 Families of model structures

Whilst a variety of models of different complexities are available (Ljung, 1999), the most general mathematical model that will be employed in this particular study is the ARMAX (Autoregressive moving-average with eXogenous input) model given by Equation (5.1).

$$y(k) = \frac{B_1(q)}{A(q)}u_1(k - n_{d1}) + \dots + \frac{B_m(q)}{A(q)}u_m(k - n_{dm}) + \frac{C(q)}{A(q)}e(k) \quad (5.1)$$

where $B_i(q)$, $A(q)$ and $C(q)$ are polynomials of order n_{bi} , n_a and n_c respectively in the delay operator q , and n_{di} is the number of pure steps delay between each input i and the output ($\tau_{n_{di}} = n_{di} \Delta T$ is the time it takes for a change in an input to affect the system output). Within a system identification framework, the index k is taken to mean a *time* index, so that $t = k \Delta T$, where t is (continuous) time and ΔT is the (fixed) sampling period, both given in seconds. It is worth noting that the analysis of data on a ‘per-beat’ basis does not allow any frequency domain calculations/interpretations.

The system is, in general, a multi-input, single-output (MISO) system. Equation (5.1) can also be represented in the form of a difference equation, as shown in Equation (5.2), which would allow the comparison to models of other researchers as in Equations (2.1) to (2.6), outlined in Section 2.2.4.

$$\begin{aligned}
 y(k) + a_1 y(k-1) + \dots + a_{n_a} y(k-n_a) = & \\
 & b_{10} u_1(k-n_{d1}) + b_{11} u_1(k-n_{d1}-1) + \dots + b_{1n_{b1}} u_1(k-n_{d1}-n_{b1}) \\
 & + \dots \\
 & + b_{m0} u_m(k-n_{dm}) + b_{m1} u_m(k-n_{dm}-1) + \dots + b_{mn_{bm}} u_m(k-n_{dm}-n_{bm}) \\
 & + e(k) + c_1 e(k-1) + \dots + c_{n_c} e(k-n_c)
 \end{aligned} \tag{5.2}$$

The ARMAX model has an output, which regresses on itself via the $A(q)$ polynomial; it has a moving-average on the noise/error term, $e(k)$, via the $C(q)$ polynomial, and includes the deterministic (exogenous) input $u(k)$. AR (AutoRegressive), MA (Moving-Average) and ARX (Autoregressive with eXogenous input) models are clearly incorporated within the ARMAX structure, by choosing $B(q) = 0$, $C(q) = 1$; $A(q) = 1$, $B(q) = 0$; and $C(q) = 1$ respectively.

5.3.2 Persistence of excitation

This section documents the conditions on the input signal, $u(k)$, which allow the parameters of a mathematical model to be uniquely determined. In general, if the spectrum, $\Phi_u(\omega)$, of $u(k)$ is different from zero at, at least, n points, a model of order n can be uniquely identified. A convenient mathematical formulation, involving the *covariance matrix*, \bar{C}_u , of $u(k)$, which is of size $n \times n$, can be given as follows:

$$\bar{C}_u = \begin{pmatrix} C_u(0) & C_u(1) & \dots & C_u(n-1) \\ C_u(1) & C_u(0) & \dots & C_u(n-2) \\ \vdots & \vdots & \ddots & \vdots \\ C_u(n-1) & C_u(n-2) & \dots & C_u(0) \end{pmatrix} \tag{5.3}$$

where:

$$C_u(\tau) = E[u(k)u(k-\tau)] \tag{5.4}$$

is defined as the *covariance* of $u(k)$, where $\tau \in \mathbb{N}$, while $E[\cdot]$ is the expectation (averaging) operator. If \bar{C}_u is non-singular, then $u(k)$ is persistently exciting of order n and a model of order n can be uniquely identified. If \bar{C}_u is singular, the number of non-zero singular values (i.e. the *rank* of the \bar{C}_u matrix, or the number of linearly independent rows or columns in the matrix) determines the order of the model that can be identified. A useful relation is that, for each separate sinusoidal frequency in $u(k)$, \bar{C}_u contains two non-zero singular values.

5.3.3 Identification in closed-loop

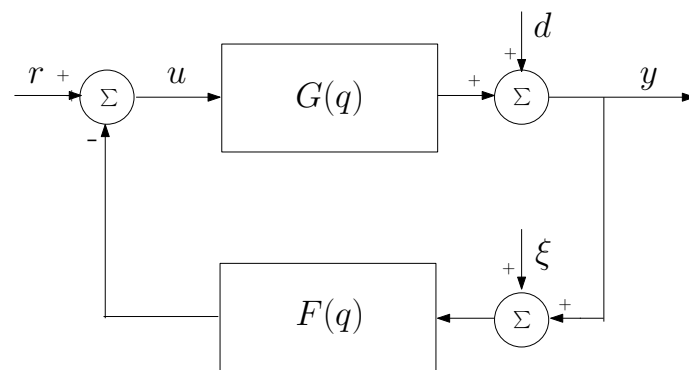


Figure 5.1: A closed-loop system

Since much of the system identification framework in this chapter is developed from a control systems perspective, a visual representation of a closed-loop system is now shown in Figure 5.1, where r is a reference (setpoint) input, y is the system output, d is an unmeasurable disturbance, ξ is measurement noise and u is the input to the $G(s)$ block in the feedforward path. There is an obvious close relationship between Figures 5.1 and 2.2. It should be noted here that in the study described in this chapter, the specific aim is to identify the $G(q)$ block in the feedforward path of Figure 5.1 (and Figure 2.2), which represents the arterial baroreflex.

In general, a number of basic conditions need to be met before identification of a system in closed loop may be attempted:

- There needs to be a delay in either the forward path $G(q)$ or the feedback path $F(q)$,
- The closed-loop system needs to be stable, and

- The range of possible model structures, used for identification, needs to contain the true system.

Three broad classes of methods for the identification of dynamical systems in closed loop are available, and each one is described briefly in the following paragraphs.

Direct method The direct method is the most popular approach for closed-loop system identification and has the following features:

- A prediction error method (PEM) (outlined in Section 5.3.4) is applied directly to the feedforward path as if no feedback exists. The signals used are the input $u(k)$ and output $y(k)$, while the reference signal $r(k)$ is ignored, even if it is known. The system is treated similarly to an open-loop system.
- The actual system needs to be described within the model structure.
- If the overall closed-loop system is stable, the forward path can still be identified even if it is unstable.
- The ARMAX model structure is well suited to this method but a good noise model is necessary.

Indirect method In the case of the indirect method, for a feedback system such as that in Figure 5.1, the regulator $F(q)$ is assumed to be known, and preferably linear. The overall closed-loop system

$$G_{cl}(q) = \frac{G(q)}{1 + G(q)F(q)} \quad (5.5)$$

is identified using the reference signal $r(k)$ and the output $y(k)$. The open-loop system $G(q)$ is then calculated, as follows:

$$G(q) = \frac{G_{cl}(q)}{1 - G_{cl}(q)F(q)} \quad (5.6)$$

This method allows the use of any open-loop technique for the identification of the overall system $G_{cl}(q)$; however, any error in the assumed feedback $F(q)$ will lead to an erroneous $G(q)$.

Joint input-output methods In the joint input-output approaches, both $u(k)$ and $y(k)$ are considered as outputs of the closed-loop system. Some characteristics of

the methods are:

- The regulator ($F(q)$) parameters can be unknown, but knowledge of its structure is required, as well as the reference signal $r(k)$.
- The closed-loop transfer function $G_{cl}(q)$ is identified using $r(k)$ and $y(k)$, using open-loop methods.
- $G(q)$ is estimated as:

$$G(q) = \frac{G_{cl}(q)}{G_{ur}(q)} \quad (5.7)$$

where the transfer function $G_{ur}(q)$ is defined as:

$$G_{ur}(q) = \frac{u(k)}{r(k)} = \frac{1}{1 + F(q)G(q)} \quad (5.8)$$

and G_{ur} is calculated using $r(k)$ and $u(k)$ also using open-loop methods.

In the case of the arterial baroreflex, the reference signal (the desired value of blood pressure), $r(k)$, is unknown. In addition, the other branch of the baroreflex ($F(q)$, or the peripheral arc in Figure 2.2) is unknown, leading to a clear default choice of the direct method. The direct method is often seen as the natural choice, due to the lack of specific knowledge and the employment of fairly standard identification routines. One particular requirement, however, is that the structure of the model must be well specified, especially the noise model.

5.3.4 Model parameter determination

Given a suitable model structure, such as the ARMAX structure described in Equation (5.1) in Section 5.3, a numerical algorithm must be employed to determine the parameters of the polynomials $A(q)$, $B(q)$ and $C(q)$. Considering the necessary requirements for identification in closed loop using the *direct method*, as described in Section 5.3.3, and noting that a single-input, single-output (SISO) system is being considered, the ARMAX model is formulated, in prediction form, as:

$$\hat{y}(k|\Theta) = \frac{B(q)}{C(q)} u(k - n_d) + \left[1 - \frac{A(q)}{C(q)} \right] y(k) \quad (5.9)$$

where the $\hat{\cdot}$ denotes an estimate which depends on Θ . Θ contains the model parameters, as follows:

$$\Theta = \left[a_1 \quad \dots \quad a_{n_a} \quad b_0 \quad \dots \quad b_{n_b} \quad c_0 \quad \dots \quad c_{n_c} \right] \quad (5.10)$$

and n_a , n_b and n_c are the orders of the $A(q)$, $B(q)$ and $C(q)$ polynomials, respectively, while n_d is the step delay.

Note that the term $\left[1 - \frac{A(q)}{C(q)}\right] y(k)$ only involves values of the output up to and including $y(k-1)$. We can now define the prediction error, $\varepsilon(k)$, as:

$$\varepsilon(k, \Theta) = y(k) - \hat{y}(k|\Theta) \quad (5.11)$$

A recursive optimisation algorithm is now employed to minimise the *performance function*:

$$J(\Theta) = \frac{1}{N} \sum_{k=1}^N \varepsilon(k, \Theta)^2 \quad (5.12)$$

over N available input/output pairs. A variety of iterative estimation algorithms (Dennis Jr. and Schnabel, 1983) may be used to determine the optimal parameter set:

$$\Theta^\circ = \underset{\Theta}{\operatorname{argmax}} J(\Theta) \quad (5.13)$$

It is worth noting that:

- A cost function can be chosen to minimise the prediction error (in Equation (5.11)), the output error, or the equation error (the difference between the left- and right-hand sides of Equation (5.2) for example). It is only possible to look at output error for models with no noise dynamics i.e. models of the form:

$$y(k) = \frac{B(q)}{F(q)} u(k) + e(k) \quad (5.14)$$

where, in this case, $e(k)$ is exactly equal to the error in the system output, $y(k)$.

- The choice of n_a , n_b , n_c and n_d is important, since the amount of excitation in the input signal limits the number of parameters that can be identified by the optimisation algorithm.

- The correct specification of the noise model structure is vital, if accurate identification within closed loop is required. In particular, for the current case of biological noise sources (dealt with in further detail in Section 5.5.2), some noise colouring is highly likely, so a noise model reflecting this (as in Equation (5.2)) is mandatory. It is well established (e.g. Ljung (1999)) that the absence or incorrect specification of the noise model invariably leads to biased estimates, in the case of misrepresented coloured noise.
- While, for a small subset of prediction-error models (those involving no noise colouring), the unknown parameter vector Θ can be determined using a once-off batch method (e.g. using least squares), the presence of the $C(q)$ polynomial necessitates the use of an iterative algorithm, where $\hat{\Theta}$ and $e(k)$ are updated in turn. Suitable recursive optimisation techniques include the Gauss-Newton, regularised Gauss-Newton, adaptive regularised Gauss-Newton and Levenberg-Marquardt methods (Dennis Jr. and Schnabel, 1983).

5.4 Results of the system identification approach to BRS estimation

The relationship between SAP and RR interval is identified for all subjects in the EuroBaVar data set, based on the framework outlined in Section 5.3 and using the direct method for identification in closed loop. Only one side of the closed loop, the baroreflex dynamics, is identified, where SAP is the system input and RR is regarded as the system output. Once the parameters of a suitable model have been determined for each subject, the BRS gain is calculated for the low-frequency and high-frequency bands, described in Section 2.2.4. A single subject from the available data set will be taken as an example (Subject 5 in the supine position), for whom the entire identification routine will be demonstrated, while the key summary results will be presented for all subjects. Detailed modelling results for all remaining subjects can be found in Appendix B.

5.4.1 Data preprocessing

In order to obtain a valid frequency domain representation of the input/output signals, the irregularly sampled per-beat data was interpolated and resampled at regular inter-

vals using cubic splines. A fixed sampling frequency of 1.5Hz was chosen in order to achieve a sampling interval of 2/3 sec, which is approximately equal to the average RR interval.

A plot of both the irregularly and regularly sampled data for Subject 5 in the supine position is shown in Figure 5.2.

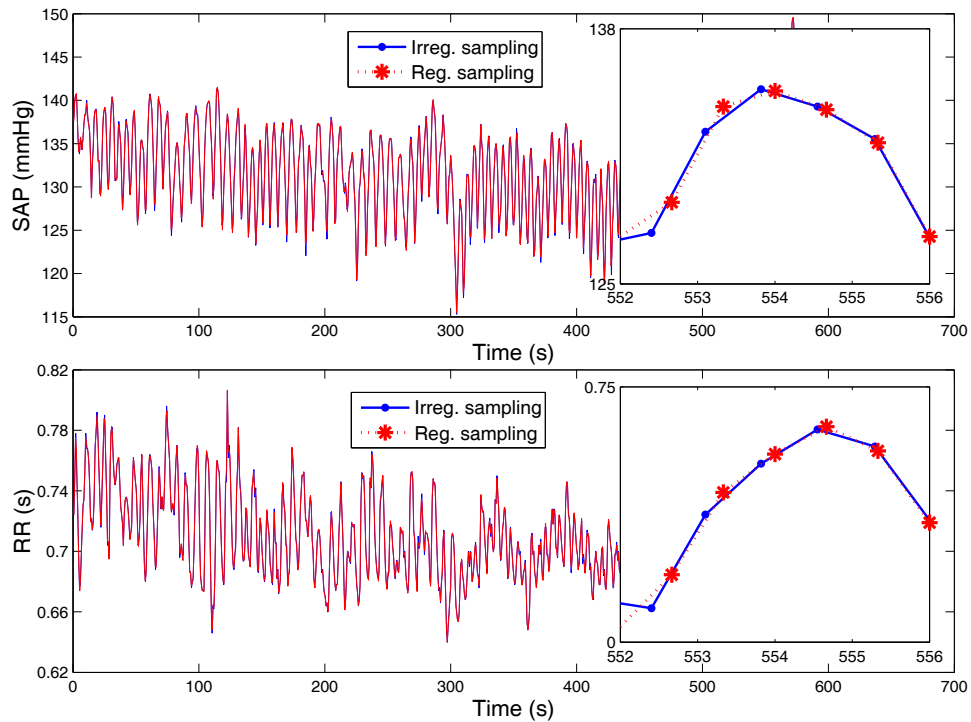


Figure 5.2: Irregularly sampled EuroBaVar beat-to-beat data compared to the interpolated regularly sampled data (Subject 5, supine position)

In addition to resampling, the input and output data were also bandpass filtered in the baroreflex region of interest (0.04-0.5 Hz) with a 7th order Butterworth filter (Parks and Burrus, 1987). The filter was applied in both forward and reverse direction, in order to avoid a phase distortion of the resulting signals (Oppenheim et al., 1999); therefore, the effective filter order is 14. A plot of the filter's response is shown in Figure 5.3, while Figure 5.4 shows the filtered data, compared to the original, unfiltered, data for Subject 5 in the supine position.

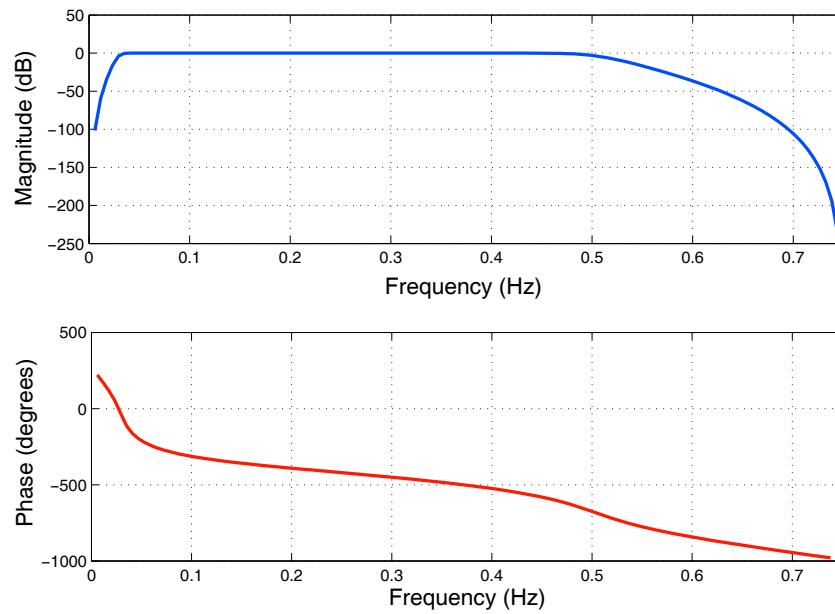


Figure 5.3: Butterworth bandpass filter response

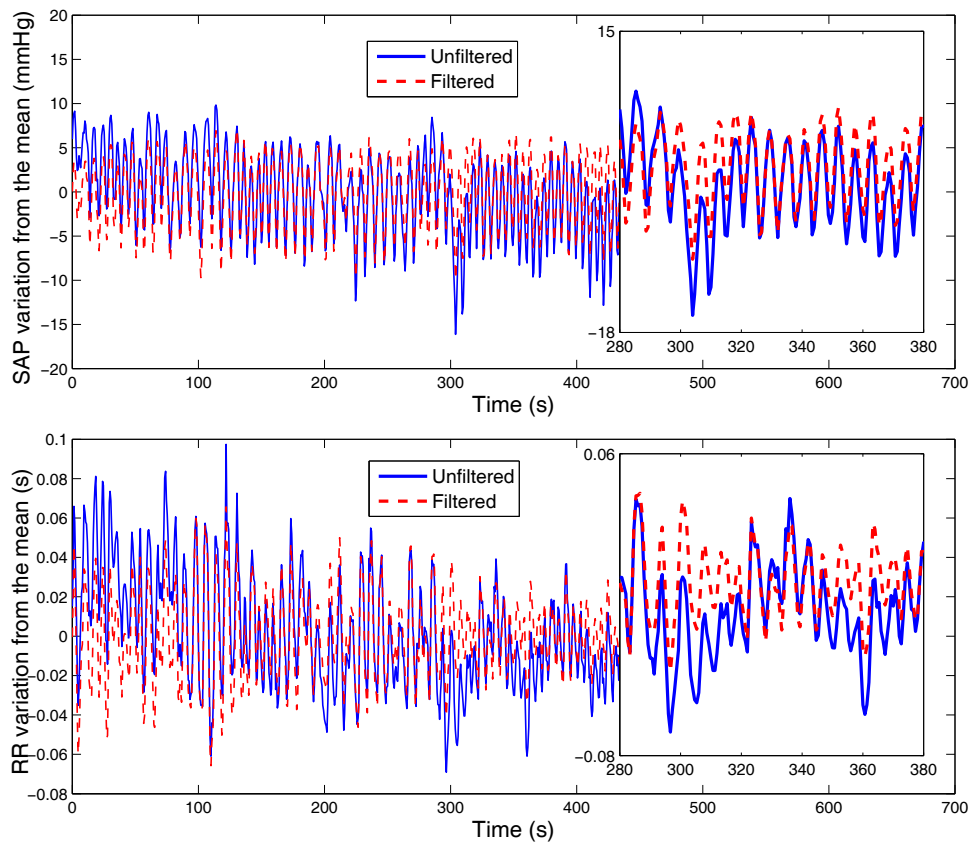


Figure 5.4: Filtered SAP and RR interval data compared with the original unfiltered data for Subject 5 in the supine position

5.4.2 Persistence of excitation

Following the specification in Section 5.3.2, the persistence of excitation is assessed up to a potential order of 50 by evaluating the singular values of a 50x50 covariance matrix (\bar{C}_u , as defined in Equation (5.4)). By way of example, the singular values of the covariance matrix for Subject 5 in the supine position are shown in Figure 5.5. Clearly, in this case, at least 15 singular values are significantly above the base value of zero, though large singular values are preferable from system identifiability perspective. The number of singular values above the base determines the number of parameters that can be comfortably estimated by the optimisation routine, as outline in Section 5.3.2.

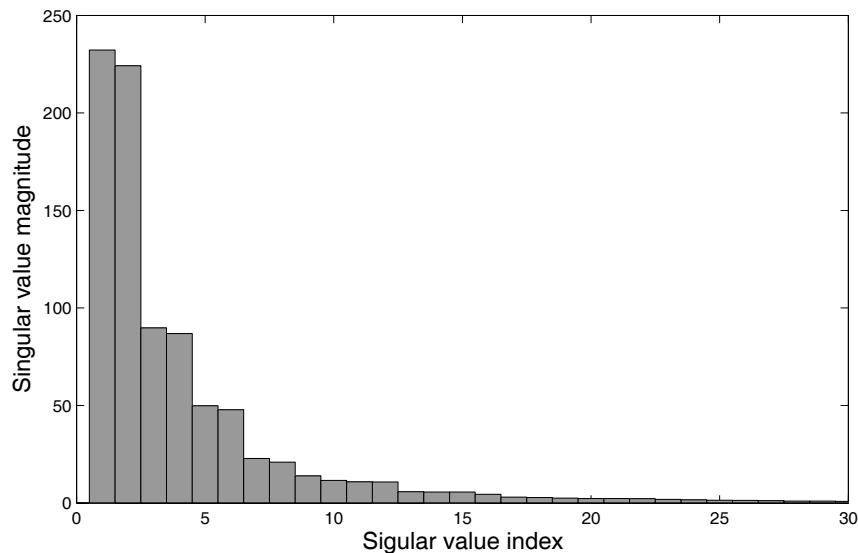


Figure 5.5: Persistence of excitation in *SAP* for Subject 5 in the supine position

In general, for all the data, the indication is that models of order 10 to 12 can be identified with the level of excitation in the *SAP* signals.

5.4.3 Model order and parameter determination

The ARMAX model, as specified in Equation (5.1), is adopted to specify the relationship between *SAP* and RR interval, as it allows modelling of some coloured unmeasured noise disturbances. The EuroBaVar data does not contain respiration data, so the ARMAX model, specified in Equation (5.1), is single input, single output, with a coloured noise

term specified by $e(k)$ and the C polynomial. The system identification problem now concerns the determination of the values of the dynamical orders n_a , n_b and n_c of the A , B and C polynomials (in Equation (5.1)), respectively, and the associated parameter values a_1, \dots, a_{n_a} , b_1, \dots, b_{n_b} and c_1, \dots, c_{n_c} . In order to facilitate the determination of open-loop characteristics from closed-loop data, a prediction error method will be employed to perform the system identification via the ‘direct method’, as articulated in Section 5.3.3.

Given the diversity of the subjects used in the collection of the EuroBaVar data, and the natural variance between individuals with seemingly similar characteristics (e.g. age, gender, mass, height, etc.), there are two options in relation to model structure determination:

1. Determine the best *average* model structure across all subjects, where only the parameter determination is specific to each subject, or
2. Use the optimal model structure for each subject.

While the methodology of option 1 above might appear to provide the best basis for inter-subject comparison (e.g. on a model parameter basis), option 2 has been chosen for the following reasons:

- The main focus is on comparing the baroreflex *frequency response* of subjects, rather than specific time domain parameters, so that overall model accuracy is paramount.
- There is significant disparity between the optimal model orders (n_a , n_b and n_c) for different subjects, making it difficult to achieve well-fitting models for any individuals using a consistent model structure.
- The ability to compare model parameters across different subjects is not a high priority (this will be discussed further in Section 5.6).

It should be noted that, since the input/output delay term, n_d , in Equation (5.1) cannot be included as a ‘linear in the parameter’ identification problem, it is included in the model order determination exercise. Thus, four parameters (n_a , n_b , n_c and n_d) need to be determined during the model order/structure identification stage. In order to choose a model structure which is not excessively complex, the overall performance function used here, Akaike’s Information theoretic Criterion (AIC) (Equation (5.15)) has a

complexity-weighting term. Akakike's information criterion is defined as follows:

$$J^*(\Theta) = \ln(J(\Theta)) + 2\frac{d}{N} \quad (5.15)$$

where

$J^*(\Theta)$ is the complexity-weighted performance function,

$J(\Theta)$ is the original performance function, as given in (5.12),

$2\frac{d}{N}$ is the complexity weighting,

d is the total number of model parameters ($d = n_a + n_b + n_c$), and

N is the number of training data points available.

The use of a complexity weighted performance function is essential in order to achieve model *parsimony*, i.e. attempting to match the model complexity to that exhibited by the training data.

For each individual in the data set, the input/output data was divided into training (2/3rd of the data) and validation (1/3rd of the data) sections. A model was estimated using the training data for a large range of structures ($n_a = 1 \rightarrow 6$, $n_b = 0 \rightarrow 6$, $n_c = 1 \rightarrow 5$ and $n_d = 0 \rightarrow 4$). The model was 'trained' using the training data, while the AIC cost function, specified in Equation (5.15) was estimated using the validation section of the data set. The model structure with the lowest resulting cost function was selected for each individual. The validation section of the data was used for cost function estimation in order to ensure that the parameterised model is capable of predicting previously 'unseen' data (Ljung, 1999), i.e. the model is robust for all data and not only the data it was trained on.

Table 5.4.3 shows the model structures returned using the performance criterion of Equation (5.15), along with the associated Mean Absolute model Errors (MAEs). The MAE, J_{MAE} is defined as:

$$J_{MAE} = \frac{1}{N} \sum_{k=1}^N |y(k) - \hat{y}(k)| \quad (5.16)$$

where N is the number of data points, and $y(k)$ and $\hat{y}(k)$ are the measured and estimated outputs.

The MAE is presented here, since it represents the exact average difference between the model predicted RR interval and the measured RR interval (in sec.).

Note that there is significant disparity in the MAEs for different subjects, indicating the lack of consistency with which a lumped-parameter model may be determined for different subjects, even with freedom in model structure selection. There is also a great variation in the model orders and delays across subjects; however, since we are primarily interested in producing accurate BRS estimates, the main objective of the time domain modelling is model fidelity, rather than enabling a direct comparison of model parameters.

As outlined in Section 5.3.4, the ARMAX model parameters were determined using a prediction error method. As an example, the model parameters, and the associated variance, for the best model structure for Subject 5 in the supine position are shown in Table 5.4.3. The variance value effectively illustrates how well that model parameter satisfies all the training points. If, conceptually, the correct model parameter for each equation represented by the training data (Equation (5.9)) is exactly the same, then the variance of the parameter estimated will be zero. In practice, it is desirable that the variance is significantly lower than the corresponding parameter value.

Table 5.1: ARMAX model structures and corresponding MAEs for each EuroBaVar subject in the standing and supine positions; n_a , n_b , n_c are the orders of the A , B and C polynomials, respectively, and n_d is the number of step delays in Equation (5.1); MAE is the mean absolute error

Subject	Standing		Supine	
	Model struc. [n_a n_b n_c n_d]	J_{MAE} (Secs.)	Model struc. [n_a n_b n_c n_d]	J_{MAE} (Secs.)
1	5 6 5 1	0.0181	5 2 0 1	0.0107
2	4 2 1 1	0.0135	1 6 1 2	0.0077
3	5 3 4 3	0.0121	2 4 0 1	0.0129
4	1 6 1 2	0.0125	3 4 0 1	0.0283
5	4 5 5 0	0.0072	6 5 1 2	0.0099
6	5 5 0 0	0.0101	4 5 0 2	0.0282
7	5 5 0 0	0.0164	1 4 1 1	0.0185
8	1 5 3 0	0.0314	2 6 0 1	0.0301
9	4 2 3 0	0.0146	1 5 0 2	0.0107
10	3 3 1 1	0.0089	1 6 3 1	0.0169
11	1 5 3 1	0.0153	2 6 4 0	0.0263
12	5 3 2 0	0.0176	1 3 3 1	0.0158
13	3 5 5 2	0.0009	1 3 5 0	0.0021
14	3 5 4 4	0.0179	5 1 0 0	0.0117
15	3 5 1 0	0.0134	2 3 0 4	0.0205
16	1 2 1 1	0.0136	6 6 2 0	0.0172
17	4 2 4 1	0.0122	3 3 0 0	0.0219
18	2 2 0 4	0.0011	1 6 0 2	0.0018
19	1 6 4 4	0.0264	5 3 5 1	0.0351
20	1 3 0 3	0.0159	1 2 2 4	0.0271
21	1 4 0 0	0.0213	1 5 1 1	0.0492

Table 5.2: ARMAX model parameters for Subject 5 in the supine position, with model structure $[6 \ 4 \ 1 \ 2]$; a_i , b_i and c_i are the parameters of the A , B and C polynomials, respectively.

Index (i)	0	1	2	3	4	5	6
a_i	1	-1.450	1.468	-1.429	1.328	-0.8189	0.4319
a_i variance	0	± 0.037	± 0.061	± 0.067	± 0.067	± 0.059	± 0.035
b_i	1.37	-1.701	0.778	-1.602	1.19		
b_i variance	± 0.186	± 0.272	± 0.310	± 0.276	± 0.1927		
c_i	1	0.951					
c_i variance	0	± 0.015					

Again, considering Subject 5 (supine position), the match between actual and modelled RR interval is shown in Figure 5.6. In general, the variations in RR interval are captured by the model, though the accuracy at the extreme values of RR is not as good, which may suggest that some nonlinear effects are present in the actual data and not captured by the linear model.

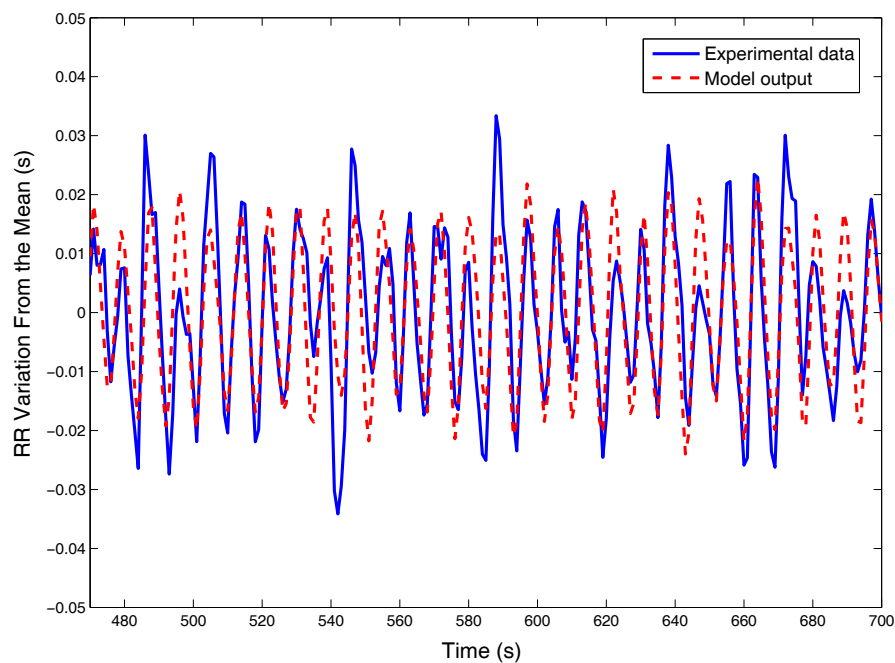


Figure 5.6: Plot of actual and modelled data for Subject 5 in the supine position

5.4.4 BRS calculation

Given that a time domain model has been identified for each subject, this can now be used to determine the magnitude of the frequency response across the frequency range of interest in the training data. In particular, we are interested in the frequency range from 0.04-0.4 Hz, containing the LF (0.04-0.15Hz) and HF (0.15-0.4Hz) baroreflex bands (Pagani et al., 1986; Davies et al., 1999; Glos et al., 2007) described in Section 2.2.4.

In the frequency domain, the magnitude response of the model is determined from input ($u(k) = SAP(k)$) to output ($y(k) = RR(k)$) as follows:

$$|G_{yu}(f)| = |[B(q)/A(q)]_{q=e^{2\pi j f T}}| \quad (5.17)$$

where f is frequency in Hertz and T is the sampling period of the data (the selected sampling interval is 2/3 sec, as previously outlined).

To demonstrate some resulting model characteristics, Figure 5.7 shows the magnitude of the frequency response for Subject 5 in the supine position.

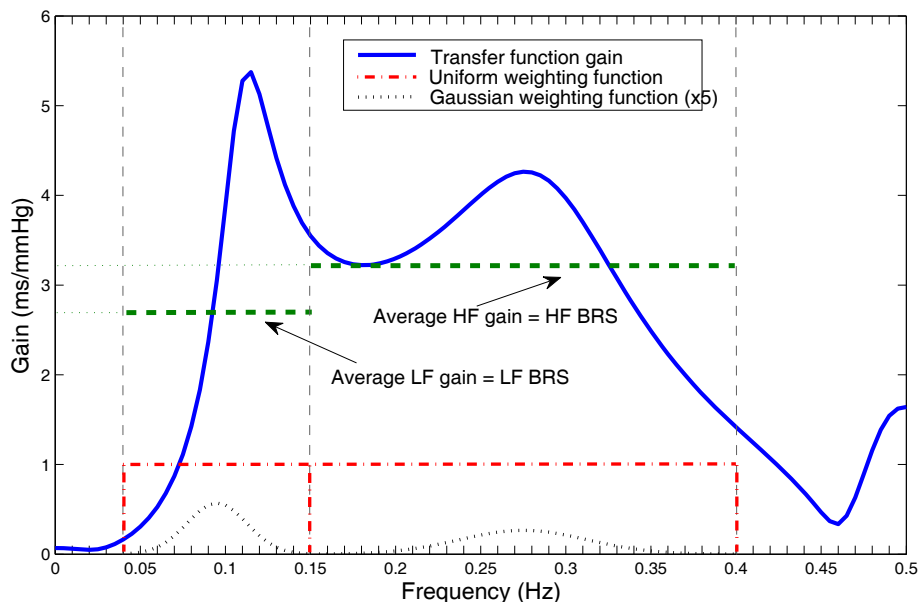


Figure 5.7: Baroreflex gain for Subject 5 in the supine position

As shown in Figure 5.7, the baroreflex sensitivity can be calculated at low (LF BRS) and high (HF BRS) frequency by evaluating an average gain over the low-frequency (0.04-0.15 Hz) and high-frequency (0.15-0.4 Hz) intervals. In general, a representative average gain value over a continuous frequency variable f can be obtained as:

$$BRS(f_{min}, f_{max}) = \frac{1}{N_w} \int_{f_{min}}^{f_{max}} W(f) \cdot |G_{yu}(f)| df \quad (5.18)$$

where $W(f)$ defines the ‘weighting’ profile applied over the interval $[f_{min}, f_{max}]$, and N_w is a normalisation factor, where

$$N_w = \int_{f_{min}}^{f_{max}} W(f) df \quad (5.19)$$

If $G_{yu}(f)$ is only available at N_f discrete frequency points $f_i = f_{min} + i \Delta f$, $i = 0, 1, \dots, N_f - 1$, with Δf being the frequency interval between points, then equation (5.18) becomes:

$$BRS = \frac{1}{N_w} \sum_{i=0}^{N_f-1} W(i) \cdot |G_{yu}(i)| \quad (5.20)$$

and

$$N_w = \sum_{i=1}^{N_f} W(i) \quad (5.21)$$

In uniform averaging, the mean BRS value over an interval $[f_{min}, f_{max}]$ is determined using $W(f) = 1$, $\forall f$. However, we can also propose non-uniform weighting using Gaussian functions, where:

$$W(f) = e^{-\frac{(f-f_0)^2}{2\sigma^2}} \quad (5.22)$$

with σ a constant which determines the width of the Gaussian weighting function and f_0 is the centre frequency of each frequency band. There are a number of reasons for considering non-uniform weighting:

- The value of the baroreflex gain at the centre of the frequency range is more important than that at the fringes,
- The relatively large variation of baroreflex gain, particularly over the low frequency range (e.g. see Figure 5.7) renders a standard average unrepresentative of the central values, and

- Applying significant weight to the baroreflex gain at the boundary between LF and HF can result in considerable contamination between the BRS_{LF} and BRS_{HF} values.

Figures 5.8 and 5.9 show the results for BRS calculation across all EuroBaVar subjects, for standing and supine positions, respectively. In general, we note that the BRS is higher in the case of the supine position compared to standing and that $BRS_{LF} > BRS_{HF}$ for standing (12 Vs 9), while $BRS_{HF} > BRS_{LF}$ for supine (18 Vs 3). We can also see that subjects with impaired baroreflex (Subjects 13 and 18) are clearly identified.

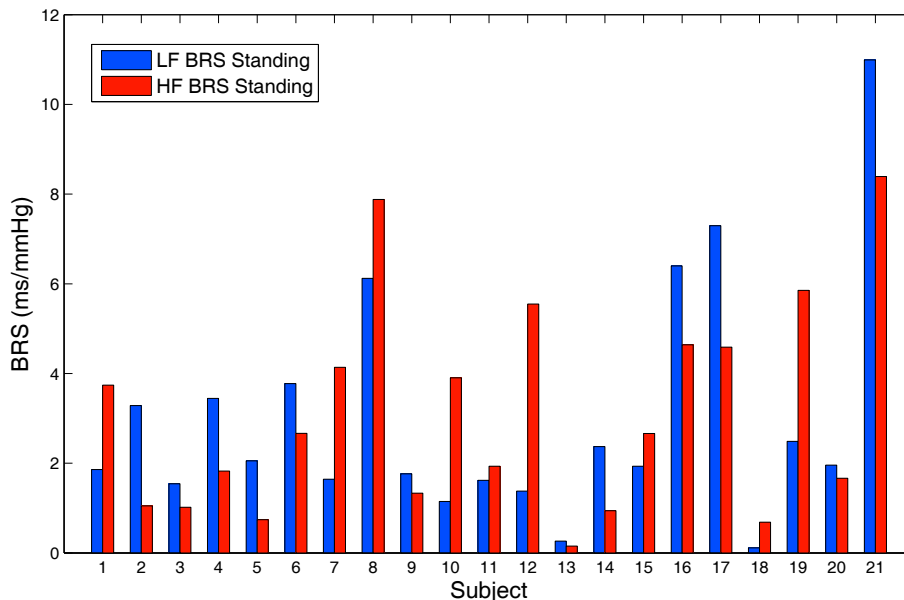


Figure 5.8: BRS estimates for all EuroBaVar subjects in the standing position

5.5 Discussion

A new systematic approach for BRS estimation has been developed in this chapter. One of the most important issues is the use for which BRS estimation is intended and whether it is fit for purpose, especially in the absence of a gold standard. One of the principal uses of BRS is the potential detection of baroreflex pathology. In this sense, we may consider BRS estimation with a classification objective, where the aim is to maximise the separation between healthy and impaired baroreflex characteristics, based on BRS calculations. There are a number of ways in which the classifier can be

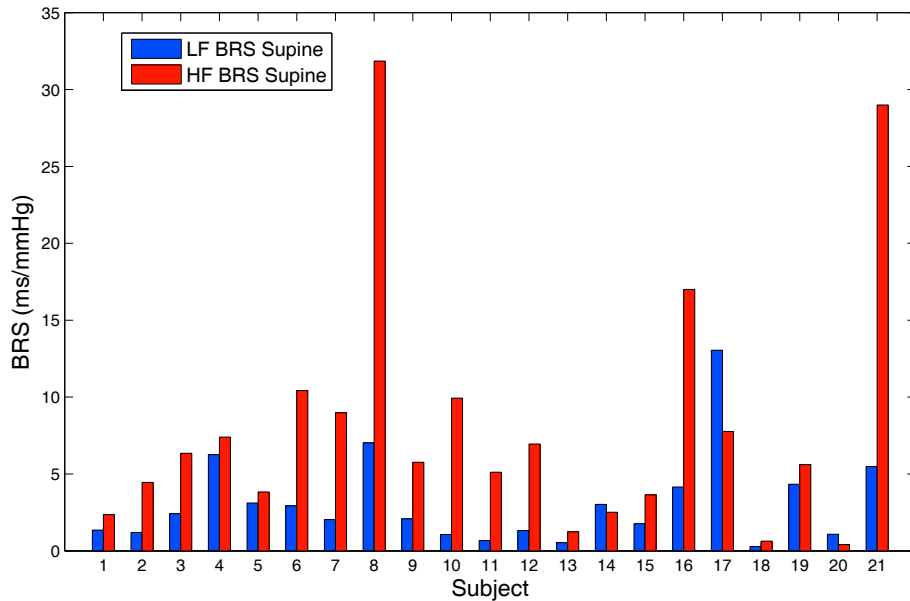


Figure 5.9: BRS estimates for all EuroBaVar subjects in the supine position

customised:

- High-frequency and low-frequency BRS values can be used or the two values can be combined,
- The weighting given to baroreflex magnitude response values to determine an ‘average’ BRS value over a frequency interval may be adapted, and
- Data recorded for supine and/or standing positions can be used or combined.

From a system identification perspective, there are a number of important observations to be made in relation to BRS estimation. The first one relates to the ability to identify BRS consistently from spontaneous baroreflex data. Within the control system community, it is well known that good regulation leads to poor identification and vice-versa (Ljung, 1999). This is due to the fact that a regulatory loop (i.e. the baroreflex) operating effectively will attempt to reduce, as much as possible, the variance of the output (i.e. BP), resulting in poor excitation of the system from a system identification perspective (see Section 5.3.2). The exception to this is where the regulatory loop is not performing well, corresponding to the case of an impaired baroreflex. This is confirmed by our results, where the modelling error is an order of magnitude less in the case of impaired baroreflex (Subjects 13 and 18) than the MAE for the remainder of the subject

population. For the standing case, the average MAE for the impaired subjects is 1ms compared to 15.7ms for the remainder of the standing population. Similarly, for the supine case, the average MAE for the impaired subjects is 1.95ms compared to 20.9ms for the remainder of the standing population. This may give some comfort, since the modelling error, and therefore corresponding BRS estimates, have less error for the case of impaired baroreflex. This phenomenon does raise the issue of what measures of accuracy in BRS estimates might be obtained, to provide some confidence to clinicians in making diagnoses. A number of alternatives exist:

1. Some measure (e.g. MAE) of the modelling error in the RR signal,
2. Some aggregate measure of the variance in the identified model parameters, and/or
3. The variance of the baroreflex gain (compared to the average BRS value) over the frequency interval.

However, the appropriate choice of error measure (which could be some aggregation of the above individual measures) is complex and requires considerable further investigation. A more comprehensive understanding of the error measures across a significantly greater variety of data sets is required; therefore, such issues are not pursued further here.

A related issue concerns the use of minimum thresholds for correlation or coherence between SAP and RR interval by various time and frequency domain methods, respectively (Laude et al., 2004). The use of minimum thresholds attempts to ensure that there is an actual relationship between variations in RR interval and SAP. The problem, however, arises when an appropriate value needs to be selected, and currently, thresholds seem to be chosen subjectively. Data not achieving the prescribed threshold are excluded from the estimation routine, resulting in an inability to form a BRS estimate in some cases. It is speculated that the consistent determination of a BRS estimate, together with an appropriate measure of confidence/error, might be more useful in a clinical setting.

5.5.1 Comparison with other methods

Based on the review of existing BRS estimation methods, it is clear that the method proposed in this chapter has some similarity with other techniques, especially those

utilising time domain models. As outlined in Section 2.2.4, a variety of models have been used to model the relationship between BP and RR interval. The most complex of these models, omitting the use of a separate external input (respiration) are those of De Cecco and Angrilli (1998) and Nollo et al. (2001) which include a coloured noise term. Our contention is that not all models have sufficient complexity to satisfy the requirement that the range of models available includes the actual system model structure, particularly due to the omission of regressor on the noise term (coloured noise), for example of Faes et al. (1999). It is clear that the noise in the system is coloured, since the active noise term (n_r in Figure 2.2) is mainly due to respiration, which has a strong harmonic component. Baselli et al. (1988) provide a very comprehensive closed-loop model identified using the joint input-output method (see Section 5.3.3), however, one drawback of their method is the use of data on a ‘per beat’ basis, so that frequency response measures (e.g. gain) cannot be reliably estimated. Notably, any frequency domain modelling exercise using ‘per beat’ data is problematic, since Equation (5.17) clearly shows the dependence of the BRS value (or at least each magnitude value) on T , the sampling period. It cannot be assumed that T is ‘naturally’ constant, as that would imply that there is no variability in RR , which violates the identifiability criterion (see Section 5.3.2). In reality, RR is not constant, hence the need to resample the signal at a regular sample period in order to eliminate the risk of frequency distortion. A further difficulty with the method of Baselli et al. (1988) is the use of an overly-simplistic model, where their relationship between SAP and RR interval is modelled by a simple gain plus a pure delay.

A brief comment is also necessary here on the variation in model orders across different subjects, documented in Table 5.4.3. As mentioned previously, the aim of this study is to provide accurate BRS estimates, rather than to build a transparent generic model across all subjects. However, it might be expected that the delay term, n_d , would be consistent across models, since the model delay is predominantly a function of the nerve conduction delays, but this ignores the complex relationship between n_d and other model orders, especially n_b . Given then that a freedom in model order variation is allowed, it would seem that the fixed model orders of Nollo et al. (2001), and Patton et al. (1996) are limited in scope. De Cecco and Angrilli (1998) and Nollo et al. (2001) seem to consider a range of model orders; however, the large number of possible parameters (in some cases over 40) cannot be easily justified due to the low levels of excitation in the

input signal and the short length of the data sets.

An additional issue with all spectral methods for BRS estimation, which employ the DFT for calculation of the signal spectra, is the inability of these methods to perform well for closed-loop data (Ljung, 1999). The popular sequence-based methods for BRS estimation also disregard the closed-loop nature of the system, by applying a simple open-loop technique and obtaining regression lines, whose slopes are taken as the BRS estimate.

5.5.2 Results comparison with other methods

In order to assess the quality of a BRS estimate, Laude et al. (2004) investigate a number of different properties of the various BRS estimation techniques used with the EuroBaVar data set.

To assess the reproducibility of the results for each technique, the EuroBaVar data set includes duplicate data for two different subjects. The modelling technique proposed in this chapter always produces identical BRS estimate for the same data sets, while some methods from Laude et al. (2004) show inconsistent reproducibility of results, due to visual selection of data segments. In addition, six of the estimation techniques reported in Laude et al. (2004) were unable to provide estimates for at least one subject, due to various data conditions not being met. Some of the frequency domain methods in Laude et al. (2004) impose minimum coherence thresholds, which were not satisfied by the data for a number of subjects. In the case of the sequence methods, the minimum correlation thresholds and minimum required number of sequences, as well as the minimum change in SAP or RR applied to some of the estimates, were also not met, leading to an absence of results for certain subjects/situations. In general, the thresholds imposed have been designed to improve the reliability of the results; however, these conditions can lead to a restriction in the use of certain methods in practice. In contrast, the procedure described in this chapter does not apply specific thresholds but yields a low baroreflex gain estimate where the data set does not show a well defined relationship between SAP and RR.

BRS estimation techniques should also be able to distinguish well between data in the standing and supine positions, since BRS tends to be higher in the supine case. Most estimation techniques reported in Laude et al. (2004) were able to distinguish

well between the two positions with an average ratio of supine to standing estimates of 2.11:1. The high-frequency BRS estimates obtained here showed a much better distinction between the standing and supine positions with an average ratio of 2.62:1, while the low-frequency estimates were similar for both positions.

The most important feature of a BRS estimation technique, however, is its ability to identify subjects with impaired baroreflex, due to the merit of its use as a prognostic factor in cardiology (La Rovere et al., 1988). Many of the previously reported BRS estimation techniques used with the EuroBaVar data set were unable to identify the two subjects with impaired baroreflex, since some methods were not able to provide an estimate due to threshold restrictions, especially in the supine position. Two techniques were unable to identify a subject with impaired baroreflex, even if a BRS estimate for that subject was available, as the values were not sufficiently different or smaller than the healthy subjects in order to be clearly identified. The BRS estimation technique developed in this thesis is well able to distinguish the two patients with baroreflex failure, as the BRS estimates are very low, especially in the standing position, compared to the other subjects. All the hypertensive subjects, numbered 3, 5 and 11 in Figures 5.8 and 5.9, also show consistently lower BRS values than the healthy population. In general, the BRS_{HF} index appears to have better selectivity, while BRS estimates for the standing position also appear to be able to discriminate better between healthy and impaired baroreflex, compared to the supine position estimates.

Figures 5.10 and 5.11 give the correlation coefficient, $R_{(x,y)}$, between the BRS estimates obtained using the technique developed in this thesis and the estimates of the 21 BRS estimation techniques reported in Laude et al. (2004).

The correlation coefficient $R_{(x,y)}$ between two signals, x and y , is defined as:

$$R_{(x,y)} = \frac{C_{(x,y)}}{\sigma_x \sigma_y} \quad (5.23)$$

where σ_x and σ_y are the standard deviations of x and y , respectively, and $C_{(x,y)}$ is the covariance of signals x and y , defined as:

$$C_{(x,y)} = \frac{1}{n-1} \sum_{i=1}^n (x - \mu_x)(y - \mu_y) \quad (5.24)$$

and μ_x and μ_y are the means of signals x and y respectively.

Methods numbered 1:11 (both in Laude et al. (2004) and in Figures 5.10 and 5.10) encompass various spectral techniques, methods numbered 12:18 are sequence-based techniques, method 19 is a trigonometric regressive spectral analysis technique, method 20 is an ‘XAR’ time domain model developed by Porta et al. (2000) and described in equation (2.2), while method 21 is a Z-coefficient statistical method (Laude et al., 2004).

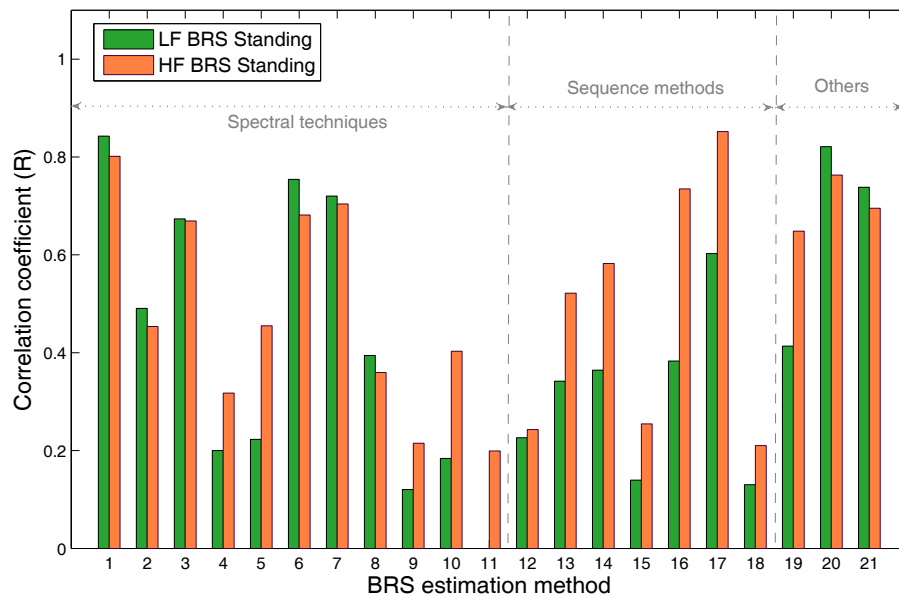


Figure 5.10: Correlation of our LF and HF BRS estimates in the standing position with results from methods reported in Laude et al. (2004)

The HF BRS estimates obtained here for the supine position seem to be well correlated with a large number of the estimation methods reported in Laude et al. (2004), as shown in Figure 5.11, while the LF BRS values have a medium correlation coefficient with most techniques of about 0.5 or less. In the standing position, the LF and HF BRS estimates reported in this chapter are well correlated with some of the spectral methods used in Laude et al. (2004) (namely methods 1, 3, 6 and 7 in Figure 5.10), which are the low-frequency estimates of the transfer function and the α -index methods. The LF BRS estimates obtained here are also well correlated with the time domain ‘XAR’ model results and those of the Z-coefficient statistical method. The HF BRS estimates in the standing position are, in addition, well correlated with the estimates of two of

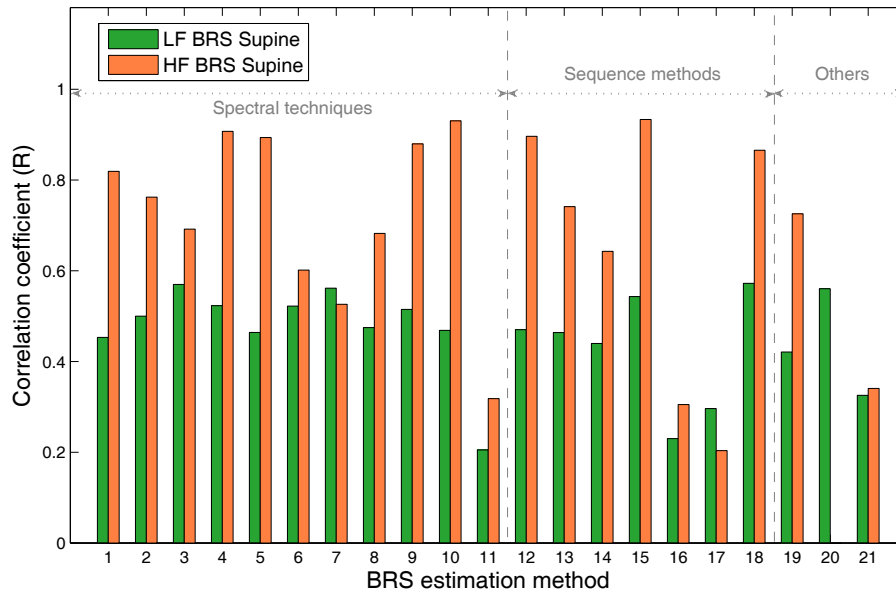


Figure 5.11: Correlation of our LF and HF BRS estimates in the supine position with results from methods reported in Laude et al. (2004)

the sequence methods (numbered 16 and 17).

The high correlation between the frequency domain methods employed in Laude et al. (2004) and the results reported in this chapter is expected since, in effect, both the method developed here and the frequency domain approaches calculate some form of a dynamic relationship or transfer function between the input and output signals (SAP and RR respectively). It is unclear whether all of the spectral methods included in Laude et al. (2004) employed the DFT to estimate the signal spectra, but it is possible that this could be the reason for the difference in actual BRS values between our results and those reported in Laude et al. (2004), with open-loop methods potentially leading to an overestimation of the BRS value. Despite the good correlation between our method and the model by Porta et al. (2000), the results still vary significantly, which is expected, since Porta's model does not include any past output regressor values.

5.6 Conclusions

The accurate and consistent determination of baroreflex sensitivity is a difficult task. This is due to the requirement to measure open-loop characteristics within a closed-

loop system, and relying exclusively on spontaneous measurements. The closed loop is a challenge for the identification method employed but, in addition, the feedback system also tries to reduce variability of the controlled variable (blood pressure), further reducing any natural excitation in the system. In order to address these challenges, this chapter proposes a rigorous procedure which can assess whether sufficient excitation in the input signal is available and then consistently provides reliable estimates of the open-loop properties. BRS estimates under spontaneous conditions may be somewhat challenging; however, it could be argued that it is preferable to using techniques where external stimulus is applied due to the difficulty of selecting an input selective enough to perturb BP without causing any other effects which might adversely affect the system characteristics. For example, the ‘Oxford method’, which utilises a bolus injection stimulus (Eckberg and Sleight, 1992) to alter BP, can also alter sinus node function, which directly alters the RR interval, therefore affecting the correlation between SAP and RR interval. Also, the intervention of external neck suction (Eckberg and Sleight, 1992) can result in conflicting signals from the two sets of baroreceptors, affecting the characteristics of the neural arc. In addition, external stimulation, of either physical or pharmacological nature, may be extremely undesirable in critically ill patients, who would also be most likely to need a BRS estimate for prognostic purposes.

It is important to highlight that the attempt to identify open-loop characteristics from closed loop-data is common in physiological system analysis. The body contains a huge variety of feedback loops, virtually all of which contribute to retaining homeostasis. It is difficult to isolate open-loop characteristics, or administer selective excitation to these feedback loops ‘in vivo’. One notable exception, pertinent to the case of BRS estimation, requires surgical intervention (e.g. denervation), but has a possible role (using animal subjects) in the assessment of the accuracy of the many methods available for BRS measurement. Until a true (non-invasive) ‘gold standard’ has been validated, a rigorous method, which respect the true nature of the systems under study (closed-loop, spontaneous irregularly-spaced measurements) must be employed.

Chapter 6

Nonlinear model of renal vasoaction

6.1 Introduction

The renal circulatory control is central to the overall long term control of blood pressure, through the mechanism of salt and water reabsorption. In addition, sympathetic stimulation of the renal nerves is the chief mechanism for mediating arterial vasoaction, effecting short-term blood pressure control. This chapter investigates the development of a non-linear model for short-term renal vasoaction, based on the dynamic relationship between sympathetic nerve activity and renal blood flow. The model is developed using experimental data obtained from New Zealand white rabbits, who have undergone renal denervation and sympathetic nerve activity is artificially simulated.

According to Equation 1.1, blood pressure regulation is mainly achieved through variation in either cardiac output or peripheral resistance. In this chapter, the focus is on mechanisms that mediate the resistance to blood flow, while CO is assumed to remain relatively constant. This assumption is acceptable, since the experimental data showed a very small standard deviation in heart rate of approximately 2beats/min.

Blood flow is differentially regulated according to physiological needs at any particular time via a variety of hormonal, neural and intrinsic factors, and a succinct overview of the local and systemic mechanisms involved in renal blood flow regulation is provided in Chapter 2. Figure 6.1 (adapted from Richardson et al. (1998)) attempts to summarise

the various factors involved in mediating vasoaction.

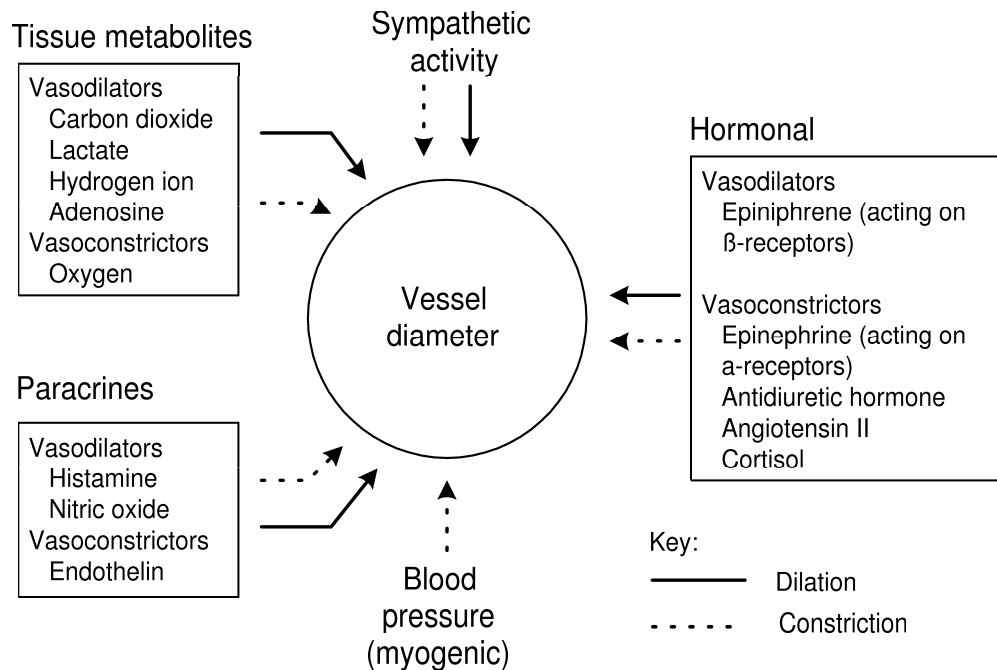


Figure 6.1: Summary of vasoactive mechanisms, adapted from Richardson et al. (1998)

Central to the short-term timescale considered in this chapter, with an approximate time delay between stimulation and response of 0.6s in rabbits (Guild et al., 2001), is the neural control of blood pressure, with sympathetic innervation of a number of major organs and areas of the vasculature, allowing rapid control of resistance via the central nervous system. Fast-acting local factors are also likely to be involved and will be considered during the model development stage as well.

Since the purpose of this chapter is to develop a model that can help improve our understanding of a complex system with multiple interactive mechanisms, it is worth considering a model type that will give us structural information about the system. A grey-box model incorporates a model structure based on *a priori* knowledge about the system under study, while the model parameters, which generally relate to specific system characteristics, are determined using experimental data. A grey-box model would provide a perfect base to construct a model structure for the vasculature response to SNA, exploiting aspects of the physical system description, while numerical methods can be used for parameter optimisation, using experimental data from New Zealand white rabbits.

In previous work (Mangourova and Ringwood, 2006) a number of optimisation techniques were compared to identify which numerical parameter optimisation method is mostly suited to the parameter identification of an initial model (Model A), which will be briefly presented in this chapter. Manual, deterministic and stochastic optimisation methods were included in the comparison in Mangourova and Ringwood (2006). Deterministic optimisation methods, such as gradient descent and Newton's method, generally yield identical solutions when the same initial conditions are used. Deterministic optimisation algorithms are relatively simple and, at least, a local minimum solution is almost guaranteed. Stochastic optimisation methods, such as genetic algorithms (GA), simulated annealing and swarm algorithms, on the other hand, use a degree of randomness in their search methodology, and not only do they give different solutions even when the same starting point is used, but they also have multiple starting points, which can help to combat premature convergence due to local minima. A combination of these two methodologies will be considered in this chapter.

6.2 Experimental protocol

Experiments were performed on anaesthetized New Zealand white rabbits at the Circulatory Control Lab., University of Auckland (Leonard et al., 2000). A transit time flow probe (type 2SB; Transonic Systems, Ithaca, NY, USA), connected to a compatible flowmeter (T106, Transonic Systems) was used to measure renal blood flow (RBF), with arterial pressure being monitored using a catheter inserted into the central ear artery and connected to a pressure transducer (Cobe, Arvarda, CO). The measured signals were sampled at 500Hz, digitized and saved continuously as 2s averages of each variable. In addition, heart rate (HR, beats/min) was derived from the MAP waveform.

For stimulation, the renal nerves were placed across a pair of hooked stimulating electrodes and were then sectioned proximal to the electrodes. Stimulation sequences using frequency modulation (FM) were applied, all using a pulse width of 2ms. Frequencies of 0.5, 1.0, 1.5, 2.0, 3.0, 5.0 and 8.0 Hz were applied in random order using a voltage equal to that required to produce a maximal RBF response. The data was recorded during the stimulation interval of 3 min., followed by a 5 min. recovery period before delivering the next stimulus. A sample of the data collected for one of the animals (Rabbit 1) is shown in Figure 6.2. The data used in this chapter was normalised, so that instead of

working with actual units of blood flow (ml/min), the percentage variation from the initial blood flow level was used. The normalisation was performed separately for each frequency of stimulation. The resulting scaled data for Rabbit 1 is shown in Figure 6.3.

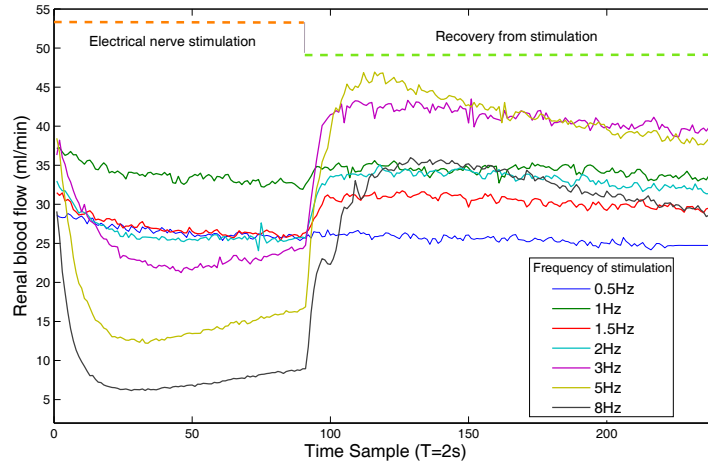


Figure 6.2: Experimental data for Rabbit 1 during electrical nerve stimulation and recovery (includes data for all 7 frequencies of stimulation)

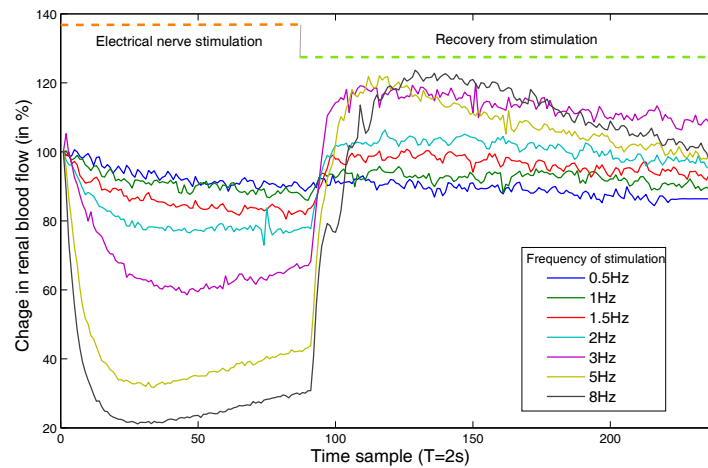


Figure 6.3: Scaled data for Rabbit 1 during electrical nerve stimulation and recovery (includes data for all 7 frequencies of stimulation)

6.3 Model structure development

An initial model structure for the RBF response to SNA stimulation was previously proposed in Mangourova and Ringwood (2006) and was parameterised for a single animal. This initial structure was based on the signal flow diagram shown in Fig. 6.4.

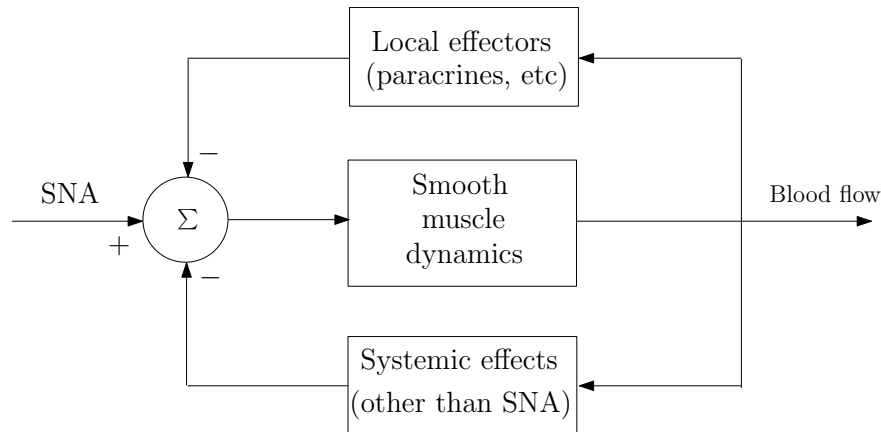


Figure 6.4: Feedforward/feedback vasoaction model configuration

The SNA input into the overall system in Figure 6.4 is outside of the closed loop, since the renal sympathetic nerves were severed, and an electric stimulation was artificially applied on them, rather than arriving from the CNS. The neural control of the renal vasculature (represented as smooth muscle dynamics in the control loop) is considered central to the model, as it is the most significant mechanism acting at the short time scale of interest, while other blood flow effectors are considered reactionary. The two feedback paths represent the effects that local and systemic blood flow/pressure control mechanisms have in response to SNA-induced reduction in RBF.

6.3.1 Model A

Model A, reported in Mangourova and Ringwood (2006), has the structure shown in Figure 6.5. The dynamics of the two feedback paths, shown in Figure 6.4, are combined in a single block in Model A. Since the renal vasculature is just one component which regulates blood pressure, the response from systemic mechanisms to renal SNA stimulation are unlikely to be as significant as that from local effectors. In addition, due to the short time scales involved (180s of renal SNA stimulation), systemic effectors may

not be activated sufficiently to be represented in the RBF signals.

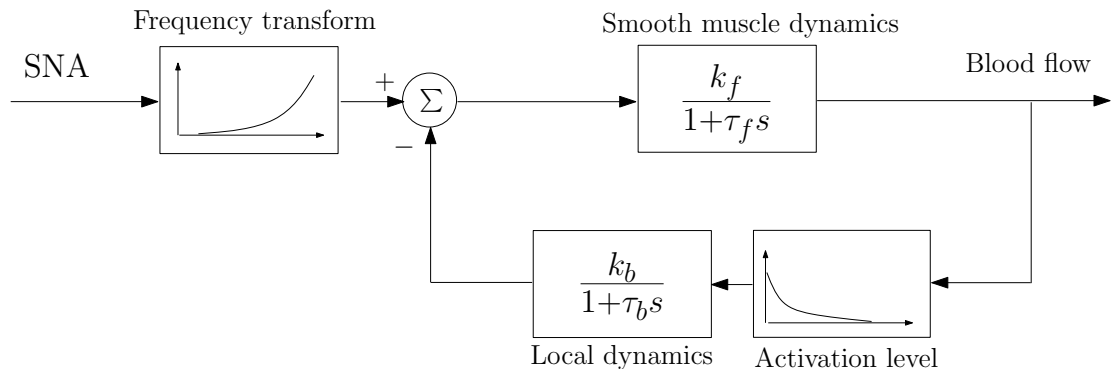


Figure 6.5: Block diagram of vasoaction Model A

Model structure A is based on the following physiological premise. Above a certain (threshold) value of (normal) blood flow, the response of blood flow to SNA is relatively linear. The ‘Smooth muscle dynamics’ block represents the dynamic response of the smooth muscle to the electrical stimulus (via a neurotransmitter) from an appropriate receptor. SNA has a vasoconstrictory effect, thus blood flow is reduced. The speed and magnitude of the response are defined by the time constant (τ_f) and gain (k_f) of the ‘Smooth muscle dynamics’ block. However, when blood flow drops below a certain value, local factors work progressively harder, as blood flow decreases, to maintain an acceptable level of local blood flow, causing reactive vasodilation. The magnitude of this nonlinear response is captured by the ‘Activation level’ block in Fig. 6.5. The ‘Local dynamics’ block in Figure 6.5 captures the speed and (linear) magnitude of response of these local reactionary mechanisms (via the τ_b and k_b parameters respectively). Finally, a representation of the relationship between the frequency of SNA stimulation and steady-state blood flow response (reduction) is added. This (mildly) nonlinear characteristic is given in Fig. 6.5 by the ‘Frequency transform’ block.

Figure 6.6 shows the typical form of the response obtained from Model A. The initial response to a step activation in SNA is roughly first order exponential but, as soon as blood flow reduction reaches a certain (low) level, local (opposite) effects temper the response. Following the release of the SNA activation, the response returns rapidly to the original level (and even overshoots it) assisted by the slowly dispersing local vasodilators.

From the above description, some aspects of the model can be clarified:

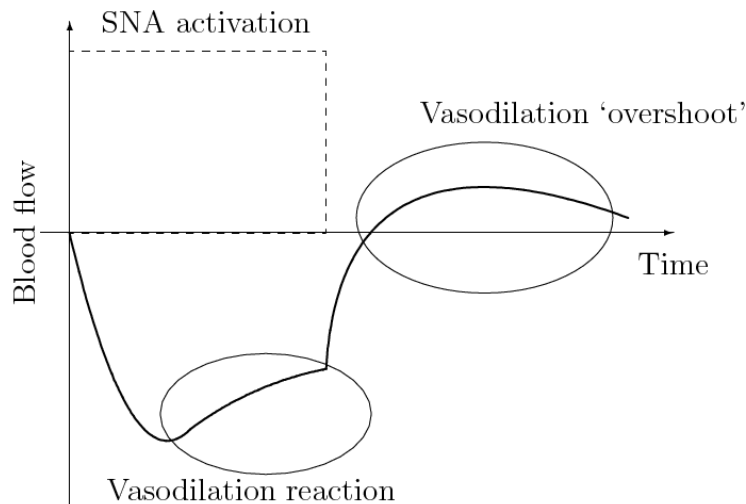


Figure 6.6: Typical large-signal response to SNA activation

- The local vasodilatory response is not linear and has some ‘threshold’ of blood flow change above which it is activated,
- The response of the local vasodilatory reaction is significantly slower than that of the smooth muscle to the SNA stimulus (i.e. $\tau_b > \tau_f$), and
- The magnitude of the action (to SNA) and reaction (by the local vasodilatory mechanism) is comparable, at least to an order of magnitude.

6.3.2 Model B

An alternative model structure is proposed in this section, and even though it employs the same static and dynamic blocks as Model A, it uses a different configuration. In Model B, as shown in Figure 6.7, the smooth muscle dynamics are taken outside of the feedback control loop. This structure again represents the reduction in blood flow due to the neural constrictory effectors being counteracted by the increase in blood flow due to the local dilatory effectors. The sympathetic input to the ‘Smooth muscle dynamics’ block, however, is not affected by the output of the local dynamics block, as it is in Model A. It is felt that this modification is justified since the smooth muscle response to SNA specifically does not change with the addition of local vasodilatory factors, but rather the *response* is a balance of the two.

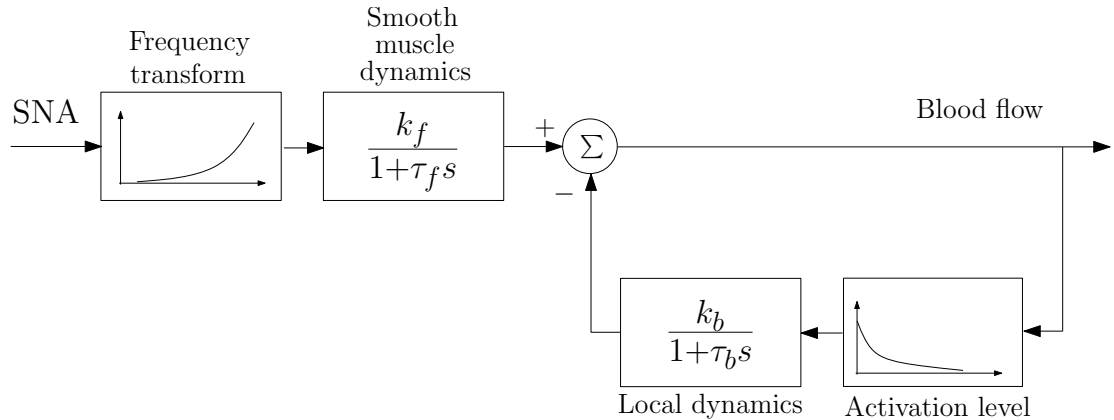


Figure 6.7: Block diagram of vasoaction Model B

6.3.3 Stimulation/recovery models

A further necessary enhancement of the model accounts for the different time constants during the stimulation and recovery stages of the experiment. These are due to different activation and dispersion rates of vasoactive substances, with the slower response during the recovery from stimulation. This is perfectly reasonable, since:

- Recovery from SNA activation is passive and the smooth muscle may take longer to relax than contract under forced activation, and
- Hormones, paracrines, etc. may take much longer to disperse than the rate at which they were formed.

Thus, though the model structure may remain the same for the two stages of the experiment, the gains, time constants and nonlinearity parameters of Model B need to be defined separately for stimulation (180s) and recovery (300s) in order to obtain a better representation of the real system. Figures 6.8 and 6.9 show the Model B structure and parameters for the stimulation and recovery phases of the experiment, respectively. Since there is no SNA stimulation during recovery, the ‘Frequency transform’ nonlinearity during recovery is obsolete.

6.4 Model optimisation

In order to determine the best model parameters, an objective function (J_{tot}) was defined as the sum of the errors, J_k obtained for each frequency of stimulation ($n =$

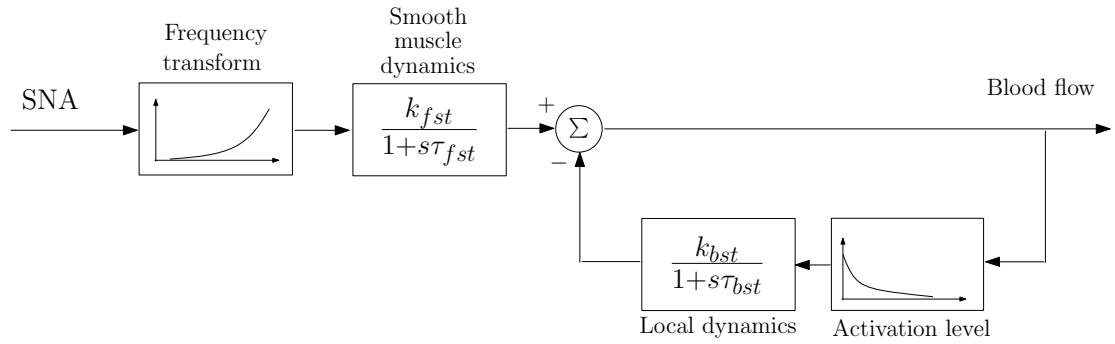


Figure 6.8: Block diagram of Model B, during stimulation

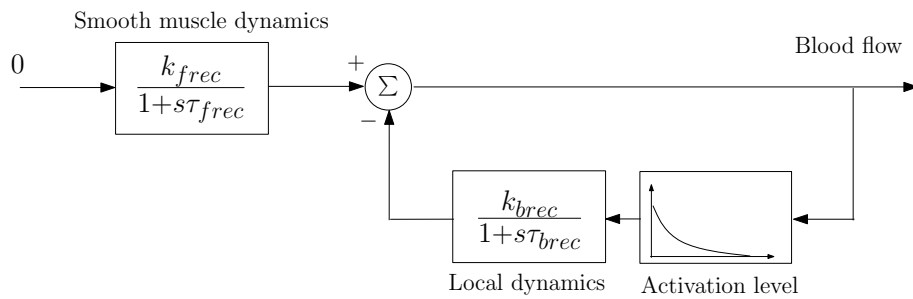


Figure 6.9: Block diagram of Model B, during recovery

number of frequencies of stimulation used):

$$J_{tot} = \sum_{k=1}^n J_k \quad (6.1)$$

where J_k , the error for each frequency of stimulation, is defined in the form of the traditional mean squared error (MSE) as:

$$J_k = \frac{1}{N} \sum_{i=1}^N (y_i - \hat{y}_i)^2 \quad (6.2)$$

- \hat{y}_i is the blood flow data obtained from the model simulations,
- y_i is the actual blood flow data, and
- N is the number of points in the data (in this case it is 240 points for each frequency of stimulation)

The purpose of the optimisation routine employed in this chapter is to minimise the objective function J_{tot} , and a number of optimisation methods are considered next.

6.4.1 Manual parametrisation

Given the intuitive nature of the initial model and the strong relationship with the underlying physiology, the first attempts focussed on tuning the model parameters by trial and error. There are 4 parameters in the dynamic blocks, as well as two piecewise linear functions, to determine. The relationship between SNA and blood flow is approximately linear above a certain threshold level of renal blood flow, hence the feedforward loop dynamics are relatively easy to determine. However, below that threshold level, local factors are activated to oppose the reduction in blood flow, thus activating the feedback path in the model. This latter relationship is nonlinear; hence, the feedback model component is more challenging to parameterise manually. Once the potential of the model was ascertained by relatively good results, more advanced numerical techniques were applied to the models, namely genetic algorithms and gradient techniques.

6.4.2 Genetic algorithms

Genetic Algorithms (GAs) are stochastic and concurrent search methods, which support a set of individuals in a population of potential solutions, where each individual contains information about the parameters to be optimised (Mitchell, 1999). These methods offer a set of solution vectors at every iteration and the fittest individuals can proliferate to improve the solution sets of future generations. GAs attempt to mimic the natural selection process by a number of specific operators: selection, mutation and crossover. At every generation (iteration), the ‘fitness’ of each individual is assessed and the fittest members of the population are selected for the recombination process. These fittest individuals recombine and then mutate in order to produce a new generation of solutions. However, the effectiveness of the algorithm can depend on the encoding technique used, the size of the population or the number of generations used. GAs can be coded either as binary strings, real numbers, integers or characters. There are many advantages to using GAs, which make them suitable for the optimisation problem of the arterial vasodilation model.

- GAs are initiated with a diverse set of potential solutions, also called hyperspace vectors and, usually, a new population of the same size is obtained at every iteration. Using a whole population of solutions facilitates the exploration of a large solution space, where multiple minima can be identified, reducing the risk

of premature convergence to a suboptimal solution.

- GAs use probabilistic methods to determine the next generation, which is an advantage over deterministic methods, as converging on a local minimum can be easily avoided.
- Even though GAs are probabilistic search methods, they are not random in their search process, as solutions with better fitness values are ranked higher, thus the search is directed to solution spaces with better a chance of convergence to a global minimum.

The above characteristics of genetic algorithms make them particularly suitable for the optimisation problem of this chapter, as the solution space is likely to be highly uneven, with multiple local minima, thus numerous concurrent searches would render the problem more manageable.

The main disadvantages of using GAs come from the fact that, in general, GAs do not guarantee to converge on a global minimum and also large population sizes and large number of iterations are needed to ensure good results. This tends to be computationally intensive and time consuming under normal laboratory conditions. Furthermore, a large numbers of parameters to be optimised can cause the algorithm to behave sub-optimally, especially if narrow bands for the parameter values are not specified.

6.4.3 Gradient techniques

Gradient descent search methods attempt to find the maximum or minimum of a cost function by taking the direction and sometimes the relative ‘steepness’ of the slope at any point in order to approximate the next point in the search. Gradient descent methods are deterministic in nature, which indicates that they will always arrive at the same solution, given the same starting point (initial conditions).

One of the advantages of using a gradient method is the speed of response from the optimiser. In cases where the initial conditions of the search are in the vicinity of the optimum solution, the function minimum can be found in a few iterations. Furthermore, these methods almost always guarantee at least a local, but accurate, minimum solution (Renders and Flasse, 1996). However, the success of the gradient technique in finding a global minimum is highly dependant on the starting point of the algorithm.

The parameters of a quadratic cost function, with a single minimum point, would be easy to optimise with a gradient search method. The cost function of a higher order optimisation problem, however, would often have an irregular surface with multiple local minima, apart from the global minimum. The problem at hand, falls into the second category of optimisation problems, i.e. there are numerous parameters to be optimised, including some nonlinearities, which indicates that a highly irregular solution surface is likely to emerge. In the case of multiple minima, it is very likely that the method would converge on the closest minimum point, rather than the global one.

6.4.4 **Combination of GAs and gradient techniques**

Despite the wide search for a global solution, genetic algorithms present an important trade off between computation time, accuracy and reliability, often leading to inefficiency and lack of precision (Renders and Flasse, 1996). An easy solution to this problem is the combination of genetic algorithms and gradient methods. Since the genetic algorithm covers a wide solution space with numerous individual solutions, the ‘best’ solution is likely to be close to, even if not exactly at, a ‘good’ minimum. The end point of a GA routine can thus be used as starting point for the gradient optimisation technique, i.e. the final parameter values obtained from the GA can be set as initial values in the gradient search algorithm. This would almost certainly lead to a cost function minimum, either local or global, depending on the original GA solution and the shape of the cost surface.

In this chapter a quasi-Newton gradient algorithm was employed to determine the minimum of the objective function. Most Newton gradient search algorithms require calculations of the gradient and Hessian (second partial derivative of the function, representing the curvature). Numerical calculation of the Hessian often entails the addition of very large, with very small, numbers. Such computer operations can cause the loss of precision and even lead to divergence from the minimum, in some cases. However, in the quasi-Newton method, the parameter approximations for the next point in the search are calculated using estimates of the Hessian, calculated in a specific manner to reduce precision loss (Schoenberg, 2001). The gradient is also approximated, so the user is not required to explicitly specify it.

Table 6.1: Dynamic parameters for the manually optimised vasoaction Model A and the computer optimised vasoaction Model A and Model B

<i>Parameter</i>	<i>ModelA(GA + Grad)</i>	<i>ModelB(GA + Grad)</i>	<i>ModelA(manual)</i>
k_f	1.04	1.12	1
k_b	72.15	83.097	80
τ_f (s)	20.09	17.86	20
τ_b (s)	179.98	150.45	200
J_{tot}	102.46	97.19	234.59

6.5 Results

A number of result sets are presented in this section. Initially, the parameters for both Model A and Model B were optimised with genetic algorithms and then the quasi-Newton method for a single animal, Rabbit 1, and these results are presented next. For comparison purposes, the parameter values obtained by manually parameterising Model A are also presented. Subsequently, a set of results will be presented for the parametrisation of Model B separately for the stimulation and recovery stages of the experiment. Parameter values are obtained for three different animals.

6.5.1 Model A vs Model B

The results for Model A and Model B, optimised with GAs and the quasi-Newton method, are compared in this section. The dynamic parameters, as well as the minimum cost function (for Rabbit 1), are presented in Table 6.1. The models were trained with all frequencies of stimulation (0.5Hz, 1Hz, 2Hz, 3Hz, 5Hz and 8Hz). The two piecewise linear functions are shown in Figures 6.10 and 6.11. They are marked as ‘Model A’ and ‘Model B’ on each of the figures. For comparison, the values for the manually parameterised model A are also shown. As can be seen in Table 6.1, the parameters for the manually optimised Model A are very similar in values to those optimised by the GAs and the gradient method. This result confirms the quality of the initial model structure. The nonlinearities in Figures 6.10 and 6.11 are also very similar.

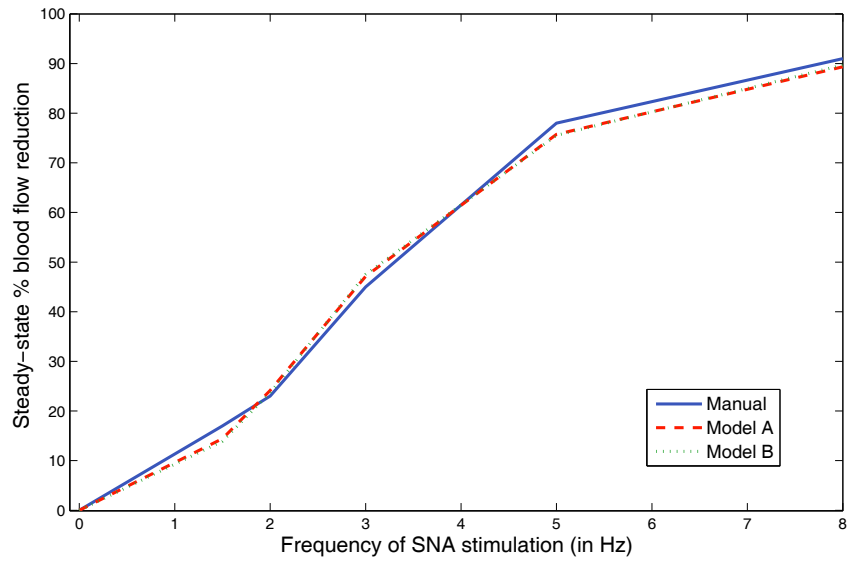


Figure 6.10: ‘Frequency’ transform function for the manually optimised Model A (Manual) and the computer optimised Model A and Model B

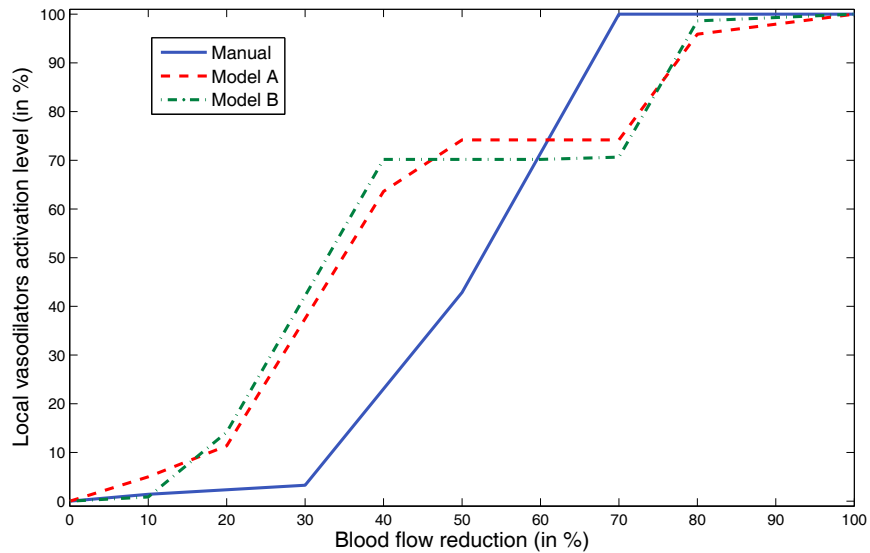


Figure 6.11: Local vasodilator ‘Activation level’ for the manually optimised Model A (Manual) and the computer optimised Model A and Model B

In terms of comparing Model A and Model B, both the parameter values and the cost functions are similar. Nevertheless, since Model B yields slightly better cost results, and also considering the hypothesis that the structure of Model B is a better representation of the true system, Model B was selected for further enhancement, namely the separate numerical optimisation of the stimulation and recovery stages of the model.

6.5.2 Stimulation/recovery models

In this section, Model B is parameterised separately for the stimulation and recovery stages of the experiment, shown in Figures 6.8 and 6.9, thus accounting for the different blood flow responses during stimulation and relaxation. Again, GAs and the quasi-Newton method were used. In the GA optimisation, the average population size used was 700 individuals. The starting values were randomly determined by the GA algorithm. The optimum GA solution was selected from a populations of solutions, after 57 generations, on average. In the case of the quasi-Newton method, applied following the GA search, the initial parameters values were taken to be the parameter values of the best solution obtained with the GA. The gradient, quasi-Newton, method provided minor improvements to converge on the local minima in the vicinity of the GA solutions in an average of 252 iterations.

The stimulation and recovery models, which have the same overall structure (Model B), but different parameter values, are optimised for three different animals. First, the models were optimised for Rabbit 1, the original data set used for model structure development. Then, the stimulation and recovery models were parameterised to fit two other animal sets (Rabbit 2 and Rabbit 3) to assess the quality of the model structure, when used across a number of animals.

In Mangourova and Ringwood (2006), Model A was both manually and numerically parameterised ('trained') using all of the data (stimulation and recovery data for all 8 frequencies of stimulation) and a total cost function (J_{tot}) was evaluated based on the difference between the training data and the model output. In this chapter, the models are trained on four frequencies of stimulation, 1.5, 2, 5 and 8Hz, and are tested with the fifth frequency of 3Hz, with J_{test} being the MSE obtained for the test frequency. This step was undertaken to evaluate the model response, given a previously 'unseen' input and data set.

Table 6.2: Dynamic blocks parameters for the stimulation vasoaction models (Model B) for 3 animals

<i>Animal</i>	k_{fst}	k_{bst}	τ_{fst} (s)	τ_{bst} (s)	J_{tot}	J_{test}
<i>Rabbit1</i>	1.0639	40.6486	15.5304	33.9248	19.89	31.85
<i>Rabbit2</i>	1.3246	39.3004	15.2996	32.8461	67.02	25.37
<i>Rabbit3</i>	1.3824	40.5726	15.5118	33.8387	152.76	46.22

Table 6.3: Dynamic blocks parameters for the recovery vasoaction models (Model B), for 3 animals

<i>Animal</i>	k_{frec}	k_{brec}	τ_{fst} (s)	τ_{brec} (s)	J_{tot}	J_{test}
<i>Rabbit1</i>	0.3058	524.568	30.7281	100.2366	65.93	87.89
<i>Rabbit2</i>	3.8658	506.744	30.48	229.3788	542.91	356.51
<i>Rabbit3</i>	0.2318	1105.89	43.7512	211.528	1003.01	242.45

Comparing the values in Tables 6.2 and 6.3, significant differences can be noted between the dynamic parameters of the stimulation and recovery models, with larger gains and time constants during recovery, as expected. It is also evident that the stimulation models perform consistently better than the recovery ones, in terms of the training and test cost function values, across all three animals. In addition, the cost function values in Tables 6.2 and 6.3 show that Rabbit 2 and Rabbit 3 are not as well represented by their models as the original data set (Rabbit 1), for which the model structure was built. It should be noted here that the cost function J_{test} is obtained for a single frequency of stimulation only (3Hz), while the training cost function J_{tot} is the sum of cost functions for all 4 training sets, thus a difference of a factor of 4 between them is expected (J_{tot} being the higher value). The test results for 3Hz are inferior to the training results, which is misleading, since including the 3Hz data as part of the training set yields very similar results to those when the 3Hz data is used for test only (i.e. unseen during training). This confirms the generalisation capability of the model and suggests that the 3Hz data has somewhat different characteristics to the rest of the data set.

Figure 6.12 shows the ‘Frequency transform’ function for all three animals for the stimulation model. During recovery the model’s input is zero, therefore this nonlinear block’s output is zero for all frequencies of stimulation and does not require graphical representation. Similar values to ours, for normalised BF response to SNA stimulation frequencies of 1.5, 2 and 3Hz were reported by DiBona and Kopp (2003).

From the plot in Figure 6.12 it is evident that there are subtle physiological differences between the three animals, leading to different steady-state percentage blood flow reductions, even if the same frequency of stimulation is applied.

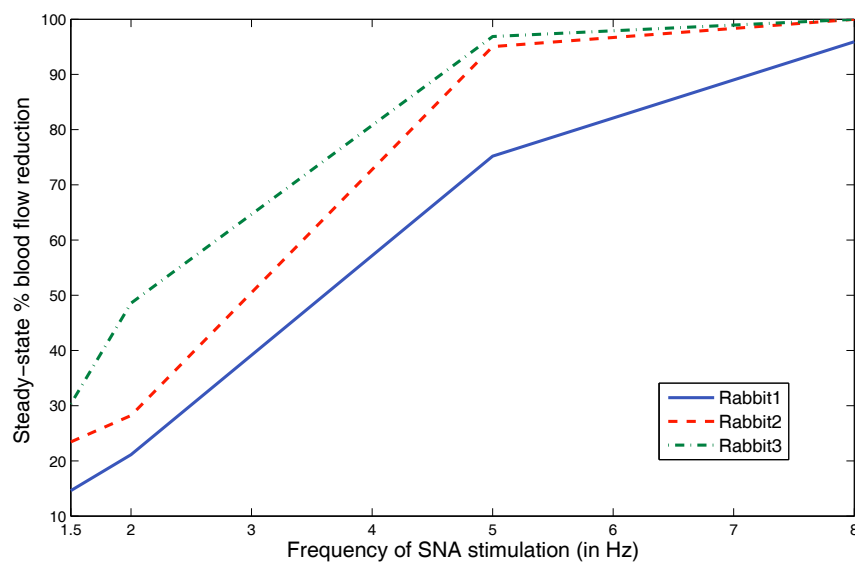


Figure 6.12: Model B (stimulation/recovery) ‘Frequency transform’ function for three animals

The ‘Activation level’ nonlinearity for the stimulation model of all three animals is shown in Figure 6.13, while Figure 6.14 shows the same nonlinearity for the recovery models. One distinctive feature of the models is the *hysteresis* effect in the identified ‘Activation level’ characteristics. These roughly take the form shown in Figure 6.15, which shows a classic hysteresis shape, typical of systems (e.g. electro-magnetic systems) which have ‘memory’ that takes some time to neutralise. In the case of local vasoaction, the memory effect possibly comes from the persistence of local vasodilators which take some time to be dispersed by the bloodstream.

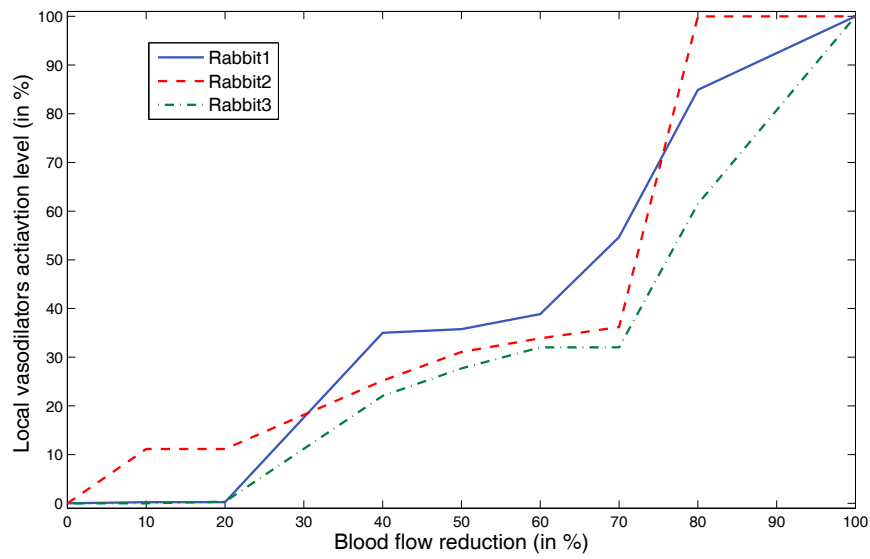


Figure 6.13: Local factors 'Activation level' function for the stimulation model of three animals (Model B)

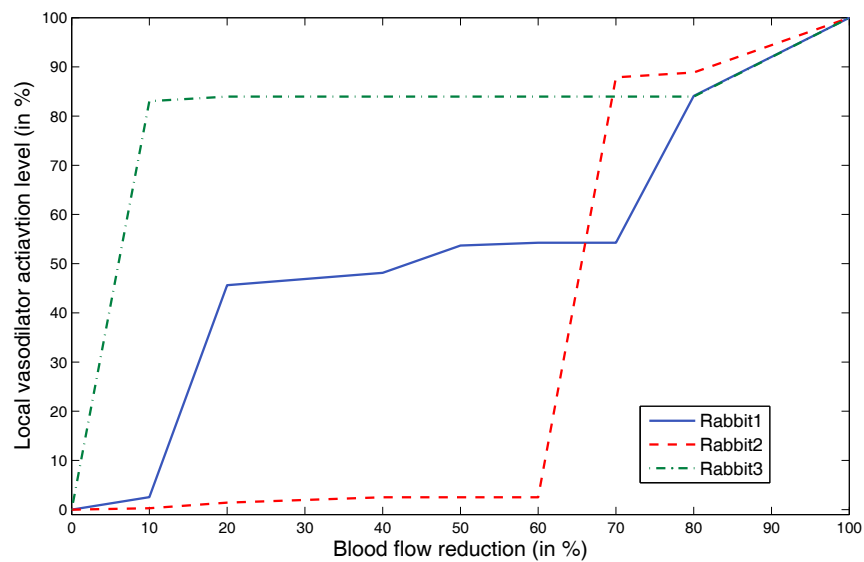


Figure 6.14: Local factors 'activation level' function for the recovery model of three animals (Model B)

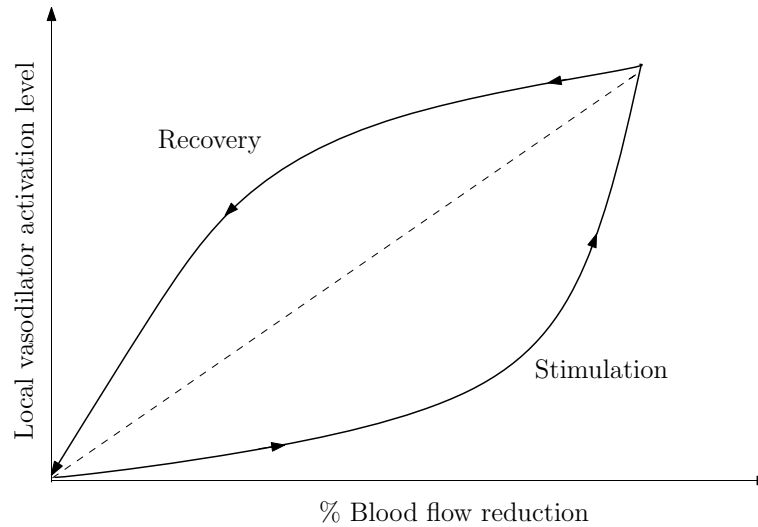


Figure 6.15: Hysteresis effect diagram

A plot of results for the stimulation and recovery stages for Rabbits 1, 2 and 3 is shown in Figures 6.16, 6.17 and 6.18, respectively. There is a noticeable deterioration in the quality of the fit for the recovery stage of Rabbits 2 and 3 compared to Rabbit 1, even though the stimulation stage of the data is relatively well represented. In addition, the data for Rabbit 3, with a stimulation frequency of 8Hz, appears to be very different in its characteristics during the recovery stage of the experiment. Since the blood flow levels during both 5Hz and 8Hz stimulation are saturated close to zero, it is possible that it took a particularly long period of time before blood pressure returned to normal levels during recovery (possibly due to very high levels of vasoconstrictory substances, or else, very low levels of local vasodilators).

6.6 Discussion

This chapter presents a number of large-signal grey-box models for neurally-induced vasoaction in the renal vasculature. The initial model (Model A), developed in Mangourova and Ringwood (2006), even when manually optimised, provided evidence that there is some merit in this proposed model structure and gives some confidence that the model maps well onto the underlying physiology. However, the new alternative model (Model B) more accurately represents the local effector activation since it better reflects the relative spatial locations of systemic and local actions, leading to slightly improved numerical results. An improvement from previous work introduces separate

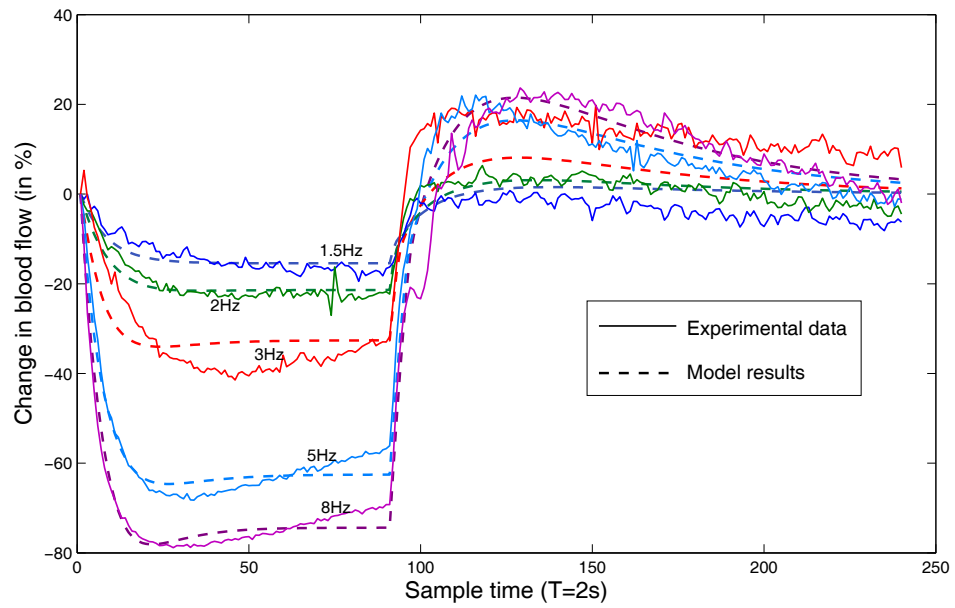


Figure 6.16: Comparison of model output and experimental results for Rabbit 1 (Model B: stimulation and recovery plotted together)

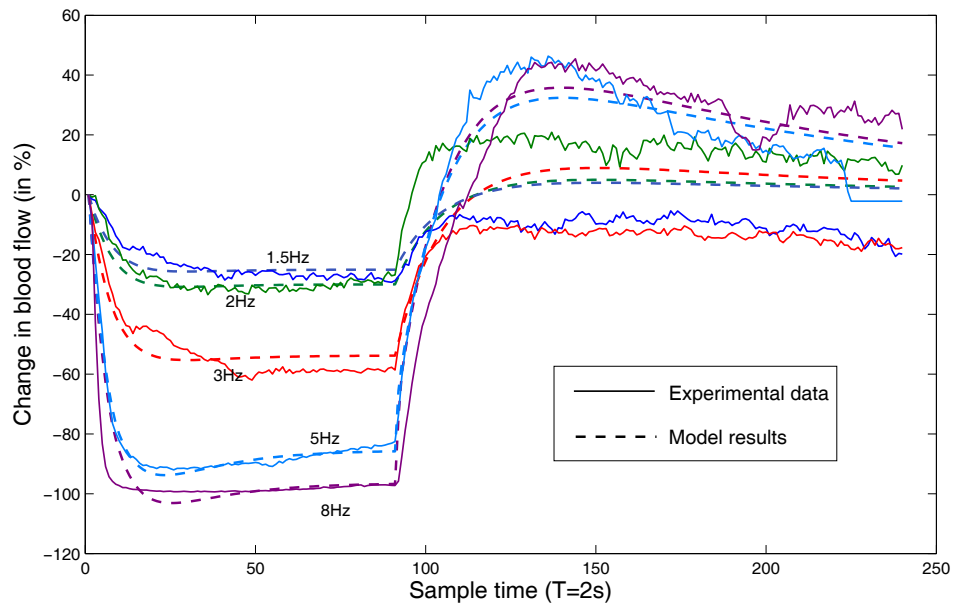


Figure 6.17: Comparison of model output and experimental results for Rabbit 2 (Model B: stimulation and recovery plotted together)

optimisation of the model parameters for the stimulation and recovery stages of Model B. This technique yields mixed results. For Rabbit 1, noting that the cost (MSE) is a

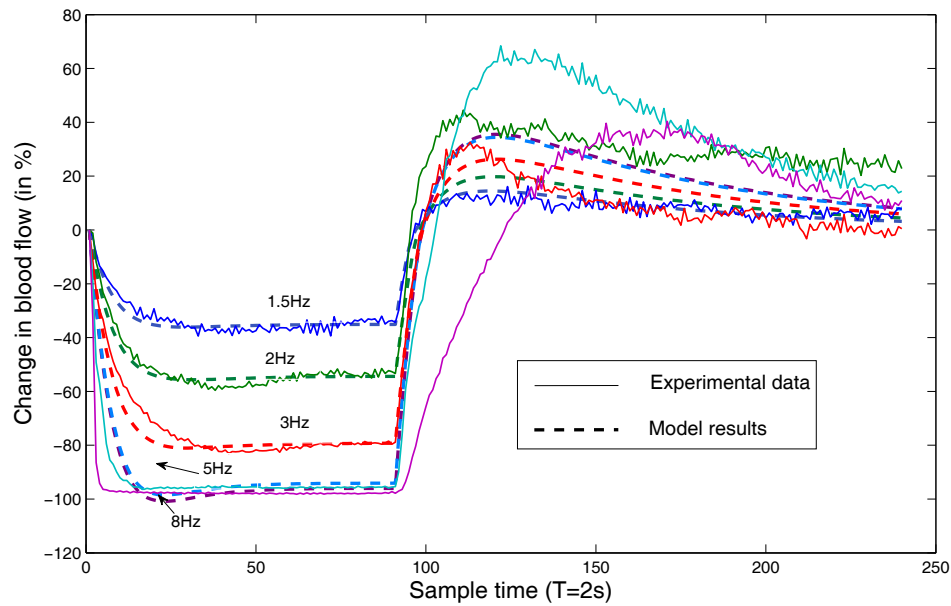


Figure 6.18: Comparison of model output and experimental results for Rabbit 3 (Model B: stimulation and recovery plotted together)

‘per sample’ (mean) measure, the training MSE for the stimulation model is 19.9 (Table 6.2), while the recovery stage has a cost value of 65.9 (Table 6.3). Additionally, the test MSE for stimulation is 31.8, with an MSE value of 87.9 for recovery, which suggests that the structure of Model B is more representative of the vasculature response during neural stimulation and may need to be altered in order to better match the recovery stage.

The work developed in this chapter also improves on previous work by presenting model results for three different animals. Prior work concentrated on Rabbit 1 only while, in this chapter, the stimulation and recovery models were optimised for two additional data sets (Rabbit 2 and Rabbit 3). Additionally, in Mangourova and Ringwood (2006), the model was trained on data for all frequencies of stimulation. An improvement here sees training of the stimulation and recovery models on four frequencies of stimulation and testing them using the remaining frequency of 3Hz.

A number of limitations of this work also need to be mentioned. As evident from the results, Model B performs better for Rabbit 1 and Rabbit 2 than for Rabbit 3. Also, the results for individual animals are relatively good, but it has been difficult to obtain a true generic model. A number of possible explanations exist:

1. Different voltage levels were used for each animal, as seen in Section 6.2.
2. The various frequencies of stimulation were applied in a random order for each animal, resulting in possibly different substances being active in each animal during the same stimulation frequency, inadvertently leading to differential response to the same input.
3. The animals were under anaesthesia, which can affect their response.
4. There was no way to ensure that the same number of nerve fibers were recruited for each animal during stimulation.

The model presented in this chapter focuses on the renal vasculature only and caution must be exercised in any attempt to extend its applicability to other vasculature components or, indeed, to TPR in general. The renal vasculature, however, is a major component of innervated resistance (approximately 30%) and therefore the models have a significant relevance to TPR.

6.7 Conclusions

In conclusion, the proposed model provides a good representation of the relationship between SNA and RBF and gives a good basis for developing a truly generic model. To date, a number of research groups have focused on modelling the relationship between blood pressure and renal blood flow, where particular attention has been paid to autoregulation and the tubuloglomerular feedback mechanism (Holstein-Rathlou and Marsh, 1994; Loutzenhiser et al., 2002). In this chapter the model represents the RBF response to SNA stimulation. It is likely that autoregulation has a contribution to the total blood flow response in the system considered in this chapter; however, it is beyond the scope of this work to quantify specific components and the magnitude of their action. Nevertheless, it is reasonable to suggest that the feedback loop represents a sum of the responses of all local mechanisms, which may be of both a vasodilatory and vasoconstrictory nature.

A study on conscious animals (Berger and Malpas, 1998), which focused on modelling the BF response to SNA and BP, demonstrated that using both SNA and BP as input to the model leads to better results than modelling separately the relationships between

SNA and BF and that between BP and BF. Therefore, future work could attempt to incorporate previously identified models for the renal blood flow response to blood pressure and nerve activity. This would be an important step forward, as it is suggested that 80% of the variation in renal blood flow can be accounted for by changes in blood pressure and SNA (Berger and Malpas, 1998).

The proposed model structures deliberately separate dynamic and nonlinear elements (with a Hammerstein structure (Ljung, 1999) in the feedback path) in an effort to make the model as transparent as possible and facilitate parameter tuning. A successful model can be helpful as part of the modelling effort to investigate the origins of low-frequency (circa 0.1 Hz in humans) oscillations in blood pressure. Current models utilise a relatively simple linear first-order dynamic element to represent the resistance component of the vasculature (Ringwood and Malpas, 2001), and while this representation is adequate for small-signal situations, it is known that oscillations of a significant amplitude can occur under certain physiological conditions e.g. haemorrhage (Malpas and Burgess, 2000). Inclusion of the counteractive vasodilatory mechanism in the models presented in this paper is likely to make a significant change to predictions of oscillation amplitudes (particularly at higher amplitudes) compared to current models utilising simple linear models.

Finally, using a slightly different modelling methodology could yield a better representation of the the physiological system. Instead of using genetic algorithms for parameter optimisation, a genetic programming (Smith and Cagnoni, 2010) approach could be taken. This would involve the use of computer software not only to tune the parameters of a predefined set of ‘blocks’ in the model, but also to select the model ‘blocks’ and configuration that are most appropriate to represent the data.

Chapter 7

Conclusions and future work

7.1 Summary and conclusions

This thesis presents the development, implementation and simulation of a number of novel mathematical models of important short- and long-term blood pressure control systems in the body.

A wide variety of mathematical models exist, including, among others, continuous- and discrete-time, linear and nonlinear, white-, grey- and black-box models. The model type is selected based on the type of system under study, the availability of *a priori* information about the system structure and parameters, and on the application and use of the resulting model. Models can also be designed using mathematical equations from first principles or they can be implemented and simulated in a modelling and simulation environment.

A nonlinear, grey-box modelling approach has been taken, in this thesis, for two different system representations. Grey box models combine the characteristics of white- and black-box models, by adopting a model structure, which is based on some known physical system characteristics, while the model parameters are identified using numerical optimisation methods and experimental data (Ljung, 2008). The modelling applications, where nonlinear grey-box modelling was applied in this thesis, were those of salt-induced hypertension and local vasoaction under SNA stimulation. The parameter identification methods, used in the two different modelling exercises, were markedly different, thus demonstrating a modest range of possible techniques for physiological

modeling.

In the local vasoaction model, described in Chapter 6, a significant external excitation is applied to the system, namely, electrical stimulation of the renal nerves, while the regulatory system operates in open loop, due to the severing of the renal nerves connection with the central nervous system. A model (Model B) was optimised separately for the stimulation and recovery stages of the model experiment with a combination of genetic algorithms and a quasi-Newton method. The parameter identification routine, proved to be very computationally intensive, while not necessarily obtaining optimum results, possibly due to the unsuitability of the model structure for the representation of the recovery part of the experiment. With the recent leap in computational power, however, genetic algorithms are now much less time-consuming and provide a very valuable technique (in combination with a gradient descent method, such as the quasi-Newton method), for physiological model parameter identification. It is worth noting that the vasoaction model, developed in Chapter 6 was very successful in representing the blood flow dynamics during nerve stimulation, but a different structure for the recovery process is needed, in order to understand and better represent the mechanisms involved in arterial vasoaction. The development of models such as the nonlinear grey-box model described in Chapter 6 is an important step in producing an overall model of the neural control of the circulation.

Similarly, modelling of the dynamics of salt-induced hypertension, using a nonlinear grey-box model (Chapter 4), proved to be very successful for a variety of experimental protocols. The model was developed to represent the blood pressure response to a high-salt diet in the Dahl rat. Three different model structures of varying complexities were proposed and their parameters were optimised using four distinct data sets (obtained from 4 separate experimental protocols). Even though the regulatory control loops of all animals were intact from a surgical and pharmacological perspective, and thus one would expect that a linear model would be adequate, this did not prove to be the case. A nonlinear model structure was necessary possibly due to a genetic predisposition of the Dahl-S rat to SIH, which would have led to one or more of the blood pressure control systems in the Dahl-S rat to malfunction, especially after prolonged exposure to a high-salt diet. Combining a model structure based on some physical characteristics of the system and the simplex method (Nelder and Mead, 1965) for parameter optimisation proved to be very successful in achieving a high-fidelity blood pressure

model response. The most complex of the three SIH models, developed in Chapter 4, showed the distinct multi-component nature of the long-term blood pressure response to a high-salt diet. Even though it is difficult to assign exact physiological meaning to each model component with certainty, the distinct components indicate the magnitudes and time scales (time constants) of the various processes involved in the development of salt-induced hypertension in the Dahl-S rat.

In contrast, a black-box modelling approach was taken to derive a mathematical model of the arterial baroreflex, with the purpose of establishing a rigorous procedure for baroreflex sensitivity estimation in humans. The ARMAX black-box model, employed to represent the baroreflex (Equation (5.1)), is linear, since it was designed to utilise spontaneous closed-loop SAP and RR interval data, as the system input and output respectively, and the RR signal variation around the equilibrium point is relatively small. The black-box structure of the model does not lend itself to assigning physiological meaning to the model components; however, the purpose of the model is quite different - the focus is on estimating the BRS index from the model's frequency response characteristics. The novel system identification approach to BRS estimation developed in Chapter 5 (based on the black-box model of the baroreflex) appears to be very successful in estimating BRS and distinguishing subjects with BRS failure. The BRS estimation method developed in this thesis also adheres tightly to the principles of system identification in closed loop, which are not commonly observed in some of the popular existing BRS estimation methods, as outlined in Chapter 5. The system identification approach to BRS estimation, employed in Chapter 5 has only been tested using the EuroBaVar (Laude et al., 2004) data set, but if tested and validated on a variety of additional data sets, it could possibly be incorporated and used in clinical settings as a predictor of future adverse outcomes (La Rovere et al., 2008). While the system identification approach described in Chapter 5 in this thesis is primarily concerned with the development of a systematic and rigorous method for BRS estimation, this modelling method can also be potentially applied to other regulatory loops within the body, where identification of open-loop properties from closed-loop data, is required.

Finally, this thesis has taken a large integrative model (Guyton et al., 1972b) and has taken its implementation to a new level. Guyton's model equations were previously implemented in a C-like programming language and the model was simulated in the MODSIM environment (Montani et al., 1989). Guyton's model conception and com-

puter implementation was, at the time, a huge achievement and provided a tremendous research tool to the physiological community; however, the potential for modernisation of the model implementation, and hopefully further development of the model itself, grew with the advent of more powerful computing and modelling and simulation software with more advanced visualisation capabilities. This thesis has taken a new approach to Guyton's model implementation, the model was implemented in a visual, hierarchical block-diagram environment (MATLAB's Simulink), where each block of the model has a specific meaning, but individual blocks are also combined into meaningful subsystems and systems. In addition, some of the most basic blocks were combined in such a way that they could visually provide basic information on parts of the system characteristics, such as steady-state gains and time constants. It is anticipated that concealing the, sometimes, visually unnecessary detail of the various systems and subsystems, would facilitate researchers in improving and building on sections of the model. Even though some other Simulink implementations of older versions of Guyton's model exist (Thomas et al., 2008; Kofranek et al., 2007), none have used the most up to date version of Guyton's model and none have employed the specific hierarchical visualisation method used in this thesis. Guyton's model has been developed further under the QHP/HumMod project (Hester et al., 2008, 2010, 2011); however, there are significant discretisation and implementation issues, due to the model being implemented in a high-level programming language in sequential code, as discussed in Chapter 3.9. In addition, the XML format of the HumMod model equation presentation is not user friendly, as the model's overall structure is not easily visualised.

Currently, Simulink-like environments remain one of a few limited options for the development and validation of an integrative model with the capability of visualising and emulating the hierarchical continuous-time nature of physiological systems (by using continuous-time dynamic blocks) and simulating the model with a numerical solver that is appropriate for the system.

The breadth of applications, and modelling and optimisation methods, in this thesis present an opportunity to make general observations about modelling of physiological systems. Even relatively uncomplicated techniques, from an engineering perspective, can significantly aid the advancement of physiological research. The variety of methods used here are applicable to many different physiological systems and there is a huge potential for future physiological exploration with the aid of mathematical mod-

elling.

7.2 Future work

There is enormous potential to further develop the work presented in this thesis. Four distinct applications of mathematical modelling were examined in this work and each of these areas can be improved on in the future.

Guyton's model implementation

There is considerable opportunity to develop Guyton's integrative physiology model further, in the form of a community project, in order for researchers to be able to use and add to and improve the existing model. The hierarchical, block-diagram, form of the Simulink implementation of the latest version of Guyton's model, presented in Chapter 3, has a very intuitive nature and visualisation. The addition of an open-access repository system for model components, where researchers can store various updates and suggestions, would benefit the whole physiology community and would help further the research into systems physiology. A potential improvement would also see the model implemented in a free open-access modelling and simulation environment, which does not suffer with compatibility issues between 'versions' of the software; however, it is currently difficult to identify a good potential solution, as the need for a stable, visual, block-diagram, hierarchical environment places a lot of constraints on the possible choice of software.

Baroreflex sensitivity estimation

The system identification approach to BRS estimation proposed in this thesis has tremendous potential for development and application in both research and clinical practice. The approach would need to be tested further, and validated, with additional experimental data, while clear guidelines for distinguishing between subjects with healthy and impaired baroreflex are required. The ARMAX model (Equation (5.1)) of the baroreflex used in Chapter 5 has a single input (SAP) and a single output (RR interval). Arguably, a better model representation of the system could be obtained

by measuring respiration and including it as an external input to the model. Another direction for further work, in the BRS estimation field, is currently being investigated. The validity of using the very popular sequence method for BRS estimation is being examined. The work is concentrating on artificially designed signals, so that the ‘correct answer’ of the estimation method is known with certainty in advance. Preliminary results show that there is a strong positive bias for a system with positive gain when a sequence method is used for gain estimation; thus, the use of sequence methods for BRS estimation may need to be reconsidered.

Modelling of salt-induced hypertension

The models of salt-induced hypertension in the Dahl rat, presented in Chapter 4 could, in the future, be tested and validated against data from other animal species, in order to investigate the generic applicability of the model structure. The models could also be used to investigate the specific physiological mechanisms that each block represents, as it would be possible to design more informative experimental protocols in the future, with the specific knowledge of the type of blood pressure response that is obtained by salt loading. Additionally, the current models, described in Chapter 4, are optimised for individual animals only, while the measurement of additional variables during future experimental protocols could potentially allow the development of an inter-animal model. Furthermore, analysis of the health status of the kidneys could also potentially provide information on the nature of some of the blocks in the model structure.

Modelling of vasoaction

Mathematical modelling of the behaviour of the renal vasculature, and the resulting renal blood flow, during and after electrical nerve stimulation (simulating SNA), has much potential for future developments. The novel model structure (Model B), developed in Chapter 6, performed better for the stimulation than recovery part of the experiment, even when the model parameters were optimised separately for stimulation and recovery. A different model structure is possibly needed to represent the recovery stage of the experiment. An attractive method for improving the model structure would be to use a genetic programming approach (Smith and Cagnoni, 2010), where the optimisation process selects not only the model parameters, but also the ‘blocks’

and 'links' in the model structure too. Once a satisfactory model is obtained, it can be used as part of an overall model for the neural control of the circulation (Ringwood and Malpas, 2001).

Appendices

Appendix A

Salt-induced hypertension model results

A.1 3-component model results

Table A.1: SIH modelling results for individual salt-sensitive animals of Protocol 1, 3-component model

Animal	MSE	MAE	G_{as}	τ_{as} (d)	G_{pr}	G_{ss}
SB1	3.7547	1.3586	3.4075	2.3076	0.0009	0.0745
SB2	4.2531	1.7405	3.4113	1.7416	0.004	0.1077
SB5	4.0675	1.5246	3.4453	1.3718	0.0027	0.0611
SB7	4.0702	1.585	3.4821	1.1801	0.0031	0.1177
SB10	4.2693	1.735	2.5603	1.2141	0.0101	0.1491
SB11	22.8316	3.6309	4.0055	0.6265	0.0112	0.1452
SB12	5.4995	1.9524	3.8247	0.9377	0.0004	0.0875
SB13	4.5589	1.5886	3.1035	0.961	0.0044	0.0855
SB16	6.6754	2.1206	3.9735	1.391	0.0034	0.1034

Table A.2: SIH modelling results for individual salt-sensitive animals of Protocol 2, 3-component model

Animal	MSE	MAE	G_{as}	τ_{as} (d)	G_{pr}	G_{ss}
R07	15.1644	3.0629	5.8042	2.2654	0	0.1257
R08	3.2228	1.4455	1.7589	1.1805	0.0132	0.0223
R10	3.5696	1.4297	2.5544	1.2678	0.0079	0.0133
R11	5.8613	1.8569	1.1525	1.7609	0.0268	0
R19	17.7748	3.2704	1.8125	0.8755	0.0172	0.2041

Table A.3: SIH modelling results for individual salt-sensitive animals of Protocol 3, 3-component model

Animal	MSE	MAE	G_{as}	τ_{as} (d)	G_{pr}	G_{ss}
SB23	8.5748	2.2531	1.4931	1.4729	0	0
SB24	5.1826	1.9478	1.2628	1.0685	0.0016	0.042
SB31	9.3277	2.409	1.4415	1.8262	0.0091	0.1298
SB32	7.7997	2.3398	2.4206	1.8306	0.0008	0.133
SB33	2.9092	1.2953	1.2535	1.8343	0.0067	0.0488
SB35	6.7102	2.1777	0.4547	1.5082	0.0391	0.0184
SB36	5.4087	1.8664	2.4207	1.6652	0	0.0404
SB37	5.7305	1.9905	2.188	1.5938	0	0.097

Table A.4: SIH modelling results for individual hybrid animals of Protocol 4, 3-component model

Animal	MSE	MAE	G_{as}	τ_{as} (d)	G_{pr}	G_{ss}
FF2	2.2176	1.1944	1.2322	1.746	0.0039	0.0252
FF5	1.6622	0.997	0.6352	2.4346	0.0108	0.0559
FF6	2.4552	1.2963	1.1463	1.3991	-0.0003	0.0068
FF8	1.8653	1.0994	1.0103	1.9893	0.0083	0.0242
FF9	1.2757	0.8091	1.7362	1.7337	0.0002	0.0351
FF11	6.8646	1.864	0.9307	1.5328	0.0056	-0.0324
FF14	1.2649	0.7888	0.6986	1.5304	0.0026	0.0162
FF17	2.4316	1.1129	1.074	1.8358	0.0062	0.0271
FF21	1.4008	0.9335	1.1121	1.7858	0.0025	0.0159
FF24	2.9448	1.221	3.0251	1.9617	-0.0011	0.0593
FF25	1.9724	0.988	1.38	2.2358	0.0054	0.0501
FF27	2.1311	1.0426	1.231	2.033	0.0042	0.0121

Table A.5: SIH modelling results for individual salt-resistant animals of Protocol 1, 3-component model

Animal	MSE	MAE	G_{as}	τ_{as} (d)	G_{pr}	G_{ss}
RB2	2.1481	0.8118	1.0061	9.0046	-0.0061	0.0095
RB3	2.5335	1.088	1.5873	0.6264	-0.0061	0.0285
RB5	1.8012	0.9586	1.503	1.2229	-0.004	0.0407
RB6	0.8892	0.5585	1.5407	1.2505	-0.0063	0.0364
RB8	3.2859	0.8598	1.5743	1.3519	-0.0074	0.0308
RB10	0.8263	0.5888	-0.5476	0.6266	-0.0012	0.0159
RB11	1.9693	1.0268	0.6223	0.6265	0.0005	0.0258

Table A.6: SIH modelling results for individual salt-resistant animals of Protocol 3, 3-component model

Animal	MSE	MAE	G_{as}	τ_{as} (d)	G_{pr}	G_{ss}
RB18	3.4655	1.3196	0.3177	1.1123	0.0141	-0.0006
RB19	3.2785	1.4388	0.4529	1.6614	0.0059	-0.0106
RB20	2.3774	1.2583	0.8742	0.7585	-0.0056	0.033
RB21	2.6686	1.2418	1.4303	27.8952	0.0333	-0.0913
RB22	2.3793	1.2072	0.3304	0.8668	0.0219	0.0163

A.2 4-component model results

Table A.7: SIH modelling results for individual salt-sensitive animals of Protocol 1, 4-component model

Animal	MSE	MAE	G_{as}	τ_{as} (d)	G_{pr}	G_{ss}	G_c	τ_c (d)
SB1	3.5517	1.2934	5.5183	4.1536	0.0007	0.0801	2.4827	8.7662
SB2	3.5951	1.5238	12.3905	5.0189	0.0021	0.1296	11.4317	8.7813
SB5	4.1402	1.5355	4.6272	2.6138	0.0028	0.0696	1.9611	10.1671
SB7	3.7503	1.5295	3.4024	1.5743	0.0031	0.1121	-0.5193	39.3592
SB10	3.9285	1.5289	3.4927	2.4075	0.01	0.1904	4.3759	22.2371
SB11	14.4892	2.8884	4.059	0.6877	0.0156	0.2101	5.7202	28.5162
SB12	4.9526	1.8528	8.8138	2.4143	0.0007	0.0946	5.7417	4.6302
SB13	4.205	1.4947	3.647	1.9484	0.0055	0.1206	3.481	26.7849
SB16	5.6452	1.9055	6.1784	2.9862	0.0042	0.1591	6.5791	18.2401

Table A.8: SIH modelling results for individual salt-sensitive animals of Protocol 2, 4-component model

Animal	MSE	MAE	G_{as}	τ_{as} (d)	G_{pr}	G_{ss}	G_c	τ_c (d)
R07	13.7273	3.1533	8.0644	4.5671	0	0.0861	0.6375	6.438
R08	1.9622	1.1137	2.8052	2.1506	0.0089	0.0493	2.8939	17.988
R10	2.4772	1.2273	2.5719	1.7242	0.009	0.0057	0	18.664
R11	4.2577	1.6309	3.475	2.7366	0.0086	0.117	10.6539	32.3719
R19	16.2897	3.0981	2.1817	1.8714	0.0195	0.4343	28.5152	77.8351

Table A.9: SIH modelling results for individual salt-sensitive animals of Protocol 3, 4-component model

Animal	MSE	MAE	G_{as}	τ_{as} (d)	G_{pr}	G_{ss}	G_c	τ_c (d)
SB23	5.0288	1.7229	5.2519	1.9077	0.0024	0.0131	5.0945	5.1413
SB24	2.1573	1.0948	2.2808	1.5697	0.0091	0.0404	2.1391	9.2932
SB31	5.6248	1.8609	0.8883	2.1761	0.0638	0.1158	1.9696	20.7528
SB32	4.1656	1.604	3.3549	2.5361	0.0092	0.138	3.4513	17.2127
SB33	2.0626	1.1599	3.4697	3.0668	0.0071	0.0543	3.5832	8.3518
SB35	4.4001	1.6518	3.3557	2.7279	0.0125	0.0199	4.5858	6.9818
SB36	2.8215	1.3286	4.2908	1.8874	0.003	0.0342	2.3302	4.0819
SB37	2.971	1.4066	19.5399	2.5113	0.0008	0.083	17.737	2.8027

Table A.10: SIH modelling results for individual hybrid animals of Protocol 4, 4-component model

Animal	MSE	MAE	G_{as}	τ_{as} (d)	G_{pr}	G_{ss}	G_c	τ_c (d)
FF2	2.3509	1.2208	1.8751	2.5606	0.0027	0.0278	0.8312	6.6798
FF5	1.5657	0.9382	2.0154	4.206	0.0039	0.0628	1.9667	10.7616
FF6	2.4852	1.3244	1.3221	2.1735	-0.001	0.0077	0.0923	1.4136
FF8	1.8733	1.0975	2.758	2.7559	0.0033	0.0229	1.8036	3.0626
FF9	1.1782	0.7964	2.0672	2.2268	0.0002	0.0366	0.4102	5.9518
FF11	6.7752	1.859	1.7351	2.3884	0.0035	-0.0274	1.1599	8.3323
FF14	1.2302	0.7733	1.6775	2.7239	0.0013	0.0236	1.4205	8.8538
FF17	2.4052	1.1269	3.4881	3.7462	0.0023	0.0293	2.7446	6.4253
FF21	1.347	0.8914	6.7723	4.5313	0.0006	0.0214	6.099	6.218
FF24	2.6244	1.2069	3.2444	1.5145	0	0.072	1.3236	16.2809
FF25	2.0147	0.9938	3.4859	3.2779	0.0022	0.0512	2.2399	4.4555
FF27	2.1541	1.053	5.1742	3.3593	0.0011	0.0139	4.1339	4.3532

Table A.11: SIH modelling results for individual salt-resistant animals of Protocol 1, 4-component model

Animal	MSE	MAE	G_{as}	$\tau_{as} (d)$	G_{pr}	G_{ss}	G_c	$\tau_c (d)$
RB2	2.1389	0.7895	1.3729	16.3126	-0.006	0.0078	0.0082	63.1923
RB3	2.4304	1.0882	1.6294	1.1208	-0.0063	0.0291	0.0533	107.6718
RB5	1.182	0.7725	6.9832	1.3551	-0.0004	0.0431	5.8375	2.0107
RB6	0.8962	0.577	1.8182	2.4093	-0.0055	0.0376	0.3031	7.3988
RB8	3.1701	0.7949	1.5502	0.7838	-0.0071	0.0309	0.0457	3.65
RB10	0.9883	0.6881	0	1.8193	0	0.019	0.6185	7.2624
RB11	1.7543	0.8841	0.8814	1.126	0.0038	0.0384	1.2188	19.2154

Table A.12: SIH modelling results for individual salt-resistant animals of Protocol 3, 4-component model

Animal	MSE	MAE	G_{as}	$\tau_{as} (d)$	G_{pr}	G_{ss}	G_c	$\tau_c (d)$
RB18	3.431	1.362	2.6261	2.4257	0.0012	0.0112	2.7551	4.6791
RB19	3.1508	1.4512	2.1927	2.3506	0.0039	0	2.5757	5.0532
RB20	1.8695	1.0586	2.4995	2.0291	0.0002	0.0492	2.7227	8.0771
RB21	2.3426	1.161	1.3444	1.8845	0.0032	0	1.502	4.3077
RB22	2.0572	1.1358	2.6179	2.2817	0.005	0.0263	3.13	5.6707

A.3 5-component model results

Table A.13: SIH modelling results for individual salt-sensitive animals of Protocol 1, 5-component model

Animal	MSE	MAE	G_{st}	τ_{st} (d)	G_{rec}	τ_{rec} (d)	G_{pr}	G_{ss}	G_c	τ_c
SB1	2.6928	1.2262	7.1025	4.029	5.9177	2.0673	0	0.0767	3.3133	2.7626
SB2	3.3133	1.4937	16.7147	4.9955	27.2904	4.7199	0.0012	0.1241	14.8307	6.9824
SB5	3.8153	1.4948	3.7756	3.6891	12.7433	2.0594	0.0034	0.1181	7.0431	71.7445
SB7	2.9125	1.3721	5.0696	5.8774	8.7936	1.2741	0	0.118	0.4389	0.9995
SB10	3.391	1.4276	10.5689	36.4752	29.99	1.914	0	0.1649	2.6967	11.5944
SB11	8.656	2.0892	14.653	10.4533	3.5932	1.1117	0	0.1832	6.36	8.8459
SB12	4.7376	1.8092	8.2252	2.8935	13.8756	2.128	0.0003	0.0949	4.7999	4.8165
SB13	3.4267	1.3206	4.8048	5.4613	16.6319	1.6048	0.0035	0.1232	4.071	18.6358
SB16	4.7098	1.7397	16.9832	5.0204	39.8196	3.1402	0.0007	0.1268	13.6714	6.0209

Table A.14: SIH modelling results for individual salt-sensitive animals of Protocol 2, 5-component model

Animal	MSE	MAE	G_{st}	τ_{st} (d)	G_{rec}	τ_{rec} (d)	G_{pr}	G_{ss}	G_c	τ_c (d)
R07	6.4887	1.9963	5.4193	1.1212	4.7085	9.679	0.0069	0.0034	0	0.7085
R08	1.5356	1.0009	9.4688	3.2723	14.5958	2.4505	0.0021	0.0482	8.2965	4.5322
R10	2.1747	1.1376	4.0396	1.6727	2.1227	1.217	0.0048	0.0152	1.3078	0.5961
R11	2.0212	1.1962	18.4811	5.1436	13.7851	3.8122	0.0011	0.0435	17.338	5.9077
R19	12.256	2.5871	10.343	4.9855	2.2702	1.7453	0	0.3215	9.3052	8.5883

Table A.15: SIH modelling results for individual salt-sensitive animals of Protocol 3, 5-component model

Animal	MSE	MAE	G_{st}	$\tau_{st} (d)$	G_{rec}	$\tau_{rec} (d)$	G_{pr}	G_{ss}	G_c	$\tau_c (d)$
SB23	3.3981	1.4907	7.4912	2.3274	4.2053	0.4508	0.0021	0.0093	3.8004	0.6395
SB24	1.5423	0.9327	4.2798	5.1064	1.6026	0.5332	0.0093	0.0392	0.9756	1.2927
SB31	3.6685	1.4777	5.8899	2.6458	0.8608	1.7024	0.0062	0.1374	3.6511	2.6298
SB32	2.885	1.327	7.1238	3.7298	0.3609	3.2111	0.0047	0.1491	5.3152	7.8237
SB33	1.4848	0.9621	6.7422	16.316	0.1151	1.073	0.0146	0.0576	0.2639	0.2887
SB35	4.0233	1.5949	9.8601	3.2347	1.9181	3.2738	0.0037	0.0283	9.2584	4.0223
SB36	2.757	1.3039	2.7859	1.5182	1.2523	1.2194	0.0037	0.0364	0.1818	0.2051
SB37	2.7867	1.3457	2.3408	1.6437	0.5545	1.5822	0.0056	0.0866	0	0.231

Table A.16: SIH modelling results for individual hybrid animals of Protocol 4, 5-component model

Animal	MSE	MAE	G_{st}	$\tau_{st} (d)$	G_{rec}	$\tau_{rec} (d)$	G_{pr}	G_{ss}	G_c	$\tau_c (d)$
FF2	2.3038	1.1995	3.0522	2.46	4.9961	3.0894	0.0025	0.019	2.2206	3.6124
FF5	1.6757	0.9972	1.0673	0.9549	2.6148	3.6389	0.0101	0.0414	0.9142	0.2077
FF6	2.2983	1.2615	2.1516	1.8135	7.7035	6.1407	0.0018	-0.0075	1.1058	3.5445
FF8	1.8942	1.0969	2.0488	1.3753	4.4309	2.4951	0.0028	0.0342	0.3732	2.8791
FF9	0.9802	0.7591	2.287	0.9734	12.4785	2.4797	0.0004	0.0342	0.4282	1.4887
FF11	6.4479	1.8315	4.0681	1.9808	0.8155	3.029	0.0007	-0.0167	2.7361	4.9829
FF14	0.9231	0.7093	3.6404	1.665	5.5883	5.2617	0.0017	0.0063	2.8305	3.576
FF17	2.1061	1.0636	3.3524	1.5827	7.8912	3.9303	0.0024	0.0256	1.9917	3.8067
FF21	1.315	0.8798	5.3994	4.2776	5.8413	4.4384	0.0007	0.0222	4.625	6.544
FF24	2.0084	1.0108	2.5756	20.941	10.2154	1.909	0.0001	0.0341	0.4234	4.3177
FF25	1.7859	0.9434	2.5496	1.0004	8.0267	2.622	0.0038	0.0447	1.3558	1.2487
FF27	2.0261	1.0295	2.0778	1.9619	4.0896	3.5843	0.003	0.0116	0.849	5.5433

Table A.17: SIH modelling results for individual salt-resistant animals of Protocol 1, 5-component model

Animal	MSE	MAE	G_{st}	τ_{st} (d)	G_{rec}	τ_{rec} (d)	G_{pr}	G_{ss}	G_c	τ_c
RB2	2.0512	0.7658	3.6076	18.417	231.1979	210.2479	0.0027	-0.0934	0.2393	2.6079
RB3	2.3587	1.0209	1.8588	0.511	11.5364	58.3347	0.0006	-0.0033	0.4063	4.9349
RB5	1.1831	0.781	2.5663	0.5463	5.8415	1.1042	0	0.0429	1.6538	3.6746
RB6	0.8077	0.5152	1.5561	0.7551	2.7628	53.2987	0.0007	0.0323	2.6185	64.1616
RB8	3.2156	0.8249	1.5092	0.641	19.892	188.3452	0.0029	0.2026	146.7916	646.8745
RB10	0.8126	0.5666	3.5197	5.8764	1.9807	8.2046	0.0013	0.0096	4.2962	5.9846
RB11	1.5666	0.8526	2.5707	3.0705	0.5419	1.2184	0.0003	0.0307	2.1069	4.1926

Table A.18: SIH modelling results for individual salt-resistant animals of Protocol 3, 5-component model

Animal	MSE	MAE	G_{st}	τ_{st} (d)	G_{rec}	τ_{rec} (d)	G_{pr}	G_{ss}	G_c	τ_c (d)
RB18	2.8892	1.1487	3.8675	1.1199	2.3014	0.5118	0	0.0104	2.8894	0.4452
RB19	2.2907	1.2156	5.4806	2.0532	1.4772	1.1464	0.0007	0.0022	3.9128	1.0391
RB20	1.5534	1.0147	5.2544	7.535	0.4354	0.8848	0	0.0432	1.2102	3.4383
RB21	1.9766	1.0894	2.9153	0.5297	1.0956	0.5694	0.0014	-0.0083	2.4826	0.3322
RB22	1.925	1.134	4.7192	2.488	1.6295	1.7834	0.0019	0.0305	3.8858	2.697

Appendix B

Baroreflex sensitivity estimation results

B.1 Persistence of excitation figures

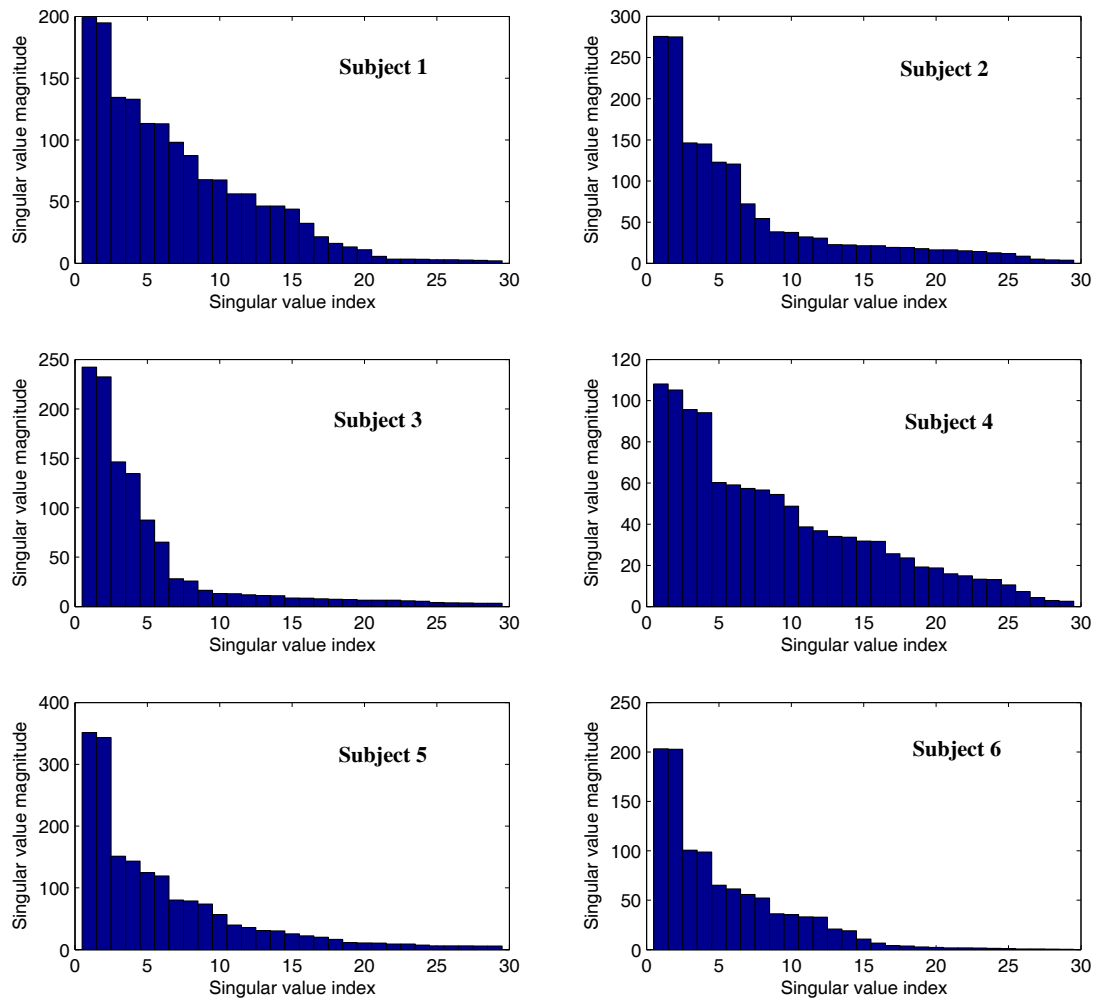


Figure B.1: Persistence of excitation in *SAP* for EuroBaVar Subjects 1-6 in the standing position

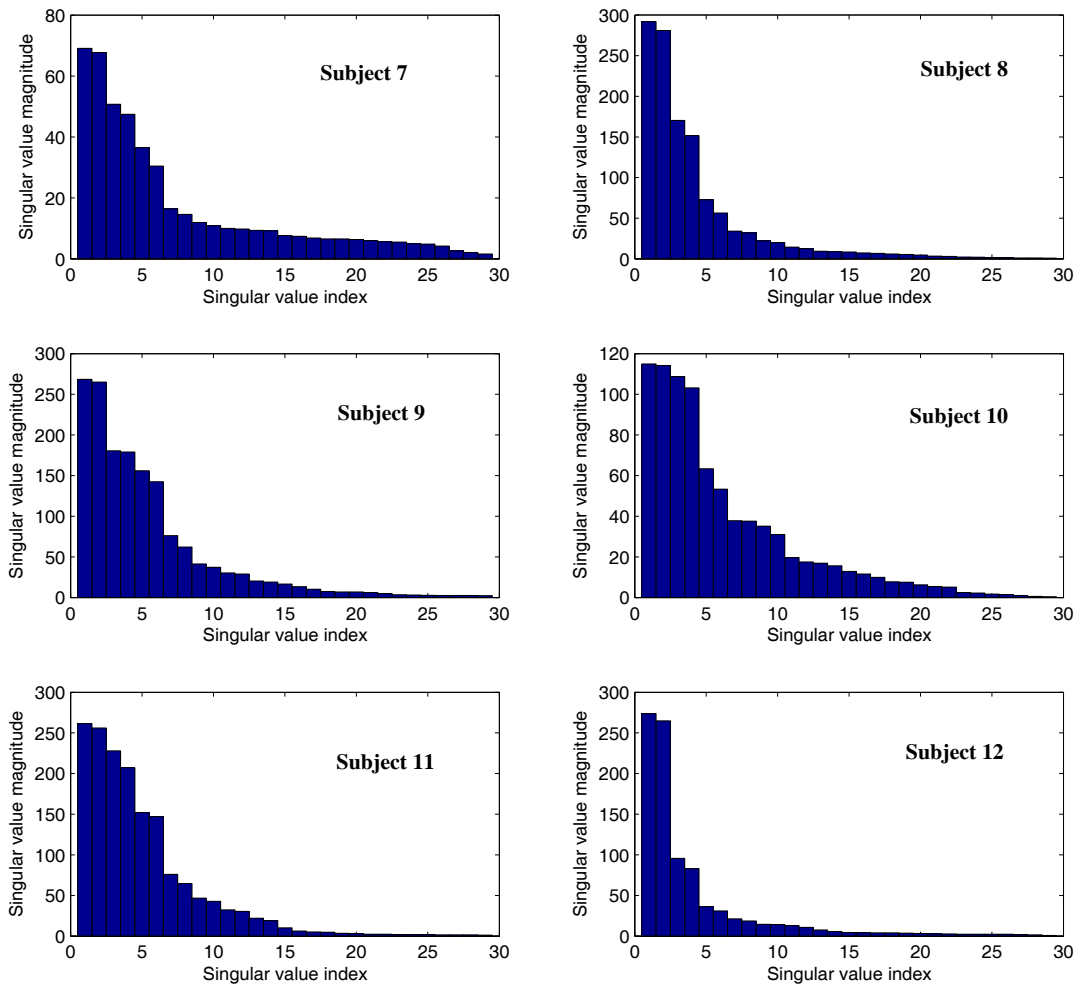


Figure B.2: Persistence of excitation in SAP for EuroBaVar Subjects 7-12 in the standing position

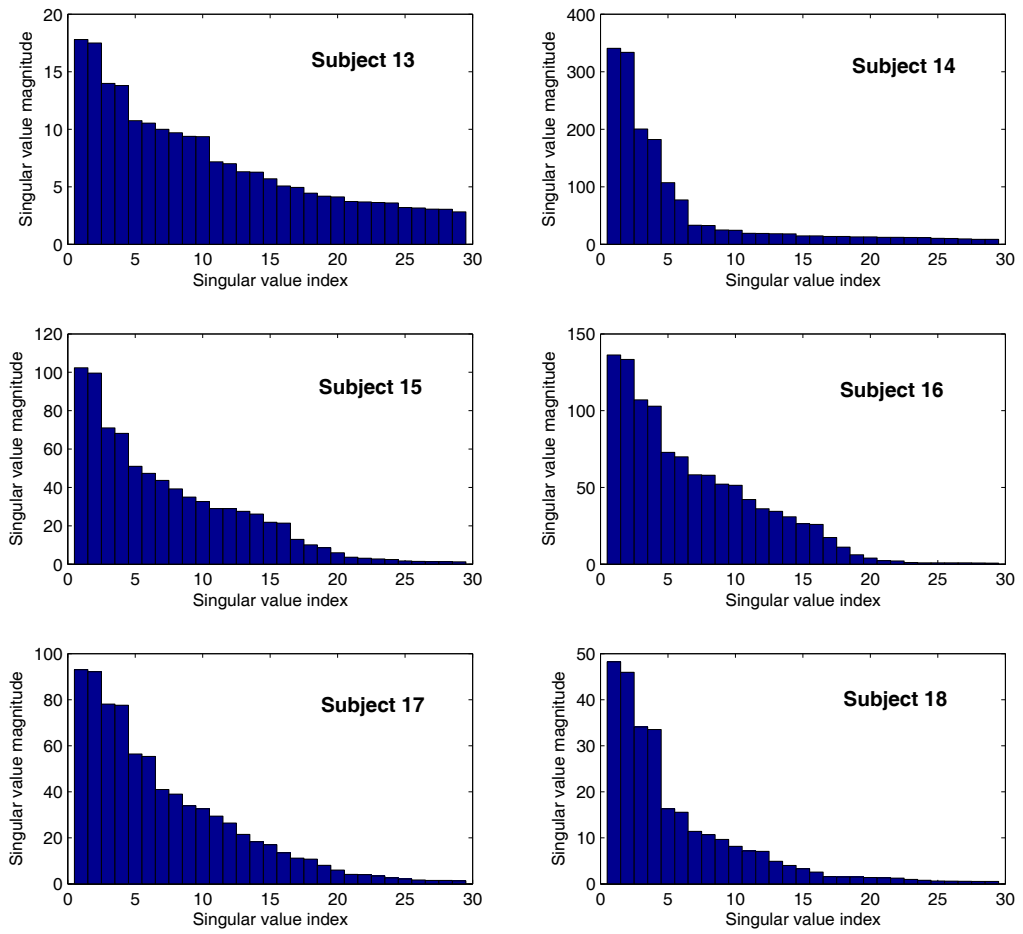


Figure B.3: Persistence of excitation in *SAP* for EuroBaVar Subjects 13-18 in the standing position

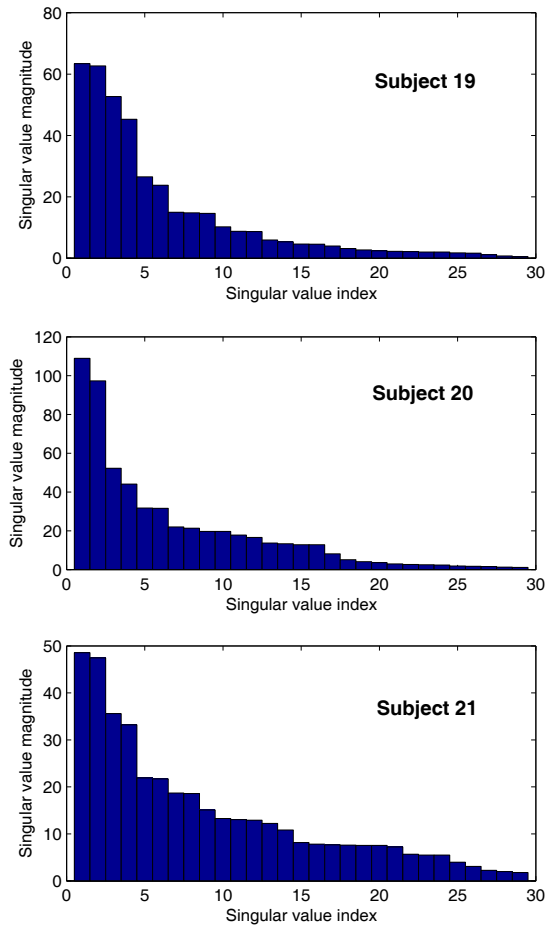


Figure B.4: Persistence of excitation in SAP for EuroBaVar Subjects 19-21 in the standing position

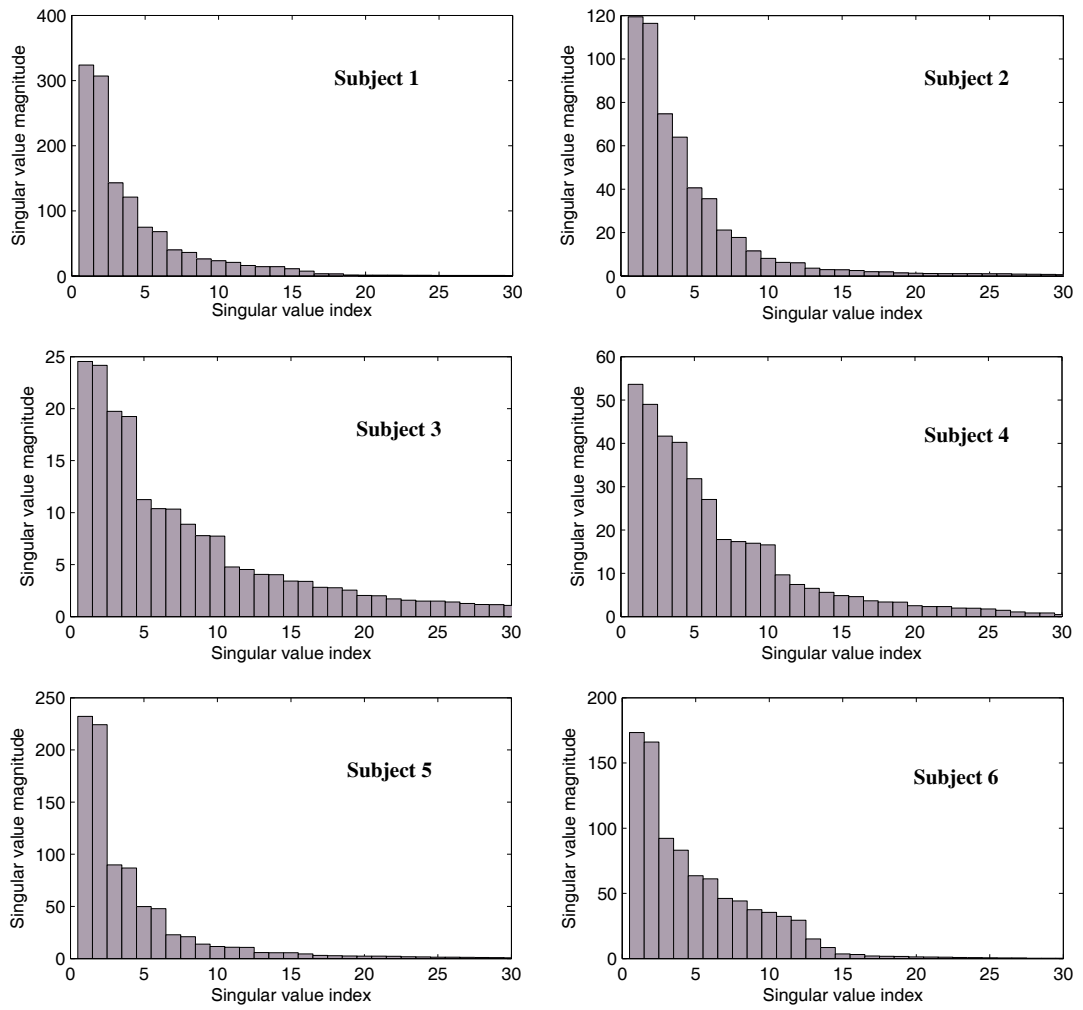


Figure B.5: Persistence of excitation in *SAP* for EuroBaVar Subjects 1-6 in the supine position

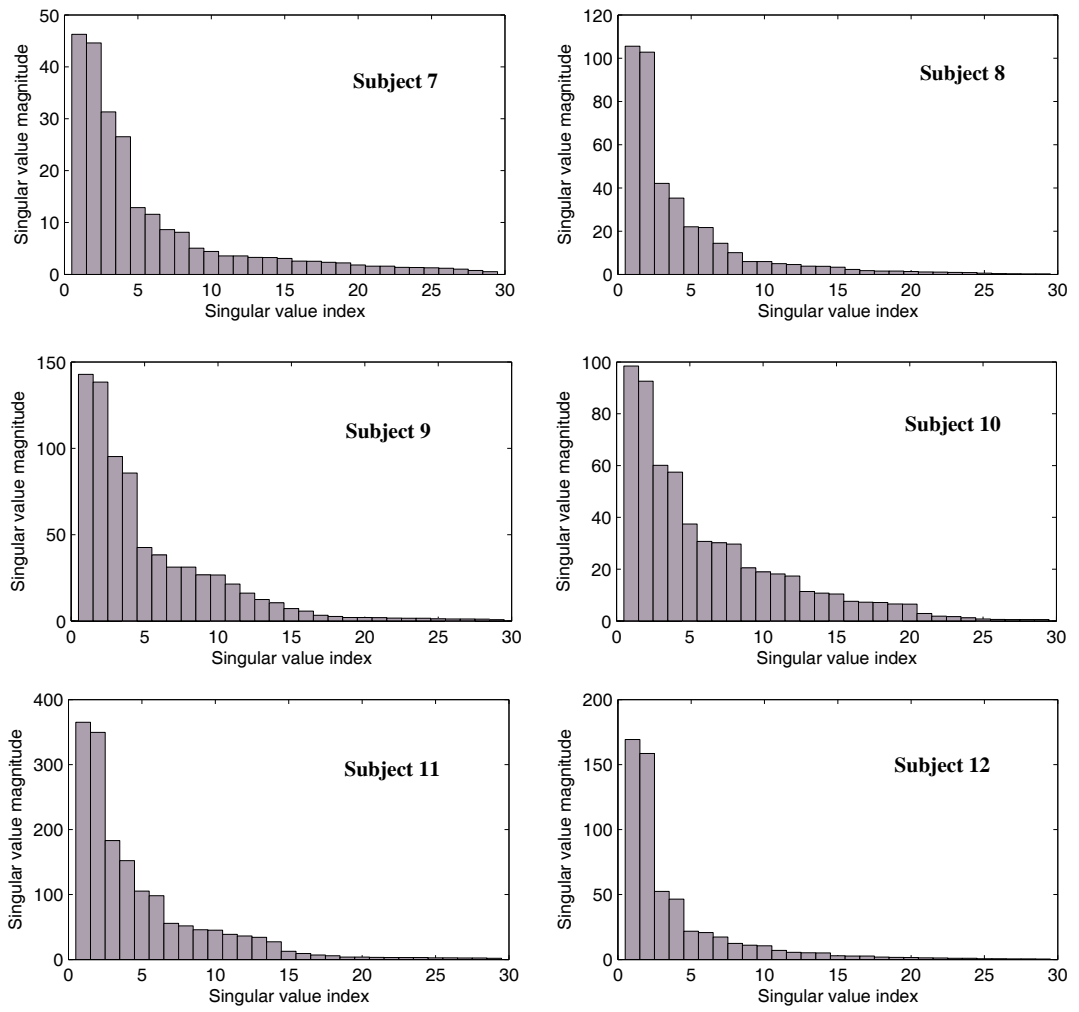


Figure B.6: Persistence of excitation in *SAP* for EuroBaVar Subjects 7-12 in the supine position

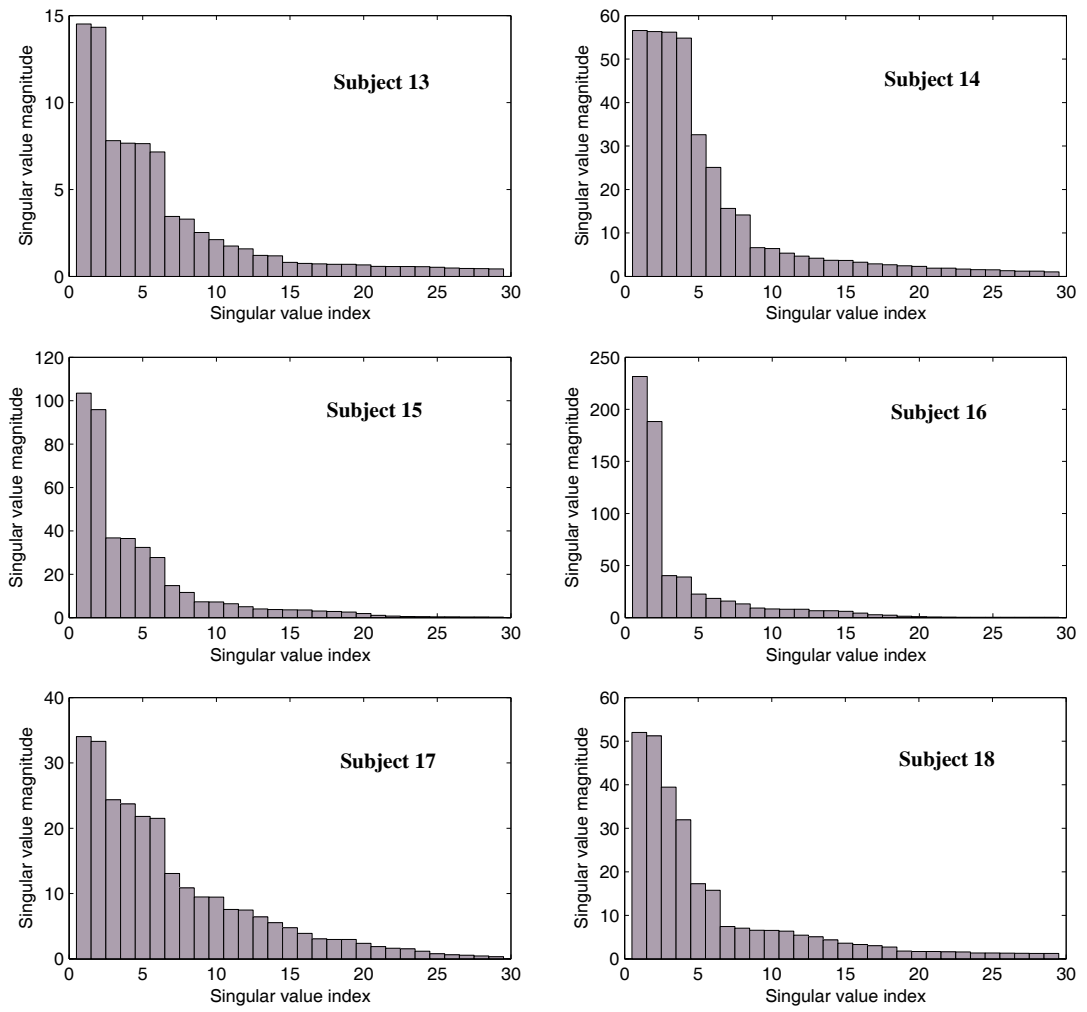


Figure B.7: Persistence of excitation in *SAP* for EuroBaVar Subjects 13-18 in the supine position

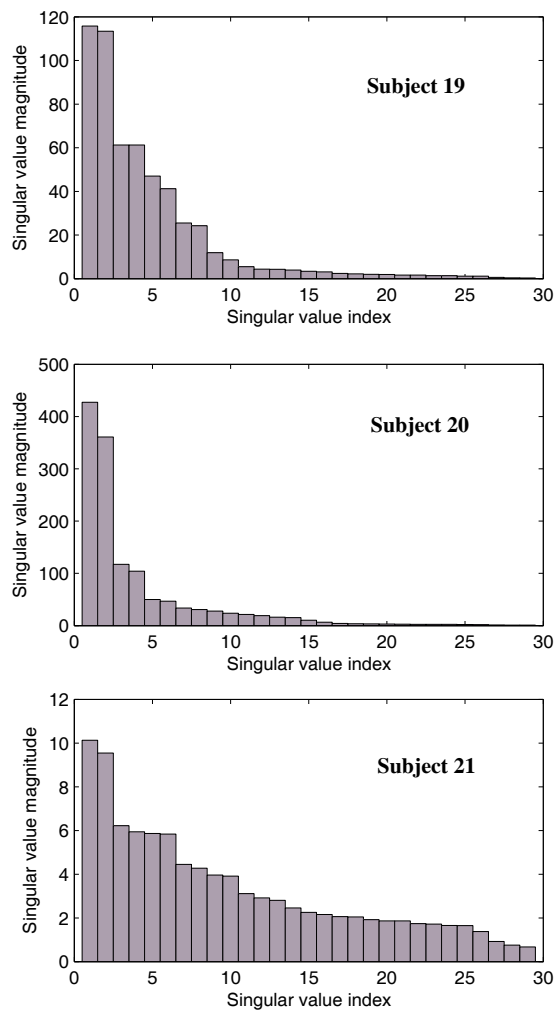


Figure B.8: Persistence of excitation in SAP for EuroBaVar Subjects 19-21 in the supine position

B.2 ARMAX model parameters - standing position

Table B.1: ARMAX model parameters, Subject 1, standing position, $n_d=1$

index (i)	1	2	3	4	5	6
a_i	1	-2.0712	1.6979	-1.279	0.9481	-0.2768
b_i	-0.3355	4.9536	-10.462	8.1577	-2.474	0.2651
c_i	1	0.6755	-1.769	-1.46	0.8025	0.7703

Table B.2: ARMAX model parameters, Subject 2, standing position, $n_d=1$

index (i)	1	2	3	4	5
a_i	1	-1.3017	0.9406	-0.8004	0.4215
b_i	0.9198	-0.1879			
c_i	1	0.9265			

Table B.3: ARMAX model parameters, Subject 3, standing position, $n_d=3$

index (i)	1	2	3	4	5	6
a_i	1	-2.089	1.614	-1.2397	1.1774	-0.4373
b_i	1.1591	-2.1667	1.0339			
c_i	1	0.1795	-1.7251	-0.1759	0.7264	0

Table B.4: ARMAX model parameters, Subject 4, standing position, $n_d=2$

index (i)	1	2	3	4	5	6
a_i	1	-0.7264				
b_i	3.608	-5.0422	4.0526	-2.4493	1.2953	-0.9252
c_i	1	0.9137				

Table B.5: ARMAX model parameters, Subject 5, standing position, $n_d=0$

index (i)	1	2	3	4	5	6
a_i	1	-1.2466	0.2269	-0.1657	0.2771	
b_i	0.3926	-0.2626	0.8468	-1.2101	0.3408	
c_i	1	1.5912	-0.7851	-1.9657	-0.211	0.3788

Table B.6: ARMAX model parameters, Subject 6, standing position, $n_d=0$

index (i)	1	2	3	4	5	6
a_i	1	-1.7521	1.7357	-1.527	1.0548	-0.3675
b_i	2.5422	-3.1296	2.837	-2.2914	1.1966	
c_i	1					

Table B.7: ARMAX model parameters, Subject 7, standing position, $n_d=0$

index (i)	1	2	3	4	5	6
a_i	1	-1.4682	1.4095	-1.277	0.8109	-0.2041
b_i	3.6829	-6.2392	4.9481	-2.8778	1.8359	
c_i	1					

Table B.8: ARMAX model parameters, Subject 8, standing position, $n_d=0$

index (i)	1	2	3	4	5
a_i	1	-0.1107			
b_i	5.0702	1.3057	-3.4039	1.8808	3.4338
c_i	1	2.5582	2.3289	0.75	

Table B.9: ARMAX model parameters, Subject 9, standing position, $n_d=0$

index (i)	1	2	3	4	5
a_i	1	-0.1388	0.1849	-0.449	0.3079
b_i	-0.2122	1.6619			
c_i	1	2.3764	2.1368	0.7032	

Table B.10: ARMAX model parameters, Subject 10, standing position, $n_d=1$

index (i)	1	2	3	4
a_i	1	-0.4956	0.4454	-0.44
b_i	4.116	-5.4588	2.2804	
c_i	1	0.7899		

Table B.11: ARMAX model parameters, Subject 11, standing position, $n_d=1$

index (i)	1	2	3	4	5
a_i	1	-0.6802			
b_i	-0.2325	0.6363	0.7715	-0.541	-0.5448
c_i	1	2.9629	2.9511	0.9874	

Table B.12: ARMAX model parameters, Subject 12, standing position, $n_d=0$

index (i)	1	2	3	4	5	6
a_i	1	-1.7461	1.672	-1.584	0.9043	-0.241
b_i	3.816	-6.6089	3.1008			
c_i	1	-0.1019	-0.8878			

Table B.13: ARMAX model parameters, Subject 13, standing position, $n_d=2$

index (i)	1	2	3	4	5	6
a_i	1	-1.8056	0.9141	-0.047	0	
b_i	-0.2061	0.4791	-0.4121	0.1588	-0.0142	
c_i	1	-0.3947	-1.3504	0.7714	0.5281	-0.5611

Table B.14: ARMAX model parameters, Subject 14, standing position, $n_d=4$

index (i)	1	2	3	4	5
a_i	1	-2.3589	1.8071	-0.433	
b_i	0.6459	-0.9593	0.6355	-0.869	0.5971
c_i	1	-0.0735	-1.7689	0.009	0.8501

Table B.15: ARMAX model parameters, Subject 15, standing position, $n_d=0$

index (i)	1	2	3	4	5
a_i	1	-1.0091	0.5447	-0.3187	
b_i	1.8094	-1.7622	2.0418	-2.3729	0.9848
c_i	1	0.9051			

Table B.16: ARMAX model parameters, Subject 16, standing position, $n_d=1$

index (i)	1	2
a_i	1	-0.648
b_i	4.7739	-2.0015
c_i	1	0.9314

Table B.17: ARMAX model parameters, Subject 17, standing position, $n_d=1$

index (i)	1	2	3	4	5
a_i	1	-1.7372	1.1893	-0.6803	0.2783
b_i	3.3306	-3.1916			
c_i	1	0.2373	-0.972	-0.4662	0.1772

Table B.18: ARMAX model parameters, Subject 18, standing position, $n_d=4$

index (i)	1	2	3
a_i	1	-0.2059	0.6689
b_i	-0.3569	0.2796	
c_i	1		

Table B.19: ARMAX model parameters, Subject 19, standing position, $n_d=4$

index (i)	1	2	3	4	5	6
a_i	1	-0.9207				
b_i	0.3118	5.3521	-7.704	3.1541	-1.775	1.5984
c_i	1	1.6463	-0.261	-1.6286	-0.7236	

Table B.20: ARMAX model parameters, Subject 20, standing position, $n_d=3$

index (i)	1	2	3
a_i	1	-0.9015	
b_i	-1.1272	0.6989	0.6827
c_i	1		

Table B.21: ARMAX model parameters, Subject 21, standing position, $n_d=0$

index (i)	1	2	3	4
a_i	1	-0.8237		
b_i	11.7197	-11.8309	4.7923	-0.8577
c_i	1			

B.3 ARMAX Model parameters - supine position

Table B.22: ARMAX model parameters, Subject 1, supine position, $n_d=1$

index (i)	1	2	3	4	5	6
a_i	1	-1.588	1.7345	-1.5448	1.1355	-0.5321
b_i	1.1987	-0.833				
c_i	1					

Table B.23: ARMAX model parameters, Subject 2, supine position, $n_d=2$

index (i)	1	2	3	4	5	6
a_i	1	-0.6261				
b_i	-2.6268	5.0026	-1.2249	-1.2462	-0.0323	0.5094
c_i	1	1.01				

Table B.24: ARMAX model parameters, Subject 3, supine position, $n_d=1$

index (i)	1	2	3	4
a_i	1	-0.942	0.3467	
b_i	-2.3194	0.5922	3.6097	-2.015
c_i	1			

Table B.25: ARMAX model parameters, Subject 4, supine position, $n_d=1$

index (i)	1	2	3	4
a_i	1	-1.5257	1.3773	-0.6665
b_i	6.1663	-11.309	12.2311	-5.4263
c_i	1			

Table B.26: ARMAX model parameters, Subject 5, supine position, $n_d=2$

index (i)	1	2	3	4	5	6	7
a_i	1	-1.4498	1.4675	-1.429	1.3277	-0.8189	0.4319
b_i	1.3699	-1.7015	0.7794	-1.6016	1.1901		
c_i	1	0.9509					

Table B.27: ARMAX model parameters, Subject 6, supine position, $n_d=2$

index (i)	1	2	3	4	5
a_i	1	-1.718	1.6885	-1.0505	0.449
b_i	6.9869	-14.848	13.6785	-8.5624	3.9228
c_i	1				

Table B.28: ARMAX model parameters, Subject 7, supine position, $n_d=1$

index (i)	1	2	3	4
a_i	1	-0.5924		
b_i	8.1488	-15.04	8.7761	0.3697
c_i	1	0.9953		

Table B.29: ARMAX model parameters, Subject 8, supine position, $n_d=1$

index (i)	1	2	3	4	5	6
a_i	1	-1.0198	0.6226			
b_i	12.0164	-36.2506	44.7118	-22.8853	8.7964	-5.1327
c_i	1					

Table B.30: ARMAX model parameters, Subject 9, supine position, $n_d=2$

index (i)	1	2	3	4	5
a_i	1	-0.6548			
b_i	8.4376	-16.0996	14.6639	-10.7776	4.8919
c_i	1				

Table B.31: ARMAX model parameters, Subject 10, supine position, $n_d=1$

index (i)	1	2	3	4	5	6
a_i	1	-0.8801				
b_i	7.6579	-16.0704	13.3912	-11.5898	11.8563	-4.967
c_i	1	0.5756	-0.8551	-0.6718		

Table B.32: ARMAX model parameters, Subject 11, supine position, $n_d=0$

index (i)	1	2	3	4	5	6
a_i	1	-0.7895	-0.0517			
b_i	-1.7155	5.7693	-5.6333	4.9267	-6.4883	4.0346
c_i	1	2.1152	0.4773	-1.4339	-0.7965	

Table B.33: ARMAX model parameters, Subject 12, supine position, $n_d=1$

index (i)	1	2	3	4
a_i	1	-0.9038		
b_i	6.9369	-12.6298	6.3217	
c_i	1	1.0037	-0.9635	-0.9673

Table B.34: ARMAX model parameters, Subject 13, supine position, $n_d=0$

index (i)	1	2	3	4	5	6
a_i	1	-0.9791				
b_i	1.5645	-2.4646	1.2703			
c_i	1	0.7161	-0.7894	-0.4645	-0.1959	-0.3111

Table B.35: ARMAX model parameters, Subject 14, supine position, $n_d=0$

index (i)	1	2	3	4	5	6
a_i	1	-1.4581	1.513	-1.4446	0.8761	-0.4037
b_i	1.3425					
c_i	1					

Table B.36: ARMAX model parameters, Subject 15, supine position, $n_d=4$

index (i)	1	2	3
a_i	1	-1.3724	0.641
b_i	-2.1361	4.7584	-2.8054
c_i	1		

Table B.37: ARMAX model parameters, Subject 16, supine position, $n_d=0$

index (i)	1	2	3	4	5	6	7
a_i	1	-1.0058	0.9613	-0.9558	0.9264	-0.5179	0.2629
b_i	-3.4929	14.329	-14.591	10.994	-12.772	6.9559	
c_i	1	2.0006	1.0201				

Table B.38: ARMAX model parameters, Subject 17, supine position, $n_d=0$

index (i)	1	2	3	4
a_i	1	-1.4971	1.048	-0.3904
b_i	7.136	-6.5916	3.7249	
c_i	1			

Table B.39: ARMAX model parameters, Subject 18, supine position, $n_d=2$

index (i)	1	2	3	4	5	6
a_i	1	-0.2726				
b_i	-0.6292	0.7752	-0.7689	0.5945	0.1241	-0.2846
c_i	1					

Table B.40: ARMAX model parameters, Subject 19, supine position, $n_d=1$

index (i)	1	2	3	4	5	6
a_i	1	-1.9629	1.353	-0.9029	0.7447	-0.2225
b_i	5.8076	-10.6862	5.1193			
c_i	1	0.2655	-1.5636	-0.9436	0.6847	0.5624

Table B.41: ARMAX model parameters, Subject 20, supine position, $n_d=4$

20	index (i)	1	2	3
	a_i	1	-0.7594	
	b_i	0.1586	0.2975	
	c_i	1	1.7994	0.8977

Table B.42: ARMAX model parameters, Subject 21, supine position, $n_d=1$

index (i)	1	2	3	4	5
a_i	1	-0.5385			
b_i	43.9352	-90.7222	80.0899	-40.9882	13.9567
c_i	1	0.9959			

References

- S. Abram, B. Hodnett, R. Summers, T. Coleman, and R. Hester. Quantitative circulatory physiology: an integrative mathematical model of human physiology for medical education. *Advances in Physiology Education*, 31 (2):202–210, 2007.
- H. Adrogué and N. Madias. Hemodynamic regulation in SHR: investigation by spectral analysis. *New England Journal of Medicine*, 356 (19):1966–1978, 2007.
- G. Aisenbrey, W. Handelman, P. Arnold, M. Manning, and R. Schrier. Vascular effects of arginine vasopressin during fluid deprivation in the rat. *Journal of Clinical Investigations*, 67:961–968, 1981.
- U. Ascher and L. Petzold. *Computer methods for ordinary differential equations and differential-algebraic equations*. SIAM, 1998.
- G. Baselli, S. Cerutti, F. Baidilni, L. Biancardi, A. Porta, M. Pagani, F. Lombardi, O. Rimoldi, R. Furlan, and A. Malliani. Model for the assessment of heart period and arterial pressure variability interactions and respiration influences. *Medical and Biological Engineering and Computing*, 32:143–152, 1994.
- G. Baselli, S. Cerutti, S. Civardi, A. Malliani, and M. Pagani. Cardiovascular variability signals: Towards the identification of a closed-loop model of the neural control mechanisms. *IEEE Transactions on Biomedical Engineering*, 35 (12):1033–1046, 1988.
- C. Berger and S. Malpas. Modelling of the dynamic relationship between arterial blood pressure, renal sympathetic nerve activity and renal blood flow in conscious rabbits. *The Journal of Experimental Biology*, 201:3425–3430, 1998.
- K. Bettenbrock, S. Fischer, A. Kremling, K. Jahreis, T. Sauter, and E. Gilles. A quantitative approach to catabolite repression in *Escherichia coli*. *Journal of Biological Chemistry*, 281(5):2578–2584, 2006.

- C. Bock. SysML and UML 2 support for activity modeling. *Systems Engineering*, 9(2): 160–186, 2006.
- F. Bolger and J. Lowry. Brain tissue oxygen: In vivo monitoring using carbon paste electrodes. *Sensors*, 5(2):473–487, 2005.
- C. Boulanger and P. Vanhoutte. The endothelium: a modulator of cardiovascular health and disease. *Dialogues in Cardiovascular Medicine*, 3 (4):187–200, 1998.
- V. Brooks, L. Keil, and I. Reid. Role of the renin-angiotensin system in the control of vasopressin secretion in conscious dogs. *Circulation Research*, 58 (6):829–838, 1986.
- D. Budgett, A. Hu, P. Si, W. Pallas, M. Donnelly, J. Broad, C. Barrett, S-J. Guild, and S. Malpas. Novel technology for the provision of power to implantable physiological devices. *Journal of Applied Physiology*, 102:1658–1663, 2007.
- M. Cabrera, G. Saidel, and S. Kalhan. Lactate metabolism during exercise: analysis by an integrative systems model. *American Journal of Physiology (Regulatory Integrative and Comparative Physiology)*, 277:R1522–R1536, 1999.
- W. Cameron. A model framework for computer simulation of overall renal function. *Journal of Theoretical Biology*, 66:552–572, 1977.
- S. Campbell, J.-P. Chancelier, and R. Nikoukhah. *Modeling and simulation in Scilab/Scicos*. Springer Verlag, 2006.
- O. Carretero and S. Oparil. Essential hypertension, Part I: definition and etiology. *Circulation*, 101:329–335, 2000.
- E. Carson and C. Cobelli. *Modelling methodology for physiology and medicine*. Academic Press, 2000.
- S. Cerutti, M. Ducher, M.-P. Gustin, J.-P. Fauvel, G. Cuisinaud, and C. Paultre. *Statistical dependence approach for the estimation of the spontaneous baroreflex sensitivity in rats and humans*. IOS Press, 1999.
- D. Chang, N. Lovell, and S. Dokos. Field Markup Language: Biological field representation in XML. In *Proceedings of the 29th International IEEE Conference on Engineering in Biology and Medicine*, pages 402–405. Lyon, 2007.
- P. Chen, P. St John, K. Kirk, D. Abrahamson, and P. Sanders. Hypertensive nephroscle-

- rosis in the Dahl/Rapp rat. Initial sites of injury and effect of dietary L-arginine supplementation. *Laboratory Investigation*, 68:174–184, 1993.
- Y. Choi, S.-B. Ko, and Y. Sun. Effect of postural changes on baroreflex sensitivity: A study on the EUROBAVAR data set. In *Proceedings of the 2006 IEEE Canadian Conference on Electrical and Computer Engineering - CCEC/CCGEI'06*, Ottawa, May 2006.
- B. Cholewa and D. Mattson. Role of the renin-angiotensin system during alterations of sodium intake in conscious mice. *American Journal of Physiology (Regulatory Integrative and Comparative Physiology)*, 281:987–993, 2001.
- A. Clement. Using differential properties of the green function in seakeeping computational codes. In *Proceedings of the 7th International Conference on Numerical Ship Hydrodynamics*, volume 6, pages 1–15. 1999.
- C. Cobelli, E. Carson, L. Finkelstein, and M. Leaning. Validation of simple and complex models in physiology and medicine. *American Journal of Physiology (Regulatory Integrative and Comparative Physiology)*, 246(2):R259–R266, 1984.
- E. Cogan. Atrial natriuretic factor and the endocrine control of electrolyte homeostasis. *Acta Cardiologica*, 46(3):377–384, 1991.
- T. Coleman. A mathematical model of the human body in health, disease, and during treatment. *ISA Transactions*, 18(3):65–73, 1979.
- T. Coleman and J. Hall. *Structuring Biological Systems: A Computer Modelling Approach*, chapter A mathematical model of renal hemodynamics and excretory function, pages 89–124. CRC Press, Oxford, 1992.
- T. Coleman and J. Randall. HUMAN: A comprehensive physiological model. *The Physiology Teacher*, 31(1):15–21, 1983.
- A. Cowley Jr. Long-term control of arterial blood pressure. *Physiological Reviews*, 72(1):231–300, 1992.
- A. Cowley Jr., J. Liard, and A. Guyton. Role of the baroreceptor reflex in daily control of arterial blood pressure and other variables in dogs. *Circulation Research*, 32:564–576, 1973.
- A. Cowley Jr., S. Swwitzer, and M. Guinn. Evidence and quantification of the vaso-

- pressin arterial pressure control system in the dog. *Circulation Research*, 46:58–67, 1980.
- A. Cuellar, C. Lloyd, P. Nielsen, D. Bullivant, D. Nickerson, and P. Hunter. An overview of CellML 1.1, a biological model description language. *Simulation*, 79(12):740–747, 2003.
- L. Dahl. Effects of chronic excess salt feeding. *The Journal of Experimental Medicine*, 114:231–236, 1961.
- L. Dahl. Possible role of salt intake in the development of essential hypertension (reprint). *International Journal of Epidemiology*, 34:967–972, 2005.
- L. Dahl and M. Heine. Primary role of renal homografts in setting chronic blood pressure levels in rats. *Circulation Research*, 36:692–696, 1975.
- L. Dahl, K. Knudsen, M. Heine, and G. Leitl. Effects of chronic excess salt ingestion. Modification of experimental hypertension in the rat by variations in the diet. *Circulation Research*, 22:11–18, 1968.
- L. Dahl and E. Schackow. Effects of chronic excess salt ingestion: Experimental hypertension in the rat. *Canadian Medical Association Journal*, 90:155–160, 1964.
- L. Davies, D. Francis, P. Jurak, T. Kara, M. Piepoli, and A. Coats. Reproducibility of methods for assessing baroreflex sensitivity in normal controls and in patients with chronic heart failure. *Clinical Science*, 97:515–522, 1999.
- M. De Burgh Daly and M. Scott. The effects of stimulation of the carotid body chemoreceptors on heart rate in the dog. *Journal of Physiology*, 144:148–166, 1958.
- M. De Cecco and A. Angrilli. Measurement of human baroreceptor reflex sensitivity by means of parametric identification. *Measurement*, 24:187–196, 1998.
- H. De Wardener and G. MacGregor. Harmful effects of dietary salt in addition to hypertension. *Journal of Human Hypertension*, 16:213–223, 2002.
- M. Dempsey. Automatic translation of Simulink models into Modelica using Simelica and the AdvancedBlocks library. In *Proceedings of the 3rd International Modelica Conference*, pages 115–124. Linköping, 2003.

- J. Dennis Jr. and R. Schnabel. *Numerical Methods for Unconstrained Optimization and Nonlinear Equations*. Prentice Hall, 1983.
- D. Denton, R. Weisinger, N. Mundy, E. Wickings, A. Dixons, P. Moisson, A. Pingard, R. Shade, D. Carey, R. Ardaillou, F. Paillard, J. Chapman, J. Thillet, and J. Michel. The effect of increased salt intake on blood pressure of chimpanzees. *Nature Medicine*, 1 (10):1009–1016, 1995.
- H. Deter, K. Buchholz, U. Schorr, H. Schchinger, S. Turan, and A. Sharma. Psychophysiological reactivity of salt-sensitive normotensive subjects. *Journal of Hypertension*, 15:839–844, 1997.
- J. Diana, S. Qian, C. Heesch, K. Barron, and C. Chien. Nicotine-induced skeletal muscle vasodilation is mediated by release of epinephrine from nerve terminals. *American Journal of Physiology (Heart and Circulatory Physiology)*, 259:H1718–H1729, 1990.
- G. DiBona. Neural control of renal function: cardiovascular implications. *Hypertension*, 13:539–548, 1989.
- G. DiBona and U. Kopp. Neural control of renal function. *Physiological Reviews*, 77:75–197, 1997.
- G. DiBona and U. Kopp. Frequency response of the renal vasculature in congestive heart failure. *Circulation*, 107:2159–2164, 2003.
- J. Dongarra, J. Bunch, G. Moler, and G. Stewart. *LINPACK users' guide*. SIAM, 1979.
- M. Ducher, J. Fauvel, M. Gustin, C. Cerutti, R. Najem, G. Cuisinaud, M. Laville, N. Pozet, and C. Paultre. A new non-invasive statistical method to assess the spontaneous cardiac baroreflex in humans. *Clinical Science*, 88:651–655, 1995.
- D. Eckberg and P. Sleight. *Human baroreflexes in health and disease*. Oxford University Press, 1992.
- Y. Egi, Y. Matsumura, S. Murata, T. Umekawa, K. Hisaki, M. Takaoka, and S. Morimoto. The effects of NG-nitro-L-arginine, a nitric oxide synthase inhibitor, on norepinephrine overflow and antidiuresis induced by stimulation of renal nerves in anesthetized dogs. *Journal of Pharmacology and Experimental Therapeutics*, 269:529–535, 1994.
- P. Elliott, L. Walker, M. Little, J. Blair-West, R. Shade, D. Rick Lee, P. Rouquet,

- E. Leroy, X. Jeunemaitre, R. Ardaillou, F. Paillard, P. Meneton, and D. Denton. Change in salt intake affects blood pressure of chimpanzees: Implications for human populations. *Circulation*, 116 (14):1563–1568, 2007.
- G. Eppel, K. Denton, S. Malpas, and R. Evans. Nitric oxide in responses of regional kidney perfusion to renal nerve stimulation and renal ischaemia. *European Journal of Physiology*, 447:205–213, 2003.
- A. Ergul. Endothelin-1 and endothelin receptor antagonists as potential cardiovascular therapeutic agents. *Pharmacotherapy*, 22:54–65, 2002.
- L. Faes, G. Nollo, A. Porta, and F. Ravelli. Noninvasive assessment of baroreflex sensitivity in post-MI patients by an open-loop parametric model of RR-systolic pressure interactions. *Computers in Cardiology*, 26:217–220, 1999.
- K. Foster. Math on the Internet. *IEEE Spectrum*, 36(4):36–40, 1999.
- M. Frenneaux. Autonomic changes in patients with heart failure and in post-myocardial infarction patients. *Heart*, 90 (11):1248–1255, 2004.
- T. Fujita, W. Henry, F. Bartter, C. Lake, and C. Delea. Factors influencing blood pressure in salt-sensitive patients with hypertension. *American Journal of Medicine*, 69:334–344, 1980.
- A. Garfinkel. A mathematics for physiology. *American Journal of Physiology (Regulatory Integrative and Comparative Physiology)*, 245:R455–R466, 1983.
- D. Gavaghan, A. Garny, P. Maini, and P. Kohl. Mathematical models in physiology. *Philosophical Transactions of the Royal Society A*, 364(2):1099–1106, 2006.
- M. Glos, D. Romberg, S. Endres, and I. Fietze. Estimation of spontaneous baroreflex sensitivity using transfer function analysis: effects of positive pressure ventilation. *Biomedizinische Technik*, 52:66–72, 2007.
- O. Gonzalez-Albarra, L. Ruilope, E. Villa, and R. Robles. Salt-sensitivity: Concept and pathogenesis. *Diabetes Research and Clinical Practice*, 39:S15–S26, 1998.
- S. Gouveia, A. Rocha, P. Laguna, and P. Lago. Time domain baroreflex sensitivity assessment by joint analysis of spontaneous SBP and RR series. *Biomedical Signal Processing and Control*, 4 (3):254–261, 2009.

- S. Gouveia, A. Rocha, P. Laguna, P. Van de Borne, and P. Lago. Improved BRS assessment using the global approach in the sequences technique. *Computers in Cardiology*, 33:641–644, 2006.
- S. Gouveia, A. Rocha, P. Van de Borne, and P. Lago. Assessing baroreflex sensitivity in the sequence technique: local versus global approach. *Computers in Cardiology*, 32:279–282, 2005.
- G. Grassi, B. Cattaneo, G. Seravalle, A. Lanfranchi, and G. Mancia. Baroreflex control of sympathetic nerve activity in essential and secondary hypertension. *Hypertension*, 31:68–72, 1998.
- F. Grodins. Integrative cardiovascular physiology: A mathematical synthesis of cardiac and blood vessel hemodynamics. *The Quarterly Review of Biology*, 34(2):93–116, 1959.
- S.-J. Guild, P. Austin, M. Navatikian, J. Ringwood, and S. Malpas. Dynamic relationship between sympathetic nerve activity and renal blood flow: a frequency domain approach. *American Journal of Physiology (Regulatory Integrative and Comparative Physiology)*, 281:R206–R212, 2001.
- A. Guyton. Acute hypertension in dogs with cerebral ischemia. *American Journal of Physiology*, 154:45–54, 1948.
- A. Guyton. *Arterial pressure and hypertension*. Saunders, 1980.
- A. Guyton. *Human physiology and mechanisms of disease*. Saunders, 1987.
- A. Guyton, T. Coleman, A. Cowley, K. Scheel, R. Manning, and R. Norman. Arterial pressure regulation: overriding dominance of the kidneys in long-term regulation and in hypertension. *The American Journal of Medicine*, 52 (5):584–594, 1972a.
- A. Guyton, T. Coleman, and H. Granger. Circulation: Overall regulation. *Annual Reviews of Physiology*, 34:13–44, 1972b.
- A. Guyton, T. Coleman, D. Young, T. Lohmeier, and J. DeClue. Salt balance and long-term blood pressure control. *Annual Review of Medicine*, 31:15–27, 1980.
- A. Guyton and J. Hall. *Textbook of medical physiology*. Saunders, 2006.

- F. Haddy and J. Scott. Metabolically linked vasoactive chemicals in local regulation of blood flow. *Physiological Reviews*, 48 (4):688–707, 1968.
- E. Hairer, S.P. Nørsett, and G. Wanner. *Solving ordinary differential equations I: Nonstiff problems*. Springer Verlag, 1993.
- E. Hairer and G. Wanner. *Solving ordinary differential equations II: Stiff and differential-algebraic problems*. Springer Verlag, 1996.
- P. Hansen and J. Schnermann. Vasoconstrictor and vasodilator effects of adenosine in the kidney. *American Journal of Physiology (Renal Physiology)*, 285:590–599, 2003.
- A. Hassan, M. El-Brawany, and M. Sharaf. A functional cardiovascular model with disorders. In *In Proceedings of the 27th IEEE Annual Conference on Engineering in Medicine and Biology*, 2005.
- A. Hassid and C. Williams. Vasoconstrictor-evoked prostaglandin synthesis in cultured vascular smooth muscle. *American Journal of Physiology (Cell Physiology)*, 245:278–282, 1983.
- J. He, M. Klag, P. Whelton, J. Chen, J. Mo, M. Qian, P. Mo, and G. He. Migration, blood pressure pattern, and hypertension: the Yi migrant study. *American Journal of Epidemiology*, 134 (10):1085–1101, 1991a.
- J. He and G. MacGregor. Effect of longer-term modest salt reduction on blood pressure. *Cochrane Database of Systematic Reviews*, 1:CD004937. DOI: 10.1002/14651858.CD004937, 2004.
- J. He, G. Tell, Y. Tang, P. Mo, and G. He. Relation of electrolytes to blood pressure in men. The Yi people study. *Hypertension*, 17 (3):378–385, 1991b.
- R. Hester, R. Summers and R. Ilescu, J. Esters, and T. Coleman. DigitalHuman (DH): an integrative mathematical model of human physiology. In *In Proceedings of Modeling and Simulation (MODSIM) World Conference*, 2010.
- R. Hester, A. Brown, L. Husband, R. Ilescu, W. Pruet, R. Summers, and T. Coleman. Hummod: A modeling environment for the simulation of integrative human physiology. *Frontiers in Physiology*, 2(12), 2011.
- R. Hester, T. Coleman, and R. Summers. A multilevel open source integrative model of human physiology. *FASEB Journal*, 22:756.8, 2008.

- K. Heusser, S. Engeli, J. Tank, A. Diedrich, J. Menne, S. Eckert, T. Peters, F. Sweep, H. Haller, A. Pichlmaier, F. Luft, and J. Jordan. Carotid baroreceptor stimulation, sympathetic activity, baroreflex function, and blood pressure in hypertensive patients. *Hypertension*, 55:619–626, 2010.
- K. Hishikawa, T. Nakaki, T. Marumo, H. Suzuki, R. Kato, and T. Saruta. Pressure enhances endothelin-1 release from cultured human endothelial cells. *Hypertension*, 25:449–452, 1995.
- N.-H. Holstein-Rathlou and D. Marsh. A dynamic model of renal blood flow autoregulation. *Bulletin of Mathematical Biology*, 56:411–429, 1994.
- N. Hori, R. Jr. Cormier, and K. Kanai. Matched pole-zero discrete-time models. *IEE Proceedings on Control Theory and Applications (Part D)*, 139(3):273–278, 1992.
- M. Horiuchi, M. Akishita, and V. Dzau. Recent progress in angiotensin II type 2 receptor research in the cardiovascular system. *Hypertension*, 33:613–621, 1999.
- R. Hornych, Hurák, and M. Sebek. MathML in Polynomial toolbox for Matlab. In *Proceedings of the International Symposium on Computer-Aided Control System Design*, pages 284–286. Glasgow, 2002.
- M. Hucka, A. Finney, M. Sauro, H. Bolouri, J. Doyle, H. Kitano, A. Arkin, B. Bornstein, D. Bray, A. Cornish-Bowden, A. Cuellar, S. Dronov, E. Gilles, M. Ginkel, V. Gor, I. Goryanin, W. Hedley, T. Hodgman, J.-H. Hofmeyr, P. Hunter, N. Juty, J. Kasberger, A. Kremling, U. Kummer, N. Le Novère, L. Loew, D. Lucio, P. Mendes, E. Minch, E. Mjolsness, Y. Nakayama, M. Nelson, P. Nielsen, T. Sakurada, J. Schaff, B. Shapiro, T. Shimizu, H. Spence, J. Stelling, K. Takahashi, M. Tomita, J. Wagner, and J. Wang. The Systems Biology Markup Language (SBML): a medium for representation and exchange of biochemical network models. *Bioinformatics*, 19:524–531, 2003.
- P. Hunter, E. Crampin, and P. Nielsen. Bioinformatics, multiscale modelling and the IUPS Physiome Project. *Briefings in Bioinformatics*, 9(4):333–343, 2008.
- P. Hunter and P. Nielsen. A strategy for integrative computational physiology. *Physiology*, 20:316–325, 2005.

- P. Hunter, P. Robbins, and D. Noble. The IUPS human Physiome Project. *European Journal of Physiology*, 445:1–9, 2002.
- H. Hytti, R. Takalo, and H. Ihalainen. Tutorial on multivariate autoregressive modelling. *Journal of Clinical Monitoring and Computing*, 20:101–108, 2006.
- M. Ikeda, M. Kohno, and T. Takeda. Endothelin production in cultured mesangial cells of spontaneously hypertensive rats. *Hypertension*, 25:1196–1201, 1995.
- N. Ikeda, F. Marumo, M. Shirataka, and T. Sato. A model of overall regulation of body fluids. *Annals of Biomedical Engineering*, 7:135–166, 1979.
- J. Imig. Eicosanoid regulation of the renal vasculature. *American Journal of Physiology (Renal Physiology)*, 279:965–981, 2000.
- D. Jaffe, L. Sutherland, D. Barker, and L. Dahl. Effects of chronic excess salt ingestion. Morphologic findings in kidneys of rats with differing genetic susceptibilities to hypertension. *Archives of Pathology*, 90:1–16, 1970.
- R. Johnson, J. Herrera-Acosta, G. Schreiner, and B. Rodriguez-Iturbe. Subtle acquired renal injury as a mechanism of salt-sensitive hypertension. *The New England Journal of Medicine*, 346 (12):913–923, 2002.
- J. Jones. The Bainbridge reflex. *Journal of Physiology*, 160:298–305, 1962.
- F. Karaaslan, Y. Denizhan, A. Kayserilioglu, and H. Gulcur. Long term mathematical model involving renal sympathetic nerve activity, arterial pressure, and sodium excretion. *Annals of Biomedical Engineering*, 33 (11):1607–1630, 2005.
- A. Kardos, G. Watterich, R. de Mendeez, M. Csanady, B. Casadei, and L. Rudas. Determinants of spontaneous baroreflex sensitivity in a healthy working population. *Hypertension*, 37:911–916, 2001.
- T. Kawasaki, C. Delea, F. Bartter, and H. Smith. The effect of high-sodium and low-sodium intakes on blood pressure and other related variables in human subjects with idiopathic hypertension. *American Journal of Medicine*, 64:193–198, 1978.
- J. Keener, J. Sneyd, L. Sirovich, S. Wiggins, L. Kadanoff, and J. Marsden. *Mathematical physiology*. Springer Verlag, 1998.
- P. Khodade, S. Malhotra, N. Kumar, M. Iyengar, N. Balkrishnan, and N. Chandra.

- Cytoview: Development of a cell modelling framework. *J. Biosci.*, 32(5):965–977, 2007.
- G. Kimura and B. Brenner. Implications of the linear pressure-natriuresis relationship and importance of sodium sensitivity in hypertension. *Journal of Hypertension*, 15: 1055–1061, 1997.
- J. Kofranek, M. Andriik, T. Kripner, and S. Matousek. Biomedical educations with golem. In *Interdisciplinary Aspects of Humanmachine Co-existence and Co-operation*, pages 142–151. Czech Technical University, Prague, 2005.
- J. Kofranek, L. Anh, H. Snaselova, R. Kerekes, and T. Velan. GOLEM multimedia simulator for medical education. In *Proceedings of the 10th World Congress on Medical Informatics*, pages 1042–1046, London, 2001.
- J. Kofranek, J. Rusz, and S. Matousek. Guyton’s diagram brought to life - from graphic chart to simulation model for teaching physiology. In *Proceedings of the 15th Annual Conference on Technical Computing*, Prague, 2007.
- J. Kofranek, M. Matejk, and P. Privitzer. Hummod - large scale physiological model in modelica. In *Proceedings of the 8th International Modelica conference*, Dresden, 2011.
- P. Korner. *Essential hypertension and its causes*. Oxford University Press, 2007.
- M. La Rovere, G. Pinna, and G. Raczak. Baroreflex sensitivity: measurement and clinical implications. *Annals of Noninvasive Electrocardiology*, 13 (2):191–207, 2008.
- M. La Rovere, G. Specchia, A. Mortara, and P. Schwartz. Baroreflex sensitivity, clinical correlates, and cardiovascular mortality among patients with a first myocardial infarction. A prospective study. *Circulation*, 78 (4):816–824, 1988.
- P. Lanfranchi and V. Somers. Arterial baroreflex function and cardiovascular variability: interactions and implications. *American Journal of Physiology (Regulatory Integrative and Comparative Physiology)*, 283:815–826, 2002.
- J. Larsson. A framework for implementation-independent simulation models. *Simulation*, 82(9):563–579, 2006.
- D. Laude, J.-L. Elghozi, A. Girard, E. Bellard, M. Bouhaddi, P. Castiglioni, C. Cerutti, A. Cividjian, M. Di Rienzo, J.-O. Fortrat, B. Janssen, J. Karemaker, G. Lefthriotis,

- G. Parati, P. Persson, A. Porta, L. Quintin, J. Regnard, H. Rdiger, and H. Stauss. Comparison of various techniques used to estimate spontaneous baroreflex sensitivity (the EuroBaVar study). *American Journal of Physiology (Regulatory Integrative and Comparative Physiology)*, 286:226–231, 2004.
- F. Leenen, M. Ruzicka, and B. Huang. The brain and salt-sensitive hypertension. *Current Hypertension Reports*, 4:129–135, 2002.
- A. Leonard, L. Chafe, J-P. Montani, and B. Van Vliet. Increased salt sensitivity in eNOS knockout mice. *American Journal of Hypertension*, 12:1264–1269, 2006.
- B. Leonard, R. Evans, M. Navakatikyan, and S. Malpas. Differential neural control of intrarenal blood flow. *American Journal of Physiology (Regulatory Integrative and Comparative Physiology)*, 297:R907–R916, 2000.
- D. Levy, M. Larson, R. Vasan, W. Kannel, and K. Ho. The progression from hypertension to congestive heart failure. *The Journal of the American Medical Association*, 275(20):1557–1562, 1996.
- K. Lewenstein. Radial basis function neural network approach for the diagnosis of coronary artery disease based on the standard electrocardiogram exercise test. *Medical and Biological Engineering and Computing*, 39(3):362–367, 2005.
- L. Ljung. *System identification: Theory for the user (2nd Ed.)*. Prentice-Hall, 1999.
- L. Ljung. Perspectives on system identification. In *Proceedings of the 17th IFAC World Congress: Plenary Papers, Milestone Reports and Selected Survey Papers*, pages 47–59, Seoul, 2008.
- L. Ljung and T. Glad. *Modeling of dynamic systems*. Prentice-Hall, 1994.
- R. Loutzenhiser, A. Bidani, and L. Chilton. Renal myogenic response: Kinetic attributes and physiological role. *Circulation Research*, 90:1316–1324, 2002.
- J. Ludbrook, Mancina G., A. Ferrari, and A Zanchetti. The variable-pressure neck-chamber method for studying the carotid baroreflex in man. *Clinical Science and Molecular Medicine*, 53 (2):156–171, 1977.
- T. Ludden, S. Beal, and L. Sheiner. Comparison of the Akaike Information Criterion, the Schwarz Criterion and the F-Test as guides to model selection. *Journal of Pharmacokinetics and Biopharmaceutics*, 22 (5):431–445, 1994.

- F. Luft. Molecular genetics of salt-sensitivity and hypertension. *Drug metabolism and disposition*, 29 (4):500–504, 2001.
- F. Luft. Mendelian forms of human hypertension and mechanisms of disease. *Clinical Medicine and Research*, 1(4):291–300, 2003.
- F. Luft and M. Weinberger. Heterogenous responses to changes in dietary salt intake: the salt-sensitivity paradigm. *The American Journal of Clinical Nutrition*, 65:612S–617S, 1997.
- X. Ma, F. Abboud, and M. Chapleau. A novel effect of angiotensin on renal sympathetic nerve activity in mice. *Journal of Hypertension*, 19:609–618, 2001.
- T. Maack. Role of atrial natriuretic factor in volume control. *Kidney International*, 49:1732–1737, 1996.
- M. Madrid, M. Garcia-Salom, J. Tornel, M. De Gasparo, and F. Fenoy. Effect of interactions between nitric oxide and angiotensin II on pressure diuresis and natriuresis. *American Journal of Physiology (Regulatory Integrative and Comparative Physiology)*, 273:1676–1682, 1997.
- R. Maestri, G. Pinna, A. Mortara, M. La Rovere, and L. Tavazzi. Assessing baroreflex sensitivity in post-myocardial infarction patients: comparison of spectral and phenylephrine techniques. *Journal of the American College of Cardiology*, 31 (2):344–351, 1998.
- A. Malliani, F. Lombardi, and M. Pagani. Power spectrum analysis of heart rate variability: a tool to explore neural regulatory mechanisms. *British Heart Journal*, 71:1–2, 1994.
- S. Malpas and D. Burgess. Renal sna as the primary mediator of slow oscillations in blood pressure during haemorrhage. *American Journal of Physiology (Heart and Circulatory Physiology)*, 279:R1299–R1306, 2000.
- V. Mangourova and J. Ringwood. Gray box modelling of arterial vasoaction. In *Proceedings of Irish Signals and Systems Conference*, Dublin Institute of Technology, Dublin, Ireland, June 2006.
- D. Manning, T. Coleman, A. Guyton, R. Norman, and R. McCaa. Essential role of

- mean circulatory filling pressure in salt-induced hypertension. *American Journal of Physiology (Regulatory Integrative and Comparative Physiology)*, 5(1):40–47, 1979.
- P. Marraccini, S. Fedele, M. Marzilli, E. Orsini, G. Dukic, L. Serasini, and A. L’Abbate. Adenosine-induced renal vasoconstriction in man. *Cardiovascular Research*, 32:949–953, 1996.
- V. McLoone, J. Ringwood, and B. Van Vliet. A multi-component model of the dynamics of salt-induced hypertension in Dahl-S rats. *BMC-Physiology*, 9:20, 2009.
- G. Meneely, R. Tucker, and W. Darby and S. Auerbach. Chronic sodium chloride toxicity in the albino rat. II. Occurrence of hypertension and of a syndrome of edema and renal failure. *The Journal of Experimental Medicine*, 98:71–80, 1953.
- P. Meneton, X. Jeunemaitre, H. De Wardener, and G. MacGregor. Links between dietary salt intake, renal salt handling, blood pressure and cardiovascular disease. *Physiological Reviews*, 85:679–715, 2005.
- M. Mitchell. *An Introduction to Genetic Algorithms*. The MIT Press, 1999.
- C. Molar and C. Van Loan. Nineteen dubious ways to compute the exponential of a matrix, twenty five years later. *SIAM Review*, 45:3–49, 2003.
- K. Monahan, F. Dinunno, D. Seals, C. Clevenger, C. Desouza, and H. Tanaka. Age-associated changes in cardiovagal baroreflex sensitivity are related to central arterial compliance. *American Journal of Physiology (Heart and Circulatory Physiology)*, 281:284–289, 2001.
- J-P. Montani. Personal communication. 2008.
- J-P. Montani, T. Adair, R. Summers, T. Coleman, and A. Guyton. A simulation support system for solving large physiological models on microcomputers. *International Journal of Bio-Medical Computing*, 24:41–54, 1989.
- R. Morris Jr, A. Sebastian, A. Forman, M. Tanaka, and O. Schmidlin. Normotensive salt sensitivity effects of race and dietary potassium. *Hypertension*, 33:18–23, 1999.
- L. Mullins, M. Bailey, and J. Mullins. Hypertension, kidney and transgenics: a fresh perspective. *Physiological Reviews*, 86:709–746, 2006.

- S. Muravchick and E. Bergofsky. Adrenergic receptors and vascular resistance in cerebral circulation of the cat. *Journal of Applied Physiology*, 40:797–804, 1976.
- P. Murray-Rust and H. Rzepa. Chemical markup, XML, and the World Wide Web. 4. CML Schema. *Journal of Chemical Information and Computer Sciences*, 43(3):757–772, 2003.
- J. Naik, T. O’Donoghay, and B. Walker. Endogenous carbon monoxide is an endothelial-derived vasodilator factor in the mesenteric circulation. *American Journal of Physiology (Heart and Circulatory Physiology)*, 284:H838–H845, 2002.
- J. Naik and B. Walker. Homogeneous segmental profile of carbon monoxide-mediated pulmonary vasodilation in rats. *American Journal of Physiology (Lung Cell and Molecular Physiology)*, 281:L1436–L1443, 2001.
- M. Navakatikyan, B. Leonard, R. Evans, and S. Malpas. Modeling the neural control of intrarenal blood flow. *Clinical and Experimental Pharmacology and Physiology*, 27:650–652, 2000.
- J. Nelder and R. Mead. A simplex method for function minimization. *The Computer Journal*, 7 (4):308–313, 1965.
- G. Nollo, A. Porta, L. Faes, M. Del Greco, M. Disertori, and F. Ravelli. Causal linear parametric model for baroreflex gain assessment in patients with recent myocardial infarction. *American Journal of Physiology (Heart and Circulatory Physiology)*, 280:1830–1839, 2001.
- M. Nuruzzaman. *Modeling and simulation in Simulink for engineers and scientists*. AuthorHouse, 2005.
- T. O’Donoghay and B. Walker. Renal vasodilatory influence of endogenous carbon monoxide in chronically hypoxic rats. *American Journal of Physiology (Heart and Circulatory Physiology)*, 279:2908–2915, 2000.
- H. Oka, S. Mochio, M. Yoshioka, M. Morita, and K. Inoue. Evaluation of baroreflex sensitivity by the sequence method using blood pressure oscillations and R-R interval changes during deep respiration. *European Neurology*, 50:230–243, 2003.
- W. Oliver, E. Cohen, and J. Neel. Blood pressure, sodium intake, and sodium related

- hormones in the Yanomamo Indians, a ‘no-salt’ culture. *Circulation*, 52 (1):146–151, 1975.
- A. Oppenheim, R. Schafer, and J. Buck. *Discrete-time Signal Processing (2Nd Ed.)*. Prentice-Hall, Inc., Upper Saddle River, NJ, USA, 1999.
- O. Ormezzano, J.-L. Cracowski, J.-L. Quesada, H. Pierre, J.-M. Mallion, and J.-P. Baguet. EVALuation of the prognostic value of BARoreflex sensitivity in hypertensive patients: the EVABAR study. *Journal of Hypertension*, 26:1373–1378, 2008.
- J. Osborn and B. Hornfeldt. Arterial baroreceptor denervation impairs long-term regulation of arterial pressure during dietary salt loading. *American Journal of Physiology (Heart and Circulatory Physiology)*, 275:1558–1566, 1998.
- K. O’Shaughnessy and F. Karet. Salt handling and hypertension. *Annual Review of Nutrition*, 26:343–365, 2006.
- K. Osterziel, D. Hanlein, R. Willenbrock, C. Eichhorn, F. Luft, and R. Dietz. Baroreflex sensitivity and cardiovascular mortality in patients with mild to moderate heart failure. *British Heart journal*, 73:517–522, 1995.
- J. Ottesen, M. Olufsen, and J. Larsen. *Applied mathematical models in human physiology*. SIAM, 2004.
- M. Pagani, F. Lombardi, S. Guzzetti, O. Rimoldi, R. Furlan, P. Pizzinelli, S. Sandrone, G. Malfatto, S. Dell’Orto, and E. Piccaluga. Power spectral analysis of heart rate and arterial pressure variabilities as a marker of sympatho-vagal interaction in man and conscious dog. *Circulation Research*, 59:178–193, 1986.
- M. Pagani, V. Somers, R. Furlan, S. Dell’Orto, J. Conway, G. Baselli, S. Cerutti, P. Sleight, and A. Malliani. Changes in autonomic regulation induced by physical training in mild hypertension. *Hypertension*, 12:600–610, 1988.
- L. Page, D. Vandever, K. Nader, N. Lubin, and J. Page. Blood pressure of Qash’qai pastoral nomads in Iran in relation to culture, diet, and body form. *American Journal of Clinical Nutrition*, 34:527–538, 1981.
- H. A. Palmero, T. F. Caeiro, D. J. Iosa, and J. Bas. Baroreceptor reflex sensitivity index derived from Phase 4 of the Valsalva maneuver. *Hypertension*, 3 (6):134–137, 1981.

- T. Parks and C. Burrus. *Digital Filter Design*. Wiley-Interscience, New York, NY, USA, 1987.
- R. Parmer, J. Cervenka, and R. Stone. Baroreflex sensitivity and heredity in essential hypertension. *Circulation*, 85:497–503, 1992.
- D. Patton, J. Triedman, M. Perrott, A. Vidian, and J. Saul. Baroreflex gain: characterization using autoregressive moving average analysis. *American Journal of Physiology (Heart and Circulatory Physiology)*, 39:1240–1249, 1996.
- A. Patzak, R. Mrowka, E. Storch, B. Hocher, and P. Persson. Interaction of Angiotensin II and nitric oxide in isolated perfused afferent arterioles of mice. *Journal of the American Society of Nephrology*, 12:1122–1127, 2001.
- S. Pedersen, J. Jørgensen, and J. Pedersen. Use of neural networks to diagnose acute myocardial infarction. II. A clinical application. *Clinical Chemistry*, 42(4):613–617, 1996.
- G. Pinna and R. Maestri. New criteria for estimating baroreflex sensitivity using the transfer function method. *Medical and Biological Engineering and Computing*, 40 (1): 79–84, 2002.
- G. Pinna, R. Maestri, and A. Mortaraz. Estimation of arterial blood pressure variability by spectral analysis: comparison between Finapres and invasive measurements. *Physiological Measurement*, 17:147–169, 1996.
- Y. Pinto, M. Paul, and D. Ganten. Lessons from rat models of hypertension: from Goldblatt to genetic engineering. *Cardiovascular Research*, 39(1):77–88, 1998.
- M. Pitzalis, F. Mastropasqua, F. Massari, A. Passantino, R. Colombo, A. Mannarini, C. Forleo, and P. Rizzon. Effect of respiratory rate on the relationships between RR interval and systolic blood pressure fluctuations: a frequency-dependent phenomenon. *Cardiovascular Research*, 38:332–339, 1998.
- H. Piuce. Effects of carbon dioxide on the cardiovascular system. *Anesthesiology*, 21 (6):652–663, 1960.
- A. Pop and P. Fritzson. ModelicaXML: A Modelica XML representation with applications. In *Proceedings of the 3rd International Modelica Conference*, pages 419–430, Linköping, 2003.

- A. Porta, G. Baselli, O. Rimoldi, A. Malliani, and M. Pagani. Assessing baroreflex gain from spontaneous variability in conscious dogs: role of causality and respiration. *American Journal of Physiology (Heart and Circulatory Physiology)*, 279:2558–2567, 2000.
- N. Poulter, K. Khaw, B. Hopwood, M. Mugambi, W. Peart, G. Rose, and P. Sever. The Kenyan Luo migration study: observations on the initiation of a rise in blood pressure. *British Medical Journal*, 300 (6730):967–972, 1990.
- M. Pueyo, J.-F. Arnal, J. Rami, and J.-B. Michel. Angiotensin II stimulates the production of NO and peroxynitrite in endothelial cells. *American Journal of Physiology (Cell Physiology)*, 274:214–220, 1998.
- S. Rajagopalan and D. Harrison. Reversing endothelial dysfunction with ACE inhibitors. A new trend? *Circulation*, 94:240–243, 1996.
- J. Rapp and H. Dene. Development and characteristics of inbred strains of Dahl salt-sensitive and salt-resistant rats. *Hypertension*, 7:340–349, 1985.
- J. Reid and M. Rand. Renal vasoconstriction is modulated by nitric oxide. *Clinical and Experimental Pharmacology and Physiology*, 19:376–379, 1992.
- H. Reinhardt, E. Seeliger, K. Lohmann, M. Corea, and W. Boemke. Changes of blood pressure, sodium excretion and sodium balance due to variations of the renin-angiotensin-aldosterone system. *Journal of the Autonomic Nervous System*, 57:184–187, 1996.
- J.-M. Renders and S. Flasse. Hybrid methods using genetic algorithms for global optimization. *IEEE Transactions on Systems, Man, and Cybernetics, PartB: Cybernetics*, 26:243–258, 1996.
- D. Richardson, D. Randall, and D. Speck. *Cardiopulmonary System*. Fence Creek Publishing, 1st edition, 1998.
- J. Ringwood and S. Malpas. Slow oscillations in blood pressure via a nonlinear feedback model. *American Journal of Physiology (Regulatory Integrative and Comparative Physiology)*, 280:R1105–R1115, 2001.
- D. Rizzoni, E. Porteri, M. Castellano, G. Bettoni, M. Muiesan, P. Muiesan, S. Giulini,

- and E. Agabiti-Rosei. Vascular hypertrophy and remodeling in secondary hypertension. *Hypertension*, 28:785–790, 1996.
- H. Robbe, L. Mulder, H. Ruddel, W. Langewitz, J. Veldman, and G. Mulder. Assessment of baroreceptor reflex sensitivity by means of spectral analysis. *Hypertension*, 10:538–543, 1987.
- H. Rüdiger, L. Klinghammer, and K. Scheuch. The trigonometric regressive spectral analysis a method for mapping of beat-to-beat recorded cardiovascular parameters on to frequency domain in comparison with Fourier transformation. *Computer Methods and Programs in Biomedicine*, 58:1–15, 1999.
- D. Russell, E. Garryb, A. Taberner, C. Barrett, J. Paton, D. Budgett, and S. Malpas. A fully implantable telemetry system for the chronic monitoring of brain tissue oxygen in freely moving rats. *Journal of Neuroscience Methods*, 204(2):242–248, 2012.
- R. Sacco, E. Benjamin, J. Broderick, M. Dyken, J. Donald Easton, W. Feinberg, L. Goldstein, P. Gorelick, G. Howard, S. Kittner, T. Manolio, J. Whisnant, and P. Wolf. Risk factors. *Stroke*, 28:1507–1517, 1997.
- N. Sasaki. High blood pressure and the salt intake of the Japanese. *Japanese Heart Journal*, 3 (4):313–324, 1962.
- R. Schoenberg. *Optimization with the quasi-Newton method*. Aptech Systems, Inc. Maple Valley, WA, 2001.
- R. Schubert and M. Mulvany. The myogenic response: established facts and attractive hypotheses. *Clinical Science*, 7796:313–326, 1999.
- P. Schwarz, R. Diem, N.J. Dun, and U. Frstermann. Endogenous and exogenous nitric oxide inhibits norepinephrine release from rat heart sympathetic nerves. *Circulation Research*, 77:841–848, 1995.
- A. Sharma, U. Schorr, C. Cetto, and A. Distler. Dietary v intravenous salt loading for the assessment of salt sensitivity in normotensive men (Abstract only). *American Journal of Hypertension*, 7 (12):1070–1075, 1994.
- D. Sigmon and W. Beierwaltes. Angiotensin II: nitric oxide interaction and the distribution of blood flow. *American Journal of Physiology (Regulatory Integrative and Comparative Physiology)*, 265:1276–1283, 1993.

- S. Simchon, W. Manger, R. Carlin, L. Peeters, J. Rodriguez, D. Batista, T. Brown, N. Merchant, K. Jan, and S. Chien. Salt-induced hypertension in Dahl salt-sensitive rats. Hemodynamics and renal responses. *Hypertension*, 13:612–621, 1989.
- B. Smith, J. Boyle, J. Dongarra, B. Garbow, Y. Ikebe, V. Klema, and C. Moler. *Matrix Eigensystem Routines, EISPACK Guide*. Lecture Notes in Computer Science, Volume 6. Springer Verlag, 1976.
- S. Smith and S. Cagnoni. *Genetic and evolutionary computation medical applications*. John Wiley & Sons, 2010.
- S. Srinivasan, G. Berenson, B. Radhakrishnamurthy, E. Dalferes, D. Underwood, and T. Foster. Effects of dietary sodium and sucrose on the induction of hypertension in spider monkeys. *American Journal of Clinical Nutrition*, 33:561–569, 1980.
- S. Srinivasan, E. Dalferes, R. Wolf, B. Radhakrishnamurthy, T. Foster, and G. Berenson. Variability in blood pressure response to dietary sodium intake among African green monkeys (*Cercopithecus aethiops*). *American Journal of Clinical Nutrition*, 39:792–796, 1984.
- J. Stamler. The INTERSALT study: background, methods, findings, and implications. *American Journal of Clinical Nutrition*, 65 (2):625S–642S, 1997.
- R. Tabrizchi and M. Pugsley. Methods of blood flow measurement in the arterial circulatory system. *Journal of Pharmacological and Toxicological Methods*, 44(2):375–384, 2000.
- E. Tan, B. Pereles, B. Horton, R. Shao, M. Zourob, and K. G. Ong. Implantable biosensors for real-time strain and pressure monitoring. *Sensors*, 8(10):6396–6406, 2008.
- Task Force of the European Society of Cardiology and the North American Society of Pacing and Electrophysiology. Heart rate variability, standards of measurement, physiological interpretation, and clinical use. *European Heart Journal*, 17:354–381, 1996.
- S. Thomas, P. Baconnier, J. Fontecave, J.-P. Francoise, F. Guillaud, P. Hannaert, A. Hernandez, V. Le Rolle, P. Maziere, F. Tahi, and R. White. SAPHIR: a physiome

- core model of body fluid homeostasis and blood pressure regulation. *Philosophical Transaction of the Royal Society A*, 366:3175–3197, 2008.
- C. Thorup, C. Jones, S. Gross, L. Moore, and M. Goligorsky. Carbon monoxide induces vasodilation and nitric oxide release but suppresses endothelial NOS. *American Journal of Physiology (Renal Physiol)*, 277:882–889, 1999.
- T. Thrasher. Baroreceptors, baroreceptor unloading, and the long-term control of blood pressure. *American Journal of Physiology (Regulatory Integrative and Comparative Physiology)*, 288:819–827, 2005.
- S. Tiinanen, M. Tulppo, and T. Seppanen. Reducing the effect of respiration in baroreflex sensitivity estimation with adaptive filtering. *IEEE Transactions on Biomedical Engineering*, 55 (1):51–59, 2008.
- M. Timio, G. Lippi, S. Venanzi, S. Gentili, G. Quintaliani, C. Verdura, C. Monarca, and P. Saronio and F. Timio. Blood pressure trend and cardiovascular events in nuns in a secluded order: a 30-year follow-up study. *Blood Pressure*, 6 (2):81–87, 1997.
- L. Tobian. Salt and hypertension: Lessons from animal models that relate to human hypertension. *Hypertension*, 17 (1):I52–I58, 1991.
- L. Tobian and S. Hanlon. High sodium chloride diets injure arteries and raise mortality without changing blood pressure. *Hypertension*, 15:900–903, 1990.
- F. Tränkle, A. Gerstlauer, M. Zeitz, and E.D. Gilles. ProMoT/Diva: A prototype of a process modeling and simulation environment. In *Proceedings of the 2nd IMACS Symposium on Mathematical Modelling (MATHMOD)*, pages 341–346. Vienna, 1999.
- R. Uttamsingh, M. Leaning, J. Bushman, E. Carson, and L. Finkelstein. Mathematical model of the human renal system. *Medical and Biological Engineering and Computing*, 23:525–535, 1985.
- H. Van de Vooren, M. Gademan, C. Swenne, B. Ten Voorde, M. Schalijs, and E. Van der Wall. Baroreflex sensitivity, blood pressure buffering, and resonance: what are the links? Computer simulation of healthy subjects and heart failure patients. *Journal of Applied Physiology*, 102:1348–1356, 2007.
- B. Van Vliet, L. Chafe, S. Halfyard, and A. Leonard. Distinct rapid and slow phases

- of salt-induced hypertension in Dahl salt-sensitive rats. *Journal of Hypertension*, 24: 1599–1606, 2006.
- B. Van Vliet and J.-P. Montani. The time course of salt-induced hypertension, and why it matters. *International Journal of Obesity*, 32:S35–S47, 2008.
- P. Wabel and S. Leonhardt. A simulink model for the human circulatory system. *Biomedizinische Technik/Biomedical Engineering*, 43:S314–S315, 1998.
- R. Ward, L. Pouchard, and J. Nutaro. Integrative computational frameworks for multiscale digital human modeling and simulation. In *Proceedings of the International Conference on Computer Science (ICCS 2006)*, pages 814–821. 2006.
- R. Waschler, O. Angeles-Palacios, M. Ginkel, and A. Kienle. Object-oriented modelling of large-scale chemical engineering processes with ProMoT. *Mathematical and Computer Modelling of Dynamical Systems*, 12(1):5–18, 2006.
- M. Weinberger. Salt sensitivity of blood pressure in humans. *Hypertension*, 27:481–490, 1996.
- M. Weinberger and N. Fineberg. Sodium and volume sensitivity of blood pressure. Age and pressure change over time. *Hypertension*, 18:67–71, 1991.
- M. Weinberger, N. Fineberg, S. Fineberg, and M. Weinberger. Salt sensitivity, pulse pressure, and death in normal and hypertensive humans. *Hypertension*, 37 (2):429–432, 2001.
- M. Weinberger, J. Miller, N. Fineberg, F. Luft, C. Grim, and J. Christian. Association of haptoglobin with sodium sensitivity and resistance of blood pressure (abstract only). *Hypertension*, 4:443–446, 1987.
- M. Weinberger, J. Miller, F. Luft, C. Grim, and N. Fineberg. Definitions and characteristics of sodium sensitivity and blood pressure resistance. *Hypertension*, 8 (Suppl II):127–134, 1986.
- M. Weinberger, J. Stegner, and N. Fineberg. A comparison of two tests for the assessment of blood pressure responses to sodium. *American Journal of Hypertension*, 6: 179–184, 1993.
- S. Weiss, C. Kulikowski, and S. Amarel. A model-based method for computer-aided medical decision-making. *Artificial Intelligence*, 11 (1-2):145–172, 1978.

-
- B. Westerhof, J. Gisolf, W. Stok, K. Wesseling, and J. Karemaker. Time-domain cross-correlation baroreflex sensitivity: performance on the EUROBAVAR data set. *Journal of Hypertension*, 22:1–10, 2004.
- P. Whelton, T. Perneger, F. Brancati, and M. Klag. Epidemiology and prevention of blood pressure-related renal disease. *Journal of Hypertension*, 10 (7):S77–S84, 1992.
- T. Wu, C. Chen, and T. Kao. Baroreflex sensitivity evaluation by Volterra-Wiener model and the Laguerre expansion technique. *Computers in Cardiology*, 35:741–744, 2008.
- S. Wunsch, J. Muller-Delp, and M. Delp. Time course of vasodilatory responses in skeletal muscle arterioles: role in hyperemia at onset of exercise. *American Journal of Physiology (Heart and Circulatory Physiology)*, 279:1715–1723, 2000.
- F. Yates. Validation of simple and complex models in physiology and medicine. *American Journal of Physiology (Regulatory Integrative and Comparative Physiology)*, 234 (5):R159–R160, 1978.
- R. Zatz and G. DeNucci. Effects of acute nitric oxide synthase inhibition on rat glomerular microcirculation. *American Journal of Physiology (Renal Physiology)*, 261:360–363, 1991.